

On the role of DNA methyltransferase 3A (DNMT3A) in myeloid cells in intestinal homeostasis and inflammatory responses

Dissertation
zur Erlangung des Doktorgrades
der Mathematisch-Naturwissenschaftlichen Fakultät der
Christian-Albrechts-Universität zu Kiel

vorgelegt von

Dora Bordoni

Kiel, 2022

First referee (supervisor): Prof. Dr. Philip Rosenstiel
Second referee: Prof. Dr. Thomas Roeder
Examiner: Prof. Dr. Petra Bacher
Chairperson: Prof. Dr. Matthias Leippe

Date of the oral examination: 20/03/2023

Approved for publication on: 20/03/2023

Acknowledgement

On the very onset of this work, I would like to extend my most sincere obligation towards all those people that directly and indirectly supported me on this scientific adventure.

First and foremost, I would like to express my deepest gratitude to Professor Philip Rosenstiel for the continuous support and guidance during my PhD, making my stay in his group an extraordinary experience.

I sincerely acknowledge all colleagues involved in this project, especially Ms. Franziska Kimming, Dr. Neha Mishra, Dr. Antonella Fazio, and Dr. Maren Falk Paulsen, for the exciting scientific discussion and for sharing their expertise.

A particular thanks goes to all those friends, before than colleagues, who were there all along and made life in Kiel not all about work.

Last and certainly not least, my most sincere and heartfelt thank you goes to my family, for their love and for their unconditional support.

Contents

1. Introduction	9
1.1 <i>Inflammatory bowel disease</i>	9
1.2 <i>Risk factors for IBD</i>	10
1.3 <i>Inflammatory Bowel Disease and Epigenetics</i>	11
1.4 <i>Epigenetic mechanisms</i>	12
1.5 <i>DNA methylation and its role in mammalian development and disease</i>	12
1.5.1 The DNMTs family	14
1.5.2 DNMT3A in development, disease and intestinal inflammation	15
1.5.3 Epithelial and immune crosstalk during IBD	17
1.6 <i>The origins of macrophages: from bone marrow to the gut</i>	17
1.6.1 Macrophages effector functions and subtypes	19
1.6.2 Classical activation: M1 macrophages	20
1.6.3 Alternative activation: M2 macrophages	20
1.6.4 Macrophage polarization in homeostasis and inflammatory bowel disease	21
1.7 <i>Arginine metabolism: arginase and nitric oxide synthase balance within macrophages polarization</i>	23
1.7.1 The nitric oxide synthase road: arginine-nitric oxide (NO) axis	24
1.7.2 The healing mode of arginase alternative pathway: the arginine-ornithine axis	24
1.8 <i>Aims of the study</i>	26
2. Materials and methods	28
2.1 <i>Molecular biology methods</i>	28
2.1.1 Total RNA isolation	28
2.1.2 cDNA synthesis	28
2.1.3 Real time quantitative polymerase chain reaction (RT-qPCR)	29
2.1.4 DNA isolation	29
2.1.5 DNA isolation for total bacteria quantification	30
2.2 <i>Biochemical methods</i>	30
2.2.1 Protein lysate preparation	30
2.2.2 Protein quantification	30
2.2.3 SDS-PAGE and Western blot	31
2.2.4 Protein transfer and immobilization	31
2.2.5 Immunoblotting and signal visualization	32

2.2.6 Signal acquisition	33
<i>2.3 Isolation and cultivation of cells</i>	33
2.3.1 Maintenance of human organoids	33
2.3.2 Generation and maintenance of murine colonic organoids	33
2.3.3 Bone marrow harvesting and macrophages differentiation	34
2.3.4 Macrophage maintenance and polarization	34
2.3.5 Splenocyte isolation	35
2.3.6 Lamina propria and intestinal epithelium dissociation from small intestine and colon	35
2.3.7 Mode-K maintenance and co-culture system establishment for <i>in vitro</i> wound healing assay	35
2.3.8 Organoid-macrophages co-culture	36
<i>2.4 Generation, handling, and treatment of mice</i>	37
2.4.1 Generation of <i>Dnmt3a</i> ^{ΔIEC} mice	37
2.4.2 Generation of <i>Dnmt3a</i> ^{LysM} mice	37
2.4.3 Animal housing and animal welfare	37
2.4.4 Acute DSS induction	38
2.4.5 Disease activity assessment	38
2.4.6 Histopathological analyses of murine colonic tissue	38
2.4.7 AOM-Chronic DSS induction	39
2.4.8 <i>In vivo</i> Fluorescein isothiocyanate (FITC)-dextran permeability assay	39
<i>2.5 Immunohistochemistry</i>	39
2.5.1 Tissue Processing	39
2.5.2 Hematoxylin and Eosin (H&E) staining	40
2.5.3 3,3'-Diaminobenzidine (DAB) staining	40
<i>2.6 Imaging and immunofluorescence</i>	40
2.6.1 Fluorescent <i>in situ</i> hybridization (FISH)	40
2.6.2 BMDMs Immunofluorescence	41
<i>2.7 NGS technology</i>	41
2.7.1 Transcriptome analysis	41
<i>2.8 Functional assays</i>	42
2.8.1 Arginase activity assay	42
2.8.2 Nitric oxide synthase assay	43
<i>2.9 Immunoassays</i>	43
2.9.1 Flow cytometry analysis	43
2.9.2 Gating strategy	44
2.9.3 Basal immune phenotyping panel	44
2.9.4 Flow cytometry analysis of hematopoietic precursors	45

2.9.5 Magnetic activated cell sorting	45
2.9.6 Mature hematopoietic cells depletion from spleen	46
2.10 Statistics	46
3. Results	47
3.1 <i>On the role of DNA methyltransferase 3A (DNMT3A) in intestinal epithelial barrier function in the colon</i>	47
3.1.1 Lack of <i>Dnmt3a</i> favours mucus layer thinning and increases bacterial translocation to mesenteric lymph nodes	47
3.1.2 <i>Dnmt3a</i> is downregulated during inflammation	49
3.2 <i>Dnmt3a in the myelomonocytic lineage during homeostasis and inflammation</i>	52
3.2.1 <i>Dnmt3a</i> deletion in macrophages of the lamina propria	52
3.2.2 <i>Dnmt3a</i> deletion in <i>Dnmt3a</i> ^{LysM} bone marrow derived macrophages (BMDMs)	54
3.2.3 Absence of <i>Dnmt3a</i> does not impact CD11b ⁺ cells frequencies after BMDM generation	54
3.3 <i>A functional characterization of macrophage polarization in Dnmt3a depleted BMDMs</i>	56
3.3.1 <i>Dnmt3a</i> expression is upregulated in M2 macrophages	56
3.3.2 Lack of <i>Dnmt3a</i> in BMDMs results in a complex transcriptional dysregulation	57
3.3.3 Lack of <i>Dnmt3a</i> results in impaired expression of polarization marker genes	62
3.3.4 Lack of <i>Dnmt3a</i> affects cytoskeletal rearrangement	64
3.3.5 Loss of <i>Dnmt3a</i> impairs phagocytosis	66
3.3.6 <i>Dnmt3a</i> contributes to arginine metabolism-dependent macrophage polarization	67
3.4 <i>Dnmt3a in the immuno-epithelial interplay</i>	69
3.4.1 <i>Dnmt3a</i> expression is beneficial for wound healing <i>in vitro</i>	69
3.4.2 <i>Dnmt3a</i> suppresses tumor-derived epithelium proliferation	71
3.5 <i>Dnmt3a</i> ^{LysM} mouse model characterization	74
3.5.1 <i>Dnmt3a</i> ^{LysM} mice: an age-dependent spontaneous phenotype	74
3.5.2 <i>Dnmt3a</i> ablation results in a spleen hypertrophy and alters splenic hematopoietic stem cell abundance	76
3.5.3 Loss of <i>Dnmt3a</i> in older mice determines splenic immune cell population composition alteration	78
3.5.4 Lack of <i>Dnmt3a</i> in macrophages during acute DSS-induced colitis	80
3.5.5 Splenic immune cell composition in <i>Dnmt3a</i> ^{LysM} mice is not affected after acute intestinal inflammation	81
3.5.6 <i>Dnmt3a</i> ^{LysM} mice are more susceptible to chronic DSS driven inflammation	82
4. Discussion	86
4.1 <i>Dnmt3a orchestrates mucosal homeostasis in the colon</i>	86
4.1.1 DNMT3A is downregulated during inflammation in intestinal epithelium	87

<i>4.2 Dnmt3a in the myelomonocytic lineage</i>	88
4.2.1 Inflammation drives <i>Dnmt3a</i> downregulation in the myelomonocytic lineage	88
4.2.2 A complex transcriptional signature portrays macrophage polarization	89
4.2.3 <i>Dnmt3a</i> depletion and its impact on polarization marker genes expression and cellular reshaping	91
<i>4.3 A comprehensive characterization of macrophagic effector functions</i>	92
4.3.1 M2 <i>Dnmt3a</i> ^{LysM} macrophages are more prone to phagocytosis	93
4.3.2 Two competitive arginine pathways in macrophage physiology	94
4.3.3 Wound repair and tumor progression	94
<i>4.4 An age-dependent phenotype</i>	95
<i>4.5 Lack of Dnmt3a impacts recovery after intestinal inflammation</i>	96
5. Conclusions and future perspectives	99
6. Summary	101
7. Zusammenfassung	104
8. References	107
9. Supplementary material	132
9.1 List of Figures	132
9.2 List of Tables	133
9.3 Abbreviations	134
9.4 Supplementary tables	139
9.5 Curriculum vitae	158
9.6 Eidesstattliche Erklärung	161

Parts of this dissertation are contained in the manuscript “DNA methyltransferase 3A controls intestinal epithelial barrier function and regeneration in the colon”.

Nat Commun. 2022 Oct 21;13(1):6266.

doi: 10.1038/s41467-022-33844-2.

Antonella Fazio^{1*}, **Dora Bordoni**^{1*}, Jan W.P. Kuiper¹, Saskia Weber-Stiehl¹, Stephanie T. Stengel¹, Philipp Arnold², David Ellinghaus¹, Go Ito^{1,4}, Florian Tran^{1,3}, Berith Messner¹, Anna Henning¹, Joana P. Bernardes¹, Robert Häslér^{1, 5}, Anne Luzius¹, Simon Imm¹, Finn Hinrichsen¹, Andre Franke¹, Samuel Huber⁶, Susanna Nikolaus³, Konrad Aden^{1,3}, Stefan Schreiber³, Felix Sommer¹, Gioacchino Natoli⁷, Neha Mishra^{1#} and Philip Rosenstiel^{1#}

* Shared first authorship

1. Introduction

1.1 Inflammatory bowel disease

Inflammatory bowel disease (IBD) is a chronic inflammatory disease affecting the intestine and it is characterized by a complex pathophysiology which involves genetic, microbiological, immunological, and epigenetic mechanisms [1]. In the last two decades, the incidence of IBD has been increasing in developing countries undergoing industrialization and urbanization [2], but the exact pathogenesis remains unknown. Symptomatic manifestations associated with IBD can include diarrhea, rectal bleeding, abdominal pain, fever, weight loss, vomiting, cramps, and muscle spasms. Up to 25% of the patients have extra-intestinal symptoms such as arthropathies, erythema nodosum and uveitis [3].

The two major clinical manifestations of IBD are Crohn's disease (CD) and ulcerative colitis (UC), both characterized by relapsing-remitting inflammatory episodes. These sub-entities of IBD can either be chronic remittent or progressive inflammatory conditions that potentially affect the entire gastrointestinal tract or the colonic mucosa, respectively. Both subtypes are associated with complications such as chronic pain, gut dysmotility and increased risk of colon cancer insurgence and progression [4]–[7]. Comparing the two from a morphological point of view, UC is a continuous inflammatory lesion that progresses from the distal colon to the proximal colon, whereas CD typically presents discontinuous patchy gut inflammation, which can occur anywhere in the GI tract. Histologically, UC displays superficial inflammation, while CD is characterized by transmural inflammation [8]. In 40% of CD cases the main affected areas are caecum and ileum. The second most common area to be affected is small intestine (30-40% cases). In the small intestine inflammation arises in segments defined as skip lesions, characterized by inflamed areas intermittent with non-inflamed segments. In UC the main affected area is the rectal-sigmoid region. Here inflammation can spread proximally from the rectal sigmoid area to the descending colon (left sided colitis) or reach transverse colon (extensive colitis) [9].

Management of IBD with drug therapy is currently restricted to drugs with significant side effects, including mesalazine, corticosteroids and immunosuppressants (azathioprine (AZA) and anti-tumor necrosis factor (TNF), monoclonal antibodies, JAK/STAT inhibitors) [10]–[14].

Despite all therapeutic advances, loss of therapy response and disease relapses are frequently observed. For this reason, further research is needed to understand the driving mechanisms of IBD, contributing to a deeper comprehension of its pathophysiology and eventually find alternative more efficient therapies.

1.2 Risk factors for IBD

The pathogenesis of IBD remains largely unknown although it is known to be related to genetic heredity, environment interaction, immunity, and gut microbiota [15].

Studies conducted on twins defined a strong correlation between genetic background and IBD [16]–[18]. In CD for example, monozygotic and dizygotic twins are characterized by concordance rates of 20-50% and 10% respectively, while in UC 16% and 4% respectively. Between 2-14% of CD and 8-14% UC patients have family history condition and it is estimated that 5% of the first degree relative of individuals affected by CD will develop the disease, whereas for UC the probability is 1,6% [19].

With the advancement of high throughput technologies, such as genome wide association analysis (GWAS), increasing number of risk genes were identified to be in correlation with this complex disease [20]–[24]. Genetic liability for disease is the main goal of genomic risk profiling studies and it is calculated using polygenic risk scores (PRSs). PRSs provide a summary of all susceptibility loci identified by GWAS, defining a total risk allele dosage by pooling together all the effects of susceptibility single nucleotides polymorphisms (SNPs) [25]. To date, more than 200 susceptibility loci have been identified and replicated through GWAS analysis [22]–[24], [26]. Furthermore, imputation-based association analysis using autosomal genotype level data from GWAS of CD and/or UC found association of risk loci specific CD or UC. Interestingly, although some loci such as Nucleotide-binding oligomerization domain containing protein-2 (NOD2), Nitric oxide synthase 2 (NOS2), Interferon gamma receptor 2 (IFNGR2), Interferon alpha and beta receptor subunit 1 (IFNAR1) and Autophagy related 16 like 1 (ATG16L1) were linked to CD only, others, such as Interleukin 10 (IL-10), Signal transducer and activator of transcription 1 (STAT1), Signal transducer and activator of transcription 4 (STAT4) and Janus kinase 2 (JAK2), were associated with only UC. More than 70% of the identified risk loci overlapped with other immune-mediated disorders such as ankylosing spondylitis and gastric cancer (interleukin-23 receptor (IL-23R)) and GvHD and Leprosy (NOD2). Genetic variants in the human DNA methyltransferase 3A (DNMT3A) and DNA methyltransferase 3B (DNMT3B) loci have also been associated with an increased risk of CD and inflammatory bowel disease, respectively [24], [26], making them novel target of further investigations.

Still, genetic variations fail to fully explain the disease risk, that was estimated to be around 20% [23], [24]. Twins' concordance rates are higher among monozygotic than among dizygotic twin pairs [27] highlighting a genetic influence on occurrence of IBD but failing to fully explain the modality of disease penetrance. This results in missed heritability [28], that includes behavioral features such as smoking and simultaneous exposure to environmental variables. Although genetic factors have been shown to strongly associate with IBD, previous studies concluded that dietary intake, lifestyle and

environmental factors were also to be considered as risk factors for IBD. These impact on IBD, suggesting that the environment might actively shape and contribute to the insurgence and severity of IBD manifestations [29] [30]–[32]. The study of how genetic variants contribute to the outcome of a disease, has surely contributed to further understanding IBD pathophysiology and occurrence, however, a system capable of controlling genetic functions and gene expression, such as how our lifestyle influences genetic-dependent processes, might sound as interesting and informative.

1.3 Inflammatory Bowel Disease and Epigenetics

In the term *epigenetic*, the prefix *epi-* (from the Greek ἐπι- "over, outside of, around") emphasizes features that are *on top of* or *in addition to* the traditional genetic basis for inheritance. *In addition to changes in genetic sequence* implies additional modifications that are extra to the classical study of genetic heritability. Epigenetic involves the regulation of genes as consequence of processes that alter gene activity without changing the DNA nominal sequence: these changes are inheritable, reversible and are maintained in the daughter cells, leading to long term modifications [33] [34].

It was 1942 when the developmental biologist Conrad Waddington published his work [35] elegantly describing how a selected population of cell could inherit specific changes in response to environmental clues. Waddington visualized developmental processes as *decisions*, occurring in response to the environment, as he represented in his developmental landscape diagram *valleys* and *forks* [36], [37]. Waddington introduced the term *epigenetic* to describe the interactions between the environment and the genes, that contributes to the development of a certain phenotype [37]. The emphasis on the importance of adaptability and canalization of phenotypic development underlines the available range for epigenetic action and the importance of environmental feedback in the development of complex traits. Further, Waddington's view emphasized the importance of the multi-directional interchange between the organism, its genome, and various aspects of the environment to the ultimate phenotype. Since epigenetics is a dynamic system, an organism is capable of adaptation to the environment by accommodating its phenotype, for example towards toxin exposure, microbial dysbiosis and nutritional changes [38]. The full set of epigenetic events are referred as *Epigenome*, and it is now at the basis of the molecular principles that shape long-term gene regulation [39].

Because of its potential heritability, epigenetics participates in the development, differentiation, and function of the host, and for this it might be crucial for IBD pathogenesis [40]. The correlation between epigenetics and IBD represents a powerful tool for early diagnosis, disease classification and treatment strategy [34].

1.4 Epigenetic mechanisms

Epigenetic changes include DNA methylation (methylation of CpG dinucleotide sequences), histone modifications [41] (methylation, acetylation, or phosphorylation of DNA packaging proteins) and alternative RNA processing [42] (alternative splicing, micro RNAs, long-noncoding RNAs). All these might as well contribute to the development and progression of IBD [40], [43]. Given its importance, it is of great interest to combine epigenetic changes to genetics so to comprehensively understand the pathogenesis and potentially treat IBD, combining multiple approaches [44].

Each epigenetic mechanism has various regulatory features that modulate gene expression to correctly equilibrate adaptation and host developments in a cell-specific manner [39]. Due to its early discovery and ability to modulate chromatin accessibility for transcription factors, DNA methylation is the best-studied mechanism. Nonetheless, DNA methylation has been described to directly mediate environmental exposures to phenotypic outcome in mammals [45], therefore becoming of pivotal interest in the field of intestinal inflammation research.

1.5 DNA methylation and its role in mammalian development and disease

DNA methylation (DNAm) in the context of CpG dinucleotides is a conserved mechanism able to control gene expression in several eukaryotic organisms [46]. The process resulting in DNAm consists in the addition of a methyl or hydroxymethyl group at cytosine base residues of DNA. The principle of DNA methylation in relation to gene transcriptional activity relies on a (here simplified) observation: high levels of DNAm at promoter sites and low levels of DNAm at gene body translates into gene expression silencing, while hypomethylation at gene promoter region and high methylation at gene body results in activation of transcriptional activity [47]. As an example of DNAm importance, *Saccharomyces cerevisiae* and *Drosophila melanogaster* have a low detectable level of DNAm, and yet perform selective gene expression control [48], supporting the hypothesis of a potent and selective gene expression regulations orchestrated by DNAm, even when present at low levels [49]. Most DNAm patterns are established in embryonic status [50] and DNAm of somatic cell lineages is maintained during embryonic development [51]. A complex process of demethylation and *de novo* methylation establishes novel DNAm patterns [52], which are maintained in successive generations by the interplay of DNA methyltransferases (DNMTs) enzymes [53]. By the blastocyst stage, *de novo* methylation is initiated. During differentiation, each cell type acquires its specific DNAm signature that is subsequently maintained during cell division [54], [55]. Although DNAm patterns are relatively stable, changes in methylation can potentially occur during early development due to environmental influences such as exposure of the mother to smoke or alcohol, which might lead to random epigenetic

mutations in the developing embryo and its germ cells [56]. Methylation profiles can be modified due to interaction with the environment, and alteration (and accumulation) of DNAm can lead to diseases as we age [57]. In fact, numerous studies consistently demonstrated an association of aging in adults with genomic DNA hypomethylation and gene-specific promoter DNA hypermethylation in a tissue-specific manner [58]–[60]. Several mechanisms were proposed for age-associated changes in DNAm during aging [61], such as: the physiological reduction of DNMT1 expression from embryo to adult (leading to DNA hypomethylation [62]), age-dependent increase of homocysteine (which contrasts DNMTs activity [63], [64]) and estrogen replacement therapies (that augment genomic DNAm of peripheral mononuclear cells [65]). Nutritional factors are as well associated with alteration in DNAm in adults, such as: folate depletion [66], [67] and trace elements deficiencies [68]. DNAm changes appear to occur more rapidly in inflamed tissues, where cell turnover is increased [69]. In a pioneer study conducted to elucidate epigenetic mechanisms of IBD, it was shown that the colonic mucosa of individuals affected by UC had significant global DNA hypomethylation compared with healthy control. Furthermore, it was shown that DNA hypomethylation was even more pronounced in patients with active UC, compared to inactive UC patients. In 1996, DNA hypomethylation of rectal mucosa of UC patients was appointed to be a hallmark of long-standing ulcerative colitis [70], and it was demonstrated that tissue specific DNAm modifications were increasing over time. This concept was proven analyzing the methylome of human intestinal-derived organoids longitudinally, supporting the hypothesis of a predetermined developmental post-natal epigenetic maturation and methylation progression after birth [71]. DNAm analysis of immune-process-related target genes, such as Interferon gamma (IFNG) and Interferon regulatory factor 5 (IRF5) suggested an association between dysregulated DNA methylation at IFNG and IRF5 genomic loci and IBD [72], [73]. Genome-wide DNAm profiling of colonic intestinal epithelial cells of children diagnosed with IBD also showed altered DNA methylation signatures [74]. Recent studies involving DNA methylation patterns in intestinal epithelial cells or IBD patients-derived organoids, concluded that demethylation of CEA cell adhesion molecule 6 (CEACAM6) promoter in CD patients correlated with CEACAM6 expression [75] as a result of a methyl-donor containing diet. Other studies based on integration analysis of methylome and transcriptome data identified 126 loci where DNA methylation patterns and RNA transcription were associated with presence of microbiome, therefore demonstrating a strong contribution of external stimuli to IECs activity [76]. Furthermore, Genome-wide DNAm analysis identified regional differences in gut epithelium functions based on DNA methylation patterns [71]. Further investigations on DNA methylation and transcriptome of paediatric IBD patients revealed that IECs from CD patients had altered DNAm and transcription patterns in colonic and ileal epithelium compared to healthy controls [77]. Another study supporting the importance of gene-environment interaction IBD was an

epigenome-wide DNA methylation analysis that revealed 439 differentially methylated positions (DMPs) and 5 differentially methylated regions (DMRs), in 240 newly diagnosed IBD cases and 190 healthy controls. Integration of DNA methylome and transcriptome identified three genetic regions where DNA was inversely correlated with gene expression, wingless-type mouse mammary tumor virus integration site family, member 2B (WNT2B) and two eicosanoid synthesis pathway enzymes (prostacyclin synthase and prostaglandin D2 synthase) respectively PTGDS and PTGIS [78]. These examples define the importance to further investigate the exact functional consequences of DNAm alterations within IBD pathogenesis, to support the development of novel potential therapies.

1.5.1 The DNMTs family

DNA methyltransferases (DNMTs) are the enzymes responsible for the establishment and maintenance of DNA methylation patterns [79]. Five enzymes belong to the family of DNMTs, namely DNMT1, DNMT2, DNMT3A, DNMT3B, DNMT3L. All five DNMTs have a similar catalytic activity consisting of the transfer of a methyl group from the universal methyl donor, S-adenosyl-methionine (SAM), to carbon-5 (C5) of the cytidine ring and it is confined to cytosine nucleotide linked to a guanosine: the so called CpG site [80]–[82]. DNMT1, the largest of the DNMTs enzymes, is responsible for maintaining DNA methylation signature in somatic cells during each cell division. The N-terminus domain of DNMT1 contains four conserved subdomains: DNMT1-associated protein (DMAP), Replication focus targeting sequence (RFTS), CXXC and Bromo adjacent homology domain (BAH) that regulate the maintenance of the DNA methylation profile between generations, acting on hemi-methylated DNA sequences [83] (Figure 1-1).

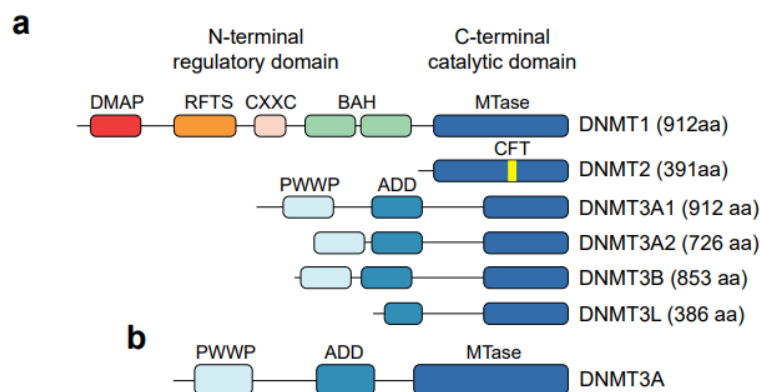


Figure 1-1: Domain architecture of the DNMTs enzyme family.

(a) Domain architecture of DNMT1, DNMT3A1, DNMT3A2, DNMT3B, DNMT3L splice isoforms. Amino acids (aa) are reported as mean of protein length. MT is the catalytic methyltransferase domain. (b) Major DNMT3A splice isoform contains a unique amino terminal domain with DNA-binding capability.

DNMT2 is a tRNA transferase, a small enzyme in charge of adding methyl groups onto cytosine 38 of anticodon loops and solely consists of the CFT motif containing catalytic domain [84]. DNMT3A, DNMT3B and DNMT3L N-terminals consist of two domains: (i) the ATRX-DNMT3-DNMT3L (ADD), mediating the interaction with the unmethylated histone H3 tail at the lysine K4 and regulating DNMT3A activity through an autoinhibitory mechanism and (ii) the Pro-Trp-Trp-Pro (PWWP) domain, present only in DNMT3A and DNMT3B, that mediates their binding to histone H3 trimethylated at lysine 36 [85][86]. DNMT3L shares homology with DNMT3A and DNMT3B, however, it is unable to bind methyl-donor SAM and does not possess any catalytic activity. DNMT3A and DNMT3B are catalytically active *de novo* methyltransferases, that exert their function by establishing new DNA methylation profiles. Finally, DNMT3L is a regulatory protein lacking catalytic activity. DNMT3L has a C-terminal domain that interacts with the catalytic domain of DNMT3A, forming a dimeric structure. This structure undergoes further dimerization through a DNMT3A-DNMT3A interaction, forming a tetrameric complex. Additionally, DNMT3L binds the unmethylated lysine 4 of histone H3 and it recruits the methyltransferases to specific DNA regions [87], [88].

Several studies have suggested a role of DNMT enzymes in transcriptional silencing, mostly through their ability to methylate promoters and change chromatin state [85]. This hypothesis was supported by research conducted using CRISPR-Cas9–DNMT3A fusion protein to induce selective gene silencing in core interactor of the DNA methylation machinery [89]–[93].

1.5.2 DNMT3A in development, disease and intestinal inflammation

DNMT3A, together with DNMT3B, is a *de novo* DNA methyltransferase with molecular weight of 130 kDa and composed of 912aa [94]. It is highly conserved within mammals, where human-murine homologues share 98% of their sequence. Murine *Dnmt3a* RNA has two splice isoforms: *Dnmt3a1* and *Dnmt3a2*. *Dnmt3a1* is expressed in both embryonic and adult tissues, and *Dnmt3a1* and *Dnmt3a2* (collectively *Dnmt3a*) are co-expressed in mouse embryonic stem cells (mESCs) and transcribed from two different promoter regions [95], [96]. *Dnmt3a2*, which is mostly expressed in ESCs, testes, ovaries, spleen and thymus [97], lacks six exons of the amino-terminus domain [98]. DNMT3A has recently emerged as one of the most important tumor suppressors in hematological malignancies [94], suggesting a critical role for DNMT3A in tumorigenic formation. Its exceptional role is rooted in stem cells, where it enables the first steps of hematopoietic differentiation. In fact, *Dnmt3a*^{-/-} hematopoietic stem cells (HSCs) and *Dnmt3a* loss-of-function mutations results in HSCs selective advantage over HSCs normally expressing *Dnmt3a* in bone marrow in both *in vitro* and *in vivo* mouse models [99]. Somatic mutations in *Dnmt3a* have been associated with increased clonal hematopoiesis (CH), hence, affecting stem cell pools over time [100], [101], with the increasing prevalence of clonal

hematopoiesis in older individuals [94], [102], [103]. Also, mutations at DNMT3A locus are associated with HSCs functions. For example, DNMT3A R878H mutation is protective towards hematopoietic stem-progenitor self-renewal capacity as a result of TNF α -induced damage and chronic inflammation [104]. Somatic mutations of DNMT3A are also associated with human acute myeloid leukemia (AML) [105]. Among DNMT3A mutations in AML patients, DNMT3A R882 is the most common and results in higher leukocyturia counts at diagnosis [106]. 22.1% of patients with AML have mutations in DNMT3A, which result in poor prognosis and adverse survival outcomes for patients [104], [107]. Finally, expression of the non-coding RNAs (lncRNAs) *Dnmt3aos* was shown to impact *Dnmt3a* expression leading to aberrant DNA methylation [108], suggesting a role for *Dnmt3a* in the differentiation and polarization of myelomonocytic cells. In turn, deletion of DNMT3A in peritoneal macrophages results in impaired production of Type I interferons, by inducing the expression of the histone deacetylase HDAC9 after PRR recognition and TBK1 activation [109].

DNMT3A loci variants have also been associated with increased risk of IBD insurgence and perpetuation [22], [24], [26]. Our group recently identified a role for DNMT3A within barrier function and colonic epithelium regeneration during homeostasis and inflammation. Specifically, RNA sequencing analysis performed on Caco-2 cells genetically depleted of DNMTA (Δ DNMT3A) and its isoforms DNMT3A1 and DNMT3A2, resulted in an isoform-specific transcriptional dysregulation. DNAm analysis performed using genome-wide based assay revealed a global hypomethylation in Δ DNMT3A cells and exceptional hypermethylated regions. Genetic deletion of *Dnmt3a* in intestinal epithelial cells (*Dnmt3a* ^{Δ IEC}) in mice alters epithelial ultrastructure (shortened apical-junctional complexes), reduced Goblet cell numbers and increased intestinal permeability. On the same line, mice treated with DSS as intestinal inflammatory agent display delayed recovery, increased disease susceptibility, impaired crypt morphology restoration, incomplete barrier function and a defective restoration of homeostasis. Additionally, during chronic inflammatory treatments, expression of genes involved in mucus formation (*Muc2*), crypts proliferation (*Notch1*) and secretory cell precursors (*Atoh1*) is impaired. *Dnmt3a* ^{Δ IEC} mice display downregulation of adherens junctional components such as E-cadherin (*Cdh1*) and *Catenin beta 1* (*Ctnnb1*), and the tight junctional proteins Occludin (*Ocln*) and Zonula occludens-1 (*Zo-1*). Epithelial cells derived from mice lacking *Dnmt3a* in intestinal epithelial cells (*Dnmt3a* ^{Δ IEC}) have defective regenerative capacity upon wounding, increased permeability and present altered architectural features such as shortened apical cell-cell adhesion complexes [110]. Finally, DNMT3A expression is downregulated in intestinal epithelial cells from IBD patients and upon tumor necrosis factor treatment in murine intestinal organoids. These data demonstrate a critical role for DNMT3A in orchestrating intestinal epithelial homeostasis and response to tissue damage and suggest an involvement of impaired epithelial DNMT3A function in the etiology of IBD.

1.5.3 Epithelial and immune crosstalk during IBD

The intestinal barrier is the first mechanical line of defense in the gut that physically separates the intestinal lumen from the underlying tissues. It consists of a single layer of intestinal epithelial cells (IECs), and it prevents water and nutrients loss while limiting the penetration of potentially pathogenic antigens. The intestinal epithelium provides homeostasis maintenance through a finely tuned mechanism of communication with the immune cells in the intestine.

IECs differentiate from a stem cell niche to form a variegated assembly of different cells, comprising enterocytes, enteroendocrine cells, Paneth cells, Goblet cells, M cells and Tuft cells [111]. Defective IECs features such as disturbed regeneration capacity, ER stress, dysregulated interleukin 22 (IL-22) pathway [112]–[114], regulation of cell death via FADD/RIP3/CASPASE-8 [115], Th17-cell-mediated intestinal inflammation [116]–[118], are linked to increased susceptibility for IBD. Little is known, however, about IECs signal transduction events and long-term regulation of differentiation programs, such as DNA methylation, as response to environmental stimuli and in relation to the disease.

Under pathological conditions such as inflammatory bowel diseases (IBD), the intestinal epithelium maintains homeostasis and coordinates the inflammatory response through a finely tuned communication with the infiltrated immune cells. Macrophages situated in the lamina propria, which is located underneath the single cell layer of IECs, are central in regulating its functions during such manifestation.

Given the proximity of the epithelium and the immune system to the environment, it would be interesting to link epigenetic patterns with the intestinal genome signature, the microbiome, and its metabolic potential. An informative investigation of this multifaceted interaction and its functional consequences will shed new light on the hypothesis that epigenetic modifications are in fact the missing link between disease manifestation, genetic predisposition, and environmental influences, contributing to a functional and clinical perspective.

1.6 The origins of macrophages: from bone marrow to the gut

The bone marrow is a semi-solid tissue situated in the spongy fraction of the bones of mammals and represents 5% of the total weight of a healthy human adult [119]. It represents the main source of hematopoietic stem cells (HSCs) niche and hematopoietic precursors that proliferate, differentiate and diverge into the diverse cellular subsets of blood components including platelets, leukocytes, and erythrocytes (Figure 1-2). HSCs give rise to two progenitor cell subtypes: common lymphoid progenitor (CLP), and common myeloid progenitor (CMP) [120]–[122]. Leukocytes are subdivided accordingly depending on progenitor cell type: CLP favours differentiation into lymphoid cells (natural

killer (NK) cells, T lymphocytes (or T cells), B lymphocytes (or B cells)) whereas CMPs favour differentiation into myeloid cells (monocytes, macrophages, and dendritic cells (DC). After differentiation, cells enter the blood stream. Among the peripheral blood mononuclear cells (PBMC) pool, monocytes represent 5-10% of circulating leukocytes and this proportion are well conserved in humans and mice. [123].

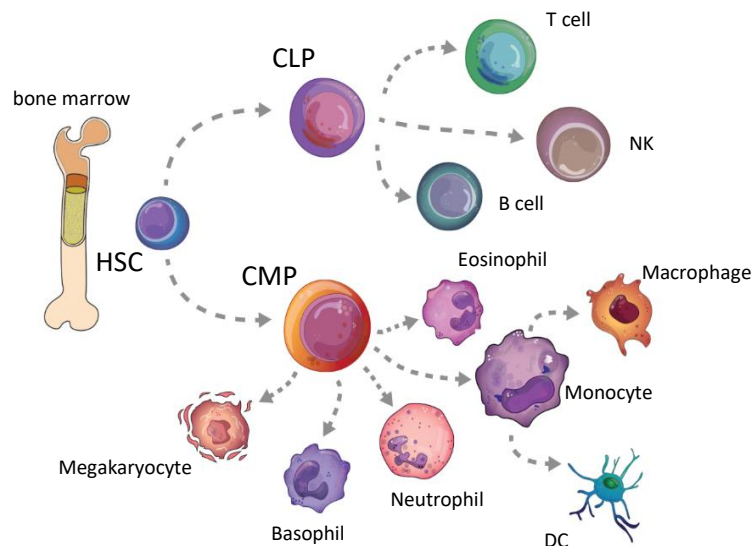


Figure 1-2: Hierarchical organization of hematopoietic stem cells differentiation.

HSCs reside at the top of the hierarchy and possess the ability of both multi-potency and self-renewal. Differentiation of HSC is possible upon loss of self-renewal capacity. From the bone marrow, HSCs can differentiate in either common lymphoid progenitor (CLP) or common myeloid progenitor (CMP), which in turn give rise to different leukocytes.

In addition, each tissue contains a proportion of professional antigen presenting cells (APCs), comprised by tissue resident macrophages and DCs, that continuously survey the tissue for pathogens and noxious insults to trigger an inflammatory response that recruits additional immune cells, or promote regulatory signals that restore tissue homeostasis. Upon tissue inflammation, circulating monocytes are recruited into designated tissues by expression of tissue-specific adhesion molecules or “homing markers” (e.g., CCR9 and integrin b7).

Previous research has tried to precisely characterize the molecular mechanisms orchestrating monocytic recruitment upon inflammation and during homeostasis, as well as monocytes trafficking and finally accommodation and differentiation within specific tissues [123]–[125]. A well accepted model proposes monocytes final differentiation as macrophages or dendritic cells. Tissue resident macrophages, compared to dendritic cells, have higher proteolytic capability, and release high numbers of cytokines which are essential for the clearance of pathogens and apoptotic cells [122],

[123]. Macrophages express a series of surface markers such as CD11b, CD14, CD68 and CCR5, along with F4/80 specifically in mouse. According to their activation status, macrophages can express surface markers that fuel inflammation or promote homeostasis restoration.

1.6.1 Macrophages effector functions and subtypes

Macrophages, from Greek μακρός/makrós (large) and φαγεῖν/phagein (to eat), are a versatile group of immune cells involved in a high number of biological processes, ranging from adaptive immunity to muscle regeneration, from iron homeostasis to wound healing.

As key actors of the innate immune response, macrophages were firstly identified as mere phagocytes, as result of the observation of their ability to engulf foreign particles [126], [127]. Macrophages contribute to tissue homeostasis and restoration of physiological conditions following inflammation derived injuries or pathogenic insult [128]. They reside in every organ and are classified accordingly to their allocation and surface markers expression. Macrophages residing in the lamina propria (LP), for example, express CD11b, CD68, F4/80 and MHC class II. This subset of macrophages are central sentinels of the immune system [129], [130]. Genetic and environmental predisposition can lead to an enhanced antimicrobial responsiveness of macrophages [131]–[133], resulting in uncontrolled activation and chronic inflammation [134]. Beside their pivotal role within the immune response, macrophages are vital within the processes of their key function: uptake and neutralization through phagocytosis, a fundamental strategy aimed to remove dying or dead cells and cellular debris [135]. Depending on their activation status, these versatile cells are categorized into two main biologically distinguishable subsets: M1 (classical activation) and M2 (alternative activation). Based on the types of factors produced, they act in a dichotomous fashion, “*fight it*” (nitric oxide production) or M1 polarization status, and “*fix it*” (ornithine production) or M2, homeostatic polarization status. Both nitric oxide and ornithine are derivative of arginine, depending on the prevalence of one of the two enzymatic pathways of Arginase or Nitric oxide synthase, which inhibit each other [136][137]. At the base of this distinction resides the different biological signature of processes in which macrophages are involved. Respectively, M1 macrophages participate in pathogen killing and inflammation, produce proinflammatory cytokines and chemokines and exacerbate inflammatory reactions and tissue damage. M2 macrophages often tolerate pathogens and promote resolution of inflammation [138], release anti-inflammatory cytokines, participate in tissue remodeling/repair after injury, remove debris and promote angiogenesis [139], [140].

1.6.2 Classical activation: M1 macrophages

It was 1876 when Karl Wilhelm von Kupffer described “reticuloendothelial cells” as phagocytosing cells of the mammalian liver [141] and 1898 when Tadeusz Browicz categorized them as tissue resident macrophages. Earlier documentation dated between the end of the 19th century and the beginning of the 20th century, testifies the effort of Ilya Metchnikoff in the study of cells able to phagocytose and killing pathogens and the impact of phagocytosis on immunity [142]–[144]. The first investigations on macrophagic phagocytosis revealed the localization (and accumulation) of this peculiar immune cell subset in inflamed tissues. Because of their plasticity and their chemotactic ability, macrophages are recruited to the site of inflammation, and because of their phagocytic (and pathogen killing ability) they were initially considered “activated” macrophages [145]. Morphologically, M1 activated macrophages display membrane protrusions that allow cellular motility and migration, and phagosome/lysosomes for the engulfment and destruction of pathogenic microorganisms. Phagocytosis is up-regulated in M1 macrophages, and it is orchestrated by intercellular adhesion molecule –1 (ICAM-1), which contributes to endocytosis, which is critical for solving inflammation and promoting wound healing [146]. Classically activated macrophages are polarized by lipopolysaccharide (LPS) either alone or in association with Th1-associated cytokines such as IFN- γ , Granulocyte-macrophage colony-stimulating factor (GM-CSF), and produce pro-inflammatory cytokines such as interleukin-1 β (IL-1 β), interleukin 6 (IL-6), interleukin 12 (IL-12), interleukin 23 (IL-23), and tumor necrosis factor alpha (TNF- α) [147], resulting in a highly phagocytic and pro-inflammatory cell population.

1.6.3 Alternative activation: M2 macrophages

Macrophages were identified as well in homeostatic tissues and outside site of inflammation. These so-called *tissue resident macrophages* seemingly appeared to be non-activated and performing a *safe disposal of waste material* [148]. With the progression of research, tissue resident macrophages become more and more attributable as sentinel cells that in homeostatic conditions perform antigen presentation to the cells of the adaptive immune system. Firstly described by Ilya Metchnikoff, this class of macrophages allowed pathogen survival in higher rates upon phagocytosis compared to when sitting extracellularly [149]. Metchnikoff’s observation led to the conclusion that some pathogens (for example *Mycobacterium tuberculosis*, *Toxoplasma gondii*, *Listeria monocytogenes*) survive longer inside the macrophages than outside of them, and that macrophages could favour certain infections by hosting pathogens, that unnoticed from the macrophages reproduce using metabolites provided by macrophages catabolism [148], [150].

In the same way, certain type of tumours can evade surveillance by macrophages, where a notable M2 signature impede the recognition and elimination of tumour cells. Here, tumour associated macrophages (TAM) promote tumour cell development, immunosuppression, and immune evasion [151]. M2 macrophages are anti-inflammatory and immunoregulatory [152]. They are polarized by Th2-associated cytokines such as interleukin 4 (IL-4) and interleukin 13 (IL-13) and produce anti-inflammatory cytokines such as interleukin 10 (IL-10) and Transforming growth factor beta (TGF- β) [147].

1.6.4 Macrophage polarization in homeostasis and inflammatory bowel disease

Gut-resident macrophages are the most abundant mononuclear phagocyte population able to recognize foreign antigens and engulf microorganisms in the intestine [153] [154]. They are located in the lamina propria which is subjacent to IECs and functionally differs from small intestine, the proximal colon and the distal colon. Macrophages composition and functions also vary between small and large intestine (given the different architecture of the tissue, different exerted functions, and different harbored microbiota) and between CD and UC [155], [156] (Figure 1-3).

As in any other tissue (in homeostatic conditions) gut-resident macrophages integrate signals from the microenvironment and adapt their phenotype and functions without necessarily inducing lymphocyte proinflammatory response [147], [157].

To do this, macrophages sample luminal content through dendritic extrusions extended between IECs and reaching into the gut lumen [158], [159] and maintain homeostasis through their tolerogenic program required for tissue homeostasis [160], [161]. Intestinal macrophages are tolerant towards luminal antigens or commensal microbiota in absence of co-stimulatory signals, due to the downregulation of recognition receptors [180], [181]. To maintain these tolerogenic properties, the expression of pattern recognition receptors (PRRs) on resident macrophages is downregulated, hence, cytokines production remains limited.

Macrophage polarization is a complex and tightly regulated biological manifestation [162], which depends on intrinsic, extrinsic, and environment stimuli including cytokines, growth factors, fatty acids, prostaglandins, and pathogen-derived molecules. A balance of M1-M2 macrophage governs the resolution of inflammation or injury [163] and evidence suggests M1-M2 balance to be responsible for intestinal homeostasis, whereas disequilibrium is involved in chronic inflammation and disease progression [164][165]. This is because M1 and M2 macrophages have different transcriptional profiles [166]–[168] and unique abilities such as destroying pathogens or repairing the inflammation-associated injury *i.e* M1 macrophages are more efficient in destroying pathogens and M2

macrophages are prone to repairing infections and inflammation-associated injuries attempting to retain homeostasis, through the secretion of IL-10 and TGF- β .

Following inflammation or mechanical insults, macrophages first exhibit the M1 phenotype and produce TNF α , IL-1 β , IL-12, and IL-23 against the stimulus. When bacteria overgrow, beneficial bactericidal activity takes place. Metallothionein is overproduced and in turn detected by nuclear factor kappa-light-chain enhancer of activated B cells (NF- κ B) and Caspase-1 (CASP1), the precursor and trigger of IL-1 β and IL-18 pro inflammatory signaling pathways [182], [183]. Furthermore, TGF β and IL-10 down-regulate triggering receptor expressed on myeloid cells-1 (TREM-1), which is in charge of amplifying immune reactions [184].

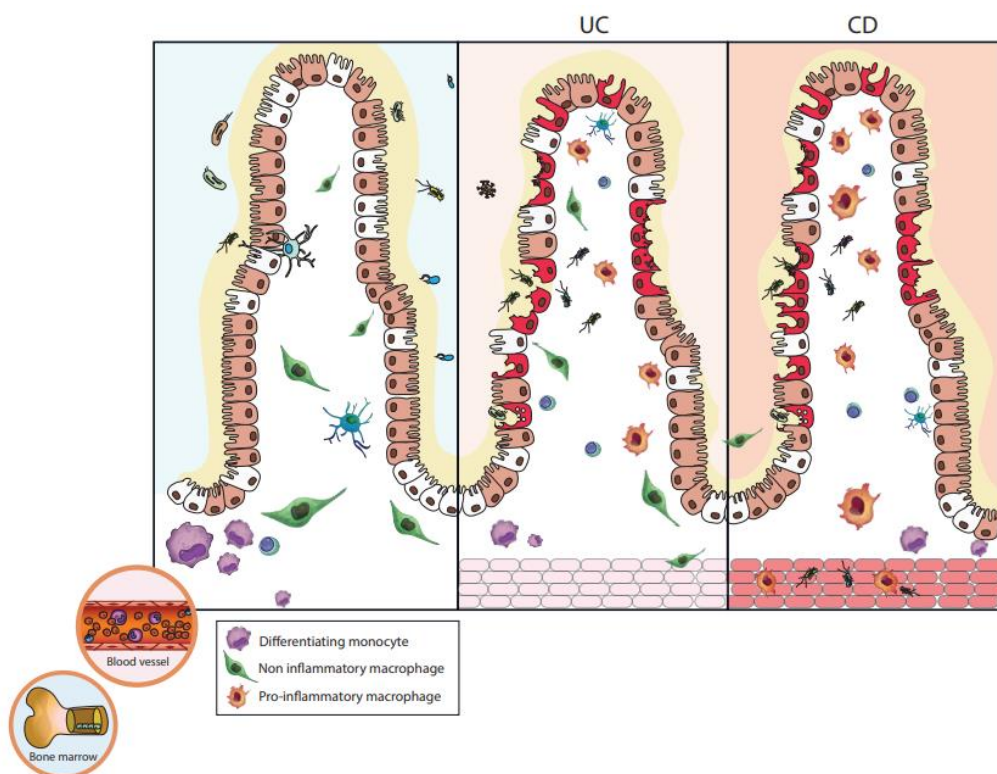


Figure 1-3: Schematic representation of intestinal macrophages distribution during IBD manifestations.

Gut-resident macrophages are responsible for apoptotic and senescent epithelial cell debris clearance. Here, they stimulate epithelial cell renewal through prostaglandin E2 (PGE2), hepatocyte growth factor (HGF) signaling. They promote epithelial integrity and homeostasis by projecting outside the intestinal epithelium and sampling luminal content. Upon pathogen infiltration, they can neutralize engulfed potential pathogens, or transfer the acquired antigens for presentation to dendritic cells for presentation to T cells in mesenteric lymph nodes. Macrophages fuel and maintain regulatory T cell expansion by producing immunoregulatory cytokines such as IL-10 or TGF β .

The original polarization can be reversible upon environmental changes [169], [170], however, when M1 phase persists, it can cause tissue damage and chronic inflammation [163]. During chronic inflammation -as the one maintained in IBD-, macrophages display distinct phenotypes and

distribution compared to tissue-resident macrophages in homeostasis as they massively infiltrate the intestinal mucosa [157]. Newly recruited macrophages from circulation derive from the bone marrow via IL-8 and TGF β [171]. Once in the gut, these transform into anergic inflammatory macrophages by TGF β induced inhibition of NF- κ B [172].

Since during IBD manifestations the intestinal barrier function is altered, local inflammation is exacerbated by invasion of microbiota. Here, macrophages upregulate PRRs, including Toll like receptors such as TLR2, TLR4, TLR5 (as a response to bacterial-derived peptidoglycans [173]), C-type-lectin receptors (CLRs) cytoplasmic nucleotide-binding oligomerization domain-containing protein (NOD)-like receptors (NLRs) and retinoic acid-inducible gene-I-like (RLRs). Equipped with this pro-inflammatory phenotype, macrophages capture, process, and present antigens to T cells, activating them to differentiate towards Th1/Th17 phenotypes and release TNF family ligand BAFF and subsequently induce B cell proliferation [174]. Furthermore, mesenchymal stem cells and T cells secrete IFN- γ , contributing to the progression of intestinal inflammation by promoting macrophages to maintain the M1 activation status [175]. Macrophages can eventually promote intestinal mucosal barrier healing and coordinate the development of immune response [176], [177], becoming attractive targets for IBD immune-mediated therapy.

Because of their central role within chronic inflammation during IBD and homeostasis restoration, studying how macrophages adapt to the microenvironment and translate into unbalanced host response might hold great promise for the treatment of IBD. [178].

1.7 Arginine metabolism: arginase and nitric oxide synthase balance within macrophages polarization

Macrophage polarization is highly dependent on the metabolism of the small, non-essential amino acid arginine. Although at the whole organism level arginine is a non-essential amino acid in healthy humans, arginine levels imbalance can result in damaging outcomes, and supplementation is usually employed during active disease flares [179], [180]. Arginine biosynthesis is complex and exclusive as it requires glutamine, ornithine, citrulline and many enzymes that are restricted to very specific cell subtypes in determined anatomic areas, such as in intestinal macrophages, where arginine is heavily involved in their polarization process. [179], [180]. Isolated in 1886, arginine was found to be part of the urea cycle and it was demonstrated to be the major precursor of citrulline and nitrite synthesis in macrophages [181]. This amino acid be catabolized by four enzymatic classes: nitric oxide synthase (NOS), arginase (ARG), arginine decarboxylase (ADC) and arginine:glycine aminotransferase (AGAT). These four groups of enzymes are localized in a cell specific fashion. The metabolites resulting from

the downstream activity of such pathways (nitric oxide (NO), urea, ornithine creatine, agmatine, glutamate, proline, polyamines) are involved in a plethora of cell regulatory pathways [182].

An interesting dichotomy relatively to arginine utilization in macrophages implicates not only different outcomes at the level of cellular metabolism, but at a higher level influence the outcome of immune responses involving macrophages participation to innate immunity [183]. Specifically, arginine processing is directed towards two possible pathways: (i) arginine is processed by inducible nitric oxide synthase (iNOS) or (ii) it is hydrolyzed by arginase (Arg). In the first case, arginine is metabolized by iNOS, resulting in NO and citrulline: alternatively, Arg hydrolyzes arginine to produce ornithine and urea.

1.7.1 The nitric oxide synthase road: arginine-nitric oxide (NO) axis

Nitric oxide (NO) synthesis is the product of iNOS activity on arginine, and it is required in macrophages for activation of cytotoxic activity and infection control. iNOS is large homodimer with two functional domains: an N-terminal oxygenase and catalytic domains and a C-terminal reductase domain with binding sites for flavin mononucleotide (FMN) and flavin-adenine nucleotide (FAD). The production of NO takes place by incorporating oxygen to the terminal guanidino nitrogen group of arginine, releasing NO and leaving citrulline as byproduct.

iNOS transcription can be triggered by a variety of pro-inflammatory cytokines *i.e* IL-1 β , IFN γ , TNF α as a result of microbial products recognition (such as LPS) and hypoxic conditions. On the other side, iNOS gene transcription downregulation (and subsequent activation of arginase transcription) can be triggered by Th2 anti-inflammatory cytokines such as IL-4, IL13, IL-10 and TGF- β (58).

Contrarily to eNOS and nNOS (the endothelial and neuronal isozymes of NOS family), iNOS expression is regulated by inducible transcription, and notably, it is the most prominent microbicidal and inflammatory pathway in macrophages.

1.7.2 The healing mode of arginase alternative pathway: the arginine-ornithine axis

Arginase controls the second possible pathway for arginine metabolism catalyzing the hydrolysis of arginine to ornithine and urea. Arginase I (ARG-1) and Arginase II (ARG 2) are the isozymes catalyzing the same reaction but differ in (sub-)cellular localization and expression [184], [185]. The mechanism of arginine transcription is tightly regulated, and its mechanism was gradually elucidated in several studies [186]–[188]. Generally, Th2 cytokines control ARG-1 mRNA induction and it is regulated by STAT6 and CEBP/ β assembly, that takes place 3kb upstream from the basal promotor of arginase. More and more levels of complexity come into place recently, demonstrating the induction of arginase I by pathogen-induced toll-like receptor (TLR) in murine macrophages [189], [190]. Macrophages

expressing arginase have been described as key players within a multitude of pathophysiological scenarios [185], from wound healing [191], [192], to tumor growth [193].

These dramatic functional and phenotypical differences observable in macrophages, together with their “argenomic” signature, resulted in the categorization of macrophages into the above mentioned M1-M2 classes [136].

Given (i) the central role of DNMT3A in immune cells-related disorders and malignancies [107], [194], (ii) its involvement in processes such as T cells differentiation and polarization [195] and (iii) its association with IBD, and finally (iv) given the key involvement of macrophages in the insurgence and perpetuation of IBD, investigating how DNMT3A in the myelomonocytic lineage impacts on the pathophysiology of IBD, would represent a powerful tool to contribute to further understanding of this complex disease and support the identification of novel, effective therapeutical solutions.

1.8 Aims of the study

Epigenetic changes such as DNA methylation, have been associated with IBD pathophysiology because of its role in regulation of gene expression. DNMT3A, one of the *de novo* methyltransferase enzymes, has been associated with IBD through genome-wide association studies. During IBD, both epithelial cells and immune cells such as macrophages have an essential role in coping with inflammation and eventually, restore homeostasis.

The first aim of this thesis is to further elucidate the role of *Dnmt3a* in the intestinal epithelium by answering the following questions:

What is the impact of the lack of Dnmt3a in IECs in vivo at steady state and how is Dnmt3a expression regulated during inflammation?

To this end, we employ murine models lacking *Dnmt3a* in IECs and analyze features such as colonic epithelium distance to luminal microbiota, bacterial translocation to mesenteric lymph nodes, Goblet cells abundance and lamina propria immune cell composition. Secondly, using human and murine IECs-derived organoids, we explore the transcriptional changes of *Dnmt3a* after pro-inflammatory stimulation.

The second aim is to perform a comprehensive investigation of the role of *Dnmt3a* in the myelomonocytic lineage during homeostasis and inflammation, by answering the following questions:

(1) What is the functional consequence of Dnmt3a deletion on gene expression regulation in macrophages?

To define the impact of *Dnmt3a* on regulation of target gene expression, we focus on the transcriptional regulation of *Dnmt3a* in resting and polarized macrophages. We employ bulk RNA sequencing and GO enrichment analysis to obtain an overview of the most affected biological processes upon deletion of *Dnmt3a*. From this, the selected polarization markers genes and dysregulated mechanisms will be targeted for more detailed analysis exploring effector macrophagic functions *in vitro*.

(2) What is the role of Dnmt3a in macrophages effector functions?

To elucidate the impact of the lack of *Dnmt3a* in macrophages on effector functions, by performing systematic *in vitro* experiments using bone marrow derived macrophages polarized *in vitro*, we attempt to elucidate the role of *Dnmt3a* in the mechanisms of polarization, phagocytosis, wound

healing response and tumor development. Following the *in vitro* work, this project continues with a comparative *in vivo* characterization of mice lacking *Dnmt3a*, aimed to elucidate the following:

(3) *What is the functional consequence of Dnmt3a deletion in myeloid cells during baseline conditions and in inflammatory responses in vivo?*

For this, we utilize a mouse model lacking *Dnmt3a* in myeloid cells (*Dnmt3a*^{LysM}) to investigate the role of *Dnmt3a* upon deletion in myelomonocytic lineage within the context of inflammation and at steady state, with particular focus on an age-dependent spontaneous phenotype. *Dnmt3a*^{LysM} mice and wild type littermates will be challenged with chemically induced inflammation to mimic both acute and chronic inflammatory episodes in the intestinal tract.

2. Materials and methods

2.1 Molecular biology methods

2.1.1 Total RNA isolation

Total RNA was isolated from cell or tissue lysates using RNeasy Mini Kit (Qiagen, Hilden, Germany) following manufacturer's instruction. Murine tissue was disrupted and homogenized using TissueLyser II (Qiagen, Hilden, Germany) in 350µl-700 µl RLT buffer (1:1 v/v) implemented with 1% β-mercaptoethanol (v/v). A minimum of 300,000 cells/well were harvested using 350µl RLT buffer and lysed on cell culture plates. The material was then transferred to QIAshredder spin columns and centrifuged for 30s at 10,000 RPM. DNase digestion was performed for 30min at room temperature using RNase-free DNase Set (Qiagen, Hilden, Germany). Following two washing steps in 500µl RPE buffer, the samples were eluted for 5min at room temperature in ultrapure 30/50µl RNase-free water. RNA concentration was determined using NanoDrop (ND-1000) spectrophotometer (PeqLab Biotechnologie GmbH, Erlangen, Germany) using 1,5µl input.

2.1.2 cDNA synthesis

Complementary DNA (cDNA) was synthesized using 1000ng total RNA and the reverse transcriptase kit Maxima H minus First Strand cDNA Synthesis (Thermo Scientific, Bremen, Germany). Reverse transcription was performed following the manufacturer's instructions (see Table 1 and Table 2 for further details). The obtained cDNA was diluted to a final concentration of 10ng/µl in ultrapure nuclease-free water for subsequent analyses and conserved at -20°C.

Table 1: Reagents and volumes used for cDNA synthesis

step	component	amount
1	RNA	100-1000ng
	Oligo (dt)18 oligonucleotide (per sample)	0.125 µl
	dNTP mix (per sample)	0.5 µl
	nuclease-free water	to 7.5 (Total) µl
2	5x RT buffer	2 µl
	Maxima H Minus RT	0.5 µl

Table 2: cDNA synthesis program

temperature	time
25°C	10 min
50°C	15 min
85°C	5 min
4°C	∞

2.1.3 Real time quantitative polymerase chain reaction (RT-qPCR)

The mRNA expression levels were quantified via quantitative real time polymerase chain reaction (RT-qPCR) after amplification of specific transcripts of interest. To target specific transcripts, exon-exon spanning primers were designed using transcript reference of the NCBI database and primer BLAST online tool (<http://www.ncbi.nlm.nih.gov/nucore/>, July 2014). Primers were synthesized by Microsynth (Lindau, Germany) and their length varied between 20-25 bases. Optimal annealing temperature was 60 °C and an amplicon size of 200-400 bp. 5ng cDNA and 0.5µL of specific primer pairs (5 µM each for Syber green) or 0.5µL of the specific TaqMan® gene expression assay was used for each reaction performed in 384-wells plates in a 7900HT Fast Real Time PCR System (Applied Biosystems, Darmstadt, Germany). Each experiment was designed with at least three biological replicates and each measurement was performed using two technical replicates. The amplification protocol was performed in duplicate on VIIA 7 PCR system (ThermoFisher, Waltham, MA). Accordingly, to the target gene, PCR program was performed following either SYBR® Select Master Mix protocol (Applied Biosystems, Darmstadt, Germany) or TaqMan Gene Expression Master Mix protocol (Applied Biosystems, Darmstadt, Germany). Cycle threshold (Ct) values of the target genes were normalized to the respective transcript expression of housekeeper genes such as β -Actin or Gadph.

2.1.4 DNA isolation

Extraction of DNA from cultured cells was performed using the DNeasy Blood and Tissue kit (Qiagen, Hilden, Germany) following the instructions provided by the manufacturer. Briefly, cultured cells were harvested delicately using a cell scraper and centrifuged at 300g for 5min. Cell pellets were resuspended in 200µl PBS equilibrated at room temperature and supplemented with 20µl proteinase K to digest proteins. 200µl AL buffer without added ethanol were added to the sample tubes and the solution was mixed vigorously using vortex at maximum intensity for 10 sec. Following 10min incubation at a 56°C, ethanol (200µl) was added and thoroughly homogenized. The mixture was transferred to DNeasy Mini Spin Columns provided in the kit, centrifuged at 6,000g and washed twice with 500µl AW1 buffer. AE buffer 50-100µl (10Mm Tris, 0.5mM EDTA, pH 9.0) was used to elute the nucleic acid after 1min incubation directly on the membrane. The eluted DNA was recovered by incubating the membranes for 5min in ultrapure nuclease-free water followed by centrifugation at 6,000g for 1min. DNA concentration was measured using NanoDrop (ND-1000) spectrophotometer (PeqLab Biotechnologie GmbH, Erlangen, Germany).

2.1.5 DNA isolation for total bacteria quantification

DNA was extracted from mesenteric lymph nodes (MLN) using Dneasy Power Soil Pro (Qiagen) following the indications of the supplier. Amplification of 16s rDNA was performed using 16S universal primers (F: ACT CCT ACG GGA GGC AG, R: GAC TAC CAG GGT ATC TAA TCC) and probe (CAG CAG CCG CGG TA) that target the V3–V4 region of the bacterial 16S ribosomal gene. Rt-qPCR was performed as previously described. A standard curve generated using serial dilution of known *E.coli* 16s rDNA was used to assess the absolute number of 16S copies in each sample. The total 16S rDNA copies were normalized to the initial weight of MLN (mg).

2.2 Biochemical methods

2.2.1 Protein lysate preparation

Cells cultivated at a minimum density of 500,000/well in 6 wells culture plates were washed with PBS after cell culture medium removal. The cells were harvested in 50/100µl RIPA buffer (Thermo Scientific, Bremen, Germany) implemented with 1% protease inhibitor cocktail Halt Protease and Phosphatase Inhibitor Cocktail (Thermo Scientific, Bremen, Germany) to avoid protein degradation. Cells were left 30min in ice cold buffer and afterwards sonicated to ensure proper cell lysis. The samples were then centrifuged for 15min at 16,000g to remove insoluble particles such as cell debris and genomic DNA. The supernatant was then transferred to clean 1.5ml reaction tubes and stored at -80°C.

2.2.2 Protein quantification

To determine the amount of total protein, 5µl of total cell lysate previously thawed on ice was diluted in 5 µl ultrapure distilled water and protein content was determined using BIO-RAD DC protein assay (BIO-RAD, Munich, Germany). This assay relies on copper ions reaction with peptides bond in alkaline conditions, providing a colorimetric determination of protein content. The 1:2 diluted protein extracts were mixed with the reagents according to the manufacturer's instructions (more details in table 3). Samples absorbance was measured after 15min reaction protected from light. Protein amount was measured normalizing the measurements with bovine serum albumin (BSA) standard curve.

Table 3: Reagents and amount used for protein quantification reaction

step	component	amount
1	Reagent A	24,5 µl
	Reagent S	0.5 µl
2	Reagent B	25 µl

2.2.3 SDS-PAGE and Western blot

Protein extracts were diluted in NuPAGE LDS Sample Buffer in a concentration 1:5 (SB:protein lysate) (Thermo Scientific, Bremen, Germany) and heated at 90°C for 5 minutes. The obtained dilution was then loaded under denaturing conditions in a concentration of 1µg/µl for a total of 15µl/well onto 15 wells gels. Total protein extracts were separated accordingly to their molecular weight using agarose gel electrophoresis in presence of adapted concentration of acrylamide depending on the size of the protein of interest (Table 4). Sodium dodecyl sulfate polyacrylamide gel electrophoresis (SDS-PAGE) was performed for 30min at 80V followed by 90min at 130V at room temperature with immersion in neutral pH buffer to minimize protein modifications.

Table 4: List of reagents used for SDS-Polyacrylamide Gel Electrophoresis

	Protein size (kDa)	50-200	30-120	20-100
Separation gel	% Acrylamide	7.5%	10%	12%
	Distilled water (ml)	5	4.15	3.5
	4x Separation Buffer (ml)	2.5	2.5	2.5
	(Bis) Acrylamide (ml)	2.5	3.35	4
	TEMED (µl)	10	10	10
	10% APS (µl)	100	100	100
Stacking gel	% Acrylamide	3%		
	Distilled water (ml)	1.95		
	4xStacking Buffer (ml)	0.75		
	(Bis)Acrylamide (ml)	0.3		
	TEMED (µl)	3		
	10% APS (µl)	30		

2.2.4 Protein transfer and immobilization

After SDS-PAGE, the separated proteins were transferred to polyvinylidene difluoride (PVDF) membrane (Bio-Rad, Munich, Germany) pre activated for 10sec in methanol with mild agitation, and rinsed 5min in distilled water twice before usage.

Protein transfer was performed using semi-dry system Trans-Blot Turbo TM Transfer System (Bio-Rad, Munich, Germany) using discontinuous gradient buffers (anode buffer I, anode buffer II and cathode buffer). Further details for buffers preparation can be found in table 5.

The activated membrane was put onto blot paper (Bio-Methods 32 Rad, Munich, Germany) matching its dimension and pre equilibrated in anode buffer 1 for 5min. On top of this, a thick transfer blot paper pre equilibrated in anode buffer II was reclined followed by another blot paper soaked in cathode buffer. The “sandwich” was then inserted in the Trans-Blot Turbo TM Transfer System cassette and exposed to continuous current of 0.1A and 25V for 60min.

Table 5: Composition of buffer used for protein transfer

	Reagent	Amount for 1000ml
Cathode buffer	Tris 25mM	25ml (from 1M stock)
	6-aminocaproic acid 40mM	4ml
	Methanol	200ml
	Distilled water	771ml
Anode buffer I	Tris 30mM	30ml (from 1M stock)
	Methanol	200ml
	Distilled water	770ml
Anode buffer II	Tris 300mM	300ml (from 1M stock)
	Methanol	200ml
	Distilled water	500ml

2.2.5 Immunoblotting and signal visualization

After transfer, membranes were rinsed in Tris-buffered saline with 0.1% Tween (TBS-T) twice to remove gel debris/methanol contamination. To avoid unspecific antibody binding, the membranes were then blocked in 5% bovine serum albumin (BSA) in tris buffered saline supplemented with 0.1% TBS-T (w/v) or 5% non-fat dry milk (w/v) in TBS-T for 1h at room temperature with constant agitation. The membranes supporting the transferred proteins were probed with suitable primary antibodies targeting the protein of interest (see table 6 for antibodies specifications) diluted in blocking solution for 1h at room temperature or overnight at 4°C in constant mild shaking, according to provider recommendations. After primary antibody incubation, the membranes were rinsed three times in 5ml TBS-T for 15 min at room temperature to remove excess antibody. Horseradish peroxidase (HRP)-labelled secondary antibody were diluted in blocking solution and incubation was performed for 1h at room temperature with constant agitation. The secondary antibody (conjugated with horseradish peroxidase (HRP)) recognizes Fc region of the primary antibody and allows the visualization of the detected antibody binding its target through chemiluminescence.

Table 6: List of primary antibodies used for immunoblotting

Antibody	Manufacturer	Reactivity	Source	Dilution
α-Dnmt3a	R & D	Hs, ms	Monoclonal, mouse IgG _{2B}	1:1000 in 5% non-fat dry milk*
α-Arg 1	Invitrogen	Hs, ms	Polyclonal, rabbit IgG	1:2000 in 5% BSA*
α-iNos	Abcam	Hs, ms	Polyclonal, rabbit IgG	1:1000 in 5% BSA**
α-Gapdh	Abcam	Hs, ms	Monoclonal, mouse	1:800 in 5% non-fat dry milk***

*Incubation: overnight at 4°C

**Incubation: 1h at room temperature

***Incubation: 45min at room temperature

2.2.6 Signal acquisition

Chemiluminescent reaction with HRP-conjugated secondary antibodies was achieved incubating the membranes for 5 min with chemiluminescent (ECL) substrate (GE Healthcare, Freiburg, Germany) following the manufacturer's instructions. For primary antibodies HRP-conjugated, the incubation with ECL was performed after primary antibody incubation. Chemiluminescent images acquisition was performed using ChemiDoc MP Imaging System (Bio Rad, Germany) and signal intensity was quantified using Image Lab software version 6.1.0 build 7 Standard edition (Bio Rad, Germany).

2.3 Isolation and cultivation of cells

2.3.1 Maintenance of human organoids

Human organoids were generated from colonic biopsies obtained from patients during endoscopic examination. Biopsies were incubated in 2.5mM EDTA and crypts were collected and embedded in matrigel in 24 wells culture plates. Crypts were maintained in IntestiCult™ Organoid Growth Medium (Stemcell) implemented with Y-27632 (10μM, Sigma-Aldrich).

Ethical approval was obtained from the Ethics Committee of the Medical Faculty, University Kiel (vote B231/98/13), the procedure was authorized by written informed consent from each patient. Current data protection policies were followed.

2.3.2 Generation and maintenance of murine colonic organoids

Murine colon was harvested and cut open longitudinally immediately after animals were sacrificed by cervical dislocation. The tissue was washed in ice cold PBS and reduced to pieces of 5mm through transversal cuts and maintained in ice cold PBS until further processing. The obtained sections were washed twice in ice cold PBS to remove mucus and luminal residues. Next, the tissue was incubated in cold PBS supplemented with 2.5mM EDTA for 40 min at 4°C to allow crypts dissociation. Crypt dissociation was mechanically favored by vigorously pipetting with 10ml serological pipettes for 10-15 times. The supernatant containing crypts was collected in separate clean tubes and the procedure was repeated three times. After centrifugation (1,200rpm, 4 °C, 10 min) the supernatants were collected and strained through a 100μm strainer and centrifuged again. After removing the supernatant, crypts were resuspended in Matrigel® (BD Bioscience/Heidelberg, Germany) with a concentration of 10 crypts/1μl Matrigel®). Matrigel® domes were left to polymerize in cell incubators at 37°C, 5%CO₂ for 15-20 min. After complete solidification, 500μl of pre-warmed organoid medium were added (50% L-WNR conditioned medium, 50% 2x basal medium supplemented with 30% FCS) were added. Medium was changed twice per week and organoids were split once fully grown.

Organoids were used at early passage and stimulations were always performed 24h after the latest passage.

2.3.3 Bone marrow harvesting and macrophages differentiation

Bone marrow derived macrophages (BMDMs) were generated *ex vivo* from mice ranging from 8-to-40 weeks old animals. After sacrifice by cervical dislocation, femurs and tibias of rear legs were removed and cleaned from muscular and tendinous tissues. The obtained bones were stored promptly into ice cold RPMI 1640 medium and promptly maintained on ice. The procedure continued in sterile conditions in a laminar flow hood, where the bones were cut at both extremities and the bone marrow was flushed with a syringe mounting a 26G needle inflated with macrophages culture medium implemented with antibiotic/antifungal mix (DMEM and Macrophage SFM medium (1:1) supplemented with 10 % (v/v) FCS, 5 % (v/v) Penicillin/Streptomycin, 5 % (v/v) Amphotericin). The bone marrow was gently resuspended using a serological 10ml pipette tip to obtain a single cell suspension. The obtained suspension was strained using a 70µm cell strainer to exclude residual debris and bone/muscle tissue contaminations. Bone marrow cells were finally poured in 15 cm petri dishes in presence of 30mL BMDM medium supplemented with 20 ng/mL macrophage colony-stimulating factor (m-CSF) and incubated at 37 °C with 5 % (w/v) CO₂ and 100 % (w/v) humidity for five days to allow monocytes differentiation into macrophages.

2.3.4 Macrophage maintenance and polarization

After five days of culture, adherent differentiated macrophages were gently washed with room temperature PBS to remove undifferentiated and/or dead cells floating within the culture medium. Then, cells were covered with ice-cold PBS and let detach for 5min at 4 °C. Ten milliliters warm BMDM medium were added to restore nourishment and physiological temperature to prevent macrophages activation or cellular stress. The cells were gently collected from the petri dish using a cell scraper and collected into 50ml tubes. Following centrifugation at 300g for 5 min at room temperature, the supernatant was discarded, and cells were resuspended in 20 mL BMDM medium and counted using the automatic cell counter Cellometer Auto T4 Plus (PeqLab, Erlangen, Germany). Cells were plated into different well formats at different concentrations accordingly to the planned experiment.

After plating, macrophages were cultivated for 4 days in BMDM medium supplemented with different cytokines cocktail to drive macrophagic polarization. Macrophages were polarized into M1 implementing BMDM medium with LPS (50 ng/ml) and IFN γ (50ng/ml). M2 polarization was obtained implementing BMDM medium with IL-4 (50ng/ml) and IL-13 (50ng/ml). Resting, unpolarized control population was maintained in BMDM medium supplemented with m-CSF.

2.3.5 Splenocyte isolation

Dnmt3a^{fl/fl} and *Dnmt3a^{LysM}* mice were sacrificed by cervical dislocation and spleens were collected and temporarily stored in RPMI 1640 medium (Invitrogen, Darmstadt, Germany) on ice. Spleens were sectioned in three parts of which, one third was used for to isolate splenocytes. To generate single cell suspensions, the splenic sections were carefully mashed through a 40µm cell strainer and splenocytes were separated from erythrocytes via gradient centrifugation (2,000rpm, 20min, room temperature) using Ficoll solution (1.099 g/ml) (Sigma-Aldrich, Taufkirchen, Germany).

After centrifugation, splenocytes were collected from the interphase and transferred to 50ml falcon tubes and RPMI supplemented with 10% FCS was added to reach 20ml final volume. Following a second centrifugation (1,600rpm, 4 min at room temperature), the pellet containing splenocytes was washed twice in RPMI supplemented with 10% FCS. Splenocytes were counted using the automatic cell counter Cellometer Auto T4 Plus (PeqLab, Erlangen, Germany) and plated in different well formats/concentrations accordingly to the experimental setup. Splenocytes that further needed processing such as MACS separation or FACS analysis, were kept on ice resuspended in 1ml RPMI-10% FCS.

2.3.6 Lamina propria and intestinal epithelium dissociation from small intestine and colon

The experiments performed in the current study involving lamina propria and intestinal epithelial cells were performed using the Lamina Propria Dissociation Kit for mouse (Miltenyi BioTech, Bergisch Gladbach, Germany) following the manufacturer's protocol. Briefly, small intestine and colon were harvested from sacrificed mice and flushed with room temperature PBS to remove contaminations from gastrointestinal content and mucus. Small intestine and colon were cut open longitudinally and reduced to 0.5cm pieces and transferred to 50ml falcon tubes prefilled with ice cold PBS. Next, the tissues were moved to ice cold PBS supplemented with 5% ethylenediaminetetraacetic acid (EDTA) and dithiothreitol (DTT), to disrupt of the structural integrity of the epithelium. In addition to the physical tissue disruption from EDTA and DTT, the digested tissue was further enzymatically dissociated into a single cell suspension using collagenase. The obtained cells were stored in ice cold PBS and freshly analyzed by FACS technology. The remaining material was reduced to a pellet and stored at -80°C until further usage.

2.3.7 Mode-K maintenance and co-culture system establishment for *in vitro* wound healing assay

Mode-K cell line is a tool to study the murine intestinal epithelium *in vitro*. Mode-K cells were used for co-culture system in presence of resting, M1 and M2 macrophages to assess the ability of each

macrophagic population in promoting or inhibiting tissue proliferation. In a first experiment, Mode-K cells were maintained in minimal essential medium (MEM) implemented with 20% fetal calf serum (FCS). Upon confluency, cells were harvested after 5min incubation at 37°C with trypsin, and 30,000 cells were seeded in Ibidi Culture-Insert 2 Well (Ibidi, Grärfelfing, Germany). The 2-wells insert provides two cell culture reservoirs, each separated by a 500µm thick wall. When confluency was reached in both reservoirs, the inserts were removed and culture medium was implemented with 30% medium harvested from resting, M1 or M2 macrophages. Mode-K proliferation was followed until the control samples covered the gap area.

In a second experiment, the 2 wells inserts were placed in 24 wells culture plates and cells were seeded in the same was described above. Once the cells in the reservoir reached confluency, transwell inserts containing macrophages previously polarized for 96h were positioned on top of the wells containing mode-K cells. Macrophages and intestinal epithelial cells were co-cultivated for 36h and fluorescent microscopy was used to assess cell proliferation. The covered area was quantified using ImageJ software.

2.3.8 Organoid-macrophages co-culture

Murine intestinal organoids were generated as described in chapter 2.3.2. Organoids were obtained from mice purchased from Jackson laboratory (C57BL/6J: RRID: IMSR_JAX:000664 and C57BL/6J-ApcMin/J: RRID: IMSR_JAX:002020). To investigate the contribution of *Dnmt3a* and macrophagic polarization to intestinal tissue proliferation, in homeostatic conditions and during tumor development, organoids were generated from C57BL/6 mice and APC^{min} mice. APC mice (APC^{min}) develop spontaneous multiple intestinal neoplasia, and for this represent a powerful model to investigate tumor development *in vitro*. Organoids from WT and APC^{min} mice were reduced to single cell suspensions through incubation for 5min with TrypLE™ Express (Gibco, Life technologies) at 37°C and vigorous pipetting. The cell suspensions were filtered through 70µm filters to avoid residual cell aggregates. 150,000 cells were seeded on membranous transwell cell culture inserts. Intestinal epithelial cells were maintained in L-WNR conditioned medium and 50% 2x basal medium supplemented with 30% FCS refreshed every second day. The transwell inserts containing intestinal epithelial cells were successively placed on top of differentiated macrophages from *Dnmt3a*^{fl/fl} and *Dnmt3a*^{LysM} mice previously seeded and polarized in 24 wells cell culture plates (30.000/well).

2.4 Generation, handling, and treatment of mice

In the current project, *Dnmt3a* conditional knock-out mice were used to elucidate the functional consequence of the deletion of *Dnmt3a* in the intestinal epithelium and the myelomonocytic lineage during homeostatic and inflammatory conditions.

2.4.1 Generation of *Dnmt3a*^{ΔIEC} mice

Mice having *Dnmt3a* flanked by loxP sites were generated by commercially available supplier (EMMA). LoxP sites were introduced to enable the excision of *Dnmt3a* upon recombination with Cre. A distal loxP site was introduced upstream exon 13 with a FRT flanked neomycin selection cassette. The mouse having this was crossed with mice expressing Flp recombinase to remove the neomycin selection cassette. The resulting *Dnmt3a*^{fl/+} mice had exon 13-17 on *Dnmt3a* flanked with two loxP sites (*Dnmt3a*^{fl/fl}). *Dnmt3a*^{fl/fl} mice were then crossed with Cre mice (mice constitutively expressing Cre recombinase) to generate offspring conditionally lacking. The Cre-deleter mice had Cre recombinase expressed under Villin promoter, ensuring the expression of Cre uniquely in intestinal epithelial cells. The resulting mouse model (*Villin(V)-cre⁺;Dnmt3a^{fl/fl}*) had an intestinal-epithelial-cell-specific *Dnmt3a* deletion (*Dnmt3a*^{ΔIEC}). Throughout this project, both male and female mice aged between 8 and 20 weeks were adopted to perform *in vivo* experiments.

2.4.2 Generation of *Dnmt3a*^{LysM} mice

The LysM Cre x *Dnmt3a*^{fl/fl} mouse model was generated to investigate the role of *Dnmt3a*, exclusively within the myeloid cell lineage (monocytes, mature macrophages and granulocytes) and the innate immune response. To this end, *Dnmt3a*^{fl/fl} mice were crossed with mice having a nuclear-localized Cre recombinase under the control of the LysM promoter. We call the resulting conditional mouse line *Dnmt3a*^{LysM}, in which the expression of LysMCre resulted in the deletion of the *Dnmt3a* gene.

2.4.3 Animal housing and animal welfare

Mice were maintained in pathogen-free facilities, in cages with controlled ventilation Central Animal Facility of the Schleswig-Holstein University Hospital Kiel, Germany. Mice were maintained with a cycle of 12 h light-12h dark at 21°C ± 2°C and 60% ± 5% humidity. Food and water were provided *ad libitum*. All research was approved by the institutional review board. Procedures involving animals were approved by ministerial decision and were performed in conformity to current national and international laws for animal care and welfare.

Appropriate permissions (acceptance no.: V242-7224.121-33, Approval no. V242-28372/2022 (29-4/22)) were obtained for all experiment performed in the current research work.

2.4.4 Acute DSS induction

Female mice aged between 10 and 12 weeks were maintained in single cages and two groups of 6 animals were included in the experiments. Mice were administered 4% dextran sodium sulfate (DSS) dissolved in drinking water for 5 days. Water containing DSS was subsequently removed and substituted with clean tap water. Food was provided *ad libitum* for the entire duration of the experiment. Body weight measurement and disease activity scoring were performed each day of experiment.

2.4.5 Disease activity assessment

Experimental mice undergoing DSS treatments were monitored throughout the duration of the experiment and disease activity index (DAI) was determined daily. The disease course was scored using a combination of values obtained from stool blood, stool consistency and body weight loss (refer to table 7 for further details).

Table 7: Disease activity scoring parameters

Score	Stool blood	Stool consistency	Body weight loss (%)
0	Negative	Formed	0
1	Slightly positive	Soft	1-4.99
2	Positive	Very soft	5-9.99
3	Visible blood in stool	Unformed	10-19.99
4	Rectal bleeding	Liquid	>20

2.4.6 Histopathological analyses of murine colonic tissue

Post mortem, the entire colon was excised and longitudinally rolled up, starting from the distal part to have distal section in the very inner layer and the proximal intestine at the very outer layer. The obtained rolls were fixed in 10% formalin. Paraffin sections were cut and stained with H&E. The histological score is represented by the sum of the combined scores of inflammatory cell infiltration and tissue damage, namely: mononuclear cell infiltrate (0=absent; 1=mild; 2=moderate; 3= severe), crypt hyperplasia (0=absent; 1=mild; 2=moderate; 3= severe), epithelial injury/erosion (0=absent; 1=mild; 2=moderate; 3= severe), and transmural inflammation (0=absent; 1=submucosal; 2=one focus extending into muscularis and serosa; 3=up to five foci extending into muscularis and serosa; 4=diffuse).

2.4.7 AOM-Chronic DSS induction

Azoxymethane (AOM)-DSS is an *in vivo* model that allows to simultaneously study the process of tumor development and inflammation. 10 to 12 weeks old female mice (n=8 per genotype) were maintained in single cages in a 12h light/dark cycle and fed *ad libitum* throughout the entire duration of the experiment. AOM (10mg/kg), a procarcinogen able to induce mutagenesis in the colonic epithelium, was intraperitoneally injected on day 1 of experiment. On day 7, the first cycle of DSS (1% DSS) was initiated by administration of dissolved DSS into drinking water. After 7 days, DSS containing water was substituted with clean water. This process was repeated twice, alternating 7 days of DSS treatment with 14 days of recovery. Body weight and disease activity were measured every second/third day. Disease activity index was scored accordingly to the description provided in table 6.

2.4.8 *In vivo* Fluorescein isothiocyanate (FITC)-dextran permeability assay

Male and female mice were fasted for 4h before the administration via oral gavage of Fluorescein isothiocyanate (FITC) conjugated dextran (Sigma-Aldrich, 60mg/100g). Mice were euthanized through cervical dislocation after 1h from administration. Peripheral blood was collected in gel containing tubes and the corpuscular components were separated from serum via centrifugation at 10,000xg for 5min. Serum was diluted 1:1 on room temperature PBS. FITC concentration in serum was calculated in 96-well plates at 528nm using the microplate reader Infinite M200 Pro (Tecan, Männedorf, Switzerland) and the associated software i-control TM 1.9 (Tecan, Männedorf, Switzerland).

FITC dextran concentrations were calculated by comparison with a standard curve with increasing concentration prepared in PBS ranging from 0 to 800µg/mL 4-kDa FITC dextran. Serum harvested from mice receiving only PBS was used as background control and subtracted to the treated serum. The experiment was performed in accordance with the guidelines for Animal Care of Kiel University.

2.5 Immunohistochemistry

2.5.1 Tissue Processing

Murine tissue was harvested from *Dnmt3a^{fl/fl}* and *Dnmt3a^{LysM}* mice and fixed promptly in 10 % (w/v) formalin in PBS for 24h at 4°C. For complete dehydration, tissues were immersed in ethanol solutions with increasing concentrations (final concentration 100%). Ethanol was gradually replaced with xylene, and eventually imbedded in paraffin for long term storage. The RM2255 microtome (Leica, Wetzlar, Germany) was used to micro dissect the paraffin embedded tissues into 3.5-4.5µm before proceeding to immunohistochemical protocol.

2.5.2 Hematoxylin and Eosin (H&E) staining

Dissected samples in paraffin were rehydrated using decreasing xylene and ethanol concentrations and washed with distilled water. Slides were stained for 2-5 min in hematoxylin. Hematoxylin in complex with aluminum salts is positively charged and reacts with negatively charged, basophilic cell components including nucleic acids which are stained blue. Counterstaining of the cytoplasm was achieved with 1 % (v/v) eosin solution for 2 min. Eosin is negatively charged and therefore reacts with positively charged, acidophilic components such as amino groups in proteins in the cytoplasm, which are stained pink. Slides were dehydrated and embedded in Roti-Histo-Kit mounting medium (Roth, Karlsruhe, Germany). Slides were examined with a Zeiss AxioImager.Z1 apotome fluorescence microscope and the AxioVision Rel 4.9 software (ZEISS, Oberkochen, Germany)

2.5.3 3,3'-Diaminobenzidine (DAB) staining

Histology slides were rehydrated, and antigen retrieval was achieved in citrate buffer (pH 6.0) for 20min. Unspecific binding sites blocking and inactivation of naturally occurring peroxidases was performed using 5% (v/v) goat serum in PBS supplemented with 3% hydrogen peroxide. Incubation times were optimized accordingly to primary antibody. Antibody incubation and 3,3'-Diaminobenzidine (DAB) staining were performed using Vectastain Elite ABC Kit (Vector Labs, Peterborough, United Kingdom), following the producer's instructions. To maximize the signal, after primary antibody incubation, the slides were incubated with biotinylated secondary antibody. Colorimetric signal of (DAB) was obtained through a second incubation with horseradish peroxidase-conjugated streptavidin antibody, to oxidize DAB and produce a brown color.

2.6 Imaging and immunofluorescence

2.6.1 Fluorescent *in situ* hybridization (FISH)

Colon sections were collected and maintained in Carnoy fixative. Tissues were hybridized and stained with the probe EUB338_Cy3 (Microsynth, 3913816), AF-488-conjugated E-Cadherin (BD Biosciences 610182) and DAPI (Sigma Aldrich, D9542). Briefly, slides were dewaxed at 60°C for 10min in xylene substitute solution. 50µl probe (0.5 µg) in Hybridization solution (prewarmed to 55°C) were added to each section and incubated at 60°C for 3h. The slides were washed in FISH washing buffer prewarmed to 50°C for 15min, and successfully washed three times in PBS for 10min. Primary antibody incubation was performed overnight at 4°C. Secondary antibody incubation was performed for 1h at room temperature. The slides were mounted using prolong antifade fluorescence mounting media (DAKO). Photomicrographs were acquired using the AxioImager.Z1 (Zeiss) fluorescent microscope. The

measurement of the distance between intestinal epithelial cells and luminal content was quantified using ImageJ software.

Table 8: Hybridization solution preparation

Component	ml	Final concentration	Stock concentration	Unit
NaCl	90	0.9	5	M
Tris-HCl pH 7.4	10	20	1000	mM
SDS	5	0.1	10	%
Formamide (5-50% final)	175	35	100	%
Distilled H ₂ O	220	n/a	n/a	-

Table 9: FISH washing buffer composition

Component	ml	Final concentration	Stock concentration	Unit
NaCl	45	0.9	5	M
Tris-HCl pH 7.4	5	20	1000	mM
H ₂ O	200	-	n/a	-
Total	500	-	-	-

2.6.2 BMDMs Immunofluorescence

Ex vivo generated BMDMs were cultivated in 8 wells chamber slides at a cellular density of 10,000 - 15,000 cells/well. After culture medium removal, the cells were washed twice with room temperature PBS and fixed with 4% PFA in PBS (w/V). After fixation, Triton X-100 0,5% (w/V) in PBS was used to permeabilize the cells for 3-5min depending on the cellular localization of the desired epitope. To prevent unspecific epitope binding, blocking was performed for 30min with 5% BSA (w/V) in PBS. Primary antibody incubation was performed at +4°C overnight or at room temperature depending on the specificity of the primary antibody. PBS was used to wash the cells three times for 5 min. The incubation with secondary antibody conjugated with Alexa Fluor 488, Alexa Fluor 700 or Alexa Fluor 555 accordingly to species specific reactivity, was performed at room temperature for 2h in a concentration of 1:200 to 1:2000 accordingly to manufacturer instruction. Following one washing in PBS, Phalloidin was used 1:500 (V/V) in PBS to visualize actin filaments (F-actin), together with DAPI and DRAQ5 (1:40,000 and 1:5,000) to visualize nuclei.

2.7 NGS technology

2.7.1 Transcriptome analysis

Transcriptome analysis was performed on *in vitro* polarized (resting, M1 and M2) macrophages obtained from 8-10 and >34 weeks old *Dnmt3a^{fl/fl}* and *Dnmt3a^{LysM}* mice. Total RNA was isolated as described in chapter 2.2.1. Sequencing was performed using Illumina total RNA stranded TruSeq

protocol on HiSeq3000 (Illumina, San Diego, United States). Analysis of differential gene expression levels performed and visualized using the Bioconductor package DESeq2 [196]. All subsequent analyses were performed using R Statistical Software (v.4.2.0; R Core Team 2022 (<https://www.R-project.org/>)). Venn diagrams were drawn using VennDiagram_R package version 1.7.3. Gene Ontology (GO) terms were obtained within the category of biological processes using topGO_R package version 2.48.0.

Differential expression of genes was calculated comparing resting and M2 groups, resting and M1 groups and M2 versus M1 groups. The comparison was performed including differentially expressed genes between young and old mice, within the polarization status. Statistical significance was calculated using Wald tests. Genes that were expressed in less than 20% of the samples were excluded from the analysis to ensure enough statistical power. For differentially expression analysis genes with a p-value below 0.05 were considered as significantly differentially expressed.

2.8 Functional assays

2.8.1 Arginase activity assay

Cells (1×10^6) were cultivated in 6 well plates and culture medium was removed. Cells were washed once in room temperature PBS and centrifuged for 10min at $1,000 \times g$ at 4°C and harvested using cell scraper. Collected samples were transferred to 1.5ml reaction tubes and lysed for 10min in $100\mu\text{l}$ lysis buffer (Tris-HCl 10mM, pH 7.4, 1:100 pepstatin A, 1:100 Leupeptin and 0,4% Triton X-100). To remove insoluble material, lysed cells were centrifuged for 10min at $13,000 \times g$, and the supernatant harvested for further processing.

Arginase activity was quantified following the manufacturer's instruction for Arginase Activity Assay Kit (Sigma- Aldrich, St. Luis, USA). $40\mu\text{l}$ of lysed cells were added to 96 wells plates in three technical replicates per sample. $10\mu\text{l}$ of 5x Substrate buffer were added to each well and incubated for 2h at 37°C . To stop the reaction, $200\mu\text{l}$ of Urea Reagent were added to all wells except for the blank wells. In the next step, $10\mu\text{l}$ of 5x Substrate buffer were added to blank wells and incubated for 1h at room temperature. The samples were measured by reading absorbance at 430nm (A_{430}). Arginase activity of a sample was determined by the following equation:

$$\text{Activity} = \frac{A_{430}(\text{sample}) - A_{430}(\text{blank})}{A_{430}(\text{standard}) - A_{430}(\text{water})} \times \frac{(1\text{mM} * 50 * 10^3)}{V * T}$$

Where T=Reaction time in minutes, V=sample volume (μL) (1–40 μL), 1 mM=concentration of Urea Standard 50=reaction volume (μL) 10^3 = mM to μM conversion factor.

2.8.2 Nitric oxide synthase assay

Nitric Oxide Synthase Activity Assay Kit was used to quantify NOS activity in cell and tissue lysates. A minimum amount of 5×10^6 cells were rinsed with room temperature PBS and 200 μ l of cold NOS Assay Buffer was used to homogenize the suspension. After centrifugation (10min 10,000x g, 4°C), the supernatant was collected, and protein concentration was determined as described in chapter 2.2.1. A minimum of 200 μ g of total protein was diluted in NOS assay buffer and the total volume equilibrated at 60 μ l. 40 μ l Reaction Mix were added and samples were incubated for 1h at 37°C.

In a next step, 95 μ l of NOS Assay Buffer and 5 μ l Enhancer were added to each sample except for background wells and incubated for 10min. For the measurement, 50 μ l Griess Reagent 1 and 50 μ l Griess Reagent 2 were added to each sample, incubated at room temperature 10min, and finally measured at OD 540nm. NOS specific activity was determined applying the following equation:

$$NOS\ Specific\ Activity = \left(\frac{B}{T + C} \right)$$

Where B=amount of Nitrite in the samples calculated from standard curve, T=reaction time, C=protein input (200 μ g).

2.9 Immunoassays

2.9.1 Flow cytometry analysis

Fluorescence activated cell sorting (FACS) analysis was performed for all experiments using Sony SA3800 spectral analyzer (SONY biotechnology, Surrey, UK). The spectral analysis technology allows to optimize sensitivity and enhances dim signal detection by collecting photons at wavelengths from 420nm to 800nm. Furthermore, the technology allows the simultaneous acquisition of spectral emission in a multicolor spectrum allowing the detection up to 10 fluorophores simultaneously.

For all flow cytometry analysis, cell viability was tested using Zombie Red™ Fixable Viability Kit Biolegend (1:1,000). Data were acquired using SA3800 Spectral Analyzer (Sony Biotechnology) and were analyzed using SA3800 Software version 2.0.5.54250.

For all experiments involving surface antigens detection, 10,000-up-to 200,000 cells were plated on standard transparent 96 well V bottom plates and washed twice in FACS Washing Buffer (FWB). The samples were centrifuged at 1,300rpm for 3 min and the supernatant was removed by inversion. After washing, Fc blocking was performed to reduce non-specific binding and background fluorescence. Fc blocking was performed for 20min on ice, protected from light. Antibody incubation was performed for 40 min at 4°C. Cells were washed three times with FWB and samples were analyzed with SA3800

software (SONY biotechnology). Used fluorochrome-conjugated antibodies, their working dilutions are listed in Table 10-11.

2.9.2 Gating strategy

Light scattered by cells is measured by two detectors: forward scatter (FSC) that detects scatter along the path of the laser, and side scatter (SSC) which measures scatter at a ninety-degree angle relative to the laser. FSC intensity is directly proportional to the dimension (or diameter) of the cell, and it is due to light diffraction around the cell. SSC is the result of refracted light from intracellular component such as granules or nodules, at the interface between the laser and intracellular structures. For all analysis, gating workflow was initially set to exclude doublets and debris by mean of SSC and FSC. After doublet exclusion, only viable cells were selected based on Zombie Red negative staining.

- For basal immuno-phenotyping panel, viable cells were gated and plotted based on CD45-FITC (leukocytes) fluorescence. CD45-FITC positive cells were plotted against CD3 ϵ -AF532 (T cells) and double positive cells were selected and stained for BV711-CD4 (CD4 T helper cells) and BV786-CD8 (CD8 cytotoxic T cells). Negative CD3 cells were gated and plotted for PerCP/Cy5.5-CD11b (monocytes), Pacific blue-CD11c (dendritic cells), BV650-CD19 (B cells), PE-NK1.1 (Natural killer) and PerCP/Cy5.5-CD11b/BV421-Ly6G (neutrophils).
- For hematopoietic stem cells proportions assessment, viable cells were selected based on negative CD3, CD19 and CD11b events. Negatively stained cells for the latter three antigens, were further plotted based on PE-Sca-1/FITC-c-Kit expression.

2.9.3 Basal immune phenotyping panel

Immune cells basal immune phenotyping was performed on lamina propria of small intestine, colon, mesenteric lymph nodes (MLN) and spleen.

Spleen, small intestinal and colonic lamina propria and MLN were immunologically characterized based on the expression of cellular markers for the main immune cell populations, namely CD45 (leukocytes), NK1.1 (natural killer T-cells), CD3 (T cell co-receptor involved in activating both the cytotoxic T cell (CD8⁺ naive T cells) and T helper cells (CD4⁺ naive T cells), CD11b (macrophages), Lys6G (common markers for monocytes, granulocytes and neutrophils), CD19 (B cells), CD11c (dendritic cells).

Table 10: list of antibodies used for basal immune phenotyping panel

Fluorochrome	Antigen	Dilution	Company
FITC	CD45	1:100	Biolegend
PE	NK1.1	1:50	eBioscience/Thermo Scientific
Alexa Fluor 532	CD3ε	1:100	eBioscience/Thermo Scientific
PerCP/Cy5.5	CD11b	1:50	Biolegend
BV421	Lys6G	1:100	Biolegend
BV711	CD4	1:100	Biolegend
BV650	CD19	1:50	Biolegend
BV786	CD8	1:100	Biolegend
Pacific Blue	CD11c	1:80	Biolegend
Zombie red	Viability	1:1000	Biolegend

2.9.4 Flow cytometry analysis of hematopoietic precursors

Lineage-negative cells (lin-) were obtained using Lineage Cell Depletion Kit (Myltenil, Germany) from mouse splenic tissue. Depleted differentiated cells were loaded into pre activated MACS MS columns and the retained cells were stained for specific stem cell surface molecules Sca-1 and c-kit and analyzed by flow cytometry. Anti- CD3ε, CD11b and CD19 antibodies were included as control for contamination of differentiate cells that were retained after MACS sorting. Table 11 summarizes the antibodies and their conjugated fluorochromes used for this analysis.

Table 11: Antibodies used for flow cytometry analysis of stem cell markers

Fluorochrome	Antigen	Dilution	Company
PE	Sca-1	1:50	
Alexa Fluor 532	CD3ε	1:100	eBioscience/Thermo Scientific
PerCP/Cy5.5	CD11b	1:100	Biolegend
FITC	c-Kit	1:60	
BV650	CD19	1:100	
Zombie red		1:1000	Biolegend

2.9.5 Magnetic activated cell sorting

CD11b positive cells were isolated from intestinal and colonic lamina propria fractions through magnetic activated cell sorting (MACS) using CD11b MicroBeads positive selection (human and mouse) from Miltenyi BioTec (Bergisch Gladbach, Germany). This method is based on the specific recognition of CD11b positive cells by magnetically active beads prelabelled with CD11b antibodies directed against CD11b. Cells expressing CD11b bind to the antibody on the surface of the magnetic beads, allowing the cells not expressing CD11b to flow through the magnetic field, to obtain a pure population of only CD11b positive cells.

Briefly, lamina propria single cells suspensions were washed twice with MACS separation buffer. The magnetic columns were activated by three washing with MACS buffer and a total number of 0.4-1 x

10⁶ cells were loaded onto the MS columns. For CD11b⁺ cells isolation, the cell suspensions were previously strained through a 30 µm pre-separation filter. To optimize the isolation and increase the purity of isolated CD11b positive population, the retained cells were eluted, and the obtained flow through was loaded again onto a second MS column. After release from the magnetic field, the cells were counted and accordingly to cell number separated into different tubes for further analysis.

2.9.6 Mature hematopoietic cells depletion from spleen

Splenocytes obtained as described above were depleted from differentiated cells. Differentiated hematopoietic-derived cells were removed using the Lineage Cell Depletion kit for mouse (Miltenyi BioTec, Bergisch Gladbach, Germany). This procedure allows the isolation of lineage-negative cells (lin⁻) from mouse splenic tissue. The Lineage Cell Depletion Kit have been developed for the efficient depletion of mature hematopoietic cells, including T cells, B cells, monocytes/macrophages, granulocytes, erythrocytes, and their committed precursors. For mature hematopoietic and differentiated cells depletion, cells labeled with an antibody cocktail against so-called lineage markers (CD5, CD45R (B220), CD11b, Gr-1 (Ly-6G/C), and Ter-119) coupled to magnetic beads. Cells were first labeled with a cocktail of biotinylated antibodies followed by labeling with Anti-Biotin MicroBeads. Cell suspensions were loaded into MACS MS Columns which were pre activated with three washing in 500µl MACS washing buffer (1% BSA w/v in PBS). Cell solutions were let precipitating by gravity through MS columns. After precipitation, the columns were released for the magnet so that magnetically retained beads coupled with lineage-positive cells could be released and the effluent collected in a separate tube. Lineage negative (lin⁻) cells were stained for specific stem cell surface molecules Stem cells antigen-1 (Sca-1) and receptor tyrosine kinase (c-kit) and analyzed by flow cytometry using a Sony SA3800 spectral analyzer (SONY biotechnology, Surrey, UK)

2.10 Statistics

Statistical analysis was performed using the GraphPad Prism 9 software package (GraphPad Software Inc., La Jolla, USA). Student's unpaired t-test was performed followed by Mann Whitney correction, unless otherwise stated. Data reported are shown as mean ± standard error of the mean (SEM). A p-value of ≤ 0,05 was considered as significant (*). A p-value of ≤ 0,01 was considered as strongly significant (**) and p-value of ≤ 0,001 as highly significant (***).

3. Results

3.1 On the role of DNA methyltransferase 3A (DNMT3A) in intestinal epithelial barrier function in the colon

3.1.1 Lack of *Dnmt3a* favours mucus layer thinning and increases bacterial translocation to mesenteric lymph nodes

To characterize the impact of *Dnmt3a* deletion in the intestinal epithelium, we generated a mouse model lacking *Dnmt3a* uniquely in intestinal epithelial cells (*Dnmt3a*^{ΔIEC}) and performed analysis at steady state. Driven by the hypothesis that *Dnmt3a* has a crucial role in maintaining gut barrier homeostasis and permeability in the colon, we further aimed to strengthen our previous findings. We assessed Goblet cells numbers (identified by PAS staining) in *Dnmt3a*^{ΔIEC} and *Dnmt3a*^{fl/fl} at baseline conditions (Figure 3-1a) and observed that *Dnmt3a*^{ΔIEC} compared to wild type littermates were characterized by lower numbers of PAS positive stained cells (Figure 3-1b). Based on this result and on the reduced expression of Mucin 2 (*Muc2*) characterizing *Dnmt3a*^{ΔIEC} mice [110], we investigated whether the lack of *Dnmt3a* might have an impact on the mucus layer thickness and could in turn favor bacterial translocation to distant sites such as mesenteric lymph nodes (MLN). Therefore, we measured the distance of luminal bacteria to epithelial cells of 10-15 weeks old steady state *Dnmt3a*^{ΔIEC} and *Dnmt3a*^{fl/fl} mice by mean of fluorescent *in situ* hybridization (FISH) using a probe targeting eubacteria (Figure 3-1c) and quantified 16S rDNA copies in MLN. By quantifying the distance between intestinal epithelial cells and luminal content, we found significantly reduced values in colonic section of *Dnmt3a*^{ΔIEC} mice (Figure 3-1d), supporting the hypothesis that *Dnmt3a* might have a determinant role in normal mucus formation. To further understand the consequence of the lack of *Dnmt3a* on mucus function, we investigated whether reduced epithelium-to-bacteria distance might favor bacterial translocation to distant sites outside the gastrointestinal apparatus. For this reason, we assessed the amount total eubacterial 16S rDNA copies in MLN of *Dnmt3a*^{ΔIEC} mice compared to *Dnmt3a*^{fl/fl} (Figure 3-1e) and observed increased 16S rDNA copies in MLN derived from *Dnmt3a* depleted mice compared to their littermate controls. To further support this observation, we tested the gut permeability *in vivo* using orally administered fluorescein isothiocyanate (FITC)-labelled dextran and quantified FITC concentration in serum 1 hour after administration (Figure 3-1f). FITC serum concentration of *Dnmt3a*^{ΔIEC} mice was significantly higher compared to *Dnmt3a*^{fl/fl} mice, indicating higher gut permeability. These results further confirm a determinant role for *Dnmt3a* in maintaining mucosal homeostasis and in allowing the formation of a healthy mucus layer.

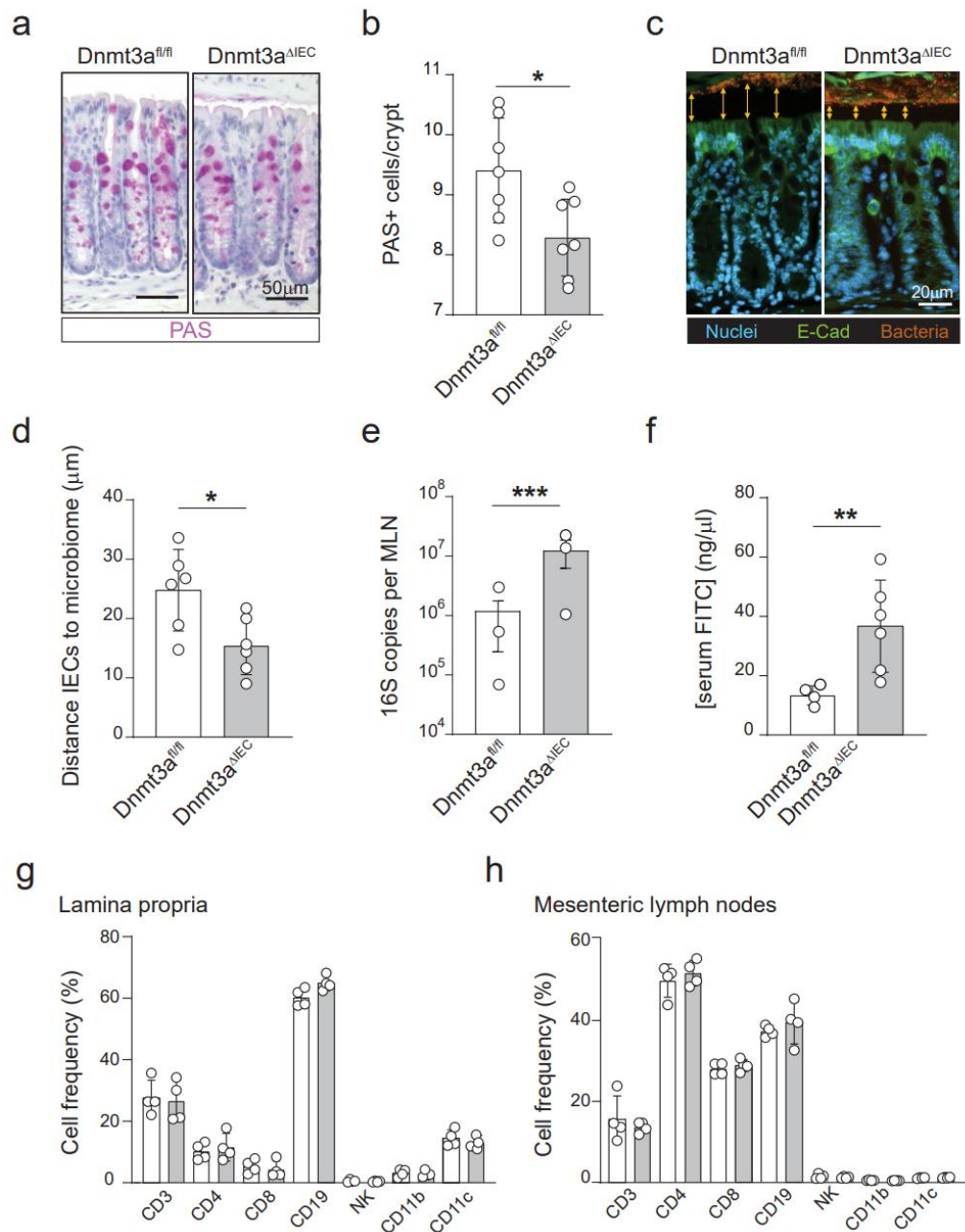


Figure 3-1: Lack of *Dnmt3a* leads to increased gut permeability and bacterial translocation.

(a) Representative photomicrographs of steady state *Dnmt3a^{fl/fl}* and *Dnmt3a^{ΔIEC}*-derived colonic sections stained for PAS and (b) quantification of positively stained cells per crypt. For each sample, a minimum of 100 crypts were counted. Each dot represents one animal, and the average of counted positive cells per 10 crypts. (c) Representative images of fluorescent *in situ* hybridization (FISH) depicting colonic sections immune-fluorescently stained for general eubacteria 16S (probe EUB338) (dark orange), E-cad (green) and nuclei (light blue) (n=6 mice/genotype) and (d) measurement of distance between intestinal epithelial cells and luminal content in colonic sections of steady state *Dnmt3a^{fl/fl}* and *Dnmt3a^{ΔIEC}* (n=6). (e) Quantification of 16S DNA copies per MLN for n=3 mice per genotype. (f) Measurement of FITC concentration in serum of steady state *Dnmt3a^{ΔIEC}* mice compared to *Dnmt3a^{fl/fl}* 1h after FITC-dextran oral administration. Serum from mice receiving PBS was used as blank control (g) Flow cytometry analysis of immune cells in colonic lamina propria obtained from steady state *Dnmt3a^{fl/fl}* and *Dnmt3a^{ΔIEC}* mice (n=4). The abundance of each population is reported as percentage of positive events on a given gated population. (h) Flow cytometry quantification of immune cell population composition in mesenteric lymph nodes of steady state *Dnmt3a^{fl/fl}* and *Dnmt3a^{ΔIEC}* mice (n=4). Data are shown as mean ± S.D. CD3: T cells, CD4: naive T cells, CD8: cytotoxic T cells, CD11b: macrophages, CD11c: dendritic cells, CD11b-Lys6G: neutrophils, CD19: B cells. Statistical significance (b), (d), (e) and (f) was calculated using student's unpaired t-test. * $p < 0.0332$, ** $p < 0.0021$ *** $p < 0.0002$.

Given (i) the substantial consequence of the lack of *Dnmt3a* in intestinal homeostasis, (ii) the importance of epithelial-immune cell communication during homeostasis and inflammation, and (iii) the increased amount of 16S rDNA copies in MLN of *Dnmt3a*^{ΔIEC} mice compared to control mice, we finally tested whether lack of *Dnmt3a* might as well determine a shift in the normal immune cells frequencies of the colonic lamina propria (LP) and of MLN (Figure 3-1g, Figure 3-1h) at baseline. To answer this question, we isolated the lamina propria from colonic epithelium of 10-15 weeks old *Dnmt3a*^{fl/fl} and *Dnmt3a*^{ΔIEC} mice and reduced MLN to single cells suspension. We used FACS technology to obtain an overview of the most abundant immune cells using surface markers characteristic for each cell population. CD3, CD4, CD8a, CD19, CD11b, CD11c, and NK1.1 were used to depict T-cells, CD4⁺T helper cells, CD8⁺ cytotoxic T cells, B cells, monocytes-macrophages, dendritic cells, and natural killer cells, respectively. The analysis did not reveal significant alteration of the composition of the immune cells compartment in LP nor MLN of *Dnmt3a*^{ΔIEC} mice when compared to *Dnmt3a*^{fl/fl} wild type littermates, suggesting that lack of *Dnmt3a* in intestinal epithelium does not impact the immune cell composition of MLN or LP at steady state.

3.1.2 *Dnmt3a* is downregulated during inflammation

Since we recently reported that DNMT3A is transcriptionally dysregulated in whole biopsy samples obtained from CD and UC patients [110], we next focused on the regulation of DNMT3A expression in intestinal epithelial cells only. To this end, we generated human intestinal organoids from endoscopically inflamed and non-inflamed tissue from CD patients and measured mRNA expression levels of DNMT3A (Figure 3-2a). We found a significant downregulation of DNMT3A mRNA levels, accompanied by reduced gene expression of CCND1 proliferative marker, and increased expression of the pro-inflammatory marker CXCL10.

To identify the molecular mechanism targeting and regulating *Dnmt3a* expression during inflammation, we measured mRNA expression levels of *Dnmt3a*, *Dnmt3b*, *Ccnd1*, *Cxcl1* and *Tnf* in murine colonic organoids and stimulated them with prototypic pro-inflammatory molecules *i.e* tumor necrosis factor-α (TNFα), interferon-γ (IFNγ) and bacterial lipopolysaccharide (LPS) (Figure 3-2b, Figure 3-2c).

TNF stimulation (but not IFNγ nor LPS) led to a unique significant downregulation of solely *Dnmt3a*, as *Dnmt3b* expression did not significantly vary. We measured the expression of pro-inflammatory genes to confirm the stimulation and found *Cxcl1*, *Cxcl10* and *Tnf* to be upregulated, therefore indicating *Dnmt3a* specific downregulation during inflammation. At protein level, the significant downregulation was even more pronounced in inflamed tissues, supporting once again a close relation between inflammation and DNMT3A downregulation.

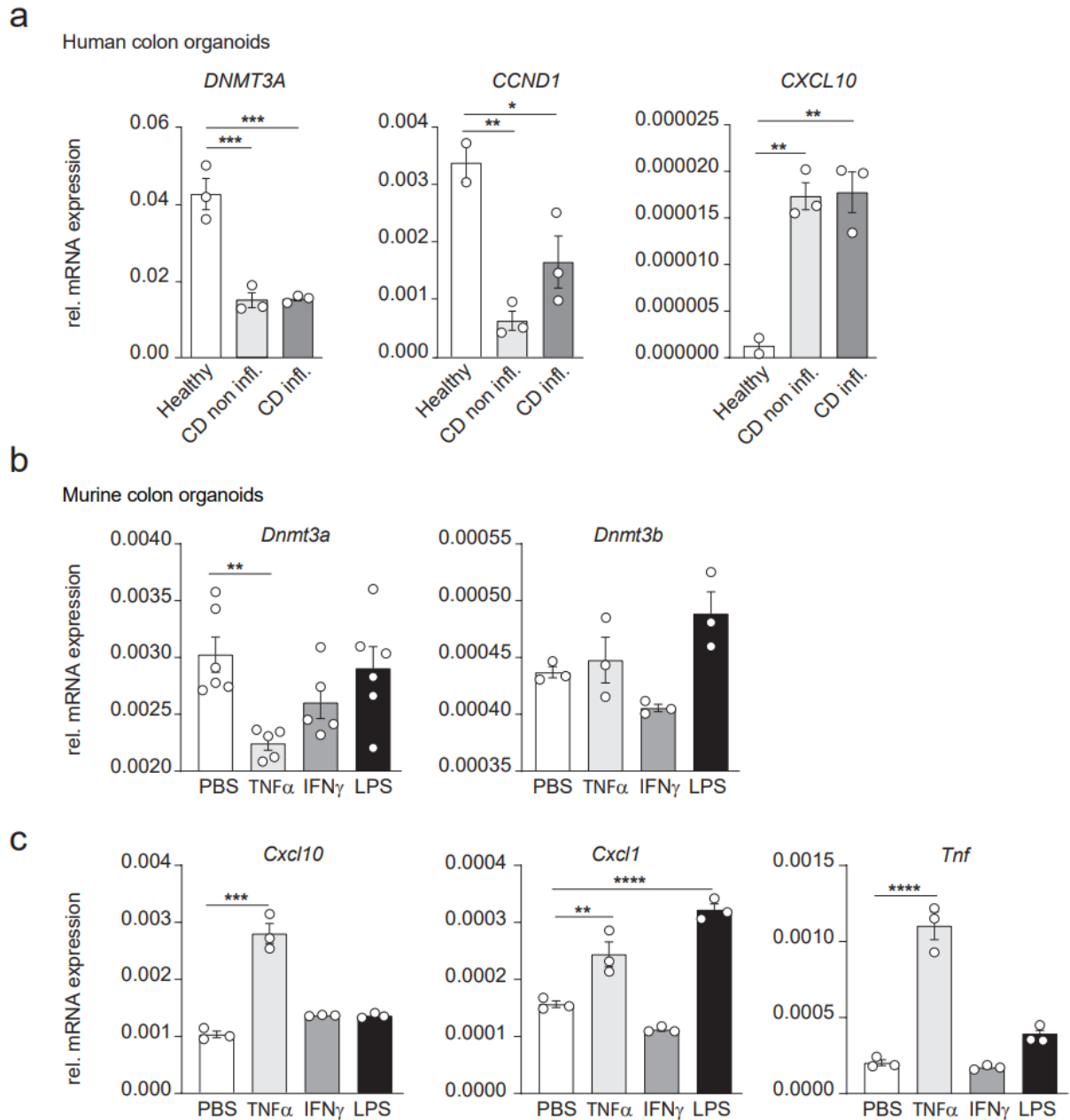


Figure 3- 2: *Dnmt3a* is downregulated upon inflammatory conditions.

(a) Relative mRNA expression of DNMT3A, CCND1 and CXCL10 in endoscopically inflamed and non-inflamed CD patient-derived organoids. Organoids were generated from human healthy, CD inflamed (CD infl.) and CD non-inflamed (CD non infl.) biopsies and mRNA was extracted at early passage. Human ACTB was used as housekeeping gene for normalization. Statistical significance was calculated using ordinary one-way Anova. *** $p < 0,0002$. (b) Relative mRNA expression analysis of *Dnmt3a* and *Dnmt3b* and (c) mRNA levels quantifications of *Cxcl1*, *Cxcl10* and *Tnfa* in murine organoids stimulated for 24h with $TNF\alpha$ (50ng/ml), $IFN\gamma$ (50ng/ml), LPS (50ng/ml) and PBS as control. *Gapdh* was used as housekeeping gene. Data shown represent two independent experiments. Statistical significance was calculated with ordinary one-way Anova. **** $p < 0,0001$.

In summary, the results suggest that *Dnmt3a* genetic ablation in mouse IECs leads to a complex transcriptional and DNA methylation dysregulation, which together result in higher susceptibility to

acute and chronic inflammatory insults [110], along with delayed recovery *in vivo*. Already at baseline conditions, lack of *Dnmt3a* leads to reduced counts of Goblet cells, decreased mucus thickness and increased intestinal permeability, which allows bacterial translocation to distant sites such as MLN. These data support the hypothesis that DNMT3A plays a decisive role in maintaining colonic epithelial homeostasis and intestinal permeability, and its dysregulation might be the result of TNF activity during inflammation.

3.2 *Dnmt3a* in the myelomonocytic lineage during homeostasis and inflammation

We further elucidated the role of *Dnmt3a* within intestinal homeostasis and inflammation using mice lacking *Dnmt3a* in the myelomonocytic lineage (hereafter referred as *Dnmt3a*^{LysM}) as primary model, obtained by crossing *Dnmt3a*^{fl/fl} mice with mice expressing Cre recombinase under LysM promoter, specifically driving the conditional expression of Cre recombinase in cells belonging to the myeloid lineage [197], [198].

We aimed to assess the effect of the hypomethylation that *Dnmt3a* depletion would cause specifically in macrophages during homeostasis and inflammation. To do so, *Dnmt3a*^{fl/fl} and *Dnmt3a*^{LysM} mice-derived macrophages were used as primary *ex vivo* model to investigate the role of *Dnmt3a* within the context of macrophages differentiation/polarization and tumor development.

We initially tested (i) the effectiveness of *Dnmt3a* deletion in macrophages residing in the lamina propria (Figure 3-3). We successively tested (ii) the efficiency of *Dnmt3a* deletion in the myelomonocytic lineage (CD11b⁺) of *Dnmt3a*^{LysM} mice (Figure 3-4) and lastly (iii) we confirmed that the lack of *Dnmt3a* does not interfere with the efficacy of monocytes-to-macrophages differentiation (Figure 3-5).

3.2.1 *Dnmt3a* deletion in macrophages of the lamina propria

We initially aimed to prove the successful deletion of *Dnmt3a* in myeloid cells residing in the intestinal lamina propria (LP) by testing the tissue-specific mRNA and protein expression levels of *Dnmt3a* in CD11b positive (CD11b⁺) cells.

Intestinal LP of *Dnmt3a*^{fl/fl} and *Dnmt3a*^{LysM} mice was dissociated from intestinal epithelial cells (IECs) and reduced to single cell suspension. Afterwards, using magnetic-activated cell sorting (MACS) on the LP fraction, an enriched macrophagic cell population was obtained through CD11b⁺ cell selection. The cell fractions (IECs, LP, LP CD11b⁻ and LP CD11b⁺) were used to assess genetic deletion of *Dnmt3a*, by measuring relative *Dnmt3a* mRNA expression levels. IECs and LP populations were used as *Dnmt3a* expressing positive controls, and LP CD11b⁻ fraction was used as additional control to ensure that *Dnmt3a* undetectable expression was CD11b⁺ cells-specific.

Dnmt3a mRNA expression levels analysis demonstrated a myelomonocytic lineage-specific deletion of *Dnmt3a* transcript (Figure 3-3a), while *Dnmt3b* expression (measured to establish whether the lack

of *Dnmt3a* might result in compensatory overexpression of other Dnmts) did not significantly vary between IECs, LP, LP CD11b⁻ cells and LP CD11b⁺ cells (Figure 3-3b).

As additional confirmation, DNMT3A protein expression levels were quantified in IECs, LP, LP CD11b⁻ and LP CD11b⁺ fractions (Figure 3-3c). On the same line as for mRNA expression levels, DNMT3A was undetectable through immunoblot in CD11b⁺ cells derived from LP of *Dnmt3a*^{LysM} mice, compared to *Dnmt3a*^{fl/fl} control. Protein expression quantification (Figure 3-3d) and gene expression level quantifications were confirmatory for a successful deletion of *Dnm3a* uniquely in myelomonocytic lineage.

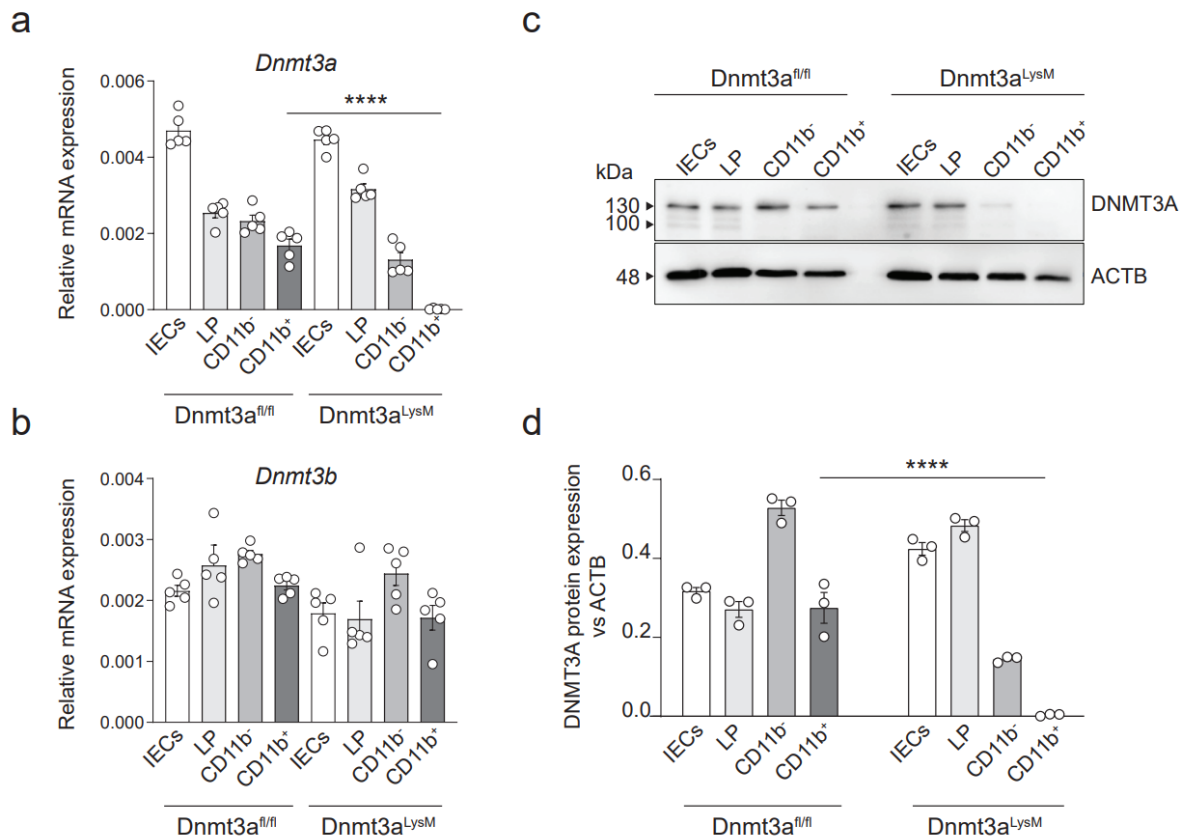


Figure 3- 3: Deletion of *Dnmt3a* in CD11b⁺ myeloid cells isolated from intestinal lamina propria.

(a) Relative mRNA expression levels of *Dnmt3a* and (b) *Dnmt3b* in IECs, LP, CD11b negative LP fraction and CD11b positive LP fractions of small intestinal lamina propria. LP CD11b⁺ and CD11b⁻ cells were selected using MACS on both fractions. *Actb* was used as housekeeping gene for normalization. Data shown are representative for n=5 mice per genotype. (c) Immunoblot and (d) relative quantification of DNMT3A protein expression levels in IECs, LP, LP CD11b negative fraction and LP CD11b positive fraction of small intestinal lamina propria obtained from *Dnmt3a*^{fl/fl} and *Dnmt3a*^{LysM} mice. Protein expression levels were assessed on 15µg protein lysate. ACTB was used as loading control. Shown immunoblot, protein and mRNA quantification result are representative for all the animals defined in the current project as *Dnmt3a*^{fl/fl} and *Dnmt3a*^{LysM}. Statistical significance was calculated using ordinary one-way Anova and Dunnett's multiple comparisons test. ****p<0,0001.

3.2.2 *Dnmt3a* deletion in *Dnmt3a*^{LysM} bone marrow derived macrophages (BMDMs)

To verify the effectiveness of deletion of *Dnmt3a* in bone marrow derived macrophages (BMDMs) (the primary *ex vivo* model used throughout the present work), mRNA and protein expression levels of BMDMs harvested from femurs and tibias of *Dnmt3a*^{fl/fl} and *Dnmt3a*^{LysM} mice were measured using RT-qPCR and immunoblotting after five days of *in vitro* differentiation (Figure 3-4). BMDM were cultivated in macrophages growing media supplemented with 20ng/ml macrophage colony-stimulating factor (M-CSF) and no further treatment was applied. *Dnmt3a*-depleted BMDM were characterized by nearly undetectable expression of *Dnmt3a* transcript (Figure 3-4a), confirming the permanent deletion of *Dnmt3a* in BMDM. On the same line, absence of protein production of both *Dnmt3a* splice isoforms (Figure 3-4b, Figure 3-4c) was observed in *Dnmt3a*^{LysM} mice derived BMDMs compared to *Dnmt3a*^{fl/fl} littermates, confirming the genomic deletion of *Dnmt3a* and the consequent missed DNMT3A protein translation.

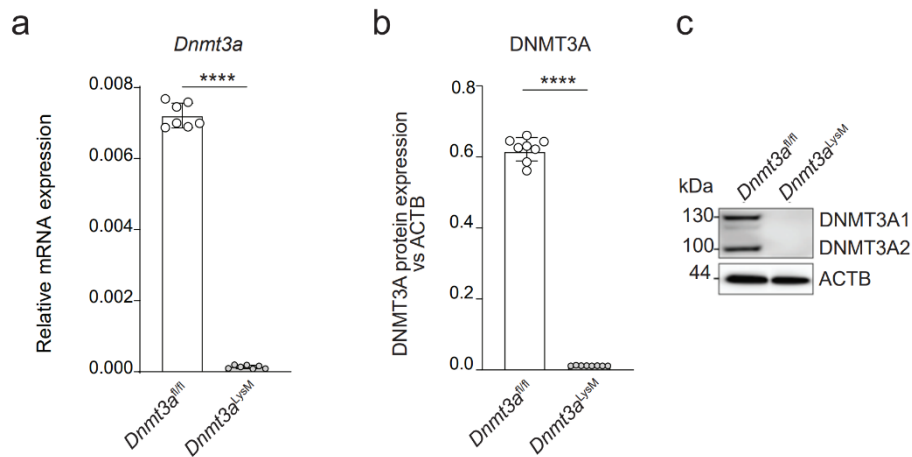


Figure 3- 4: *Dnmt3a* deletion in *Dnmt3a*^{LysM} derived BMDM.

(a) Relative *Dnmt3a* mRNA expression levels analysis of BMDMs five days after isolation from rear leg bones. Data shown are representative for n=7 mice included in the mRNA expression measurement, and for the genotype of all animals used in the current study. TaqMan assay data shown represent mean \pm SEM. (b) Protein level measurement and (c) representative Immunoblotting performed to evaluate DNMT3A protein level (n=8/genotype) using ACTB as loading control on 15 μ g protein lysate input. Data shown represent mean \pm SD. Statistical significance in (a) and (b) was calculated using unpaired Student's *t*-test. **** $p < 0,0001$.

3.2.3 Absence of *Dnmt3a* does not impact CD11b⁺ cells frequencies after BMDM generation

The bone marrow is the main source of hematopoietic stem cells (HSC) and it contains the three major subsets of blood cells (leukocytes, erythrocytes, and platelets). It contains a unique microenvironment that supports self-renewal and differentiation of HSC, multipotent progenitors (MPP), and lineage committed progenitors [199]. The efficiency of macrophagic M-CSF-driven differentiation from the

bone marrow was tested using flow cytometry on BMDM isolated from femurs and tibias of *Dnmt3a^{fl/fl}* and *Dnmt3a^{LysM}* mice. Differentiated macrophages were here intended as cells expressing CD11b cell surface marker (CD11b⁺). The proportions of CD11b⁺ cells were measured at day 5 of differentiation and cultivated in presence of macrophage culture media implemented with M-CSF (20ng/ml). The cell population was plotted based on cellular dimension, by mean of forward scatter (FSC), and granularity, by mean of side scatter (SSC) (Figure 3-5a, left). This population was plotted accordingly to zombie red negatively stained cells (viable cells) (Figure 3-5a middle) and finally based on PerCP-Cy5.5-CD11b positivity. FITC-CD3 was included as negative control staining (Figure 3-5a, right).

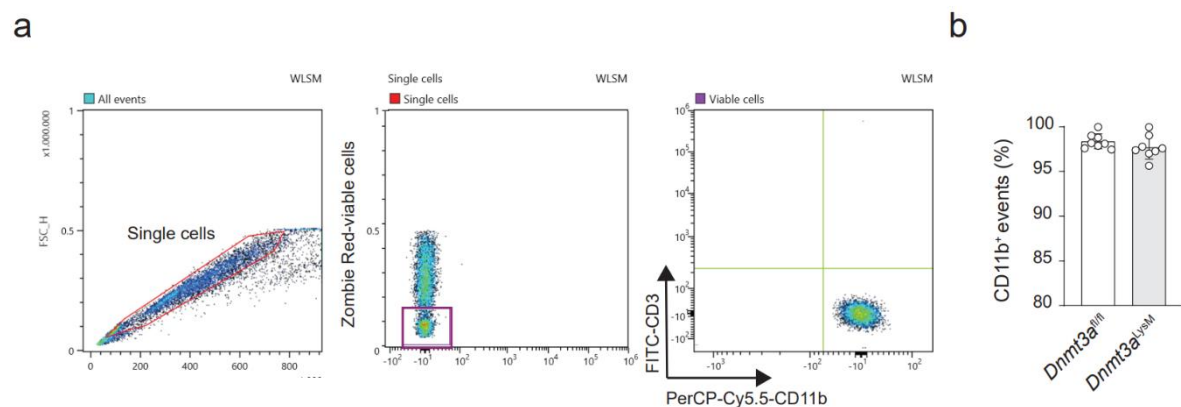


Figure 3- 5: Proportions of CD11b⁺ events in *ex vivo* differentiated BMDM do not change between *Dnmt3a^{fl/fl}* and *Dnmt3a^{LysM}* mice.

(a) Representative workflow depicting gating strategy to exclude doublets, debris, and dead cells (left, middle) and CD11b positive events (right). Flow FSC: forward scatter. SSC: sideward scatter. (b) CD11b events percentages measured through flow cytometry. Each dot represents one animal (n=8 mice per genotype). The quantification of CD11b positive cells was assessed after 5 days *in vitro* differentiation. BMDM were obtained from flushed femurs and tibias of *Dnmt3a^{fl/fl}* and *Dnmt3a^{LysM}* mice and the extracts were cultivated for five days in macrophages culture media supplemented with 20ng/ml m-CSF, until monocytes-to-macrophages differentiation.

The efficiency of macrophages *in vitro* differentiation from bone marrow, in terms of CD11b positive event percentage, was up to 98% (±1,02/1,98%) independently of the genotype (Figure 3-5b). Therefore, an interference of *Dnmt3a* depletion in CD11b⁺ *in vitro* differentiated BMDMs was excluded.

3.3 A functional characterization of macrophage polarization in *Dnmt3a* depleted BMDMs

Given *Dnmt3a* relevance in the immune response and the importance of macrophages within the pathophysiology of IBD, we next aimed to investigate the impact of *Dnmt3a* during monocyte-to-macrophages differentiation and polarization processes both at protein and mRNA level (Figure 3-6). Secondly, we investigated the functional consequence that *Dnmt3a* deletion on the transcriptome of resting, M2 and M1 macrophages (Figure 3-7, Figure 3-8, Figure 3-9) might have on marker gene expression (Figure 3-10) and morphological reshaping upon polarization and during phagocytosis (Figure 3-11, Figure 3-12), as representation of some of the main macrophagic effector functions during host protection against potential pathogenic particles derived from the gut lumen. As discrimination between M1 and M2 population, some well recognized polarization markers such as Arginase-1 (*Arg-1*) and inducible nitric oxide synthase, (iNos, *Nos2*) were used as M2 and M1 markers respectively, and their enzymatic activity was tested (Figure 3-13).

3.3.1 *Dnmt3a* expression is upregulated in M2 macrophages

Dnmt3a has been linked with T-cell development and polarization [195] [200], cancer progression [201], hematopoietic stem cell differentiation and proliferation [101] [202], aberrant DNA methylation and macrophages polarization [108], defining a central role for *Dnmt3a* in the above-mentioned processes.

To investigate if the lack of *Dnmt3a* might impact on the process of macrophagic polarization, we analyzed DNMT3A, protein expression of wild type BMDM from the day of harvesting to M1 and M2 polarized macrophages for a total of 9 days (Figure 3-6). Along with DNMT3A, protein expression levels of iNOS (M1) and ARG-1 (M2) were analyzed, to confirm BMDM polarization status. DNMT3A protein levels increased only in M2 macrophages in latest time points (day 6, 7, 8, 9), whereas, in M1 macrophages, DNMT3A protein expression remained almost undetectable throughout the entire duration of the time course follow-up.

A predictable increase in iNOS levels was observed as well in later time points in M1 polarized BMDM, while remained almost undetectable compared to M2 control. On the same line, ARG-1 protein expression increased in M2 polarized BMDMs towards the end of the surveilled timeframe, while remaining lower (but clearly detectable) in the M1 counterpart.

From this observation we concluded that DNMT3A protein level is lower in M1 macrophages, while increases in M2 macrophages: consequently, *Dnmt3a* is downregulated upon inflammatory conditions

(M1), while it is upregulated upon homeostatic stimuli (M2), suggesting a role for *Dnmt3a* in *in vitro* BMDM polarization.

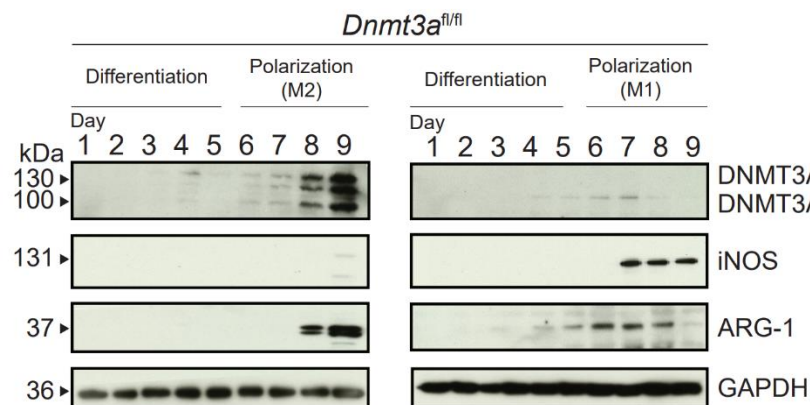


Figure 3- 6: DNMT3A protein expression varies during wild type BMDMs polarization.

Western blot analysis of DNMT3A and the polarization markers ARG-1 (M2) and iNOS (M1) in wild type BMDM along the polarization time course of 9 days. BMDM were harvested from flushed femurs and tibias and cultivated for 5 days in macrophages culture medium supplemented with M-CSF and polarized with cytokines cocktails (M2: IL-4 50ng/ml, IL-13 50ng/ml and M1: LPS 100ng/ml, IFN- γ 50ng/ml) for 4 additional days. 15 μ l of total protein lysates were used and GAPDH served as loading control. ARG-1: Arginase 1. iNOS: inducible nitric oxide synthase. The shown immunoblots are representative of two independent experiments.

3.3.2 Lack of *Dnmt3a* in BMDMs results in a complex transcriptional dysregulation

Dnmt3a is associated with age-dependent defective HSC self-renewal and clonal hematopoiesis [99], [103] and it is frequently mutated in myeloid malignancies [203] [194]. Since macrophages originate from hematopoietic stem cell (HSC), which self-renew and proliferate under strict control mechanisms, and since *Dnmt3a* deficiency in HSC results in increased self-renewal and malignant transformation of hematopoietic stem cells [101], [204], elucidating the role of *Dnmt3a* in macrophages biology will contribute to a better understanding of immune-related pathologies such as IBD.

Based on the observation of an age-dependent HSC defect in self-renewal [205] and on our previous experiment reporting that M1 and M2 polarization statuses are characterized by different DNMT3A expression, we next aimed to understand the functional consequences that the deletion of *Dnmt3a* might induce during the processes of macrophages differentiation and polarization.

To this end, BMDM from young (8-10 weeks old) and old (>34 weeks old) *Dnmt3a*^{fl/fl} and *Dnmt3a*^{LysM} mice were generated, and RNA sequencing analysis was performed on resting, M1 and M2 polarized BMDMs. To have a comprehensive overview on the complex transcriptional signature characterizing each BMDM population, differential gene expression analysis was performed according to genotype, age and polarization status (resting-to-M2, resting-to-M1 and M2-to-M1) (Figure 3-7). The analysis identified 1692 and 480 uniquely differentially expressed genes (DEGs) in young and old *Dnmt3a*-deleted BMDM respectively, compared to *Dnmt3a*^{fl/fl} controls in the comparison resting-M1.

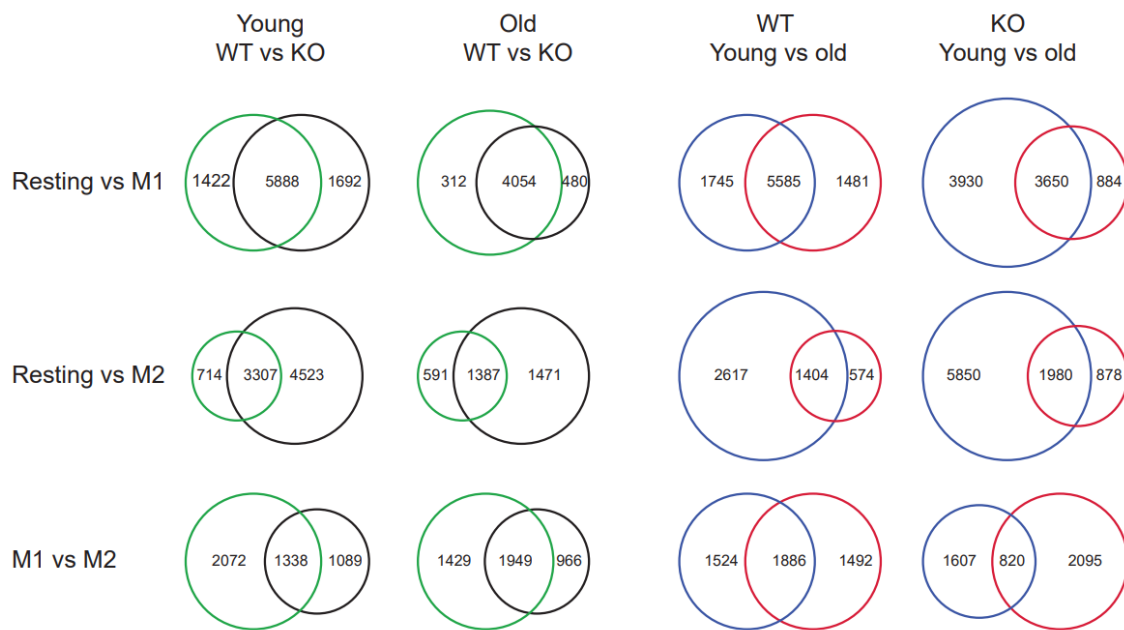


Figure 3- 7: Venn diagrams summarizing unique DEGs in young and old *Dnmt3a*^{fl/fl} vs *Dnmt3a*^{LysM} BMDM.

Graphic representation of the comparison between wild type and *Dnmt3a*-depleted resting vs M1, resting vs M2 and M1 vs M2 macrophages identifies sets of uniquely DEGs in each population. Venn diagrams are summarizing the number of DEGs found in each subset. Only genes found to be significantly differentially expressed were included in the analysis ($p < 0.05$). Venn diagrams are representative for visualization of intersections and set differences found within the different categories.

In the comparison resting-M2, 4523 and 1471 unique DEGs were identified in young and old *Dnmt3a*-deleted BMDM compared to wild type control. Finally, the M1-M2 comparison revealed 1089 and 966 DEGs uniquely for the young and old *Dnmt3a*-ablated group. Similarly, we generated Venn diagrams to visualize the comparison between young and old polarized BMDMs to find 1481 DEGs specific for old wild type and 884 DEGs unique for *Dnmt3a*-ablated BMDMs in the resting versus M1 comparison. When comparing M2 with resting macrophages, we observed 574 and 878 DEGs in old wild type and old *Dnmt3a*-depleted BMDMs, respectively, compared to young control. Finally, the M2-M1

comparison revealed 1492 DEGs specific for old wild type BMDMs and 2095 DEGs for old *Dnmt3a*-depleted BMDMs, compared to young controls.

To have a more comprehensive view on the complex transcriptional variation between the different categories, we generated Venn diagrams to visualize DEGs unique for each polarization category (Figure 3-8). When comparing M2 with resting BMDM, we observed 1079 and 1503 DEGs in wild type and *Dnmt3a*-depleted BMDMs, respectively. Wild type M1 group, compared to resting, had 2375 uniquely DEGs, while *Dnmt3a*-depleted BMDMs was characterized by 943 unique DEGs. In the comparison M1-M2, wild type and *Dnmt3a*^{LysM} mice-derived BMDMs displayed 180 and 64 unique DEGs, respectively.

On the same line, we generated Venn diagrams to visualize the set of unique DEGs in old *Dnmt3a*^{fl/fl} vs *Dnmt3a*^{LysM}-mice derived BMDM. Here, we found 2949 and 1305 unique DEGs in the comparison resting to M1 and 397 and 910 unique DEGs in the comparison resting to M2. When comparing M1 with M2 polarization status, old wild type BMDM revealed 160 unique DEGs while *Dnmt3a*-depleted BMDMs were characterized by 411 unique DEGs. We successively selected the significantly unique top 50 up and down regulated genes (Supplementary Tables 1-12) for each comparison and performed gene ontology (GO) term enrichment analysis within each comparison (Figure 3-9). In the resting versus M2 comparison, GO analysis revealed biological processes typically found in the respective polarization phases, such as *positive regulation of ERK1 and ERK2 cascade*, *Phosphatidylinositol 3-kinase signaling*, and *positive regulation of interleukin 10 production* for M2 polarization status in both wild type and *Dnmt3a*-depleted macrophages.

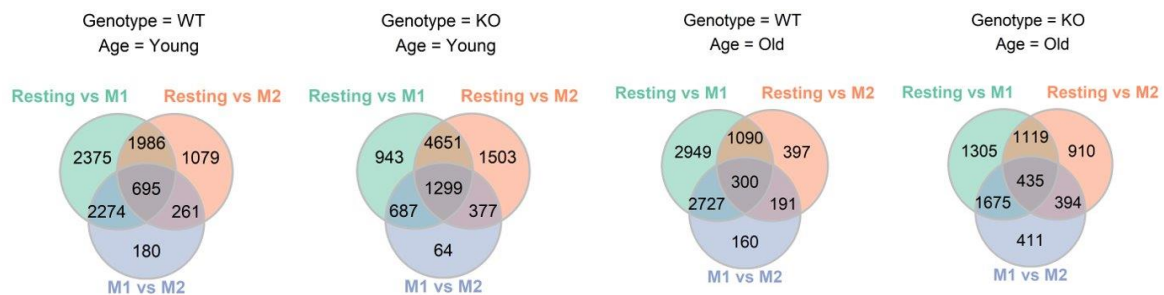


Figure 3- 8: Absence of *Dnmt3a* results in a complex dysregulated transcriptional signature.

Venn diagrams summarizing the subsets of overlapping and unique DEGs transcriptionally dysregulated in resting-M1, resting-M2 and M1-M2 categories, based on genotype and age.

On the same line, in the M1 comparison versus resting macrophages, characteristic M1-related biological processes such as *positive regulation of tumor necrosis factor production* were found, confirming the typical pro-inflammatory molecular signature of M1 activation. Intriguingly, in the

comparison resting versus M1, biological processes such as *positive regulation of nitric oxide biosynthetic process* and *positive regulation of phagocytosis* (strongly associated with the M1 phenotype) were found not only in wild type M1 macrophages, but also in *Dnmt3a*-ablated macrophages in the comparison resting versus M2, in both young and old datasets. Additionally, *positive regulation of NF-κB transcription factor activity* was found in both M1 and M2 *Dnmt3a*^{LysM} macrophages (Figure 3-9).

These observations although confirming, in part, the canonical M1-M2 molecular phenotype of polarized macrophages, revealed for *Dnmt3a*^{LysM} macrophages a concomitant M1 and M2 signature. We therefore hypothesize that lack *Dnmt3a* does not only results in a complex transcriptional dysregulation, but also that *Dnmt3a* might have a central role in orchestrating multiple metabolic pathways which are disbalanced during macrophages polarization upon *Dnmt3a* loss. Instructed by these results, we next aimed to investigate whether the observed co-existing M1-M2 phenotype observed *in silico*, could translate in an *ex vivo* functional consequence affecting the major macrophages effector functions *in vitro*.

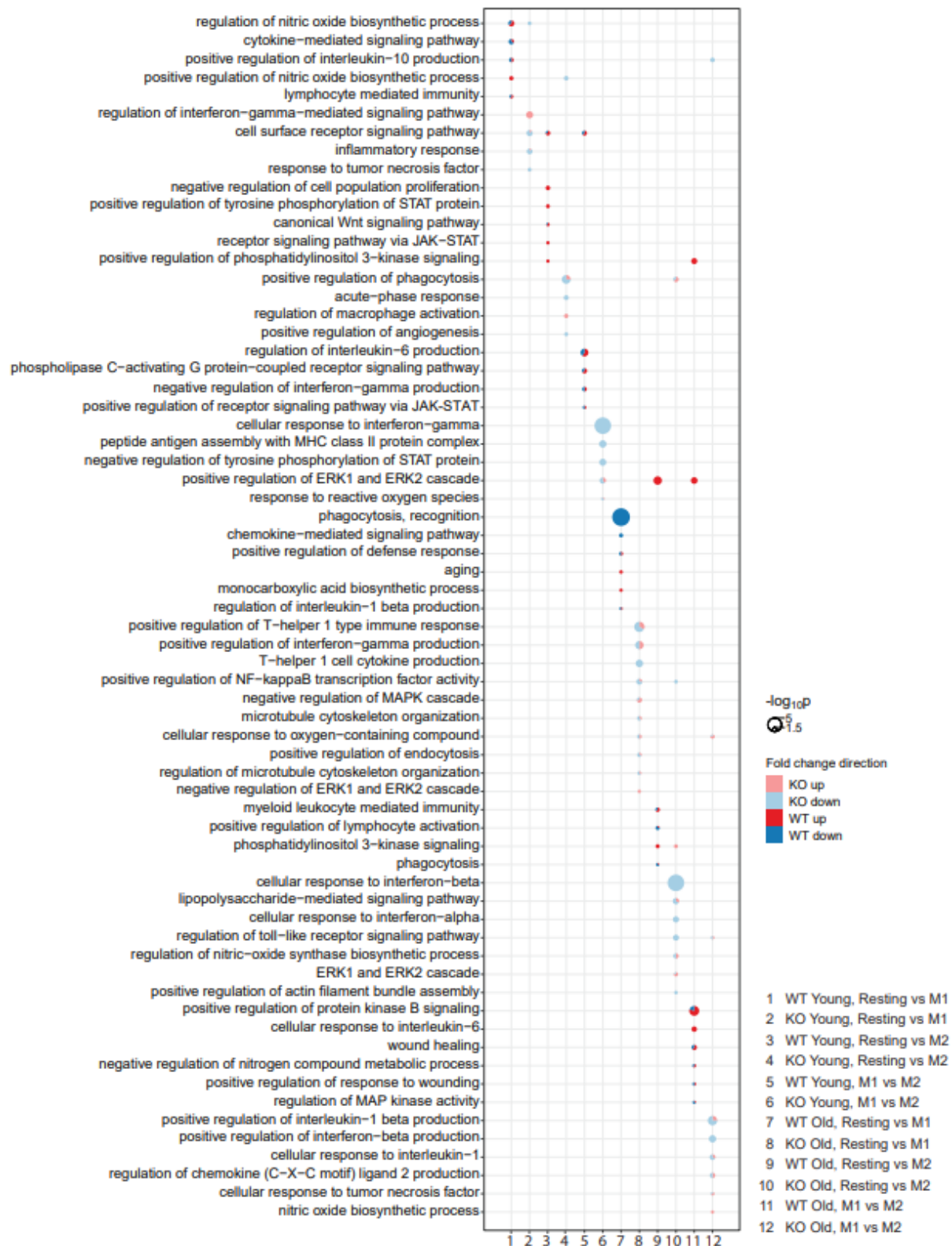


Figure 3- 9: GO enrichment analysis for the 50 most up- and downregulated genes between resting-M1, Resting-M2 and M1-M2 for young and old wild type vs *Dnmt3a*^{LysM} BMDM.

GO term analysis reporting 5 selected representative biological processes for each comparison. The size of the dot is proportional to the significance of the term where bigger dots represent higher significance. Each dot is a pie chart consisting of the significant genes annotated to the corresponding GO term.

3.3.3 Lack of *Dnmt3a* results in impaired expression of polarization marker genes

We next validated the expression of M1 and M2 defining marker genes for each polarization group by measuring mRNA expression level of representative polarization marker genes. Along with *Arg-1*, *Retnla* (M2 markers) and *Tnf*, *Irg-1* (M1 markers), mRNA levels of *Dnmt3b* were measured to investigate whether the lack of *Dnmt3a* might result in compensatory up or down regulation of other Dnmts (Figure 3-10a).

We first confirmed that *Dnmt3a* RNA expression was downregulated in wild type M1 macrophages and upregulated in M2 wild type macrophages (Figure 3-10b), as reported in our previous findings (chapter 3.3.1), indicating an inflammatory environment-driven downregulation of *Dnmt3a*. Expression levels of *Dnmt3a* mRNA from wild type BMDMs followed the expression levels of DNMT3A protein reported in Figure 3-6 and correlated with the M1-M2 phenotype marked by iNOS and ARG-1 respectively.

Arg-1 mRNA expression levels resulted to be upregulated in both *Dnmt3a*^{fl/fl} and *Dnmt3a*^{LysM} M2 BMDMs at 96h compared to time 0 (Figure 3-10c). Of note, *Arg-1* was significantly more expressed in *Dnmt3a*-depleted M2 BMDM at 96h compared to BMDM expressing *Dnmt3a*.

On the same line, *Retnla* expression levels were upregulated in 96h M2 polarized *Dnmt3a*^{fl/fl} and *Dnmt3a*^{LysM} BMDMs compared to time 0. Interestingly, *Retnla* transcript resulted to be slightly, but significantly, less expressed in *Dnmt3a*-depleted M2 BMDM at 96h (Figure 3-10d). These results confirmed the specificity of *Arg-1* and *Retnla* as M2 markers.

Tnf, was uniformly expressed in almost all compared groups (Figure 3-10e), with exception of M1 *Dnmt3a*^{fl/fl} and *Dnmt3a*^{LysM} macrophages polarized towards M1 at 96h, confirming their specificity for the M1 population. *Tnf* mRNA levels were significantly higher in *Dnmt3a*^{LysM} compared to *Dnmt3a*^{fl/fl} at 96h. The same trend was observed for *Irg-1* (Figure 3-10f) that was more expressed in M1 *Dnmt3a*^{LysM} BMDMs compared to *Dnmt3a*^{fl/fl} at 96h. Interestingly, *Irg-1* mRNA expression at 96h was increased as well in *Dnmt3a*^{LysM} BMDMs compared to *Dnmt3a*^{fl/fl} when comparing M2 BMDMs at 96h, suggesting an unbalanced M2 polarization, with a tendency towards M1 polarization.

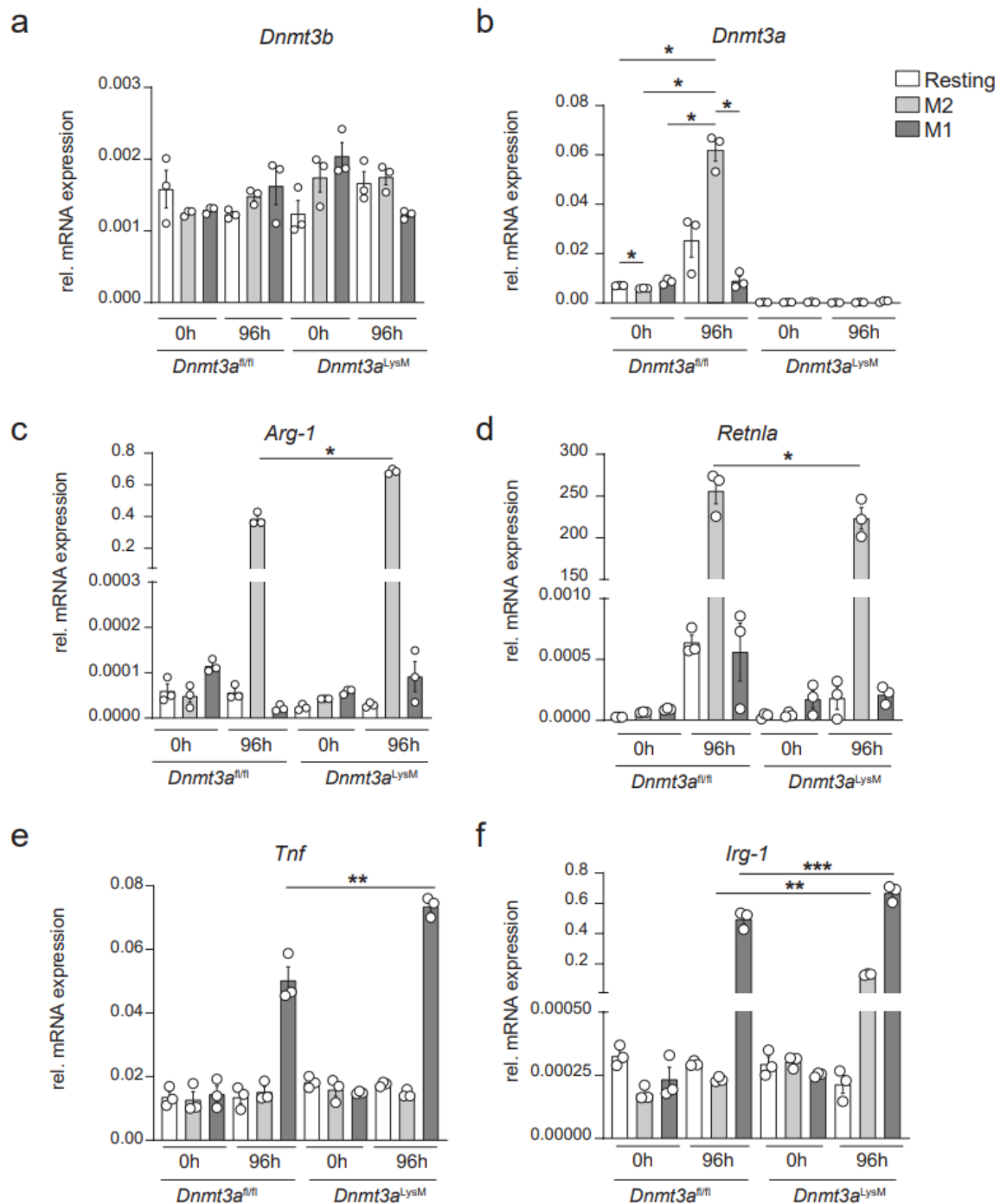


Figure 3- 10: Lack of *Dnmt3a* leads to impaired polarization marker genes expression.

Relative mRNA quantification of (a) *Dnmt3b*, (b) *Dnmt3a*, (c) *Arg-1*, (d) *Retnla*, (e) *Tnf* and (f) *Irg-1* transcripts. BMDMs from *Dnmt3a^{fl/fl}* and *Dnmt3a^{LysM}* mice were cultivated for 5 days in presence of the differentiation factor m-CSF. BMDMs were subsequently polarized in vitro for 96h by addition in culture medium of IL-4 (50ng/ml) and IL-13 (50ng/ml) for M2, and LPS (50 ng/ml) and IFN γ (50ng/ml) for M1. *Actb* was used as housekeeper gene for normalization. *Arg-1*: Arginase 1; *Irg-1*: immune-responsive gene 1, *Tnf*: tumor necrosis factor; *Retnla*: resistin like alpha. Data represents mean \pm SEM. Statistical significance was calculated using one-way Anova followed by Dunnet's test for multiple comparisons. Shown data are representative for n=3 biological replicates. *p<0,0332, **p<0,0021, ***p<0,0002 ****, p<0,0001.

These experiments together concluded that *Dnmt3a* expression levels vary significantly accordingly to the polarization status of macrophages. In particular, *Dnmt3a* mRNA expression levels increase in 96h *in vitro* polarized M2 macrophages, supporting the hypothesis that *Dnmt3a* is central in the maintenance of homeostasis, and its expression is suppressed upon inflammation.

Concluding, we could therefore hypothesize a role for *Dnmt3a* within macrophages polarization and suggest functional implication of the lack of *Dnmt3a* in perturbing the molecular phenotype of differently polarized macrophages during of inflammatory and homeostatic conditions.

3.3.4 Lack of *Dnmt3a* affects cytoskeletal rearrangement

GO term enrichment analysis performed on resting, M1 and M2 wild type and *Dnmt3a*-depleted *in vitro* polarized BMDMs, revealed for most of the comparison a recurrent GO term: *cytoskeletal rearrangement*. Reorganization of cytoskeleton is a fundamental for macrophages plasticity. Due to their multifaced involvement within different biological processes, a hallmark of macrophages is to fast react to changing microenvironment. Macrophages undergo drastic cytoskeletal changes during processes such as activation, migration, or phagocytosis. In a conventional scenario, M2 macrophages assume an elongated spindle-like shape resembling fibroblast-like cellular morphology while M1 macrophages are characterized by a highly reactive rounded and compact cellular morphology.

To study the impact of *Dnmt3a* deletion on macrophage polarization-driven cytoskeletal reshaping, BMDM were obtained from *Dnmt3a^{fl/fl}* and *Dnmt3a^{LysM}* mice and polarized *in vitro*. Their morphology was microscopically analyzed using fluorescence microscopy on day 9 of polarization (Figure 3-11a, Figure 3-11b). Wild type resting macrophages exhibited a slightly elongated morphology, that resembles the homeostatic “resting” shape of inactive macrophages (Figure 3-11a upper panel, left). *Dnmt3a^{LysM}* mice-derived resting macrophages on the other hand, displayed increased proportions of rounded cells already at baseline, resting condition, resembling the M1 activation status (Figure 3-11a lower panel, left). As expected, wild type macrophages polarized towards M2 status had a physiological, spindle-like, elongated morphology (Figure 3-11a upper panel, middle) while M1 counterpart mainly assumed a flat, rounded cell morphology (Figure 3-11a upper panel, right). Noticeably, BMDM lacking *Dnmt3a* and polarized in the M2 status displayed a disorganized cellular architecture and failed to assume the typical M2-defining elongated cellular morphology (Figure 3-11a lower panel, middle), that in contrast is well maintained in wild type M2 macrophages.

Taken together, these results show a failure in morphological lengthening of *Dnmt3a*-depleted BMDMs during *in vitro* M2 polarization, hence, producing a morphologically disorganized population of macrophages interspersed with rounded M1-like cells.

Thus, a potential underlying M1-like pro-inflammatory polarization phenotype might be the result of *Dnmt3a* depletion. Also, these observations support the hypothesis of a role for *Dnmt3a* in orchestrating architectural re-adaptation during M2 macrophages polarization.

a

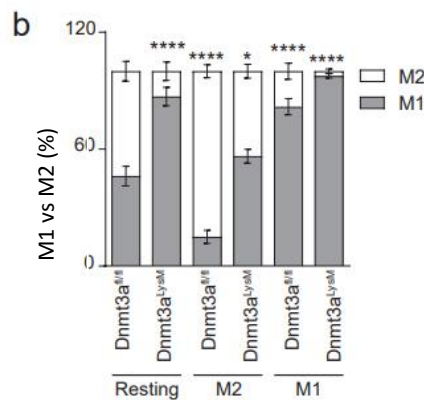
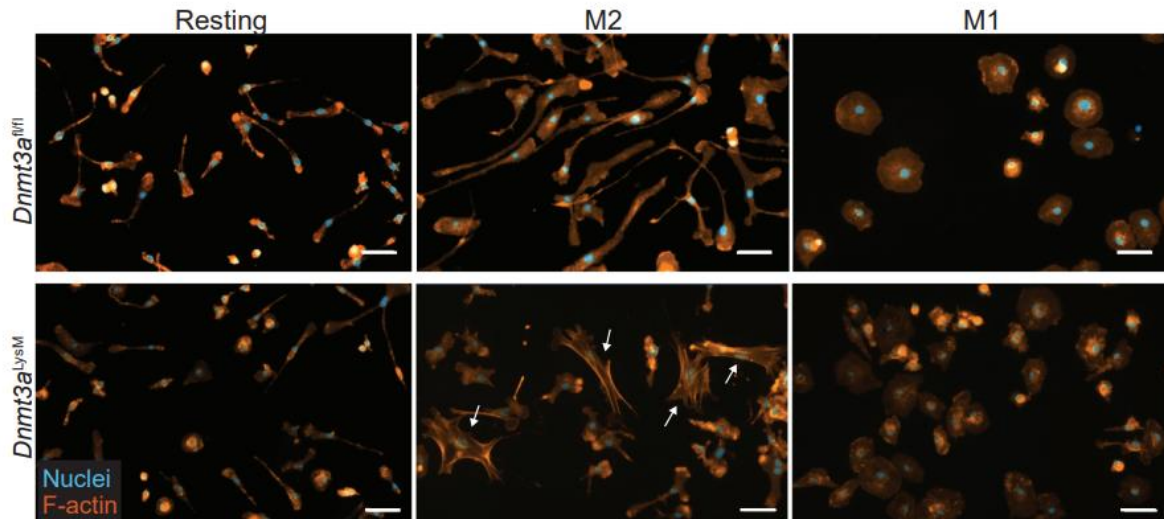


Figure 3-11: *Dnmt3a*-null BMDM undergo cytoskeletal organization towards M1 phenotype and display improper M2 phenotype.

(a) Representative fluorescent photomicrographs depicting BMDM cytoskeleton of macrophages generated from wild type and *Dnmt3a*^{LysM} mice and polarized *in vitro* for 96h. Upper panel from left to right depicts resting, M2 and M1 wild type macrophages. Lower panel, in the same order, depicts *Dnmt3a*^{LysM}-derived resting, M2 and M1 BMDM. Phalloidin (dark orange) and DAPI (light blue) were used to visualize F-actin filaments and nuclei, respectively. Scale bar: 20μm. (b) Quantification of M1 and M2 population based on canonical cellular morphology (M1: rounded, compact; M2: elongated, spindle-like). A minimum of 10 optic fields were analyzed per n=3 technical replicates, and n=5 biological replicates. Statistical significance was calculated using two-way Anova. **p*<0,0332, **** *p*<0,0001.

Exploring whether this could be a consequence of failing cytoskeletal reorganization during M2 programming or the result of a preference for M1 polarization (despite the homeostatic environment) would provide further insight of *Dnmt3a*'s impact on macrophage polarization and consequent functionality.

3.3.5 Loss of *Dnmt3a* impairs phagocytosis

Given (i) the evidence supporting an altered molecular phenotype of polarized macrophages upon lack of *Dnmt3a* and (ii) the observation of a dysregulated cytoskeletal rearrangement in *Dnmt3a*-null M2 BMDM, we generated and polarized macrophages from 8-10 and >34 weeks old *Dnmt3a^{fl/fl}* and *Dnmt3a^{LysM}* animals, to study the impact of *Dnmt3a* and age on macrophagic phagocytosis ability *in vitro* (Figure 3-12). Phagocytic capacity was assessed on resting and *in vitro* polarized macrophages. BMDMs were exposed for 3h to pre-fluorescently labeled Green Zymosan particles supplemented to culture medium. To quantify the phagocytosed particles, flow cytometry was used to assess the percentages of engulfed green zymosan on the total of viable cells (Figure 3-12a).

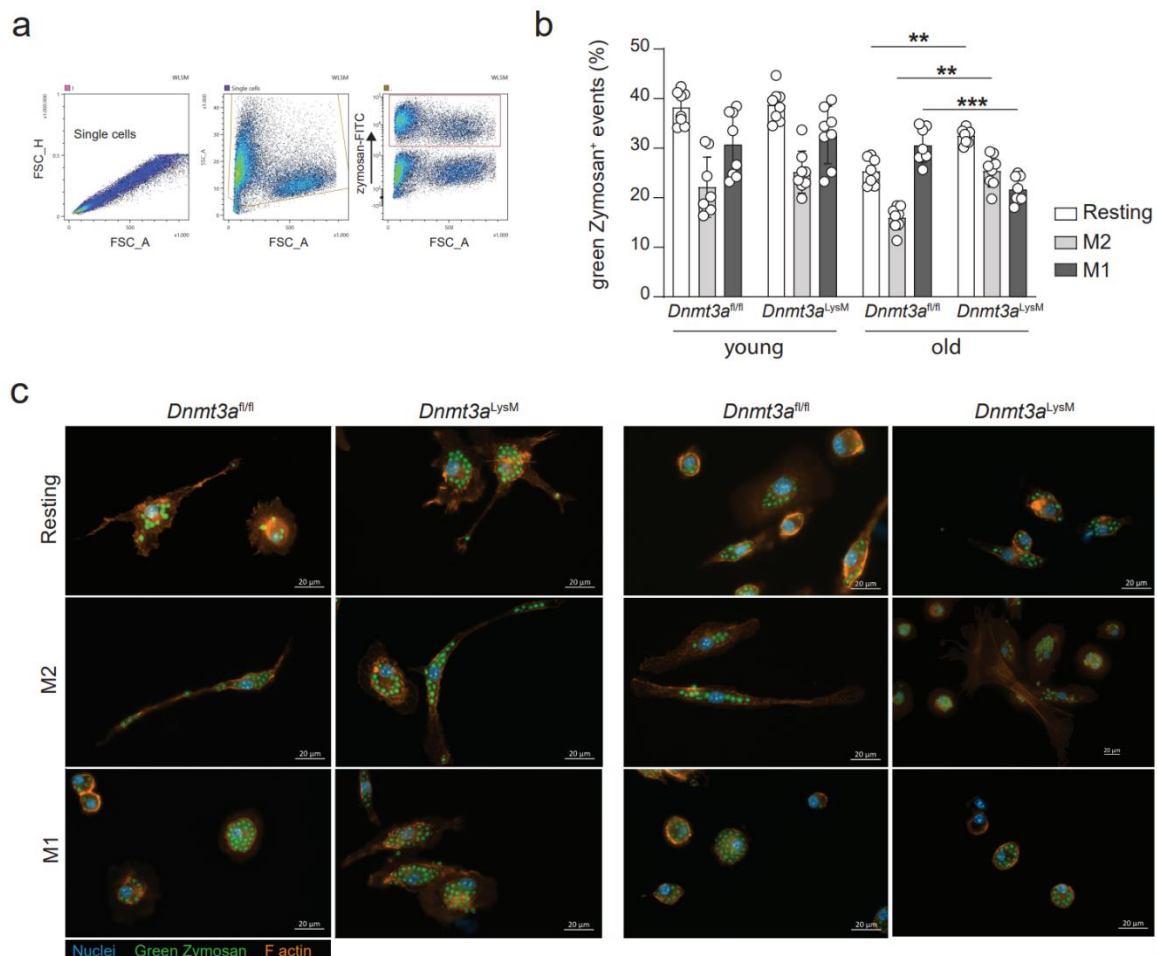


Figure 3-12: Lack of *Dnmt3a* results in increased phagocytotic ability of M2 BMDMs and decreases it in M1 BMDMs.

(a) Representative gating workflows depicting doublets and debris exclusion and FITC positive events gating. (b) Abundance (depicted as percentages) of green zymosan positive events in young and old resting, M2 and M1 populations measured through flow cytometry (n=8 per genotype/polarization/age group). Percentages represents positive FITC events on the total viable population. (c) Representative Immunofluorescent photomicrographs of resting and M1-M2 polarized BMDM generated from young and old *Dnmt3a^{LysM}* and *Dnmt3a^{fl/fl}* mice. BMDM growth medium was implemented with fluorescently stained Zymosan particles for 3 hours to allow engulfment. Nuclei, cytoskeleton and Zymosan particles are depicted in blue, dark orange and green, respectively. Data shown (b) are representative for n=5 independent experiments and represent mean \pm SEM. Statistical significance was calculated using two-way Anova followed by Tukey's correction test for multiple comparisons. **p<0,0021, ***p<0,0002.

Macrophages belonging to the wild type and *Dnmt3a*-depleted 10 weeks-old group maintained the same engulfing capacity between resting and M2 population (Figure 3-12b, Figure 3-12c), and displayed higher positive events counts in the M1 population.

As a general concept, M1 macrophages are more prone to phagocytosis compared to M2: resting macrophages on the same line, due to their *naïve* status, activate upon encounter with foreign particles, therefore quickly evolving into a highly responsive and phagocytic population, consistent with the M1 phenotype.

BMDM derived from older mice on the other hand, had an overall decreased phagocytic capacity. We observed increased percentages of engulfed Zymosan particles in resting *Dnmt3a*-depleted BMDMs compared to control. When polarized into the M2 status, *Dnmt3a*^{LysM} BMDMs revealed higher percentages of positive green Zymosan events, while the M1 population phagocytized less Zymosan particles compared to the wild-type control. The increased Zymosan positive events rates that we measured for old, *Dnmt3a*-depleted M2 BMDM support the hypothesis of a subtle but effective perpetuation of an M1-like activation status, which translates in higher phagocytic activity. Controversially, the diminished phagocytic capacity of old *Dnmt3a*-knock out macrophages compared to wild type M1, at the same time suggests an attenuation of the M1 status upon lack of *Dnmt3a*.

These results taken together strongly points toward a decisive role of *Dnmt3a* within macrophages polarization, cytoskeletal re-arrangement, and phagocytosis. We therefore hypothesize an involvement of *Dnmt3a* in the regulation of transcription of genes involved in cytoskeleton reshaping upon polarization and phagocytosis process.

3.3.6 *Dnmt3a* contributes to arginine metabolism-dependent macrophage polarization

Polarization of macrophages towards M1 or M2 occurs accordingly to the activities of the arginase (ARG) and nitric oxide synthase (NOS) enzyme families [183], [185], [206]. ARG catalyzes the final step of the urea cycle, resulting in the conversion of arginine to urea and ornithine. This enzyme participates in multiple anti-inflammatory reactions such as tissue repair [206]–[208]. On the other hand, during M1 response, inducible nitric oxide synthase (iNOS) generates nitric oxide (NO) species with anti-proliferative effects which are necessary for protection against pathogens and aberrant cells.

To investigate the role of *Dnmt3a* in arginine metabolism and macrophages polarization, ARG and NOS activity levels were measured on resting, M1 and M2 BMDMs generated from 10 and >34 weeks old *Dnmt3a*^{fl/fl} and *Dnmt3a*^{LysM} mice (Figure 3-13).

Arginase activity was measured by chemically inducing the arginine-to-ornithine/urea production *in vitro* (Figure 3-13a) while NOS activity was measured by assessing the amount of nitrite present in

each sample and intended as amount of enzyme required to yield 1 μmol of nitric oxide/minute at 37° (Figure 3-13b).

Comparable levels of arginase activity were observed in all resting populations (both young, old, *Dnmt3a^{fl/fl}* and *Dnmt3a^{LysM}* macrophages). This analysis revealed an (expected) increased arginase activity in M2 macrophages in both young wild type and *Dnmt3a^{LysM}* mice-derived macrophages. Higher arginase activity is in fact (as extensively described in chapter 1.7) a preponderant feature of M2 macrophage polarization. Controversially, old mice-derived *Dnmt3a* depleted M2 macrophages, revealed a significant decreased arginase activity compared to old M2 BMDMs. As controversially, we observed increased levels of arginase activity in old, *Dnmt3a* knock-out M1 macrophages.

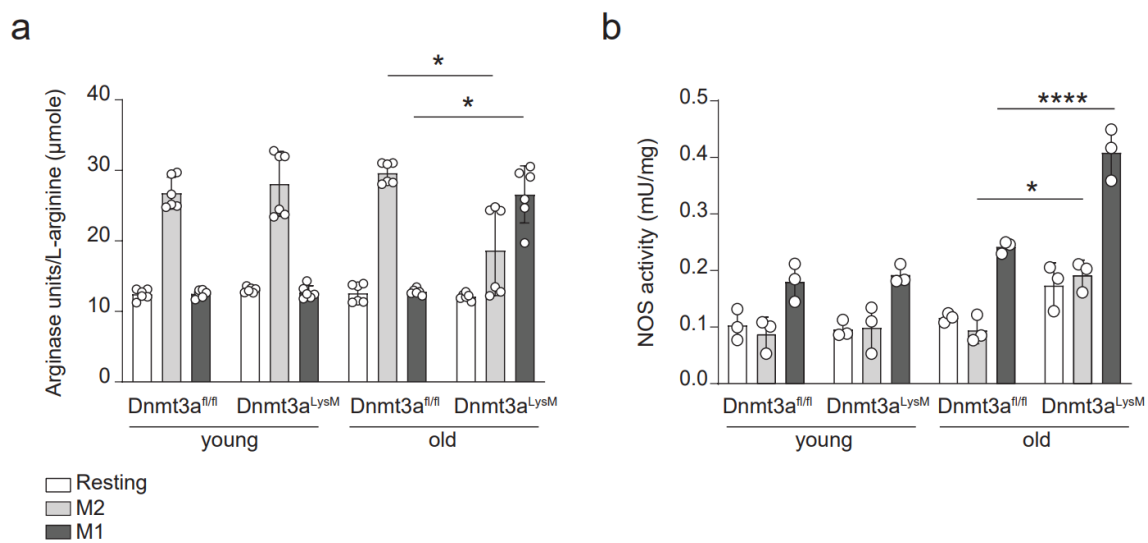


Figure 3-13: Arginase and nitric oxide synthase activity is dysregulated in old *Dnmt3a^{LysM}* mice.

(a) Arginase activity assay performed on *Dnmt3a^{fl/fl}* and *Dnmt3a^{LysM}* mice-derived *in vitro* polarized BMDM (n=6 biological replicates over two independent experiments). Arginase enzymatic activity was measured by providing macrophages with pre-determined arginine substrate and allowing the reaction to take place for two hours. Units/L: amount of enzyme converting 1 μmol L-arginine in ornithine and urea per minute at pH 9.5, 37°C. (b) NOS enzymatic activity performed on *Dnmt3a^{fl/fl}* and *Dnmt3a^{LysM}* mice-derived *in vitro* polarized BMDM (n=3 biological replicates). A series of chemical conversions allowed the reaction with Griess reagents to generate a colored product with absorbance at OD 540 nm. 50 to 200 μg of total cell lysate were used as input material. Statistical significance was calculated using two-way Anova with Dunnett's multiple comparison test. *p<0,0332, ****p<0,0001

On the same line, an expected increased NOS activity was present all M1 populations, with a slight increase in old M1 wild type and with even (significantly) greater extent in old *Dnmt3a*-depleted macrophages. Resting and M2 macrophages derived from young and old *Dnmt3a^{fl/fl}* and *Dnmt3a^{LysM}* mice, and resting and M2 BMDMs derived from old *Dnmt3a^{fl/fl}*, displayed similar levels of NOS activity in all groups. Resting and M2 old *Dnmt3a*-null BMDMs, showed higher levels of NOS activity,

suggesting NOS pathway activation despite the absence of M1 polarizing cytokine cocktail, supporting the hypothesis that lack of *Dnmt3a* results in an M1-like phenotype in an age-dependent manner. Taken together, these results reveal, specifically in old *Dnmt3a*^{LysM} mice-derived macrophages, an exacerbation of the M1 phenotype (augmented NOS activity). Also, lower levels of arginase activity in old *Dnmt3a*-depleted M2 population (compared to old *Dnmt3a*^{fl/fl} control BMDMs) suggest the concomitant coexistence of both M1 and M2 phenotypes. This resumes in an essential role of *Dnmt3a* in determining the arginine metabolic direction, which translates in a dysregulated metabolic polarization signature that favours M1 polarization status.

3.4 *Dnmt3a* in the immuno-epithelial interplay

Promoting tissue regeneration and resolution of inflammation is a key feature of macrophages in a healthy system [209], [210]. To elucidate the role of *Dnmt3a* in macrophages during wound repair, we established an in vitro co-culture system consisting of Mode-K cells, on which a “wound” was inflicted utilizing fixed inserts of known dimensions. Mode-K cells were firstly cultivated in presence of resting *Dnmt3a*^{fl/fl} and *Dnmt3a*^{LysM} macrophages (Figure 3-14). In a second experiment, the cells were co-cultivated with M1 or M2 macrophages, polarized *a priori* in membranous well inserts (Figure 3-15). Finally, a co-culture system of C57BL/6- and APC^{min} derived intestinal organoids and macrophages was set up to investigate the contribution of *Dnmt3a* on healthy and tumor-derived intestinal epithelium proliferation (Figure 3-16).

3.4.1 *Dnmt3a* expression is beneficial for wound healing *in vitro*

To study the ability of *Dnmt3a*-depleted macrophages in promoting tissue regeneration in response to mechanical wounding, Mode-K cells were seeded in silicon inserts and let grow until confluency. Once the cells covered the entire area of the two reservoirs, the inserts were removed, generating a gap. Immediately after gap generation, Mode-K cells were co-cultivated in presence of resting wild type and *Dnmt3a*-depleted BMDMs that were previously accommodated in membranous inserts as illustrated in Figure 3-14a.

Gap area (Figure 3-14b) was measured after 36 hours (Figure 3-14c). Exposure of Mode-K cells to wild-type resting BMDMs, resulted in an almost complete coverage of the gap (wound) after 36h. Co-culture with *Dnmt3a*^{LysM} BMDMs resulted in less gap coverage, which meant a decreased proliferation of Mode-K cells and increased gap area compared to *Dnmt3a*^{fl/fl} derived BMDM -Mode-K co-culture. These results suggest a direct genotype-dependent effect of *Dnmt3a* in macrophages within epithelial proliferation already in resting conditions.

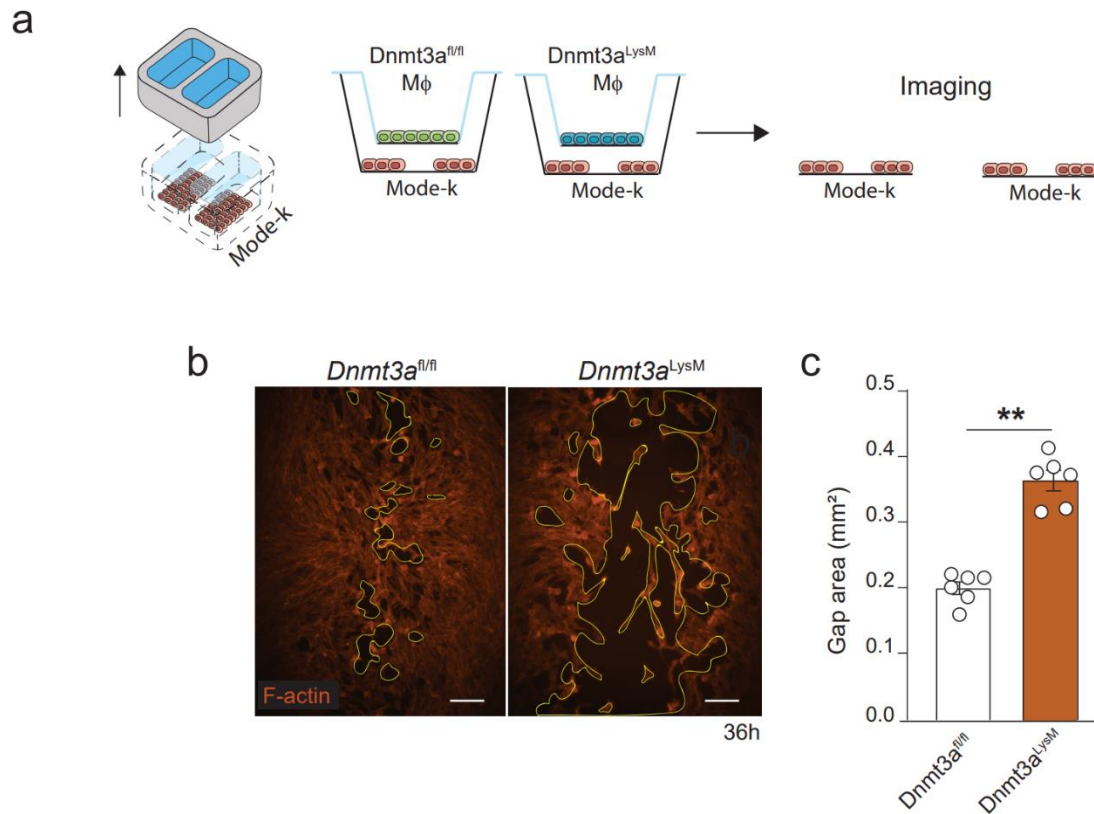


Figure 3-14: *Dnmt3a* promotes IEC monolayer regeneration after wounding.

(a) Schematic representation of the wound healing assay where two-reservoirs inserts with Mode-K cells were cultured (left) and the subsequent exposure to resting *Dnmt3a^{fl/fl}* and *Dnmt3a^{LysM}* macrophages by placing a transwell insert on top of the culture well for 36h. Mode-K cells were cultivated in inserts (30.000 cells/reservoir) until confluency. BMDM were cultivated for 5 days in presence of m-CSF (20ng/ml) and combined with confluent Mode-K culture immediately after inserts removal. (b) fluorescent photomicrographs of Mode-K cells after 36h wound healing assay in co-culture with *Dnmt3a^{fl/fl}* control (left) or *Dnmt3a^{LysM}* (right) resting BMDMs. F-actin is depicted in dark orange. (c) Wound closure quantification after wounding and co-culture establishment. Data point represent the average of n=3 technical replicates for n=6 biological replicates over three independent experiments. Statistical significance was calculated using nonparametric student's t-test followed by Mann Whitney test. **p<0,0021.

We have previously shown that lack of *Dnmt3a* impairs macrophagic polarization promoting a M1 like phenotype. Therefore, we further investigated the functional consequence of this impaired polarization effect on tissue regeneration upon wounding. To this end, co-culture including M1 and M2 macrophages was established (Figure 3-15a).

In the previous set up (Figure 3-14), the co-culture of Mode-K cells with *Dnmt3a*-depleted macrophages resulted in delayed wound closure compared to *Dnmt3a^{fl/fl}* control BMDM-Mode-K co-culture. We therefore included M1-M2 polarized BMDMs in the co-culture system (Figure 5-15a) and measured wound closure after 36h of co-culture (Figure 3-15c). *Dnmt3a^{fl/fl}* M2 macrophages allowed almost complete wound closure (Figure 3-15b, upper left). Co-culture with M1 *Dnmt3a^{fl/fl}* macrophages on the other hand resulted in partial confluency (Figure 3-15b, upper right). On the

contrary, Mode-K cells co-cultivated in presence of M2 *Dnmt3a*-depleted macrophages resulted in less wound closure rates compared to *Dnmt3a*^{fl/fl} M2 BMDMs, (Figure 3-15b, lower left) and an exacerbated missed wound closure when comparing the M1 subtypes (Figure 3-15b, lower right).

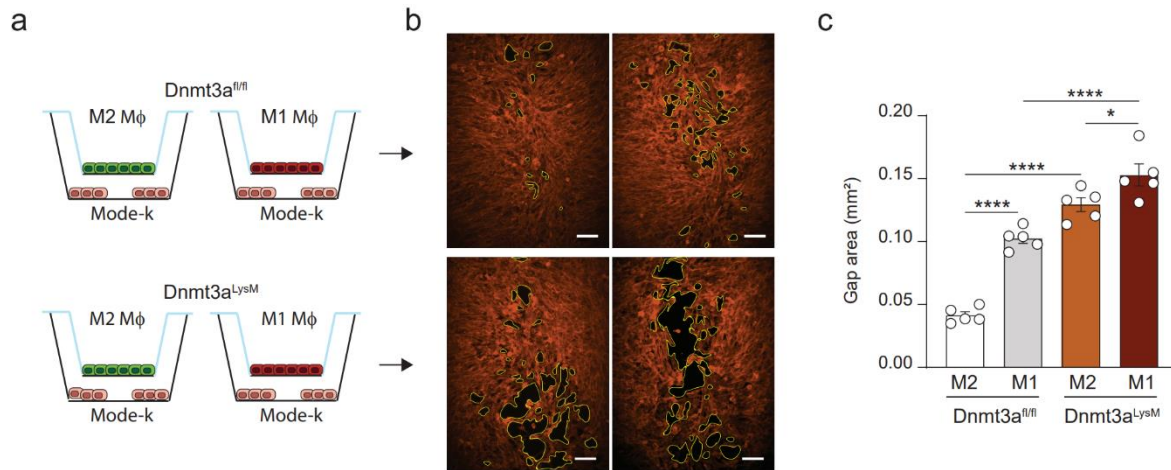


Figure 3-15: Lack of *Dnmt3a* in M2 macrophages results in less tissue proliferation.

(a) Schematic representation of experimental set up. Mode-K cells were cultivated until confluency using inserts consisting of two reservoirs separated by a separator creating a 500µm gap upon removal. After insert removal, cells were cultivated in presence of M2 and M1 macrophages for 36h and Mode-K cellular proliferation was quantified by mean of wound area measurement. (b) Representative photomicrographs depicting Mode-K gap closure after 36h of co-culture with M1 (upper and lower panels, right) and M2 macrophages (upper and lower panel, left). (c) Gap area measurement after 36h of co-culture. Data shown represents mean ± SEM over two independent experiments. Statistical significance was calculated with one-way Anova with Tuckey's test for multiple comparison. *p<0,0332, and ****p<0,0001.

Overall, these observations suggest that the lack of *Dnmt3a* in resting macrophages affects cellular proliferation of co-cultured monolayers of Mode-K cells. In addition, *Dnmt3a* genetic absence in M1 macrophages inhibit Mode-K cell monolayer proliferation to an even greater extent, compared to M1 BMDM expressing *Dnmt3a*. Thus, *Dnmt3a* in macrophages might be central during tissue proliferation, and its lack might as well result in a spontaneous M1-like epithelial-immune signaling and unbalanced M2 resolatory phenotype.

3.4.2 *Dnmt3a* suppresses tumor-derived epithelium proliferation

As reported previously (refer to chapter 3.3, Figure 3-6, Figure 3-10), the lack of *Dnmt3a* in the myelomonocytic lineage is responsible for defective macrophage polarization. M1 activity inhibits cell proliferation and causes tissue damage, while M2 activity promotes cell proliferation and tissue repair [209]. We therefore combined intestinal epithelial cells and macrophages in a co-culture model to assess a potential involvement of *Dnmt3a* within tissue proliferation of intestinal epithelial cells *ex vivo*. Since a class of M2 macrophages, the so-called tumor associated macrophages (TAM), promotes

tumor development [211], we implemented our co-culture model with monolayers generated from intestinal organoids derived from wild type (C57BL/6) and APC^{min} mice that spontaneously develop tumors in the intestine.

Since expression of *Dnmt3a* in macrophages promotes intestinal cells proliferation, I concluded this chapter with *in vitro* investigation aiming to assess if this effect could also contribute to intestinal epithelial tumor formation. To gather further insight on *Dnmt3a*-dependent tissue proliferation, *in vitro* polarized *Dnmt3a*^{fl/fl} and *Dnmt3a*^{LysM} macrophages were cultivated with C57BL/6 (Figure 3-16a). and APC^{min}-derived intestinal organoids (Figure 3-16b).

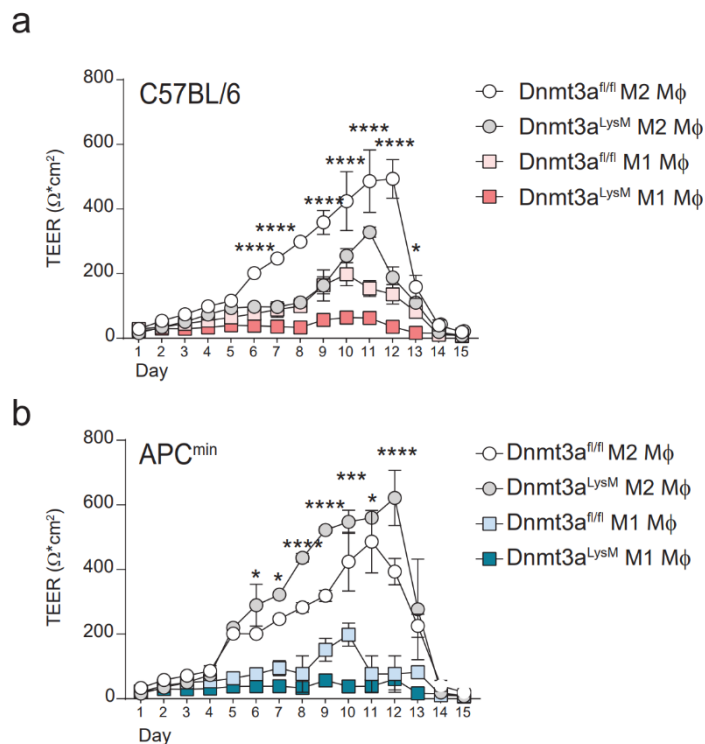


Figure 3-16: *Dnmt3a* expression in M2 polarized BMDMs is required to induce IEC proliferation and promotes IEC-derived tumorous cell expansion.

(a) TEER measurements of C57BL/6-*Dnmt3a*^{fl/fl}/*Dnmt3a*^{LysM} resting, M1, and M2 macrophages co-culture. Single cells suspensions were seeded on porous membrane inserts and cells were cultivated in presence of polarized macrophages from *Dnmt3a*^{fl/fl} mice *Dnmt3a*^{LysM}. (b) TEER measurements of APC^{min} *Dnmt3a*^{fl/fl}/*Dnmt3a*^{LysM} resting, M1, and M2 macrophages co-culture. Data shown are representative for n=3 independent experiments. Statistical significance was calculated using two-way Anova followed by Tukey's correction test. *p<0,0332, ****p<0,0001.

Transepithelial electrical resistance (TEER) measurement was assessed to monitor monolayers integrity and therefore their proliferative status. Single cell layers of intestinal cells from C57BL/6- and APC^{min} mice were seeded onto porous wells inserts and combined with BMDM obtained from *Dnmt3a*^{fl/fl} and *Dnmt3a*^{LysM} previously cultivated and polarized *in vitro*. TEER was monitored for two weeks after the establishment of the co-culture. Intestinal C57BL/6-derived monolayers co-cultivated

with M2 *Dnmt3a*^{fl/fl} macrophages displayed a significantly higher TEER compared to the ones cultivated in presence of *Dnmt3a*^{LysM}-derived M2 macrophages, proving that (i) wild type M2 macrophages (as expected) promote wild type epithelial proliferation and that (ii) *Dnmt3a* is involved in not only correct M2 polarization but as well in the successive physiological activity of macrophages polarization, such as tissue proliferation.

As assumed, co-culture with *Dnmt3a*^{LysM}- M1 macrophages revealed a tragic effect on monolayer growth, as displayed by the low TEER value indicative of absence of monolayer formation, in both *Dnmt3a*^{fl/fl} and *Dnmt3a*^{LysM} M1 macrophages/C57BL/6 derived epithelium co-cultures (Figure 3-16 a). Co-culture of APC^{min} derived intestinal epithelial cells with *Dnmt3a*^{fl/fl} and *Dnmt3a*^{LysM}-mice-derived M2 BMDM resulted in a significant increase of TEER (Figure 3-16b). M2 macrophages lacking *Dnmt3a* however, provoked a drastic increase in tissue proliferation compared to *Dnmt3a*^{fl/fl} M2 DMBMs. M1 *Dnmt3a*-depleted macrophages on the other side, did not allow monolayer formation.

Taken together, these data reveal a role for *Dnmt3a* in directing macrophage M1/M2 polarization. Loss of *Dnmt3a* results in imbalanced M1-M2 polarization status, compromising the function of macrophages on promoting or delaying tissue regeneration. Indeed, *Dnmt3a* deficient M2 macrophages are not capable of promoting monolayer formation *in vitro*, suggesting a defect in promoting tissue regeneration upon damage. We therefore hypothesized *Dnmt3a* to be beneficial in the process of resolution of inflammation and tissue proliferation upon mechanical insult. Furthermore, we observed a drastic contribution of wild-type *Dnmt3a* in M2 macrophages in promoting monolayer formation compared to *Dnmt3a*^{LysM} M2 macrophages. On the contrary, lack of *Dnmt3a* in M2 macrophages resulted in promotion of tumor-derived monolayer formation, compared to wild-type M2 macrophages, suggesting an involvement of *Dnmt3a* in suppressing tumor formation.

3.5 *Dnmt3a*^{LysM} mouse model characterization

To study the role of *Dnmt3a* in the myeloid lineage during homeostasis and inflammation *in vivo*, we characterized the phenotype of *Dnmt3a*^{-LysM} mouse model. The conditional mouse model was characterized at baseline conditions (young and aged animals) and upon inflammatory conditions using intestinal inflammation *in vivo* models.

3.5.1 *Dnmt3a*^{LysM} mice: an age-dependent spontaneous phenotype

Following the confirmation of successful conditional deletion of *Dnmt3a* specifically in the myelomonocytic lineage (data shown in chapter 3.2), the phenotype of *Dnmt3a*^{LysM} mouse model was characterized (Figure 3-17). Eight-to-12 and >34 weeks old mice from *Dnmt3a*^{fl/fl} and *Dnmt3a*^{LysM} were used to study the effect of LysMCre-mediated deletion of *Dnmt3a*.

Dnmt3a^{LysM} mice were born following the expected mendelian ratios (Figure 3-17a) and deficiency of *Dnmt3a* in younger animals did not have an impact on the development, gross morphology of the analyzed organs, nor the overall anatomy of the mice. As well, no altered behavioral/motor alterations nor defects in reproduction capacity were observed. Measurements of liver, spleen, caecum and kidney weight, together with small intestinal and colonic length and body weight, did not result in significant differences between 8-12 weeks old males and females *Dnmt3a*^{LysM} compared to *Dnmt3a*^{fl/fl} littermates (Figure 3-17e-k (left)).

Basal comparison of older animals did not result in significant differences in colon and small intestinal lengths (Figure 3-17h, Figure 3-17i (right)), nor kidney and caecum weight (Figure 3-17k, Figure 3-17j (right)). *Dnmt3a*^{LysM} mice however, exhibited spontaneous hepato-splenomegaly starting from 34 weeks of age (Figure 3-17c, Figure 3-17e, Figure 3-17f (right)), that determined impaired motility due to abdominal enlargement (Figure 3-17b) and significantly higher body weight compared to *Dnmt3a*^{fl/fl} littermates (Figure 3-17g). Of note, bone marrow the rear legs of >34 weeks old mice were characterized by a pale pink (almost white) color compared to the *Dnmt3a*^{fl/fl} control (Figure 3-17d).

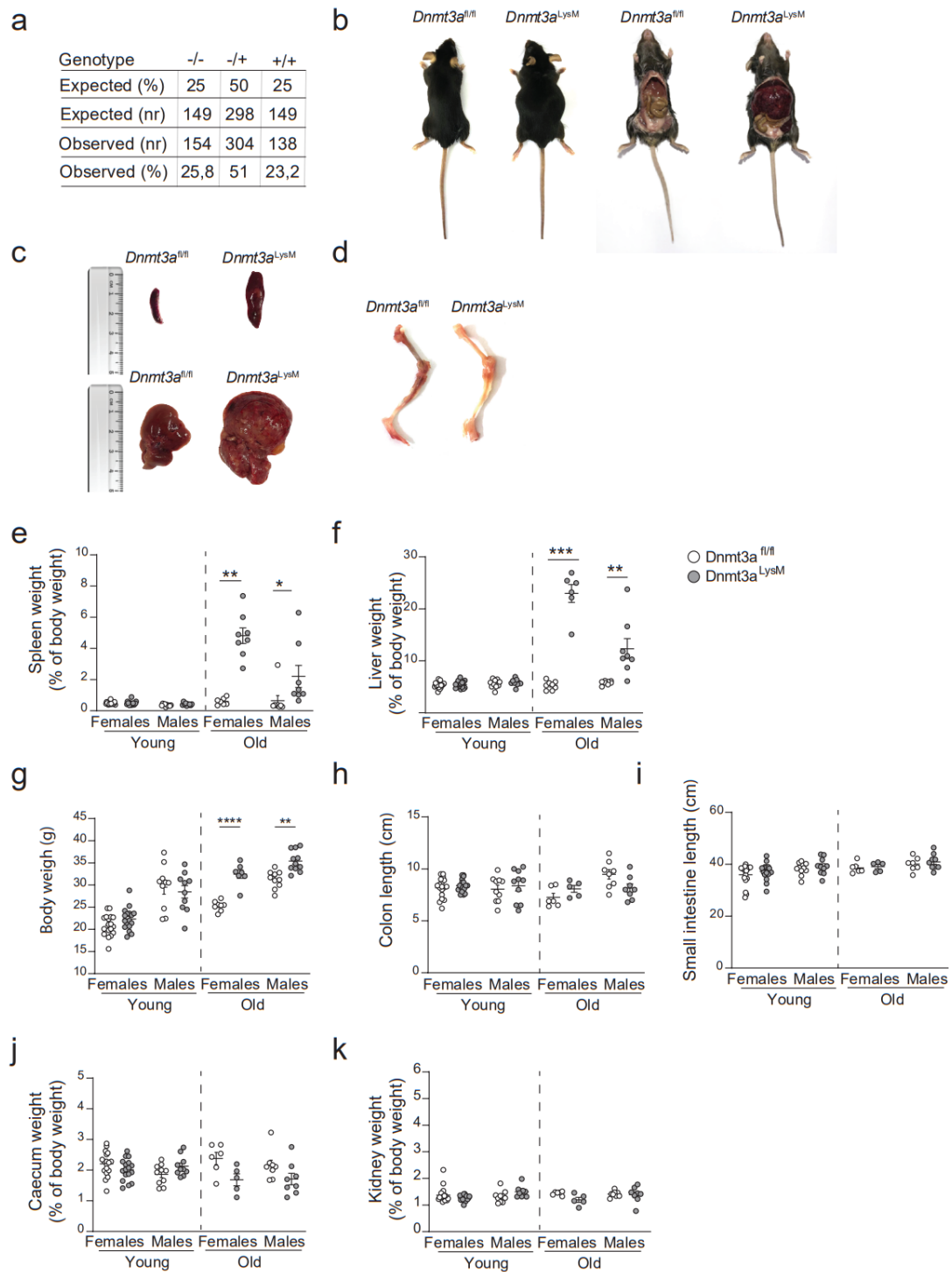


Figure 3-17: Basal phenotyping of *Dnmt3a^{LysM}* mouse line.

(a) Birth rates of wild type and *Dnmt3a^{LysM}* reflected the expected mendelian ratio. (b) Representative comparison of body morphology of *Dnmt3a^{fl/fl}* (left) and *Dnmt3a^{LysM}* (right) mice at >34 weeks of age. (c) Liver/spleen gross morphology of *Dnmt3a^{fl/fl}* mice (left) compared to *Dnmt3a^{LysM}* mice (right) at >34 weeks of age. (d) Depiction of bones of femurs and tibias of *Dnmt3a^{LysM}* mice (right) versus the control littermate (left). (e) spleen, (f) liver, (g) body, (h) colon, (i) small intestine, (j) caecum and (k) kidney (weight and/or length) of 8-12 and >34 weeks old males and females wild-type and *Dnmt3a^{LysM}* mice (n=18 for 8-10 weeks old females, n=10 for 8-12 weeks old males, n=5 vs 6 for >34 weeks old females and n=8 for >34 weeks old males). Statistical significance was calculated using multiple unpaired t-test with Mann Whitney test. *p<0,0332, **p<0,0021, ***p<0,0002 and **** p<0,0001.

3.5.2 *Dnmt3a* ablation results in a spleen hypertrophy and alters splenic hematopoietic stem cell abundance

The basal phenotypical observation of *Dnmt3a*^{LysM} mouse model revealed a drastic (age-dependent) effect of the lack of *Dnmt3a* that results in - presumably - leukemic malignancies accompanied by rapidly evolving hepato-splenomegaly.

Small intestine, colon, liver and spleen were histologically evaluated for microscopic anatomy by hematoxylin and eosin staining to assess tissue morphology and spontaneous immune cell infiltration (Figure 3-18a). The overall tissue anatomy appeared normal in all the assessed organs from young *Dnmt3a*^{LysM} mice compared to fl/fl mice. Cellular proliferation assessment by Ki67 (Figure 3-18b) staining did not reveal differences in proliferation rates on the small intestine nor the colon and no signs of spontaneous intestinal inflammation were observed.

Dnmt3a^{LysM} mice above 34 weeks of age however, displayed a severe alteration of the normal anatomy and cellular proliferation rates of spleen and liver.

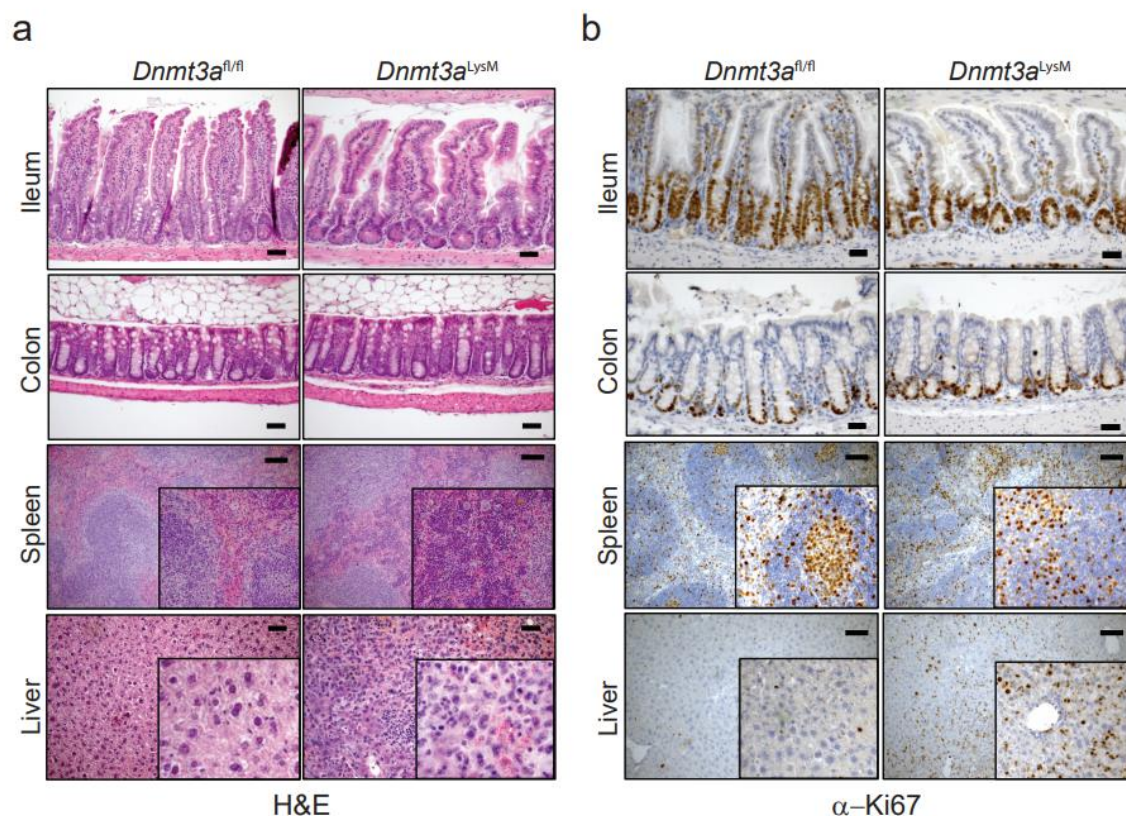


Figure 3-18: Spleen and liver of *Dnmt3a*^{LysM} mice have higher proliferation rates.

Representative photomicrographs depicting histological evaluation of (a) H&E staining and (b) Ki67 positive cells in colonic/ileal sections and spleen and liver from >34 weeks old *Dnmt3a*^{fl/fl} (left) and *Dnmt3a*^{LysM} (right) mice animals, representative for n=5-8 per genotype. Scale bar=100μm.

Noticeably, the splenic germinal centers (GCs) of >34 weeks old *Dnmt3a*^{LysM} mice were characterized by increased proliferation rates compared to their control littermates. Considering the striking difference in proliferation rates in the GCs, we investigated whether the observed hyperproliferation might be due to impaired hematopoietic stem cells proliferation. For this, we analyzed the number of hematopoietic stem cells (HSCs) residing in the spleen of young and old *Dnmt3a*^{fl/fl} and *Dnmt3a*^{LysM} mice (n=6) (Figure 3-19).

To exclude differentiated splenocytes from the analysis, the latter were depleted through MACS technology using cell type-specific lineage antigens. Differentiated splenocytes were retained by sorting of magnetic beads coupled with a cocktail of biotinylated antibodies against a panel of “lineage” antigens (CD5, CD45R (B220), CD11b, Anti-Gr-1 (Ly6G/C), and Ter-119 antibodies) and Anti-biotin micro beads targeting differentiated cells.

Remaining lineage negative cells (lin⁻) were stained for the HSC markers stem cell antigen-1 (Sca-1) and proto-oncogene c-Kit (c-Kit) (Figure 3-19a).

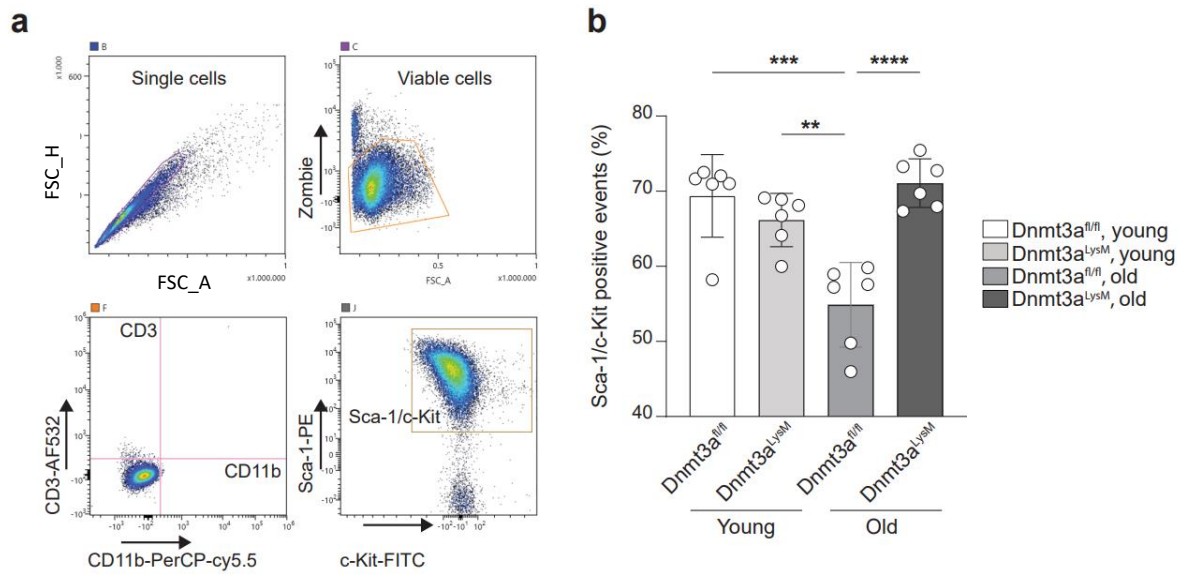


Figure 3-19: Increased frequencies of HSCs in the spleen of older *Dnmt3a*^{LysM} mice.

(a) Representative gating strategy depicting doublet exclusion, viable cells selection (upper row, first two dot plots), contamination assessment for differentiation markers CD3 and CD11b positive events (lower row) and Sca-1/c-Kit percentage. Sca-1 and c-Kit fluorophores intensities were corrected with WLSM compensation algorithm. Negative selection of lin⁻ cells was performed using MACS-based cell-type specific lineage depletion kit. Lin⁻ cells from spleens of *Dnmt3a*^{fl/fl} and *Dnmt3a*^{LysM} mice (n=6 biological replicates) were stained for cell type-specific and HSC antigens and positive events were measured by flow cytometry. (b) Percentages of Sca-1/c-Kit positive events as percentage of viable gated population. Data are shown as mean ± S.D. Statistical significance was calculated using one-way Anova. $p < 0.021$ ***, $p < 0.0002$ and ****, $p < 0.0001$. FSC: forward scatter, SSC: sideward scatter.

To confirm the purity of the lin⁻ retained cells, the cell population was stained for common differentiation antigens of abundant cell types such as CD19, CD3 and CD11b and analyzed through FACS. The retained population of differentiated cells was tested for differentiated cells contaminations and the analysis revealed $1.15\% \pm 0.68$ of CD3⁺ and $1.1\% \pm 0.14$ of CD19⁺ events. Staining of CD11b⁺ cells revealed $1.58\% \pm 0.5$ in the lin⁻ population (Figure 3-19b). Contaminations of differentiated cells were detectable in both genotypes, therefore allowing the comparison of abundances of HSC in both sample groups. Interestingly, lin⁻ population was significantly lower in old wild type mice compared to the young counterpart, suggesting an age-dependent loss of hematopoietic cells renewal in older animals. In contrast, we observed increased Sca-1/c-Kit events in the spleen of >34 weeks-old *Dnmt3a*^{LysM} mice, suggesting that loss of *Dnmt3a* might result in increased hematopoietic cell proliferation.

3.5.3 Loss of *Dnmt3a* in older mice determines splenic immune cell population composition alteration

Considering the significant increase in Sca-1/cKit hematopoietic cells rates and given the evident alteration of the gross morphology of the spleen at baseline conditions in >34 weeks old *Dnmt3a*^{LysM} mice, we next aimed to define whether lack of *Dnmt3a* impacts on to the splenic immune cell frequencies. The most abundant immune cells residing in the spleen were quantified using FACS (Figure 3-20). Flow cytometry analysis was performed to assess the frequencies of T cells (CD3) (Figure 3-20a), T helper cells (CD4) (Figure 3-20b), cytotoxic T cells (CD8) (Figure 3-20c), monocytes-macrophages (CD11b) (Figure 3-20d), dendritic cells (CD11c) (Figure 3-20e), natural killer cells (NK1.1) (Figure 3-20f), neutrophils (CD11b-Lys6G) (Figure 3-20g) and B cells (CD19) (Figure 3-20h).

T cells and monocytes differed when comparing young mice based on the genotype. Young *Dnmt3a*^{fl/fl} mice had moderate but significant less T cells and increased numbers of monocytes compared to *Dnmt3a*^{LysM} mice. When comparing young and old wild type mice, we found increased frequencies of T cells and cytotoxic (CD8⁺ T cells) T cells. Comparing the two old groups based on their genotype, we observed diminished counts of T cells, T helper cells, but increased cytotoxic T cells. Old *Dnmt3a*^{LysM} mice had less CD11b positive cells but increased frequencies of dendritic cells. No differences in regard to natural killer, B cells or neutrophils counts were found in any of the comparisons that were taken in consideration. These results testify that not only the lack of *Dnmt3a* results in impaired immune cell composition, but also underlines how age, in combination with the genotype, is determinant in promoting specific cell lineages expansion.

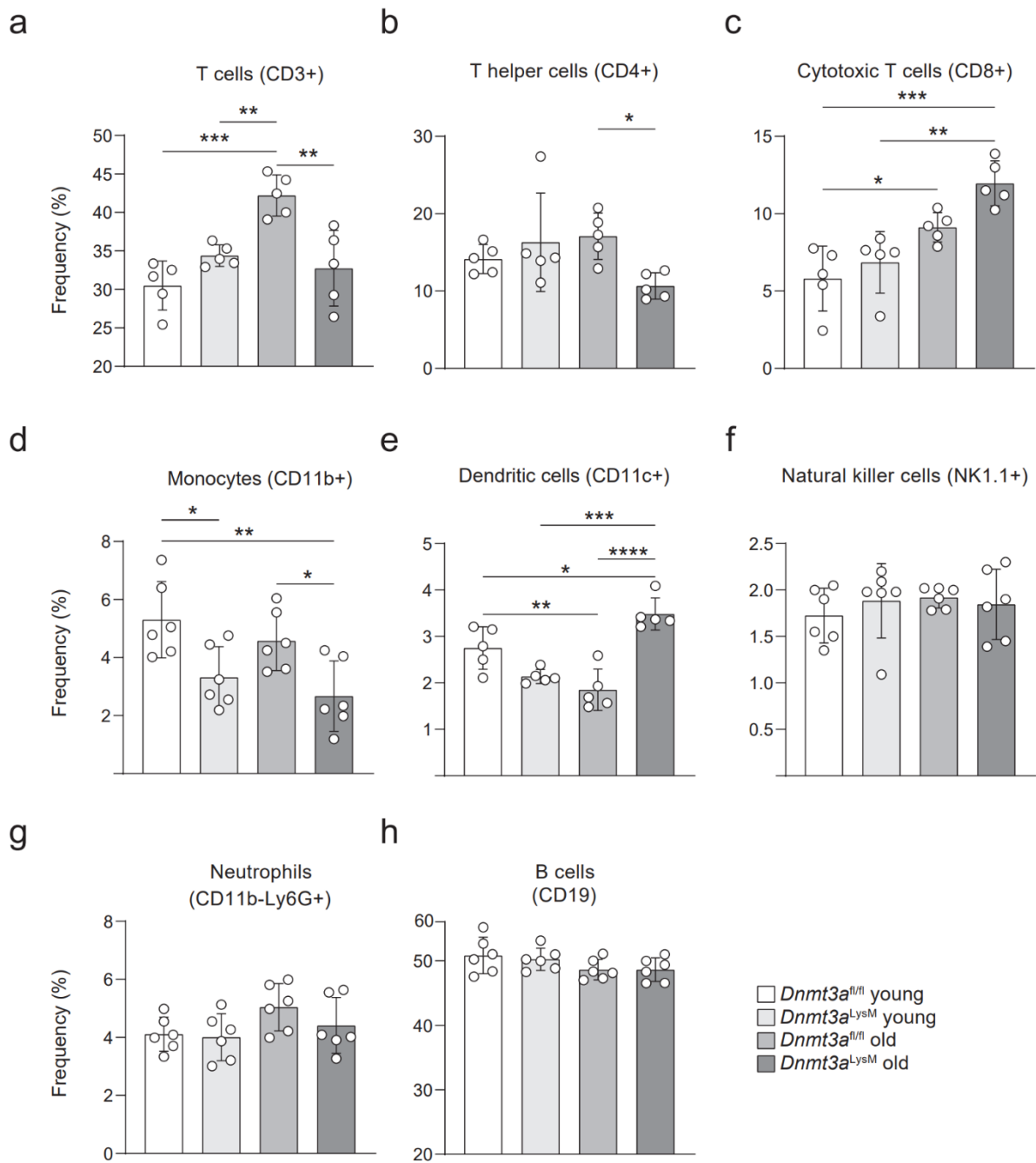


Figure 3-20: Lack of *Dnmt3a* in myeloid cells results in impaired splenic immune cell composition.

Bar plots summarizing the quantification of most abundant immune cells frequencies in the spleen of *Dnmt3a*^{fl/fl} and *Dnmt3a*^{LysM} mice by flow cytometry. Spleen were harvested, reduced to single cell suspensions, and stained for cell-specific antigens to identify (a) T cells, (b) T helper cells, (c) cytotoxic T cells, (d) monocytes, (e) dendritic cells (f) natural killer cells, (g) neutrophils and (h) B cells. Statistical significance was calculated using one-way Anova (* $p < 0.0332$, ** $p < 0.0021$, *** $p < 0.0002$ and **** $p < 0.0001$). Data shown are representative for $n = 5/6$ over three independent experiments.

3.5.4 Lack of *Dnmt3a* in macrophages during acute DSS-induced colitis

To investigate the impact of *Dnmt3a* deficiency in macrophages during inflammation *in vivo*, DSS - a synthetic dextran-derived polysaccharide that induces inflammation - was used to mimic an acute manifestation of inflammation in the gastrointestinal tract. DSS was administered for 5 days in drinking water (4%) followed by 7 days recovery phase where clean drinking water was administered to 12 (n=6 per genotype) 10-week-old female mice (Figure 3-21). Upon removal of DSS we observed a noticeable weight loss (up to 75-80%), indicating the effectiveness of the treatment in both groups (Figure 3-21a). *Dnmt3a*^{fl/fl} and *Dnmt3a*^{LysM} body weight loss curves did not significantly differ throughout the duration of the experiment. However, we observed a moderate but significant increase of disease activity index, as representation of worsening of the overall condition of *Dnmt3a*^{LysM} group (Figure 3-21b). Disease activity index (DAI) was quantified by mean of a subjective classification system based on weight loss, presence of blood in feces, and stool consistency (refer to Chapter 2.4.5 for further details). Measurement of small intestinal and colonic length, together with caecum, spleen, liver and kidney weight did not result in significant variations between the two experimental groups (Figure 3-21c-h).

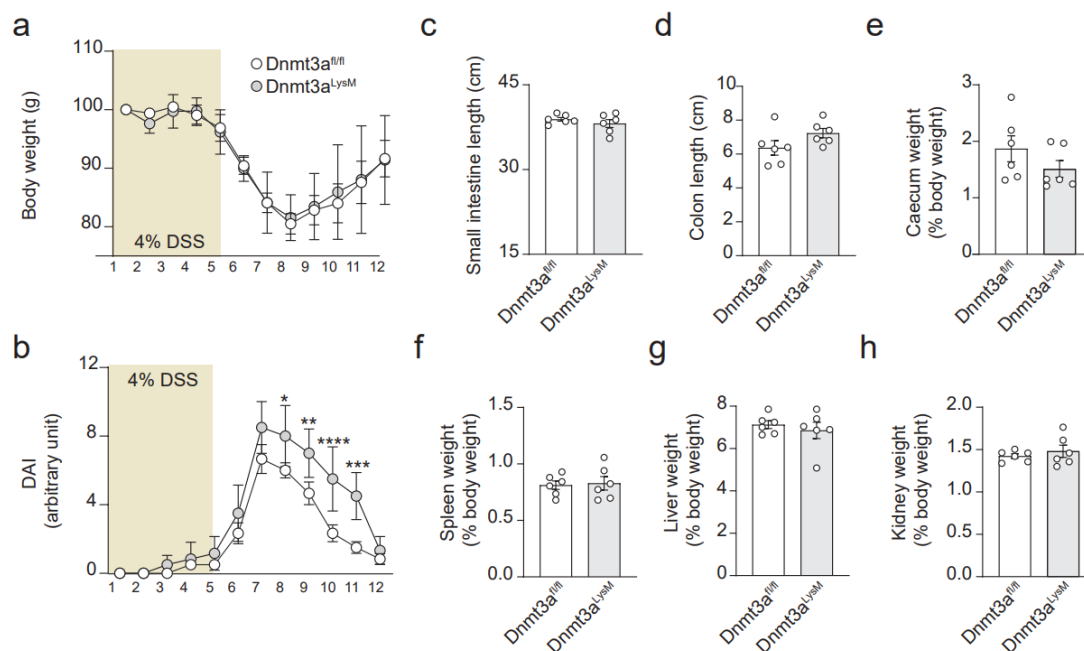


Figure 3-21: Acute DSS colitis model impacts *Dnmt3a*^{LysM} mice on DAI score but not in overall or organ weight or length of intestines in young female mice.

(a) Body weight and (b) disease activity index (DAI) were monitored daily for the entire duration of the experiment. DSS-induced damage was scored through DAI, combining severity in body weight loss, stool consistency and bleeding. Data shown in (a) and (b) represent mean \pm SEM. Statistical significance was calculated using two-way Anova followed by Tukey correction test; ****p<0,0001. (c-h) Organ weight of *Dnmt3a*^{fl/fl} and *Dnmt3a*^{LysM} mice (n=6 per group) assessed on day 12, which was the end of the recovery phase and of the experiment. Small intestine length (upper left), colon length (upper middle) and caecum (upper right), spleen (lower left), liver (lower middle), and kidney (lower right) weights (in % relative to total body weight) are represented as mean \pm SEM.

3.5.5 Splenic immune cell composition in *Dnmt3a*^{LysM} mice is not affected after acute intestinal inflammation

Although the overall outcome of DSS induced acute inflammation did not differ between genotypes (except for DAI score) but considering the alteration of the immune cell frequencies observed in >34 weeks old steady state *Dnmt3a*^{LysM} mice, we investigated whether the lack of *Dnmt3a* following DSS-induced inflammation affected the composition of the immune composition of spleen (Figure 3-22a) and small intestinal lamina propria (Figure 3-22b). For this, immune cells from spleen and small intestine were harvested and analyzed using FACS technology. No difference in immune cell frequencies was observed between *Dnmt3a*^{fl/fl} and *Dnmt3a*^{LysM} at the end of the recovery phase after DSS induced colitis.

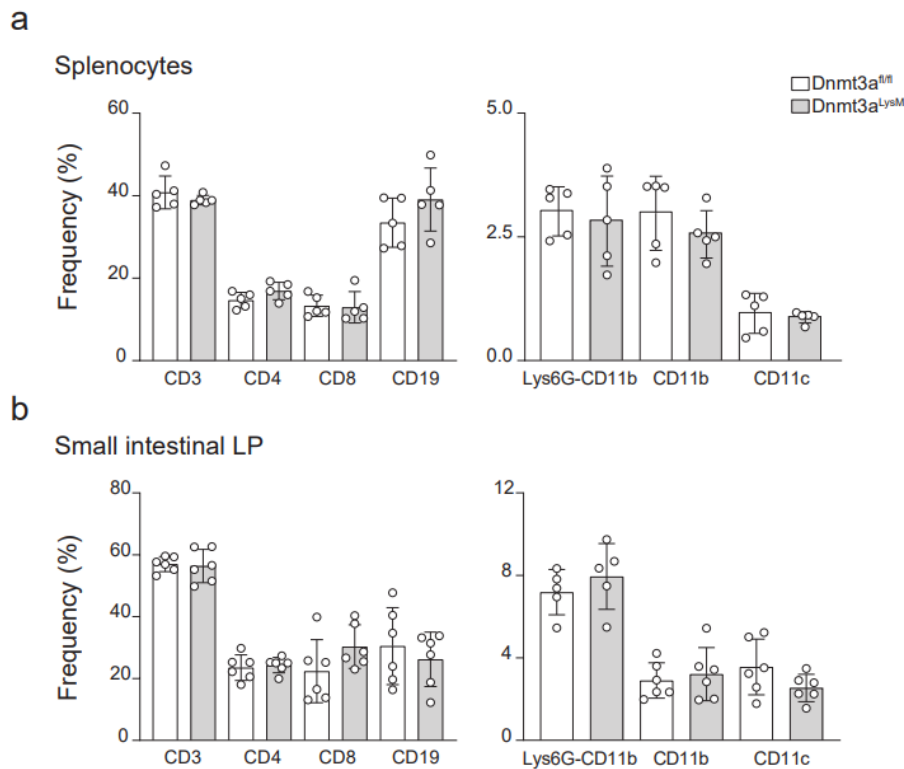


Figure 3-22: Splenic immune cell composition and small intestinal lamina propria immune phenotyping after acute DSS colitis.

Percentages of positive events rates measured by flow cytometry for (a) spleen (n=5) and (b) small intestinal lamina propria of n=6 *Dnmt3a*^{fl/fl} and n=6 *Dnmt3a*^{LysM} littermates at the end of recovery phase following acute DSS colitis (4%) and stained for cell line-specific antigens. Lamina propria of small intestinal sections were dissociated from IECs at the end of recovery phase (day 12) after 5 days of DSS treatment. The abundance of each population is reported as percentage of positive events on a given gated population. Data are shown as mean ± S.D. CD3: T cells, CD4: naive T cells, CD8: cytotoxic T cells, CD19: B cells, CD11b: macrophages, CD11c: dendritic cells, CD11b-Lys6G: neutrophils. CD45 served as a primary leukocyte common antigen for initial gating.

3.5.6 *Dnmt3a*^{LysM} mice are more susceptible to chronic DSS driven inflammation

Since *Dnmt3a* is involved in tumor progression, we further treated 10-week-old *Dnmt3a*^{fl/fl} and *Dnmt3a*^{LysM} female mice (n=8 per genotype) with a chronic DSS regime, *i.e.* 3 periods of DSS administration in alternance to recovery, combined with intraperitoneal injections of Azoxymethane (AOM) at the beginning and mid-term of the experiment. AOM is a potent colorectal cancer inducer. Thus, DSS and AOM combination is a model that could both provoke intestinal inflammation and tumor insurgence.

Mice were therefore exposed to three cycles of DSS treatment, regularly interspersed with intraperitoneal injections of AOM. (Although DSS treatment was effective in inducing inflammation, no tumor insurgence was detectable. This could be due to ineffective AOM treatment or chemical decay of the compound used. We therefore interpreted the experiment as a chronic DSS treatment). During the first cycle, 1% DSS was dissolved in drinking water and administered to the mice for 7 days, followed by 14 days of recovery phase where only pure drinking water was administered. The cycle was repeated two times, increasing DSS to 1,5% in the following two cycles. Body weight was monitored daily during DSS treatment and every second day during recovery phase (Figure 3-23a). DAI was monitored every second/third day for the entire duration of the experiment (Figure 3-23b).

During first and second cycles of DSS induced inflammation, no difference was observed between body weight of *Dnmt3a*^{LysM} and wild type littermates until later time points. DAI as well did not vary between the two groups during cycle one. After cycle two, *Dnmt3a*^{LysM} body weight curve showed a slight increasement, however without reaching statistical significance. Disease activity did not reveal increased susceptibility in the *Dnmt3a*^{LysM} group compared to control group. During the follow up phase after cycle three, the increase of body weight of *Dnmt3a*^{LysM} mice was higher although not significant. Disease activity did not show differences in *Dnmt3a*^{LysM} mice during the third and last cycle of DSS. On the last day of experiment, body weight of *Dnmt3a*^{LysM} mice resulted significantly higher than *Dnmt3a*^{fl/fl} control littermates (Figure 3-23c), while DAI scoring did not differ in terms of disease susceptibility. Spleen and liver weight did not differ when comparing the two groups (Figure 3-23d, Figure 3-23e). *Dnmt3a*^{LysM} mice displayed increased epididymal white adipose tissue (EWAT) weight (Figure 3-23f) but no difference in colon length was observed (Figure 3-23g). Longer small intestinal tracts characterized *Dnmt3a*^{LysM} mice compared to *Dnmt3a*^{fl/fl} (Figure 3-23h), while kidney and caecum weight did not result in significant difference (Figure 3-23i, Figure 3-2j). Histological evaluation of colonic tissue revealed increased degree of inflammation *Dnmt3a*^{LysM} mice compared to *Dnmt3a*^{fl/fl} (Figure 3-23k, Figure 3-23l), suggesting increased susceptibility to chronic DSS treatment upon lack of *Dnmt3a* in the myelomonocytic lineage.

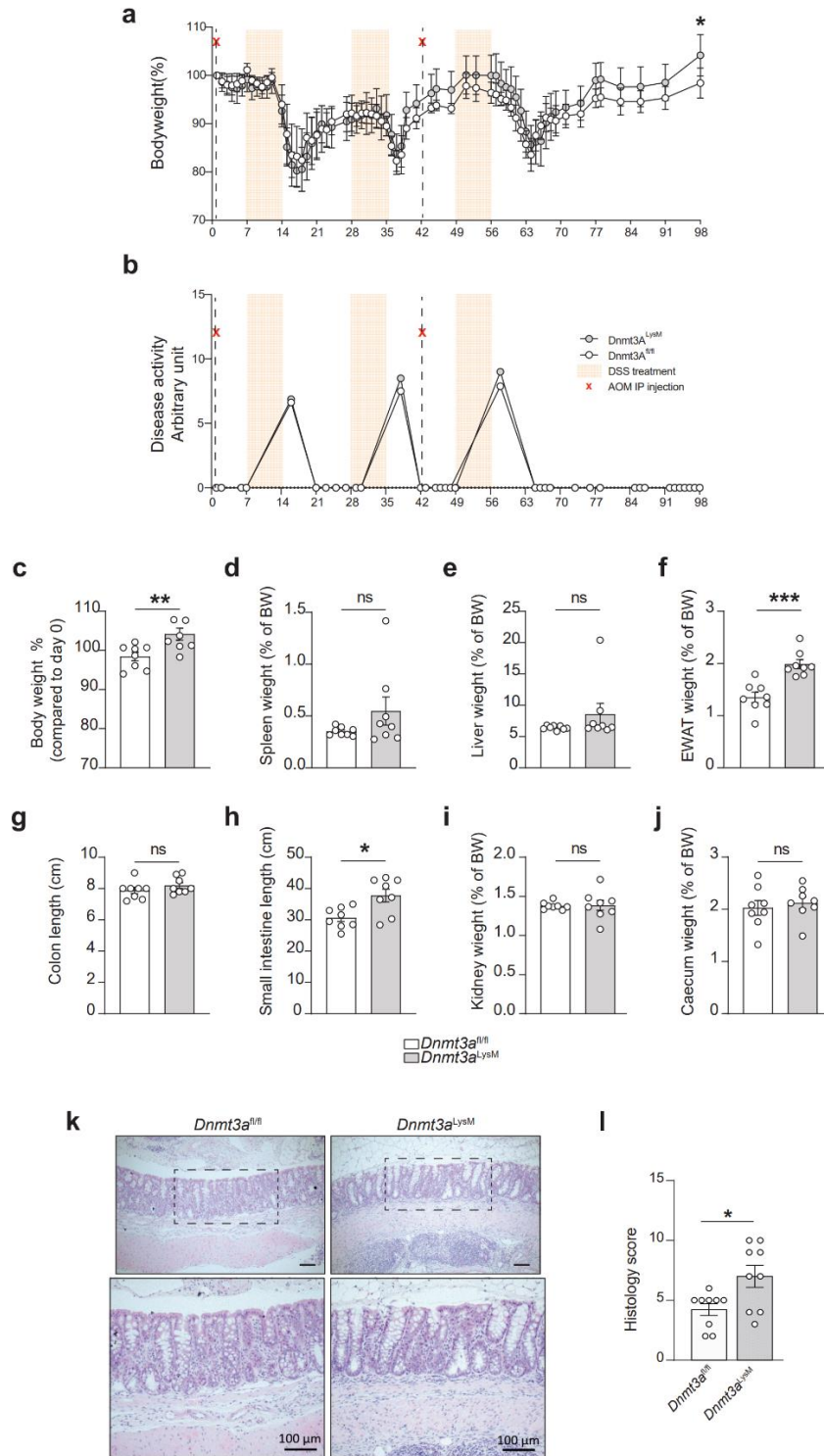


Figure 3-23: Conditional deletion of *Dnmt3a* in myeloid lineage determines a subtle increase in body weight and disease activity upon chronic/AOM inflammation.

(a) Body weight loss variation during AOM-chronic DSS induced colitis and (b) disease activity calculated using DAI scoring during DSS treatment and recovery phase. (c) Body weight, (d) spleen, (e) liver and (f) EWAT weight. (g) Colon and (h) small intestine length. (i) Kidney and (j) caecum weight on the last day of experiment. (k) representative photomicrograph displaying increased immune cell infiltration in colonic section of *Dnmt3a^{LYM}* (right) compared to *Dnmt3a^{fl/fl}* mice (left) and (l) statistical evaluation of the histological inflammation score in colon sections. Data represent mean \pm SEM of n=8 biological replicates per group. Statistical significance was calculated using unpaired t-test followed by Mann Whitney correction. * $p < 0.0332$, ** $p < 0.0021$, *** $p < 0.0002$ and **** $p < 0.0001$.

3.5.6.1 Chronic inflammation does not alter the immune cell composition of spleen, colonic or small intestinal lamina propria of *Dnmt3a*^{LysM} mice

To further elucidate the consequence of the conditional deletion of *Dnmt3a* in the myeloid-monocytic lineage during inflammation, the immune composition of intestinal and colonic lamina propria (Figure 3-24a, Figure 3-24b), and spleen (Figure 3-24c) were analyzed by FACS. Spleen and lamina propria were harvested from *Dnmt3a*^{LysM} and wild type littermates after the induction of chronic inflammation. Spleen, small intestinal and colonic lamina propria of n=8 *Dnmt3a*^{LysM} and wild type littermate were harvested and reduced to single cell suspension and stained with a cocktail of cell-specific antigens detecting the most abundant immune cells composing spleen and lamina propria.

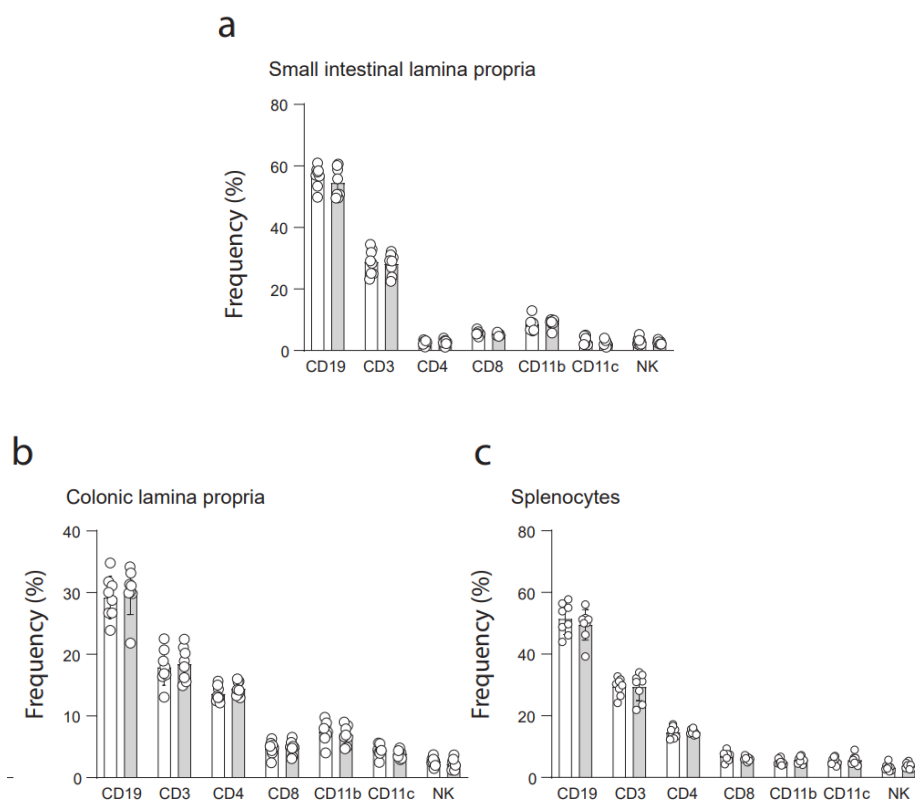


Figure 3-24: Immune cell composition of spleen, colonic and small intestinal lamina propria do not change in *Dnmt3a*^{LysM} mice after chronic DSS-induced inflammation.

Bar plots summarizing the frequencies of cell specific antigens in (a) small intestinal LP, (b) colonic LP and (c) spleen quantified by flow cytometry after chronic inflammation in wild type and *Dnmt3a*^{LysM} mice. The abundance of each population is reported as percentage of positive events on a given gated population. Data are shown as mean \pm S.D. CD3: T cells, CD4: T helper cells, CD8: cytotoxic T cells, CD11b: macrophages, CD11c: dendritic cells, CD11b-Lys6G: neutrophils, CD19: B cells. CD45 served as a primary leukocyte common antigen for initial gating.

The analysis of the proportions of different immune cell population did not result in statistically significant difference between *Dnmt3a*^{LysM} and control littermates, indicating that *Dnmt3a* did not

impact on the overall immune population proportion on the last day of experimental *in vivo* chronic inflammation.

4. Discussion

During intestinal inflammation, a complex and essential interplay between intestinal epithelium and immune cells takes place: here macrophages mediate the resolution of inflammation and mucosal healing. Although many studies have found an association with DNA methylation and IBD [212]–[214], little is known about the role of DNMT3A in the myelomonocytic lineage and intestinal epithelial cells. This thesis investigates how the lack of *Dnmt3a* in the intestinal epithelium impacts on the maintenance of intestinal homeostasis and gut barrier functions in the colon, and explores the role of *Dnmt3a* in the myelomonocytic lineage during cell homeostasis and inflammation.

4.1 *Dnmt3a* orchestrates mucosal homeostasis in the colon

The *de novo* DNA methyltransferase DNMT3A is part of the tightly regulated epigenetic machinery of DNA methylation (DNAm) and it is responsible of establishing new DNAm patterns on the genome. DNAm earned the definition of “link” between genetic regulation and environment [215] and it is involved in maintaining cellular homeostasis development, and differentiation [216], [217]. Genome-wide association studies have found IBD, and more particularly CD, to be associated with genetic variants of DNMT3A [24], [218]. In our recent investigation we explored the consequence of the genomic deletion of *Dnmt3a* in IECs during *in vivo* inflammatory models and revealed a decisive role for *Dnmt3a* in mucosal homeostasis, epithelial regeneration, and response to intestinal inflammation [110], [219]. This, however, contrasts other groups’ hypothesis that in murine models, *Dnmt3a* do not appear to be necessary to maintain intestinal homeostasis nor DNA methylation patterns [202].

An efficient intestinal epithelial barrier is vital for nutrients absorption and mechanical defense against potentially pathological luminal antigens [220], [221]. Aberrant DNAm at promoter sites of genes involved in mucus abundance [222] linked the human mucin genes MUC4 and MUC2 within intestinal homeostasis with the activity of DNA methyltransferases in epithelial cancer cell lines [222]–[224]. Here we additionally demonstrate that *Dnmt3a* might be causative for reduced mucus thickness. Using a murine model lacking *Dnmt3a* exclusively in IECs (*Dnmt3a*^{ΔIEC}), we show that already at steady state the ablation of *Dnmt3a* results in diminished distance of IECs to luminal microbiota, which we confirmed by fluorescent *in situ* hybridization. Interestingly, this feature phenocopies the thinner mucosa of IBD patients which is observed in IBD [225]. CD patients in fact present dysfunctional intestinal barrier [226], [227] and altered tight junction ultrastructure [227] as consequence of the downregulation of epithelial junctional proteins [228], [229] such as β -catenin or E-cadherin [230], [231] and a more penetrable mucus layer [232].

Reduction of Goblet cells number is associated with development of colitis [233]. Notably, we found the same reduction of Goblet cell counts in the colon of *Dnmt3a*^{ΔIEC} mice already at steady state. This might be explanatory for the augmented disease susceptibility of *Dnmt3a*^{ΔIEC} mice that was observed during *in vivo* inflammatory models [110].

The epithelium of affected patients is characterized as well by increased epithelial permeability [226], [227], [232] and this is predictive of relapse in patients with quiescent IBD [232], [234], [235]. In our murine model we observed increased epithelial permeability which could be the consequence of the diminished Goblet cell count, and therefore the thinning of the mucus layer separating the intestinal epithelium from the luminal content.

As a direct consequence of a more permeable epithelium, augmented bacterial translocation is as well common in IBD [236], [237]. In support to this, we reported increased bacterial DNA in mesenteric lymph nodes (MLN) of steady state *Dnmt3a*^{ΔIEC} mice. Thus, the baseline phenotype that we observed, might be explanatory for the augmented disease susceptibility during chemically induced intestinal inflammation that were demonstrated in previous studies performed by our group [110]. However, although we report increased amount of bacterial DNA in MLN, we could not demonstrate spontaneous inflammation nor alteration in the immune cell composition of MLN nor colonic lamina propria as the observed translocation might not involve viable bacteria.

These novel observations together support our initial hypothesis of a perturbed epithelial barrier capacity due to the lack of *Dnmt3a*, which in turn do not directly translates in spontaneous inflammation but identifies an essential role of *Dnmt3a* in maintaining epithelial barrier function and epithelial integrity.

Limitations in this approach might be identified in the necessity to perform the same assessment during, for example, *in vivo* inflammatory models *i.e* acute/chronic DSS colitis, to define whether inflammatory conditions might exacerbate the features we observed already at baseline conditions.

4.1.1 DNMT3A is downregulated during inflammation in intestinal epithelium

Site-specific methylation and gene expression patterns characterize the ascending and sigmoid colon compared to the terminal ileum of pediatric IBD cohorts [77], suggesting a causative link between inflammation and DNAm/gene expression dysregulation in a site-specific manner. DNMT3A polymorphisms were associated with the accumulation of gene methylation in gastric mucosa during *Helicobacter pylori* infection. These polymorphisms are linked to the severity of gastric mucosal atrophy, which in turn is accompanied by chronic inflammation and potential development of gastric cancer [238], [239]. Thus, the genetic association of DNMT3A with CD, suggest a causative link of DNA

methylation to IBD [24]. In murine models, intestinal ablation of both *Dnmt1* and *Dnmt3b* is lethal [202], indicating the essential role of Dnmts in maintaining DNA methylation and genomic integrity in the intestinal epithelium [240]. However, to date, knowledge about how inflammation directs DNMT3A regulation in the intestinal epithelium is still missing.

Although other groups proposed no alteration of DNMT3A expression levels in colonic mucosa of UC patients [241], in our comparative study we demonstrate a significant downregulation of DNMT3A transcript levels compared to healthy controls in endoscopically inflamed and non-inflamed CD patients-derived organoids. To confirm ongoing inflammation, we included *CCND1* and *CXCL10* as proliferative and inflammatory markers, respectively.

To circumvent the high genetic variability that characterizes human-derived organoids [242], we employed colonic organoids from *Dnmt3a^{fl/fl}* and *Dnmt3a^{ΔIEC}* mice to pinpoint which trigger is responsible for the observed decreased *Dnmt3a* transcriptional expression. We monitored gene expression levels of *Dnmt3a* and *Dnmt3b* upon stimulation with prototypic pro-inflammatory stimuli and we demonstrated that *Dnmt3a* is consistently downregulated at both mRNA and protein level not only in clinically inflamed whole tissues but also specifically in human- and murine-derived IECs. These findings support our hypothesis that the IBD genetic risk at DNMT3A locus is mediated by suppression of DNMT3A, potentially in response to pro-inflammatory stimuli *i.e* TNF.

4.2 *Dnmt3a* in the myelomonocytic lineage

The Immune response in IBD takes place upon strict communication between intestinal epithelium and the underlying immune compartment residing in the lamina propria (LP). Here, macrophages and their polarization play a central role mediating the inflammatory response. [154], [157], [163], [178], [243]. Immune cells involvement during such manifestations is of great importance to cope with inflammation and produce an effective resolutive action [243], [244]. In this scenario, macrophages are central to discriminate innocuous from potentially pathogenic antigens maintaining tolerance. Furthermore, genetic and epigenetic predisposition leads to impaired immune responses that can lead to chronic relapsing pathologies such as IBD. Evidence suggests a causal link between monocyte-macrophages differentiation/polarization and missed resolution of inflammation [210], making macrophages an interesting target for further investigations.

4.2.1 Inflammation drives *Dnmt3a* downregulation in the myelomonocytic lineage

Macrophages have been subcategorized into two main biologically distinct populations: M1 (or pro-inflammatory macrophages) and M2 (or homeostatic, anti-inflammatory) macrophages [245]. M1-M2

balance alteration is linked with IBD [178] and perpetuation of inflammation [246]. So far, epigenetic regulation of macrophage polarization has been shown for DNMT3B in the context of obesity and inflammation [247]. Loss-of-function studies of *Dnmt3a* in murine models had been limited to hematopoietic stem cells [204], T cells [195], primordial germ cells [248], embryonic stem cells [249], [250] and neural stem cells [251]. How the lack of *Dnmt3a* in macrophages contributes to inflammatory diseases- such as IBD- and homeostasis restoration, has not been investigated yet.

Here, we employ a murine model depleted of *Dnmt3a* uniquely in the myelomonocytic lineage and we show that *Dnmt3a* is linked to macrophages polarization. Other groups postulated that Dnmt3aos (long noncoding RNA (lncRNA) Dnmt3a-opposite strand) to be highly expressed in M2 macrophages and to play a key role in macrophage polarization [108]. On the same line, our measurement of *Dnmt3a* mRNA expression level in macrophages expressing *Dnmt3a* revealed higher levels of Dnmt3a mRNA in M2 polarized macrophages and almost undetectable amounts in M1 macrophages. We report that this is also reflected at protein level. We monitored DNMT3A abundance in a 9-days follow up in wild type macrophages, demonstrating an inflammation-dependent DNMT3A protein production, similarly to what was previously observed in intestinal murine and human epithelium [110].

Macrophage polarization strictly depends on the metabolic balance of arginase activity [252]. Together with DNMT3A, we show ARG-1 to be more abundant in M2 macrophages, confirming previous findings linking ARG-1 with DNMT3A mutations in lower-grade myelodysplastic syndromes and chronic myelomonocytic leukemia mouse models [253]. We thus conclude that *Dnmt3a* expression is strictly regulated in accordance with homeostatic-or-inflammatory conditions and might play a central role during macrophage polarization.

We acknowledge that this experiment might be even more informative when including (in the same 9-days follow up set up), *Dnmt3a*-depleted macrophages, to address whether the absence of *Dnmt3a* might as well impact on polarization marker genes expression during monocyte-to-macrophage differentiation.

4.2.2 A complex transcriptional signature portrays macrophage polarization

Dnmt3a is highly expressed in macrophages [109], where it is involved in efferocytosis, tissue resolution [254], and in regulating inflammatory pathways in a context-specific manner [255]. However, how the lack of *Dnmt3a* in the myelomonocytic lineage impacts the transcriptional signature of polarized macrophages has not been investigated yet. We demonstrate that *Dnmt3a* is differentially expressed accordingly to macrophage polarization by performing comparative RNA sequencing

analysis of resting and M1-M2 *in vitro* polarized BMDMs obtained from young (8-10 weeks old) and (>34 weeks old) *Dnmt3a^{fl/fl}* and *Dnmt3a^{LysM}* mice. The polarization status that we found is defined by a complex dysregulation of the transcriptional signature of the different macrophage populations, in the same line as previously observed in human [165] and murine wild type macrophages [256]. Overall, the analysis highlighted a complex transcriptome adaptation, specific for M1 and M2 polarization status, confirming what already reported by other groups [257]. More in detail, we identified 1692 and 480 unique differentially expressed genes (DEGs) when comparing resting-M1 polarization of young and old *Dnmt3a*-deleted BMDM compared to wild type controls. When comparing resting with M2, we found 4523 and 1471 unique DEGs in young and old *Dnmt3a*-deleted BMDM. M1-M2 comparison resulted in 1089 and 966 unique DEGs in young and old *Dnmt3a*-ablated group. Young and old polarized BMDMs revealed 1481 DEGs specific for old wild type and 884 DEGs unique for *Dnmt3a*-ablated BMDMs in the resting versus M1 comparison. Comparing M2 (young and old) with resting macrophages, we observed 574 and 878 DEGs in old wild type and old *Dnmt3a*-depleted BMDMs. The M2-M1/young-old comparison resulted in 1492 DEGs specific for old wild type BMDMs and 2095 DEGs for old *Dnmt3a*-depleted BMDMs.

We interrogated our dataset for GO term enrichment for each comparison including genes that were uniquely up or down regulated in *Dnmt3a^{fl/fl}* or in *Dnmt3a^{LysM}* macrophages, and those that were found significantly differentially expressed in both. For the comparisons young (wild type versus *Dnmt3a^{LysM}*) and old (wild type versus *Dnmt3a^{LysM}*) in the category M1 versus resting, we found GO processes such as *positive interferon-gamma (IFN- γ) production* and *positive regulation of IL-8 production*, which are known hallmark of M1 polarization [258]. When comparing M2 and resting macrophages, we found *wound healing involved in inflammatory response* in the overlapping DEGs dataset and *positive regulation of phosphatidylinositol 3-kinase (PI3K) signaling* (already described to be associated with M2 status [259]) unique for wild type. Interestingly, *nitric oxide mediated signal transduction* and *regulation of macrophages activation* (both normally found in M1 macrophages [260], [261]) were found to be unique for *Dnmt3a^{LysM}* M2 BMDM. Comparing M2 to M1 macrophages, we observed *positive regulation of ERK1 and ERK2 cascade*, which is associated with M2 polarization [262], to be unique for *Dnmt3a^{LysM}* macrophages. In line to extensive work describing the complexity of transcriptional changes during M1-M2 polarization [165], [263]–[265], our analysis confirms that macrophage polarization results in drastic transcriptional change which not only is specific for each subtype, but also affects biological processes that are central in macrophage biology.

Perhaps most interesting, these results strongly support a key role of *Dnmt3a* on macrophage polarization and function, encouraging more specific experiments to further elucidate the relevance of *Dnmt3a* in pathogenesis.

4.2.3 *Dnmt3a* depletion and its impact on polarization marker genes expression and cellular reshaping

Previous findings deciphering macrophage polarization transcriptome [170], [246], [256], categorized macrophage polarization based on gene expression profiles. Here we validated the specificity of polarization marker genes that strongly associate with M1 and M2 macrophages polarization status. We found that *Dnmt3a*, *Arg-1*, *Retnla*, *Tnf* and immune responsive gene 1 (*Irg-1*) mRNA transcript levels vary significantly according to M1-M2 status. We observed that *Dnmt3a* mRNA expression was significantly higher in M2 BMDM, while being close to undetectable levels in the M1 counterpart. The relative expression levels of *Dnmt3b* mRNA did not follow such variation, suggesting that the lack of *Dnmt3a* does not translate in compensatory expression of other Dnmts. Controversially, previous works report an involvement of *Dnmt3b* in macrophage polarization [247] and that its deficiency aggravates pathologies such as pulmonary fibrosis by enhancing fibrotic macrophages activation [266]. Also, it was proposed that transient silencing of *Dnmt3b* promotes M2 and suppress macrophages M1 activation in adipose tissue macrophages (ATMs) and proved that its overexpression prevents IL-4 induced expression of *Arg-1* and LPS-induced TNF secretion [247]. We report that *Arg-1* and *Retnla* transcript levels significantly varied between *Dnmt3a*^{LysM}-derived and control macrophages. Comparing the M2 scenario, increased mRNA expression of *Arg-1* indicates an exacerbated M2 profile in *Dnmt3a*-null macrophages. On the other hand, we observed lower expression of *Retnla* mRNA in the same comparison, that might be indicating a reduction of the M2 signature in *Dnmt3a*-depleted BMDMs.

Prior studies reported that, upon activation, tissue resident or recruited macrophages can attract and activate other immune cells by releasing soluble stimuli such as pro inflammatory cytokines (*i.e* interleukin-1 β (IL-1 β) or tumor necrosis factor alpha (TNF α)) or chemokines (*i.e* , C-X-C motif chemokine ligand 8 (CXCL8, IL-8) and C-X-C motif ligand 2 (CXCL2)), resulting in lymphocytes activation and increased vascular permeability [267]. We therefore measured *Tnf* and *Irg-1*, mRNA transcript and showed that both are significantly higher in the M1 *Dnmt3a*-depleted subset compared to wild type control, suggesting an exacerbation of the M1 phenotype, which is typically defined by high *Tnf* and *Irg-1* expression [268], [269]. Interestingly, other groups reported that silencing of *Irg-1* gene expression in macrophages resulted in significantly reduced antimicrobial activity during bacterial

infections [269], linking *Irg-1* with M1 activation. We reported (Chapter 3.3.5) augmented phagocytosis ability in M2-*Dnmt3a* depleted macrophages, hypothesizing a propensity towards M1 polarization upon lack of *Dnmt3a*, which might be explained by the increased expression of *Irg-1* as central mediator of macrophage bactericidal activity.

These results, although counterintuitive, delineate a clear macrophage polarization impairment upon lack of *Dnmt3a* which propends towards the M1 activation. Even more importantly, these findings underline, for the first time, a critical role for *Dnmt3a* in the regulation of transcription of macrophage polarization marker genes, which so far was observed only for *Dnmt1* and *Dnmt3b* [270], [271].

M2 macrophages are described to be highly plastic, and able to adapt their morphology in response to environmental influences [163], [164], [209], where actin remodeling is critical for motility, phagocytosis and antigen presentation [272]. In our gene ontology (GO) analysis performed on the top 50 (up and down) differentially expressed genes (DEGs), we found controversial GO terms such as *positive regulation of phagocytosis* to be specific for *Dnmt3a*^{LysM} M2 macrophages.

We observed recurrent GO terms such as *Cytoskeleton organization* and *Cytoskeleton rearrangement*, which strongly associate with the M2 phenotype [273]. Hence, we stained actin filaments of *Dnmt3a*^{LysM} and control mice-derived BMDMs (resting, M1, M2) and demonstrated a phenotypically impaired cytoskeletal morphology proper of M2 *Dnmt3a*^{LysM} BMDMs. M2 cellular morphology is elongated, almost spindle like and evolving in a loglinear fashion [274]. M1 macrophages on the contrary are rounded, compact and highly reactive [166]. We propose that lack of *Dnmt3a* in M2 BMDMs leads to failure to elongate and acquire the typical spindle-like conformation, that we report to be maintained in the *Dnmt3a*^{fl/fl} control.

An exacerbation of the pro-inflammatory phenotype was already illustrated upon overexpression of *Dnmt1* in peripheral blood monocytes obtained from atherosclerosis (AS) patients [275]. We assessed the proportions of M1 and M2 macrophages based on the morphological features described above and observed that (in contrast to what observed for *Dnmt1* overexpression [275]), *Dnmt3a*-depleted macrophages have an overall propensity to adopt an M1 like morphology, supporting our hypothesis of an underlying activation of M1 phenotype upon lack of *Dnmt3a* in *in vitro* polarized BMDMs.

4.3 A comprehensive characterization of macrophagic effector functions

Within macrophages effector functions, phagocytosis is surely an outstanding feature and represents one of their main effector mechanisms [267]. Alongside phagocytosis, immune cell recruitment and activation are two major macrophage effector abilities [244], [267], [276]. We explored in a comprehensive approach the functional consequence of the deletion of *Dnmt3a* in macrophages

effector functions during differentiation/polarization and upon homeostasis and inflammation. For our systematic description, we employed a mouse model lacking *Dnmt3a* specifically in the myelomonocytic lineage (*Dnmt3a*^{LysM}) and generated *ex vivo* bone marrow derived macrophages (BMDMs) from wild type and *Dnmt3a*^{LysM} young and old (>34 weeks old) mice and used them as primary *ex vivo* model.

4.3.1 M2 *Dnmt3a*^{LysM} macrophages are more prone to phagocytosis

Macrophages are specialized phagocytes that can modulate adaptive immunity by recruiting other cells through chemokines secretion [276]. Phagocytosis is a process which is more pronounced in M1 macrophages due to their highly reactive phenotype [146], [254], [277], and DNMT3A was reported to be involved in *Staphylococcus aureus* response and efferocytosis, a type of phagocytosis [254]. We therefore challenged the concomitant M1-M2 phenotype that we previously observed in older *Dnmt3a*-deleted macrophages by testing their phagocytic capacity. We assessed the ability of young-old wild type and *Dnmt3a* knock out macrophages (resting, M1 and M2) to engulf foreign (Zymosan) particles. The phagocytic capacity of macrophages varies accordingly to their activation status and age [278]. Accordingly, the phagocytic capacity of resting, M2 and M1 BMDMs isolated from old mice, decreased compared to the young controls. Intriguingly, we detected in old mice-derived BMDMs increased rates of engulfed particles in the M2-polarized *Dnmt3a*^{LysM} subset, compared to the control expressing *Dnmt3a*.

As mentioned before, induction of phagocytosis is a mechanism widely associated with M1 phenotype [299], [279], [280]. In our analysis, M1-polarized *Dnmt3a*-depleted macrophages revealed reduced phagocytosis rates, pointing out the reduced effectiveness of *Dnmt3a*^{LysM}-derived M1 BMDMs compared to the control group. Notably, resting macrophages resembled the same feature. We might explain this considering that upon encounter with external particles, *naïve* macrophages can quickly activate and polarize into M1 phenotype, as previously reported [281]. This quick activation capacity might translate into increased phagocytic activity in the *Dnmt3a* knock out population, demonstrating that upon lack of *Dnmt3a*, a preponderant M1 phenotype takes place to cope with pathogen clearance.

Since we show these features in *naïve* BMDM, it would be informative to expand this experimental set up to macrophages isolated from different tissues - *ex vivo* - such as peritoneal macrophages, small intestinal or colonic macrophages, and implement our understanding of the phagocytosis ability of macrophages that already possess tolerogenic capacity.

4.3.2 Two competitive arginine pathways in macrophage physiology

Macrophages' key biological functions are mainly driven by the arginine metabolism: M1 macrophages express the enzyme nitric oxide synthase (NOS), which transforms arginine into nitric oxide and citrulline [282], [283]. M2 macrophages strongly express arginase, which hydrolyzes arginine to ornithine and urea. The fundamental hub is that arginase pathway limits arginine availability for NOS-dependent NO synthesis. NOS/arginase balance results in M1 versus M2 polarization that leads to biologically contrasting outcomes, mainly represented by inflammation initiation and tissue repair, respectively [183], [185]. We tested arginase and NOS activity, in young- and old- resting, M1 and M2 wild type and *Dnmt3a*-deleted macrophages and observed that old M2 *Dnmt3a*-depleted macrophages displayed lower arginase activity, while M1 macrophages had significantly higher arginase activity compared to control BMDMs. Although contrasting to what expected, this observation recalls and confirms the hypothesis of a dual M1-M2 coexistence, where M1 knock out macrophages exert a M2-like biological signature, and M2 *Dnmt3a*-null macrophages phenotypically resemble the M1 physiology.

Limitations in this approach might be individuated in the lack of a *in vivo* metabolic activity characterization, such as measurement of tissue-resident macrophage arginase and NOS activity, which might be instructive to further elucidate the impact of *Dnmt3a* on the arginine catabolism during for example, inflammation.

4.3.3 Wound repair and tumor progression

In a recent study we demonstrated that *Dnmt3a* is essential for tissue proliferation and regeneration at steady state and after inflammation in colonic epithelium [110]. Interestingly, not only *Dnmt3a* is essential in homeostatic colonic epithelium, but also in certain types of cancer, such as pancreatic cancer, where its silencing provokes G1-S phase transition arrest by downregulation cyclin D1 and IL8, with subsequent inactivation of STAT3 signaling pathway [284]. The association of *Dnmt3a* in macrophages with tissue repair and proliferation upon wounding has not been investigated yet.

Especially M2 macrophages are prone to induce tissue repair and regeneration [163], [170], [178]. For the first time, we show that the lack of *Dnmt3a* affects the ability of M2 macrophage to positively influence IECs growth and tumorous IECs proliferation. In a biomicritic experiment, we tested the proliferation rates of Mode-K cells grown in monolayer and co-cultivated with resting, M1 and M2 macrophages obtained from *Dnmt3a*^{fl/fl} and *Dnmt3a*^{LysM} mice. The drastic lack of wound closure characterizing the monolayer co-cultivated with *Dnmt3a*-depleted M2 macrophages, suggests a defective M2 polarization phenotype, unable to cope with tissue repair upon wounding. Additional

co-culture models involving organoid-derived monolayer from wild type C57BL/6 mice and APC^{min} mice (developing spontaneous multiple intestinal neoplasia) and macrophages, provide further proof of an inefficient M2 activity. M2 macrophages lacking *Dnmt3a* were less effective in promoting wild type monolayer formation. The same M2 macrophages, however, were able to significantly promote the growth of monolayers obtained from APC^{min} intestinal organoids, suggesting an important role for *Dnmt3a* in contrasting tumor advancement. We could therefore postulate that *Dnmt3a* might be fundamental in limiting tumor progression by orchestrating macrophage polarization and could in fact be essential for tissue homeostasis maintenance and tumor progression silencing.

Additional experiments *i.e* wounding assay *in vivo* might further elucidate the effect of *Dnmt3a* conditional deletion in the myelomonocytic lineage on epithelial wound healing in a (patho-) physiological scenario.

4.4 An age-dependent phenotype

Dnmt3a mutations are recurrent in myeloid malignancies [106], [285], and are linked to hematopoietic cells malignant transformation [101], [204]. Previous research concluded that simultaneous loss of *Dnmt3a* and *Dnmt3b* is lethal, proving their fundamentality in early development [250]. Whole body *Dnmt3a* deletion results in 100% mortality by week 4 after birth, and ablation of *Dnmt3a* in HSCs results into increased differentiation of hematopoietic lineages [101]. We therefore performed phenotypical and pathological comparison of mice lacking *Dnmt3a* uniquely in the myelomonocytic lineage at steady state.

Our analysis concluded that this conditional mouse model does not translate in lethality and that basal characterization of younger animals (8-20 weeks old mice) does not result in significant changes (in both males and females) in gross morphology, organ weight, motor ability or fertility.

We describe for the first time a fast-progressing hepato-splenomegaly (HPM) with spontaneous insurgence after 34 weeks of age. A similar phenotype was observed in 2016 in a study using Mx1-Cre-driven *Dnmt3a* deletion in HSC, that resulted in lethal hematologic disease, myeloid progenitor expansion, increased HSC self-renewal capacity and hepatomegaly due to liver-specific myeloproliferation and extramedullary hematopoiesis [194]. Our findings are in line with previous studies linking the lack of *Dnmt3a* in hematopoietic precursors with the aberrant tissue tropism and marked extramedullary hematopoiesis (EMH) with liver involvement [194].

The splenic and hepatic abnormal growth that we report might be a secondary manifestation of hematological malignancies such as leukemia or myeloproliferative disorders.

In support to our hypothesis, we demonstrated that the frequency of hematopoietic cells (Sca-1/c-Kit positive cells) in the spleen of old *Dnmt3a*-depleted mice (compared to old control littermates) is significantly higher, strengthening the already formulated hypothesis that maintenance of epigenetic regulation by *Dnmt3a* in the myelomonocytic lineage is necessary for the regulation of HSC self-renewal ability [103], [286].

Interestingly, previous studies concluded that *Dnmt3a* represses hematopoietic cells stemness and activate their transcriptional differentiation program [105], [287] and that its (and *Tet2*) deficiency converge into aberrant inflammatory signaling. In addition, we demonstrated an age-dependent diminishment in the proportion of Sca-1/c-Kit positive rates in WT mice. This phenotype was abolished in the old *Dnmt3a*-depleted mice, indicating that *Dnmt3a* might be essential for the fine tuning of HSC self-renewal regulation during aging. We assessed the proportions of the preponderant populations of immune cells residing in the spleen of young and old mice. For young mice, only CD11b⁺ cells were significantly less compared to *Dnmt3a*^{LysM} group. Most of the immune cell proportions were significantly different in old *Dnmt3a*^{LysM} mice compared to wild type spleens, in particular: significantly less CD3⁺ T cells and CD4⁺ helper T cells, and significantly more CD8⁺ cytotoxic T cells and CD11c⁺ (dendritic cells). In line with evidence supporting the diminished HSC self-renewal capacity [286], [288], the increased hematopoietic cells frequencies in spleens of >34 weeks old *Dnmt3a*-depleted mice confirmed an age-and-genotype-dependent effect on the splenic basal immune cell composition and proved a critical role for *Dnmt3a* in the regulation of hematopoietic cells self-renewal and differentiation capacity.

Additional experiments would greatly contribute to establish whether this dysregulation might in turn affect, *i.e* worsen, the response to inflammatory insults involving macrophage such as sepsis models or viral/bacterial infectious models.

4.5 Lack of *Dnmt3a* impacts recovery after intestinal inflammation

Our group previously demonstrated that *Dnmt3a* is central in restoration after inflammation in intestinal epithelial cells [110], and that lack of *Dnmt3a* results in worsening of the overall ability of coping with inflammation. We also found *Dnmt3a* to be downregulated in macrophages during inflammation, resulting in a M1-like or non-resolutive M2-like phenotype *in vitro*. We hypothesized that the absence of *Dnmt3a* in the myelomonocytic lineage might influence the pathophysiological response upon chemically induced *in vivo* inflammatory models.

Acute and chronic DSS colitis models are useful to study the contribution of the innate immune system to the development of intestinal inflammation [289]. Contrastingly to the downregulation of *Dnmt3a* that we systematically observed, it was recently proposed that during DSS treatment *Dnmt3a* transcript is upregulated in intestinal epithelial tissue, resulting in aggravated colitis [290]. In our acute model, we could not demonstrate an effect of the lack of *Dnmt3a* during the acute inflammatory phase based on body weight variation nor disease activity. On the same line, we did not find significant differences in body weight nor immune cell composition of spleen and intestinal LP after the recovery phase. However, in support to our hypothesis, we observed significantly higher disease activity during the resolution phase in mice lacking *Dnmt3a*, suggesting *Dnmt3a* to have a protective role against inflammation.

Dnmt3a mutations in the hematopoietic system are associated with colitis-associated colon cancer development [291]. Also, in our *in vitro* co-culture system, we observed that *Dnmt3a* is dysregulated accordingly to inflammatory conditions and its lack in macrophages favours tumor tissue proliferation. AOM-DSS is a useful model that mimics IBD-colorectal cancer (CRC) by chemical induction of DNA damage followed by repeated cycles of DSS [292], [293]. We adopted this strategy to define the contribution of *Dnmt3a* in macrophages in response to chronic inflammation and tumorigenesis. Our AOM-DSS model did not allow any conclusion concerning the role of *Dnmt3a* in tumor formation during inflammation *in vivo* (ineffectiveness of AOM treatment). Nonetheless, we observed increased body weight in the *Dnmt3a*^{LysM} group at the latest experimental time point. Interestingly, previous work highlighted a central role for *Dnmt3a* in the regulation of adipocytes differentiation [294] and a drastic occurrence of a fast-progressing obesity with significant increased amount of abdominal and subcutaneous fat in mice lacking *Dnmt3a* in neurons [295]. On the same line, heterozygous germline mutations in *Dnmt3a* lead to obesity, indicating that *Dnmt3a* coordinates energy storage required to maintain normal weight and prevent inflammatory obesity [294]. In our analysis, *Dnmt3a*^{LysM} group was characterized by significantly higher epididymal white adipose tissue (EWAT) weight compared to the control group. This phenotype could be the result of EWAT expansion due to the interference of the lack of *Dnmt3a* in energy storage related pathways.

Overall, our *in vivo* investigations comprising acute and chronic (AOM-DSS) treatments are indicative for a role of *Dnmt3a* during the course of the disease. The significantly worse histopathological conditions in the colon of *Dnmt3a*^{LysM} might reinforce our hypothesis of a delayed/aggravated response to inflammation due to the lack of *Dnmt3a*. Considering our *in vitro* data showing an involvement of *Dnmt3a* in wound repair and M2 polarization, we can speculate that *Dnmt3a* in

macrophages is fundamental for tissue regeneration via the control of resolutive M2 macrophages, and that its deletion results in delayed restoration of homeostasis.

5. Conclusions and future perspectives

Genome-wide association studies (GWAS) had labeled DNMT3A as a risk gene for CD, raising the hypothesis of a pivotal role for DNMT3A in IBD pathophysiology. With the advance of genome-wide DNA methylation profiling technologies, the study of how DNMT3A contribute to the methylome, and subsequent genetic regulation has received more and more interest.

This thesis brings novel insights into the pivotal role of *Dnmt3a* in directing gene transcription and the functional consequence of its myelomonocytic specific deletion, with particular emphasis on macrophage polarization. Although these informative findings shed new light on the effect of DNA methylation on homeostasis and inflammation, some open points and questions remain to be addressed.

The basis for the investigation of the biological consequence of the lack of *Dnmt3a* in the myelomonocytic lineage upon macrophages polarization was found in a simple, but essential, 9 days follow up experiment where DNMT3A protein levels were measured in wild type M1 and M2 macrophages. DNMT3A expression was strictly dependent on the polarization status, in particular, it was up regulated in homeostatic (M2) macrophages, and almost undetectable in pro-inflammatory (M1) macrophages. Bulk RNA sequencing analysis of resting, M1 and M2 bone marrow derived macrophages polarized *in vitro*, demonstrated a profound but specific dysregulation of the transcriptome of macrophages belonging to each polarization groups. From here, polarization-defining genes (*i.e Arg-1, Retnla, iNos* and *Irg-1*) were selected and served as confirmatory markers for further investigations aimed to assess cellular morphology, phagocytic capacity, enzymatic activity and macrophage-epithelial communication upon wound healing and tissue proliferation.

Our *ex vivo* polarization-based experiments demonstrated that genomic deletion of *Dnmt3a* results in a dichotomous co-existing M1-M2 phenotypical and transcriptional signature, that affects normal macrophages effector functions. *Dnmt3a* was found to be essential for correct macrophage polarization, as M2 *Dnmt3a*-depleted macrophages failed to morphologically resemble the canonical elongated, spindle-like shape characteristic of M2 macrophages. Increased levels of phagocytosis rates and unbalanced arginase and NOS activity were observed in M2 macrophages generated from older (>34) mice, indicating that not only *Dnmt3a* is essential for correct macrophage morphological adaptation during polarization, but also is central in defining the direction of arginine metabolic processing, which is determinant in macrophage physiology. In this context, metabolomics analysis might be crucial in deciphering differentially regulated metabolic pathways upon *Dnmt3a* genomic depletion.

In addition to an unconventional M1-M2 polarization, this work proves that *Dnmt3a* deletion in the myelomonocytic lineage results in transcriptional perturbation of genes involved in cytoskeletal rearrangement, cellular polarization, macrophage effector functions and dysregulation of metabolic hubs such as arginase and nitric oxide synthase. Methylome profiling would be of primary importance to decipher how DNA methylation dysregulation affects the transcription of the genes involved in the beforehand mentioned biological mechanism. Surely, further analysis is required to fully untangle the complex DNA methylation-gene expression cooperation in a multi-omics comprehensive approach.

Our *in vivo* studies revealed two main findings. The first, that *Dnmt3a* deficiency results in spontaneous age-dependent hepatosplenomegaly starting at 34 weeks of age, as supposedly secondary result of malignant myeloproliferative defects with consequent extramedullary hyperproliferation. Second, we showed that *Dnmt3a* depletion in macrophages might have an impact on disease activity after acute chemically-induced colitis, especially during the recovery phase.

Thus, it would be of great interest to perform additional *in vivo* models such as LPS shock to further elucidate the role of *Dnmt3a* in the myelomonocytic lineage upon inflammation. Whole genome methylation analysis linking DNA methylation and gene expression changes during inflammation and resolution might ultimately result in the identification of novel targets that might in turn contribute to the development of more effective intervention approaches.

6. Summary

The intestinal epithelium and the immune cells residing in the lamina propria are in close relation and their tightly regulated communication is necessary to maintain homeostasis. During inflammatory bowel disease (IBD) manifestations, inflammatory cascades are over activated and failure to restore homeostasis results in chronic inflammatory responses, such as the one observed in IBD. The insurgence of IBD depends on multiple factors, between which epigenetics has a central role. Epigenetic modifications such as DNA methylation regulate gene transcription through a tightly regulated and inheritable mechanism that can be shaped according to environmental conditions.

DNA methylation orchestrates gene expression in a cell and tissue-specific manner interfering with transcription factor binding sites accessibility: in a simplified model, DNA hypermethylation and hypomethylation result in gene transcription silencing and activation, respectively. The family of enzymes responsible for establishment and maintenance of DNA methylation signature during development are the so-called DNA methyltransferases (DNMTs), which genomic deletion results in lethality already at embryonic stage. Genetic investigations associated DNA methyltransferase 3A (DNMT3A), a *de novo* methyltransferase, with IBD. Furthermore, DNMT3A (and mutations occurring at DNMT3A locus) were also associated with hematopoietic stem cells self-renewal during aging and hematopoietic malignancies, suggesting a pivotal role for DNMT3A in orchestrating hematopoietic cell developmental programs and making DNMT3A a novel, interesting target for research.

The first part of this thesis (reported in chapter 3.1) consists of experiments aimed to fortify our understanding of the role of *Dnmt3a* in the intestinal epithelium. Here, we demonstrated increased bacterial translocation to distant sites (mesenteric lymph nodes) as a result of an alteration of intestinal permeability, reduced Goblet cells count and thinning of colonic mucus layer in mice lacking *Dnmt3a* in intestinal epithelial cells (IECs) compared to control littermates, already at baseline conditions. Further investigations revealed an inflammation-dependent *DNMT3A* transcriptional downregulation in IBD patients-derived colonic organoids, and stimulation experiments in murine organoids demonstrated a decreased expression of *Dnmt3a* transcript, which is likely to be via TNF α . Therefore, we confirmed that *Dnmt3a* is downregulated during inflammation and that perturbs gut permeability and mucus formation, finally disrupting intestinal barrier homeostasis.

The second part of this work (reported from chapter 3.2 to 3.5) explores the functional consequences of *Dnmt3a* deletion in the myelomonocytic lineage of conditional murine models. Since the impact of *Dnmt3a* in myeloid lineage during intestinal homeostasis and inflammation has not been investigated

yet, we explored the functional consequence of the lack of *Dnmt3a* in macrophages *in vitro* and *in vivo*. In this section we show that *Dnmt3a* is downregulated both mRNA and protein level in murine macrophages during inflammatory conditions (M1 macrophages) and upregulated during M2 polarization (anti-inflammatory, tolerogenic, “homeostatic” conditions). Based on this strong observation, we performed RNA sequencing in resting, M1 and M2 macrophages generated from young and old mice either expressing or lacking *Dnmt3a* in the myelomonocytic lineage. A complex dysregulation of the gene expression profiles characterized the groups included in the analysis, evincing a disbalanced transcriptional polarization signature. GO enrichment analysis of the 50 most differentially regulated unique genes revealed, between many others, phagocytosis, and positive nitric oxide synthesis not only in the (expected) M1 category, but also in the M2 subtype of *Dnmt3a*-null bone marrow derived macrophages (BMDMs), suggesting that lack of *Dnmt3a* might impact the regulation of specific metabolic pathways that in turn results into an impaired polarization phenotype.

Furthermore, we functionally assessed the contribution of *Dnmt3a* on macrophage polarization. Absence of *Dnmt3a* resulted in impaired gene expression of polarization marker. The dysregulated gene expression profile translated into an alteration of the canonical M1-M2 defining macroscopical phenotypic characteristics, including cellular morphology and ability to engulf foreign particles.

Moreover, we performed a series of *in vitro* functional assays to demonstrate that myelomonocytic ablation of *Dnmt3a* induces dysregulation of arginine metabolism - crucial to the resolution of macrophage polarization - and favors M1 phenotype (even in the presence of M2 macrophage polarizing conditions). In depth characterization of mice lacking *Dnmt3a* expression in myelomonocytic lineage cells resulted in overt phenotype manifestations only in aged mice. Young *Dnmt3a* KO mice displayed a decreased number of monocytes in the spleen, while all organs maintained, in general, normal morphology. Mice lacking *Dnmt3a* developed a severe, fast progressing hepatosplenomegaly starting at 34 weeks of age, and had increased circulating numbers of hematopoietic stem cells. These experiments demonstrate that the lack of *Dnmt3a* impacts macrophage polarization towards M1-subtype, and that ablation of *Dnmt3a* in macrophages might have an effect in inflammation and in tumor development.

Collectively, the findings reported in this thesis underline the extensive contribution of *Dnmt3a* in maintaining intestinal homeostasis, not only when confined to the intestinal epithelium, but also in immune cells belonging to the myelomonocytic lineage. We conclude that *Dnmt3a* is key in maintaining mucosal permeability in the intestinal epithelial compartment. If disrupted, intestinal epithelial cells might have a compromised capability for regeneration and tissue repair, hence,

hijacking tissue integrity. In addition, *Dnmt3a* is crucial in directing macrophage polarization as its depletion favors the proinflammatory M1 phenotype. Thus, genetic disturbances in DNMT3A gene could provoke a decreased threshold for developing an exacerbated proinflammatory immune response in IBD patients. Finally, since *Dnmt3a*^{LysM} mice develop hepatosplenomegaly and display increased hematopoietic stem cell numbers with age, we conclude that *Dnmt3a* might also have a role in tumorigenesis, hence in the development of (extra)-gastrointestinal complications and tumors in IBD patients. In conclusion, we could postulate that *Dnmt3a* is essential for tissue integrity and mucosal permeability in the intestinal epithelium, and that it is central in tuning macrophages polarization in response to detrimental insults in an age-dependent manner.

7. Zusammenfassung

Das intestinale Epithel und die in der Lamina propria lokalisierten Immunzellen stehen in enger Beziehung zueinander. Ihre streng regulierte Kommunikation ist dabei für die Aufrechterhaltung der intestinalen Homöostase erforderlich. Bei Manifestation einer chronisch-entzündlichen Darmerkrankung (CED), hierzu zählen Morbus Crohn und Colitis ulcerosa, werden zunächst Entzündungskaskaden aktiviert. Kann im weiteren Verlauf die Homöostase nicht wiederhergestellt werden, entsteht eine chronische Entzündung. Die CED-Pathogenese ist multifaktoriell; Epigenetik spielt dabei eine zentrale Rolle: Epigenetische Veränderungen wie die DNA-Methylierung steuern die Gentranskription durch einen streng regulierten und vererbaren Mechanismus, der in Abhängigkeit von äußeren Bedingungen aber auch modifiziert werden kann. Die DNA-Methylierung steuert die Genexpression dabei zell- sowie gewebespezifisch, indem sie die Zugänglichkeit der Bindungsstellen für Transkriptionsfaktoren steuert: In einem vereinfachten Modell führen DNA Hypermethylierung und Hypomethylierung zu einer Unterdrückung (silencing) bzw. Aktivierung der Gentranskription.

Für die Etablierung und Aufrechterhaltung der DNA-Methylierung während der Entwicklung sind die sogenannten DNA-Methyltransferasen (DNMTs) verantwortlich. Deren genomische Deletion führt dagegen bereits im Embryonalstadium zur Letalität. Außerdem deuten genetische Analysen auf eine Assoziation zwischen der *de novo* Methyltransferase DNMT3A, und CED hin. Darüber hinaus wurde DNMT3A (und Mutationen im *DNMT3A*-Locus) auch mit der Selbsterneuerung hämatopoetischer Stammzellen im Rahmen des Alterungsprozesses und mit malignen hämatologischen Erkrankungen in Verbindung gebracht. Dies deutet auf eine entscheidende Rolle von *Dnmt3a* bei der Steuerung der Entwicklung von hämatopoetischen Zellen hin. Somit stellt DNMT3A ein interessantes, vielversprechendes Target für die Forschung dar.

Der erste Teil dieser Arbeit (dargestellt in Kapitel 3.1) knüpft an Forschungsergebnisse unserer Arbeitsgruppe an, die bereits im Rahmen der Publikation „DNA-Methyltransferase 3A controls intestinal epithelial barrier function and regeneration in the colon“ (Fazio and Bordoni et. al., Nat. Comm, 2022) zusammengefasst wurden und beinhaltet weiterführende Experimente, um unser Verständnis der Rolle von *Dnmt3a* im intestinalen Epithel weiter zu vertiefen.

Wir konnten demonstrieren, dass Mäuse, die eine Deletion von *Dnmt3a* im intestinalen Epithel aufweisen, im Vergleich zu Kontrollmäusen eine erhöhte bakterielle Translokation aufweisen. Diese wird durch eine erhöhte Darmpermeabilität, einer Reduktion von Goblet-Zellen und einem Rückgang der Mucusschicht begünstigt. Außerdem wurde eine entzündungsabhängige, reduzierte Transkription von *DNMT3A* in Colon-Organoiden, generiert aus Biopsien von CED-Patienten, beobachtet.

Gleichermaßen wurde in murinen Organoiden eine TNF α -vermittelte verringerte Expression von *Dnmt3a* auf mRNA-Ebene beobachtet.

Diese Beobachtungen bestätigen, dass *Dnmt3a* während einer Entzündung herunterreguliert wird. Dies führt zu einer Beeinträchtigung der Darmpermeabilität sowie der Mucusbildung, wodurch die intestinale Homöostase gestört wird.

Im zweiten Teil dieser Arbeit (siehe Kapitel 3.2 bis 3.5) werden die funktionellen Folgen einer Deletion von *Dnmt3a* in Zellen der myelomonozytären Linie mittels eines konditionalen Mausmodells untersucht. Da die Rolle von *Dnmt3a* in myeloischen Zellen für die Aufrechterhaltung der intestinalen Homöostase und bei der Entstehung von Entzündung bisher nicht näher beschrieben wurde, analysierten wir sowohl in vitro als auch in vivo die funktionellen Folgen einer Deletion von *Dnmt3a* in Makrophagen.

In diesem Abschnitt wird gezeigt, dass *Dnmt3a* sowohl auf mRNA- als auch auf Proteinebene in murinen Wildtyp-Makrophagen unter pro-inflammatorischen Bedingungen (M1 Makrophagen) herunterreguliert und während der M2-Polarisierung (entzündungshemmende, tolerogene, "homöostatische" Bedingungen) hochreguliert wird. Ausgehend von dieser Beobachtung führten wir eine RNA-Sequenzierung in ruhenden M1- und M2 Makrophagen durch, die aus *Dnmt3a*^{fl/fl}- und *Dnmt3a*-depletierten Makrophagen junger und alter Mäuse gewonnen wurden. Es zeigte sich eine komplexe Dysregulation der Genexpressionsprofile der analysierten Gruppen, was auf eine unausgewogene genetische Signatur der Polarisierung hindeutet. Die Gene Ontology (GO)-Anreicherungsanalyse der 50 am stärksten differenziell regulierten Gene identifizierte unter anderem die Phagozytose und die positive Stickoxid-Synthese sowohl in der (erwarteten) M1-Kategorie, aber auch im M2 Subtyp der *Dnmt3a*-depletierten Makrophagen. Wir vermuten daher, dass das Fehlen von *Dnmt3a* die Regulierung spezifischer Stoffwechselwege beeinflusst und in Folge zu einem gestörten Polarisationsphänotyp führt.

Basierend auf diesen Ergebnissen haben wir im nächsten Schritt die Rolle von *Dnmt3a* bei der Polarisierung von Makrophagen auch funktionell untersucht. Das Fehlen von *Dnmt3a* führte zu einer veränderten Genexpression verschiedener Polarisationsmarkern. Diese Dysregulation ging mit einer Veränderung der klassischen M1-M2 phänotypischen Merkmale, einschließlich der Zellmorphologie, einher.

Darüber hinaus konnte ich anhand von verschiedener in vitro Funktionstests aufzeigen, dass die myelomonozytäre Ablation von *Dnmt3a* zu einer Dysregulation des Arginin-Stoffwechsels führt – dieser ist für die Auflösung der Makrophagenpolarisierung entscheidend – und damit den M1-

Phänotyp begünstigt (selbst bei Vorliegen von Bedingungen, die eine M2-Makrophagenpolarisierung induzieren würden). Die umfassende Charakterisierung von Mäusen mit einer Deletion von *Dnmt3a* in den Zellen der myelomonozytären Linie (Dnmt3LysM) ergab, dass sich dieser Phänotyp allerdings nur bei älteren Mäusen manifestiert. Junge Mäuse mit dieser Deletion wiesen zwar eine verringerte Anzahl von Monozyten in der Milz auf, bei den Organen wurden aber keine Besonderheiten hinsichtlich ihrer Morphologie festgestellt. Dagegen entwickelten gealterte Dnmt3LysM-Mäuse eine Hepatosplenomegalie. Außerdem wurde eine erhöhte Anzahl zirkulierender hämatopoetischer Stammzellen detektiert. Diese Experimente zeigen, dass das Fehlen von *Dnmt3a* die Polarisierung von Makrophagen in Richtung des M1-Subtyps verschiebt und dass die Ablation von *Dnmt3a* in Makrophagen Auswirkungen auf Entzündungen und die Tumorentwicklung hat.

Insgesamt unterstreichen die in dieser Arbeit berichteten Ergebnisse die entscheidende Funktion von *Dnmt3a* in der Aufrechterhaltung der intestinalen Homöostase sowohl in intestinalen Epithelzellen als auch in Immunzellen der myelomonozytären Linie. Unsere Beobachtungen demonstrieren, dass *Dnmt3a* eine Schlüsselrolle bei der Aufrechterhaltung der Barrierefunktion des intestinalen Epithels besitzt. Eine Schädigung der Funktion von DNMT3A könnte die intestinalen Epithelzellen in ihrer Fähigkeit zur Regeneration und Wundheilung beeinträchtigen, wodurch die Integrität des Gewebes gestört wird. Darüber hinaus ist *Dnmt3a* für die Steuerung der Polarisierung von Makrophagen von entscheidender Bedeutung: Eine Deletion von *Dnmt3a* führt zu einer Verschiebung in Richtung des proinflammatorischen M1-Phänotyps. Genetische Störungen, die DNMT3A betreffen, könnten zu der verstärkten proinflammatorischen Immunantwort bei CED-Patienten beitragen.

Die Beobachtung, dass *Dnmt3a*^{LysM}-Mäuse mit zunehmendem Alter eine Hepatosplenomegalie entwickeln und eine erhöhte Anzahl hämatopoetischer Stammzellen aufweisen, deutet darauf hin, dass DNMT3A auch eine Rolle bei der Tumorgenese und damit bei der Entwicklung von intestinalen als auch extraintestinale Komplikationen sowie Tumoren bei CED-Patienten spielen könnte. Zusammenfassend konnten wir zeigen, dass *Dnmt3a* für die Integrität des Gewebes und die Barrierefunktion des intestinalen Epithels essentiell ist und dass *Dnmt3a* eine zentrale Rolle bei der Makrophagenpolarisierung als Reaktion auf schädliche Einflüsse spielt, die altersabhängig erfolgt.

8. References

- [1] M. Agrawal, K. H. Allin, F. Petralia, J.-F. Colombel, and T. Jess, “Multiomics to elucidate inflammatory bowel disease risk factors and pathways,” *Nat Rev Gastroenterol Hepatol*, Mar. 2022, doi: 10.1038/s41575-022-00593-y.
- [2] J. Burisch and P. Munkholm, “The epidemiology of inflammatory bowel disease.,” *Scand J Gastroenterol*, vol. 50, no. 8, pp. 942–51, Aug. 2015, doi: 10.3109/00365521.2015.1014407.
- [3] T. F. Malik and D. M. Aurelio, *Extraintestinal Manifestations of Inflammatory Bowel Disease*. 2022.
- [4] B. E. Sands, “From symptom to diagnosis: clinical distinctions among various forms of intestinal inflammation.,” *Gastroenterology*, vol. 126, no. 6, pp. 1518–32, May 2004, doi: 10.1053/j.gastro.2004.02.072.
- [5] C. N. Bernstein *et al.*, “World Gastroenterology Organization Practice Guidelines for the diagnosis and management of IBD in 2010.,” *Inflamm Bowel Dis*, vol. 16, no. 1, pp. 112–24, Jan. 2010, doi: 10.1002/ibd.21048.
- [6] L. M. Spekhorst *et al.*, “Performance of the Montreal classification for inflammatory bowel diseases.,” *World J Gastroenterol*, vol. 20, no. 41, pp. 15374–81, Nov. 2014, doi: 10.3748/wjg.v20.i41.15374.
- [7] D. S. Keller, A. Windsor, R. Cohen, and M. Chand, “Colorectal cancer in inflammatory bowel disease: review of the evidence.,” *Tech Coloproctol*, vol. 23, no. 1, pp. 3–13, 2019, doi: 10.1007/s10151-019-1926-2.
- [8] T. Bennike, “Biomarkers in inflammatory bowel diseases: Current status and proteomics identification strategies,” *World J Gastroenterol*, vol. 20, no. 12, p. 3231, 2014, doi: 10.3748/wjg.v20.i12.3231.
- [9] Z. Cai, S. Wang, and J. Li, “Treatment of Inflammatory Bowel Disease: A Comprehensive Review,” *Front Med (Lausanne)*, vol. 8, Dec. 2021, doi: 10.3389/fmed.2021.765474.
- [10] P. L. Lakatos, L. Lakatos, L. S. Kiss, L. Peyrin-Biroulet, A. Schoepfer, and S. Vavricka, “Treatment of extraintestinal manifestations in inflammatory bowel disease.,” *Digestion*, vol. 86 Suppl 1, pp. 28–35, 2012, doi: 10.1159/000341950.
- [11] C. Mowat *et al.*, “Guidelines for the management of inflammatory bowel disease in adults.,” *Gut*, vol. 60, no. 5, pp. 571–607, May 2011, doi: 10.1136/gut.2010.224154.
- [12] G. R. D’Haens *et al.*, “The London Position Statement of the World Congress of Gastroenterology on Biological Therapy for IBD with the European Crohn’s and Colitis Organization: when to start, when to stop, which drug to choose, and how to predict

- response?," *Am J Gastroenterol*, vol. 106, no. 2, pp. 199–212; quiz 213, Feb. 2011, doi: 10.1038/ajg.2010.392.
- [13] G. van Assche *et al.*, "The second European evidence-based Consensus on the diagnosis and management of Crohn's disease: Definitions and diagnosis.," *J Crohns Colitis*, vol. 4, no. 1, pp. 7–27, Feb. 2010, doi: 10.1016/j.j.crohns.2009.12.003.
 - [14] A. Dignass *et al.*, "Second European evidence-based consensus on the diagnosis and management of ulcerative colitis part 1: definitions and diagnosis.," *J Crohns Colitis*, vol. 6, no. 10, pp. 965–90, Dec. 2012, doi: 10.1016/j.j.crohns.2012.09.003.
 - [15] M. Sobczak *et al.*, "Current overview of extrinsic and intrinsic factors in etiology and progression of inflammatory bowel diseases," *Pharmacological Reports*, vol. 66, no. 5, pp. 766–775, Oct. 2014, doi: 10.1016/j.pharep.2014.04.005.
 - [16] M. Orholm, V. Binder, T. I. Sørensen, L. P. Rasmussen, and K. O. Kyvik, "Concordance of inflammatory bowel disease among Danish twins. Results of a nationwide study.," *Scand J Gastroenterol*, vol. 35, no. 10, pp. 1075–81, Oct. 2000, doi: 10.1080/003655200451207.
 - [17] S. C. Ng, S. Woodrow, N. Patel, J. Subhani, and M. Harbord, "Role of genetic and environmental factors in British twins with inflammatory bowel disease," *Inflamm Bowel Dis*, vol. 18, no. 4, pp. 725–736, Apr. 2012, doi: 10.1002/ibd.21747.
 - [18] L. Halme, P. Paavola-Sakki, U. Turunen, M. Lappalainen, M. Farkkila, and K. Kontula, "Family and twin studies in inflammatory bowel disease.," *World J Gastroenterol*, vol. 12, no. 23, pp. 3668–72, Jun. 2006, doi: 10.3748/wjg.v12.i23.3668.
 - [19] H. Yang, C. McElree, M. P. Roth, F. Shanahan, S. R. Targan, and J. I. Rotter, "Familial empirical risks for inflammatory bowel disease: differences between Jews and non-Jews.," *Gut*, vol. 34, no. 4, pp. 517–24, Apr. 1993, doi: 10.1136/gut.34.4.517.
 - [20] K. M. de Lange *et al.*, "Genome-wide association study implicates immune activation of multiple integrin genes in inflammatory bowel disease," *Nat Genet*, vol. 49, no. 2, pp. 256–261, Feb. 2017, doi: 10.1038/ng.3760.
 - [21] Y. Momozawa *et al.*, "IBD risk loci are enriched in multigenic regulatory modules encompassing putative causative genes," *Nat Commun*, vol. 9, no. 1, p. 2427, Dec. 2018, doi: 10.1038/s41467-018-04365-8.
 - [22] A. Franke *et al.*, "Genome-wide association study for ulcerative colitis identifies risk loci at 7q22 and 22q13 (IL17REL)," *Nat Genet*, vol. 42, no. 4, pp. 292–294, Apr. 2010, doi: 10.1038/ng.553.
 - [23] C. A. Anderson *et al.*, "Meta-analysis identifies 29 additional ulcerative colitis risk loci, increasing the number of confirmed associations to 47," *Nat Genet*, vol. 43, no. 3, pp. 246–252, Mar. 2011, doi: 10.1038/ng.764.

- [24] A. Franke *et al.*, “Genome-wide meta-analysis increases to 71 the number of confirmed Crohn’s disease susceptibility loci,” *Nat Genet*, vol. 42, no. 12, pp. 1118–1125, Dec. 2010, doi: 10.1038/ng.717.
- [25] U. M. Marigorta, “Genetic Risk Prediction in IBD,” in *Molecular Genetics of Inflammatory Bowel Disease*, Cham: Springer International Publishing, 2019, pp. 141–156. doi: 10.1007/978-3-030-28703-0_7.
- [26] L. Jostins *et al.*, “Host–microbe interactions have shaped the genetic architecture of inflammatory bowel disease,” *Nature*, vol. 491, no. 7422, pp. 119–124, Nov. 2012, doi: 10.1038/nature11582.
- [27] V. B. T. I. A. S. M. Orholm, “Concordance of Inflammatory Bowel Disease among Danish Twins: Results of a Nationwide Study,” *Scand J Gastroenterol*, vol. 35, no. 10, pp. 1075–1081, Jan. 2000, doi: 10.1080/003655200451207.
- [28] B. Maher, “Personal genomes: The case of the missing heritability,” *Nature*, vol. 456, no. 7218, pp. 18–21, Nov. 2008, doi: 10.1038/456018a.
- [29] E. W. Lopes *et al.*, “Risk Factors for Incident Inflammatory Bowel Disease According to Disease Phenotype,” *Clin Gastroenterol Hepatol*, Jan. 2022, doi: 10.1016/j.cgh.2022.01.003.
- [30] A. Kaser, S. Zeissig, and R. S. Blumberg, “Inflammatory bowel disease,” *Annu Rev Immunol*, vol. 28, pp. 573–621, 2010, doi: 10.1146/annurev-immunol-030409-101225.
- [31] X. C. Zhu and R. P. MacDermott, “A Primer on IBD: Phenotypes, Diagnosis, Treatment, and Clinical Challenges,” in *Molecular Genetics of Inflammatory Bowel Disease*, New York, NY: Springer New York, 2013, pp. 3–21. doi: 10.1007/978-1-4614-8256-7_1.
- [32] I. Loddio and C. Romano, “Inflammatory Bowel Disease: Genetics, Epigenetics, and Pathogenesis,” *Front Immunol*, vol. 6, Nov. 2015, doi: 10.3389/fimmu.2015.00551.
- [33] I. Lacal and R. Ventura, “Epigenetic Inheritance: Concepts, Mechanisms and Perspectives,” *Front Mol Neurosci*, vol. 11, Sep. 2018, doi: 10.3389/fnmol.2018.00292.
- [34] J. Xu *et al.*, “New Insights Into the Epigenetic Regulation of Inflammatory Bowel Disease,” *Front Pharmacol*, vol. 13, p. 813659, 2022, doi: 10.3389/fphar.2022.813659.
- [35] C. H. Waddington, “The Epigenotype,” *Int J Epidemiol*, vol. 41, no. 1, pp. 10–13, Feb. 2012, doi: 10.1093/ije/dyr184.
- [36] C. H. Waddington, “GENETIC ASSIMILATION OF THE *BITHORAX* PHENOTYPE,” *Evolution (N Y)*, vol. 10, no. 1, pp. 1–13, Mar. 1956, doi: 10.1111/j.1558-5646.1956.tb02824.x.
- [37] E. Tronick and R. G. Hunter, “Waddington, Dynamic Systems, and Epigenetics,” *Front Behav Neurosci*, vol. 10, Jun. 2016, doi: 10.3389/fnbeh.2016.00107.

- [38] W. Chan, A. Chen, D. Tiao, C. Selinger, and R. Leong, "Medication adherence in inflammatory bowel disease," *Intest Res*, vol. 15, no. 4, p. 434, 2017, doi: 10.5217/ir.2017.15.4.434.
- [39] A. Fazio, D. Bordoni, and P. Rosenstiel, "Inflammatory Bowel Disease and Epigenetics," in *Molecular Genetics of Inflammatory Bowel Disease*, Cham: Springer International Publishing, 2019, pp. 183–201. doi: 10.1007/978-3-030-28703-0_9.
- [40] N. T. Ventham, N. A. Kennedy, E. R. Nimmo, and J. Satsangi, "Beyond Gene Discovery in Inflammatory Bowel Disease: The Emerging Role of Epigenetics," *Gastroenterology*, vol. 145, no. 2, pp. 293–308, Aug. 2013, doi: 10.1053/j.gastro.2013.05.050.
- [41] M. Scarpa and E. Stylianou, "Epigenetics: Concepts and relevance to IBD pathogenesis," *Inflamm Bowel Dis*, vol. 18, no. 10, pp. 1982–1996, Oct. 2012, doi: 10.1002/ibd.22934.
- [42] G. Koukos *et al.*, "A MicroRNA Signature in Pediatric Ulcerative Colitis," *Inflamm Bowel Dis*, vol. 21, no. 5, pp. 996–1005, May 2015, doi: 10.1097/MIB.0000000000000339.
- [43] A. Unnikrishnan, W. M. Freeman, J. Jackson, J. D. Wren, H. Porter, and A. Richardson, "The role of DNA methylation in epigenetics of aging," *Pharmacol Ther*, vol. 195, pp. 172–185, Mar. 2019, doi: 10.1016/j.pharmthera.2018.11.001.
- [44] T. Kucharzik *et al.*, "Recent understanding of IBD pathogenesis: Implications for future therapies," *Inflamm Bowel Dis*, vol. 12, no. 11, pp. 1068–1083, Nov. 2006, doi: 10.1097/01.mib.0000235827.21778.d5.
- [45] R. Kellermayer, "Epigenetics and the developmental origins of inflammatory bowel diseases.," *Can J Gastroenterol*, vol. 26, no. 12, pp. 909–15, Dec. 2012, doi: 10.1155/2012/526408.
- [46] R. Fujii, S. Sato, Y. Tsuboi, A. Cardenas, and K. Suzuki, "DNA methylation as a mediator of associations between the environment and chronic diseases: A scoping review on application of mediation analysis," *Epigenetics*, pp. 1–27, Aug. 2021, doi: 10.1080/15592294.2021.1959736.
- [47] M. M. Suzuki and A. Bird, "DNA methylation landscapes: provocative insights from epigenomics," *Nat Rev Genet*, vol. 9, no. 6, pp. 465–476, Jun. 2008, doi: 10.1038/nrg2341.
- [48] F. Capuano, M. Müllender, R. Kok, H. J. Blom, and M. Ralser, "Cytosine DNA Methylation Is Found in *Drosophila melanogaster* but Absent in *Saccharomyces cerevisiae*, *Schizosaccharomyces pombe*, and Other Yeast Species," *Anal Chem*, vol. 86, no. 8, pp. 3697–3702, Apr. 2014, doi: 10.1021/ac500447w.
- [49] A. Razin and H. Cedar, "DNA methylation and gene expression," *Microbiol Rev*, vol. 55, no. 3, pp. 451–458, Sep. 1991, doi: 10.1128/mr.55.3.451-458.1991.

- [50] T. Chen, Y. Ueda, J. E. Dodge, Z. Wang, and E. Li, "Establishment and Maintenance of Genomic Methylation Patterns in Mouse Embryonic Stem Cells by Dnmt3a and Dnmt3b," *Mol Cell Biol*, vol. 23, no. 16, pp. 5594–5605, Aug. 2003, doi: 10.1128/MCB.23.16.5594-5605.2003.
- [51] D. M. Messerschmidt, B. B. Knowles, and D. Solter, "DNA methylation dynamics during epigenetic reprogramming in the germline and preimplantation embryos.," *Genes Dev*, vol. 28, no. 8, pp. 812–28, Apr. 2014, doi: 10.1101/gad.234294.113.
- [52] W. Dean, "DNA methylation and demethylation: A pathway to gametogenesis and development," *Mol Reprod Dev*, vol. 81, no. 2, pp. 113–125, Feb. 2014, doi: 10.1002/mrd.22280.
- [53] J. R. Edwards, O. Yarychivska, M. Boulard, and T. H. Bestor, "DNA methylation and DNA methyltransferases," *Epigenetics Chromatin*, vol. 10, no. 1, p. 23, Dec. 2017, doi: 10.1186/s13072-017-0130-8.
- [54] E. Li, "Chromatin modification and epigenetic reprogramming in mammalian development," *Nat Rev Genet*, vol. 3, no. 9, pp. 662–673, Sep. 2002, doi: 10.1038/nrg887.
- [55] J. H. A. Martens and H. G. Stunnenberg, "BLUEPRINT: mapping human blood cell epigenomes," *Haematologica*, vol. 98, no. 10, pp. 1487–1489, Oct. 2013, doi: 10.3324/haematol.2013.094243.
- [56] M. Breton-Larivière, E. Elder, and S. McGraw, "DNA methylation, environmental exposures and early embryo development," *Anim Reprod*, vol. 16, no. 3, pp. 465–474, 2019, doi: 10.21451/1984-3143-AR2019-0062.
- [57] K. Kim, S. Friso, and S.-W. Choi, "DNA methylation, an epigenetic mechanism connecting folate to healthy embryonic development and aging," *J Nutr Biochem*, vol. 20, no. 12, pp. 917–926, Dec. 2009, doi: 10.1016/j.jnutbio.2009.06.008.
- [58] V. L. Wilson and P. A. Jones, "DNA Methylation Decreases in Aging But Not in Immortal Cells," *Science (1979)*, vol. 220, no. 4601, pp. 1055–1057, Jun. 1983, doi: 10.1126/science.6844925.
- [59] B. C. Richardson, "Role of DNA Methylation in the Regulation of Cell Function: Autoimmunity, Aging and Cancer," *J Nutr*, vol. 132, no. 8, pp. 2401S–2405S, Aug. 2002, doi: 10.1093/jn/132.8.2401S.
- [60] T. Ono, N. Takahashi, and S. Okada, "Age-associated changes in DNA methylation and mRNA level of the c-myc gene in spleen and liver of mice," *Mutation Research/DNAging*, vol. 219, no. 1, pp. 39–50, Jan. 1989, doi: 10.1016/0921-8734(89)90039-8.
- [61] B. Richardson, "Impact of aging on DNA methylation," *Ageing Res Rev*, vol. 2, no. 3, pp. 245–261, Jul. 2003, doi: 10.1016/S1568-1637(03)00010-2.

- [62] M. F. FRAGA, R. AGRELO, and M. ESTELLER, "Cross-Talk between Aging and Cancer: The Epigenetic Language," *Ann N Y Acad Sci*, vol. 1100, no. 1, pp. 60–74, Apr. 2007, doi: 10.1196/annals.1395.005.
- [63] P. Yi, S. Melnyk, M. Pogribna, I. P. Pogribny, R. J. Hine, and S. J. James, "Increase in Plasma Homocysteine Associated with Parallel Increases in Plasma S-Adenosylhomocysteine and Lymphocyte DNA Hypomethylation," *Journal of Biological Chemistry*, vol. 275, no. 38, pp. 29318–29323, Sep. 2000, doi: 10.1074/jbc.M002725200.
- [64] P. F. Jacques, J. Selhub, A. G. Bostom, P. W. F. Wilson, and I. H. Rosenberg, "The Effect of Folic Acid Fortification on Plasma Folate and Total Homocysteine Concentrations," *New England Journal of Medicine*, vol. 340, no. 19, pp. 1449–1454, May 1999, doi: 10.1056/NEJM199905133401901.
- [65] S. Friso, S. Lamon-Fava, H. Jang, E. J. Schaefer, R. Corrocher, and S.-W. Choi, "Oestrogen replacement therapy reduces total plasma homocysteine and enhances genomic DNA methylation in postmenopausal women," *British Journal of Nutrition*, vol. 97, no. 4, pp. 617–621, Apr. 2007, doi: 10.1017/S0007114507433013.
- [66] R. A. Jacob *et al.*, "Moderate Folate Depletion Increases Plasma Homocysteine and Decreases Lymphocyte DNA Methylation in Postmenopausal Women," *J Nutr*, vol. 128, no. 7, pp. 1204–1212, Jul. 1998, doi: 10.1093/jn/128.7.1204.
- [67] G. C. Rampersaud, G. P. Kauwell, A. D. Hutson, J. J. Cerda, and L. B. Bailey, "Genomic DNA methylation decreases in response to moderate folate depletion in elderly women," *Am J Clin Nutr*, vol. 72, no. 4, pp. 998–1003, Oct. 2000, doi: 10.1093/ajcn/72.4.998.
- [68] C. D. Davis, E. O. Uthus, and J. W. Finley, "Dietary Selenium and Arsenic Affect DNA Methylation In Vitro in Caco-2 Cells and In Vivo in Rat Liver and Colon," *J Nutr*, vol. 130, no. 12, pp. 2903–2909, Dec. 2000, doi: 10.1093/jn/130.12.2903.
- [69] J. P. Issa, N. Ahuja, M. Toyota, M. P. Bronner, and T. A. Brentnall, "Accelerated age-related CpG island methylation in ulcerative colitis," *Cancer Res*, vol. 61, no. 9, pp. 3573–7, May 2001.
- [70] L. Glória *et al.*, "DNA hypomethylation and proliferative activity are increased in the rectal mucosa of patients with long-standing ulcerative colitis," *Cancer*, vol. 78, no. 11, pp. 2300–2306, Dec. 1996, doi: 10.1002/(SICI)1097-0142(19961201)78:11<2300::AID-CNCR5>3.0.CO;2-Q.
- [71] J. Kraiczy, A. D. B. Ross, J. L. Forbester, G. Dougan, L. Vallier, and M. Zilbauer, "Genome-Wide Epigenetic and Transcriptomic Characterization of Human-Induced Pluripotent Stem Cell-Derived Intestinal Epithelial Organoids," *Cell Mol Gastroenterol Hepatol*, vol. 7, no. 2, pp. 285–288, 2019, doi: 10.1016/j.jcmgh.2018.10.008.

- [72] R. Gonsky, R. L. Deem, and S. R. Targan, "Distinct Methylation of *IFNG* in the Gut," *Journal of Interferon & Cytokine Research*, vol. 29, no. 7, pp. 407–414, Jul. 2009, doi: 10.1089/jir.2008.0109.
- [73] V. Dideberg *et al.*, "An insertion deletion polymorphism in the Interferon Regulatory Factor 5 (IRF5) gene confers risk of inflammatory bowel diseases," *Hum Mol Genet*, vol. 16, no. 24, pp. 3008–3016, Sep. 2007, doi: 10.1093/hmg/ddm259.
- [74] L. D. Moore, T. Le, and G. Fan, "DNA Methylation and Its Basic Function," *Neuropsychopharmacology*, vol. 38, no. 1, pp. 23–38, Jan. 2013, doi: 10.1038/npp.2012.112.
- [75] J. Denizot *et al.*, "Diet-induced hypoxia responsive element demethylation increases CEACAM6 expression, favouring Crohn's disease-associated *Escherichia coli* colonisation," *Gut*, vol. 64, no. 3, pp. 428–437, Mar. 2015, doi: 10.1136/gutjnl-2014-306944.
- [76] W.-H. Pan *et al.*, "Exposure to the gut microbiota drives distinct methylome and transcriptome changes in intestinal epithelial cells during postnatal development," *Genome Med*, vol. 10, no. 1, p. 27, Dec. 2018, doi: 10.1186/s13073-018-0534-5.
- [77] K. J. Howell *et al.*, "DNA Methylation and Transcription Patterns in Intestinal Epithelial Cells From Pediatric Patients With Inflammatory Bowel Diseases Differentiate Disease Subtypes and Associate With Outcome," *Gastroenterology*, vol. 154, no. 3, pp. 585–598, Feb. 2018, doi: 10.1053/j.gastro.2017.10.007.
- [78] T. Sadler *et al.*, "Genome-wide analysis of DNA methylation and gene expression defines molecular characteristics of Crohn's disease-associated fibrosis," *Clin Epigenetics*, vol. 8, no. 1, p. 30, Dec. 2016, doi: 10.1186/s13148-016-0193-6.
- [79] F. Lyko, "The DNA methyltransferase family: a versatile toolkit for epigenetic regulation," *Nat Rev Genet*, vol. 19, no. 2, pp. 81–92, Feb. 2018, doi: 10.1038/nrg.2017.80.
- [80] G. Egger, G. Liang, A. Aparicio, and P. A. Jones, "Epigenetics in human disease and prospects for epigenetic therapy," *Nature*, vol. 429, no. 6990, pp. 457–463, May 2004, doi: 10.1038/nature02625.
- [81] P. A. Jones and S. B. Baylin, "The fundamental role of epigenetic events in cancer," *Nat Rev Genet*, vol. 3, no. 6, pp. 415–428, Jun. 2002, doi: 10.1038/nrg816.
- [82] K. D. Robertson, "DNA methylation and chromatin – unraveling the tangled web," *Oncogene*, vol. 21, no. 35, pp. 5361–5379, Aug. 2002, doi: 10.1038/sj.onc.1205609.
- [83] A. Hermann, H. Gowher, and A. Jeltsch, "Biochemistry and biology of mammalian DNA methyltransferases," *Cellular and Molecular Life Sciences*, vol. 61, no. 19–20, pp. 2571–2587, Oct. 2004, doi: 10.1007/s00018-004-4201-1.

- [84] M. G. Goll *et al.*, "Methylation of tRNA^{Asp} by the DNA Methyltransferase Homolog Dnmt2," *Science* (1979), vol. 311, no. 5759, pp. 395–398, Jan. 2006, doi: 10.1126/science.1120976.
- [85] F. Lyko, "The DNA methyltransferase family: a versatile toolkit for epigenetic regulation," *Nat Rev Genet*, vol. 19, no. 2, pp. 81–92, Feb. 2018, doi: 10.1038/nrg.2017.80.
- [86] A. Jeltsch and R. Z. Jurkowska, "Allosteric control of mammalian DNA methyltransferases – a new regulatory paradigm," *Nucleic Acids Res*, vol. 44, no. 18, pp. 8556–8575, Oct. 2016, doi: 10.1093/nar/gkw723.
- [87] S. K. T. Ooi *et al.*, "DNMT3L connects unmethylated lysine 4 of histone H3 to de novo methylation of DNA," *Nature*, vol. 448, no. 7154, pp. 714–717, Aug. 2007, doi: 10.1038/nature05987.
- [88] D. Jia, R. Z. Jurkowska, X. Zhang, A. Jeltsch, and X. Cheng, "Structure of Dnmt3a bound to Dnmt3L suggests a model for de novo DNA methylation," *Nature*, vol. 449, no. 7159, pp. 248–251, Sep. 2007, doi: 10.1038/nature06146.
- [89] R. J. Klose and A. P. Bird, "Genomic DNA methylation: the mark and its mediators," *Trends Biochem Sci*, vol. 31, no. 2, pp. 89–97, Feb. 2006, doi: 10.1016/j.tibs.2005.12.008.
- [90] A. Amabile *et al.*, "Inheritable Silencing of Endogenous Genes by Hit-and-Run Targeted Epigenetic Editing," *Cell*, vol. 167, no. 1, pp. 219–232.e14, Sep. 2016, doi: 10.1016/j.cell.2016.09.006.
- [91] A. Vojta *et al.*, "Repurposing the CRISPR-Cas9 system for targeted DNA methylation," *Nucleic Acids Res*, vol. 44, no. 12, pp. 5615–5628, Jul. 2016, doi: 10.1093/nar/gkw159.
- [92] X. S. Liu *et al.*, "Editing DNA Methylation in the Mammalian Genome," *Cell*, vol. 167, no. 1, pp. 233–247.e17, Sep. 2016, doi: 10.1016/j.cell.2016.08.056.
- [93] P. Stepper *et al.*, "Efficient targeted DNA methylation with chimeric dCas9–Dnmt3a–Dnmt3L methyltransferase," *Nucleic Acids Res*, vol. 45, no. 4, pp. 1703–1713, Feb. 2017, doi: 10.1093/nar/gkw1112.
- [94] L. Yang, R. Rau, and M. A. Goodell, "DNMT3A in haematological malignancies," *Nat Rev Cancer*, vol. 15, no. 3, pp. 152–165, Mar. 2015, doi: 10.1038/nrc3895.
- [95] Y. Yanagisawa, E. Ito, Y. Yuasa, and K. Maruyama, "The human DNA methyltransferases DNMT3A and DNMT3B have two types of promoters with different CpG contents," *Biochimica et Biophysica Acta (BBA) - Gene Structure and Expression*, vol. 1577, no. 3, pp. 457–465, Sep. 2002, doi: 10.1016/S0167-4781(02)00482-7.
- [96] D. J. Weisenberger *et al.*, "Identification and characterization of alternatively spliced variants of DNA methyltransferase 3a in mammalian cells," *Gene*, vol. 298, no. 1, pp. 91–99, Sep. 2002, doi: 10.1016/S0378-1119(02)00976-9.

- [97] Y. Tadokoro, H. Ema, M. Okano, E. Li, and H. Nakauchi, "De novo DNA methyltransferase is essential for self-renewal, but not for differentiation, in hematopoietic stem cells," *Journal of Experimental Medicine*, vol. 204, no. 4, pp. 715–722, Apr. 2007, doi: 10.1084/jem.20060750.
- [98] T. Chen, Y. Ueda, S. Xie, and E. Li, "A Novel Dnmt3a Isoform Produced from an Alternative Promoter Localizes to Euchromatin and Its Expression Correlates with Activated De Novo Methylation," *Journal of Biological Chemistry*, vol. 277, no. 41, pp. 38746–38754, Oct. 2002, doi: 10.1074/jbc.M205312200.
- [99] E. Eudy, M. Loberg, R. Bell, T. Stearns, and J. Trowbridge, "Dnmt3a Mutation Confers a Selective Advantage Specifically to Cells within the Long-Term Hematopoietic Stem Cell (LT-HSC) Compartment," *Blood*, vol. 134, no. Supplement_1, pp. 448–448, Nov. 2019, doi: 10.1182/blood-2019-124540.
- [100] O. A. Guryanova *et al.*, "DNMT3A mutations promote anthracycline resistance in acute myeloid leukemia via impaired nucleosome remodeling," *Nat Med*, vol. 22, no. 12, pp. 1488–1495, Dec. 2016, doi: 10.1038/nm.4210.
- [101] G. A. Challen *et al.*, "Dnmt3a is essential for hematopoietic stem cell differentiation," *Nat Genet*, vol. 44, no. 1, pp. 23–31, Jan. 2012, doi: 10.1038/ng.1009.
- [102] W. Abplanalp *et al.*, "DNMT3A clonal hematopoiesis-driver mutations are associated with profound changes in monocyte and T cell signatures in humans with heart failure," *Eur Heart J*, vol. 41, no. Supplement_2, Nov. 2020, doi: 10.1093/ehjci/ehaa946.3626.
- [103] M. Liao *et al.*, "Aging-elevated inflammation promotes DNMT3A R878H-driven clonal hematopoiesis," *Acta Pharm Sin B*, vol. 12, no. 2, pp. 678–691, Feb. 2022, doi: 10.1016/j.apsb.2021.09.015.
- [104] S. F. Chaudry and T. J. T. Chevassut, "Epigenetic Guardian: A Review of the DNA Methyltransferase DNMT3A in Acute Myeloid Leukaemia and Clonal Haematopoiesis," *Biomed Res Int*, vol. 2017, pp. 1–13, 2017, doi: 10.1155/2017/5473197.
- [105] M. Y. Shah and J. D. Licht, "DNMT3A mutations in acute myeloid leukemia," *Nat Genet*, vol. 43, no. 4, pp. 289–290, Apr. 2011, doi: 10.1038/ng0411-289.
- [106] O. Blau, F. Behrenbeck, M. Bayanova, I.-W. Blau, and L. Bullinger, "Characteristics of DNMT3A-R882 Mutation in AML," *Blood*, vol. 132, no. Supplement 1, pp. 5263–5263, Nov. 2018, doi: 10.1182/blood-2018-99-116652.
- [107] T. J. Ley *et al.*, "DNMT3A Mutations in Acute Myeloid Leukemia," *New England Journal of Medicine*, vol. 363, no. 25, pp. 2424–2433, Dec. 2010, doi: 10.1056/NEJMoa1005143.

- [108] X. Li *et al.*, “LncRNA *Dnmt3aos* regulates *Dnmt3a* expression leading to aberrant DNA methylation in macrophage polarization,” *The FASEB Journal*, vol. 34, no. 4, pp. 5077–5091, Apr. 2020, doi: 10.1096/fj.201902379R.
- [109] X. Li *et al.*, “Methyltransferase *Dnmt3a* upregulates HDAC9 to deacetylate the kinase TBK1 for activation of antiviral innate immunity,” *Nat Immunol*, vol. 17, no. 7, pp. 806–815, Jul. 2016, doi: 10.1038/ni.3464.
- [110] A. Fazio *et al.*, “DNA methyltransferase 3A controls intestinal epithelial barrier function and regeneration in the colon,” *Nat Commun*, vol. 13, no. 1, p. 6266, Oct. 2022, doi: 10.1038/s41467-022-33844-2.
- [111] L. G. van der Flier and H. Clevers, “Stem Cells, Self-Renewal, and Differentiation in the Intestinal Epithelium,” *Annu Rev Physiol*, vol. 71, no. 1, pp. 241–260, Mar. 2009, doi: 10.1146/annurev.physiol.010908.163145.
- [112] W. Bao *et al.*, “Interleukin-22 Mediates Early Host Defense against *Rhizomucor pusillus* Pathogens,” *PLoS One*, vol. 8, no. 6, p. e65065, Jun. 2013, doi: 10.1371/journal.pone.0065065.
- [113] G. Pickert *et al.*, “STAT3 links IL-22 signaling in intestinal epithelial cells to mucosal wound healing,” *Journal of Experimental Medicine*, vol. 206, no. 7, pp. 1465–1472, Jul. 2009, doi: 10.1084/jem.20082683.
- [114] K. Aden *et al.*, “ATG16L1 orchestrates interleukin-22 signaling in the intestinal epithelium via cGAS–STING,” *Journal of Experimental Medicine*, vol. 215, no. 11, pp. 2868–2886, Nov. 2018, doi: 10.1084/jem.20171029.
- [115] P.-S. Welz *et al.*, “FADD prevents RIP3-mediated epithelial cell necrosis and chronic intestinal inflammation,” *Nature*, vol. 477, no. 7364, pp. 330–334, Sep. 2011, doi: 10.1038/nature10273.
- [116] I. I. Ivanov *et al.*, “Induction of Intestinal Th17 Cells by Segmented Filamentous Bacteria,” *Cell*, vol. 139, no. 3, pp. 485–498, Oct. 2009, doi: 10.1016/j.cell.2009.09.033.
- [117] K. Atarashi *et al.*, “Th17 Cell Induction by Adhesion of Microbes to Intestinal Epithelial Cells,” *Cell*, vol. 163, no. 2, pp. 367–380, Oct. 2015, doi: 10.1016/j.cell.2015.08.058.
- [118] K. Aden *et al.*, “Epithelial IL-23R Signaling Licenses Protective IL-22 Responses in Intestinal Inflammation,” *Cell Rep*, vol. 16, no. 8, pp. 2208–2218, Aug. 2016, doi: 10.1016/j.celrep.2016.07.054.
- [119] C. Hindorf, G. Glatting, C. Chiesa, O. Lindén, and G. Flux, “EANM Dosimetry Committee guidelines for bone marrow and whole-body dosimetry,” *Eur J Nucl Med Mol Imaging*, vol. 37, no. 6, pp. 1238–1250, Jun. 2010, doi: 10.1007/s00259-010-1422-4.
- [120] M. Jagannathan-Bogdan and L. I. Zon, “Hematopoiesis,” *Development*, vol. 140, no. 12, pp. 2463–2467, Jun. 2013, doi: 10.1242/dev.083147.

- [121] M. Kondo, I. L. Weissman, and K. Akashi, "Identification of Clonogenic Common Lymphoid Progenitors in Mouse Bone Marrow," *Cell*, vol. 91, no. 5, pp. 661–672, Nov. 1997, doi: 10.1016/S0092-8674(00)80453-5.
- [122] K. Akashi, D. Traver, T. Miyamoto, and I. L. Weissman, "A clonogenic common myeloid progenitor that gives rise to all myeloid lineages," *Nature*, vol. 404, no. 6774, pp. 193–197, Mar. 2000, doi: 10.1038/35004599.
- [123] S. W. Russell and J. L. Pace, "Both the Kind and Magnitude of Stimulus Are Important in Overcoming the Negative Regulation of Macrophage Activation by PGE₂," *J Leukoc Biol*, vol. 35, no. 3, pp. 291–301, Mar. 1984, doi: 10.1002/jlb.35.3.291.
- [124] R. P. Bourette, "The biological role of interferon-inducible P204 protein in the development of the mononuclear phagocyte system," *Frontiers in Bioscience*, vol. 13, no. 13, p. 879, 2008, doi: 10.2741/2728.
- [125] Y. Luan, P. Lengyel, and C.-J. Liu, "p204, a p200 family protein, as a multifunctional regulator of cell proliferation and differentiation," *Cytokine Growth Factor Rev*, vol. 19, no. 5–6, pp. 357–369, Oct. 2008, doi: 10.1016/j.cytogfr.2008.11.002.
- [126] J. Dauffy, G. Mouchiroud, and R. P. Bourette, "The interferon-inducible gene, Ifi204, is transcriptionally activated in response to M-CSF, and its expression favors macrophage differentiation in myeloid progenitor cells," *J Leukoc Biol*, vol. 79, no. 1, pp. 173–183, Jan. 2006, doi: 10.1189/jlb.0205083.
- [127] R. J. Salo, D. K. Bleam, V. L. Greer, and A. P. Ortega, "Interferon Production in Murine Macrophage-Like Cell Lines," *J Leukoc Biol*, vol. 37, no. 4, pp. 395–406, Apr. 1985, doi: 10.1002/jlb.37.4.395.
- [128] T. A. Wynn, A. Chawla, and J. W. Pollard, "Macrophage biology in development, homeostasis and disease," *Nature*, vol. 496, no. 7446, pp. 445–455, Apr. 2013, doi: 10.1038/nature12034.
- [129] L. Franken, M. Schiwon, and C. Kurts, "Macrophages: sentinels and regulators of the immune system," *Cell Microbiol*, vol. 18, no. 4, pp. 475–487, Apr. 2016, doi: 10.1111/cmi.12580.
- [130] X. Pan, Q. Zhu, L.-L. Pan, and J. Sun, "Macrophage immunometabolism in inflammatory bowel diseases: From pathogenesis to therapy," *Pharmacol Ther*, vol. 238, p. 108176, Oct. 2022, doi: 10.1016/j.pharmthera.2022.108176.
- [131] M. Steinbakk, C.-F. Naess-Andresen, M. K. Fagerhol, E. Lingaas, I. Dale, and P. Brandtzaeg, "Antimicrobial actions of calcium binding leucocyte L1 protein, calprotectin," *The Lancet*, vol. 336, no. 8718, pp. 763–765, Sep. 1990, doi: 10.1016/0140-6736(90)93237-J.

- [132] M. C. GRIMM, P. PAVLI, E. van de POL, and W. F. DOE, "Evidence for a CD14+ population of monocytes in inflammatory bowel disease mucosa—implications for pathogenesis," *Clin Exp Immunol*, vol. 100, no. 2, pp. 291–297, Jun. 2008, doi: 10.1111/j.1365-2249.1995.tb03667.x.
- [133] R. J. Ulevitch and P. S. Tobias, "Recognition of Gram-negative bacteria and endotoxin by the innate immune system," *Curr Opin Immunol*, vol. 11, no. 1, pp. 19–22, Feb. 1999, doi: 10.1016/S0952-7915(99)80004-1.
- [134] S. T. Gren and O. Grip, "Role of Monocytes and Intestinal Macrophages in Crohn's Disease and Ulcerative Colitis," *Inflamm Bowel Dis*, vol. 22, no. 8, pp. 1992–1998, Aug. 2016, doi: 10.1097/MIB.0000000000000824.
- [135] P. Sharma *et al.*, "Particle uptake driven phagocytosis in macrophages and neutrophils enhances bacterial clearance," *Journal of Controlled Release*, vol. 343, pp. 131–141, Mar. 2022, doi: 10.1016/j.jconrel.2022.01.030.
- [136] C. Mills, "M1 and M2 Macrophages: Oracles of Health and Disease," *Crit Rev Immunol*, vol. 32, no. 6, pp. 463–488, 2012, doi: 10.1615/CritRevImmunol.v32.i6.10.
- [137] S. P. Arlauckas *et al.*, "Arg1 expression defines immunosuppressive subsets of tumor-associated macrophages," *Theranostics*, vol. 8, no. 21, pp. 5842–5854, 2018, doi: 10.7150/thno.26888.
- [138] T. Rószler, "Understanding the Mysterious M2 Macrophage through Activation Markers and Effector Mechanisms," *Mediators Inflamm*, vol. 2015, pp. 1–16, 2015, doi: 10.1155/2015/816460.
- [139] A. J. Chan, J. C. Jang, and M. G. Nair, "Tissue Remodeling and Repair During Type 2 Inflammation," in *The Th2 Type Immune Response in Health and Disease*, New York, NY: Springer New York, 2016, pp. 115–130. doi: 10.1007/978-1-4939-2911-5_7.
- [140] L. Wang *et al.*, "Clinical Significance of M1/M2 Macrophages and Related Cytokines in Patients with Spinal Tuberculosis," *Dis Markers*, vol. 2020, pp. 1–8, May 2020, doi: 10.1155/2020/2509454.
- [141] C. Kupffer, "Ueber Sternzellen der Leber," *Archiv für Mikroskopische Anatomie*, vol. 12, no. 1, pp. 353–358, Dec. 1876, doi: 10.1007/BF02933897.
- [142] S. Gordon, "Phagocytosis: The Legacy of Metchnikoff," *Cell*, vol. 166, no. 5, pp. 1065–1068, Aug. 2016, doi: 10.1016/j.cell.2016.08.017.
- [143] Z.-L. Chang, "Recent development of the mononuclear phagocyte system: in memory of Metchnikoff and Ehrlich on the 100th Anniversary of the 1908 Nobel Prize in Physiology or Medicine," *Biol Cell*, vol. 101, no. 12, pp. 709–721, Dec. 2009, doi: 10.1042/BC20080227.

- [144] A. Sródka, R. W. Gryglewski, and W. Szczepariski, "Browicz or Kupffer cells?," *Pol J Pathol*, vol. 57, no. 4, pp. 183–5, 2006.
- [145] P. A. Ward, "CHEMOTAXIS OF MONONUCLEAR CELLS," *Journal of Experimental Medicine*, vol. 128, no. 5, pp. 1201–1221, Nov. 1968, doi: 10.1084/jem.128.5.1201.
- [146] D. Hirayama, T. Iida, and H. Nakase, "The Phagocytic Function of Macrophage-Enforcing Innate Immunity and Tissue Homeostasis," *Int J Mol Sci*, vol. 19, no. 1, p. 92, Dec. 2017, doi: 10.3390/ijms19010092.
- [147] A. Shapouri-Moghaddam *et al.*, "Macrophage plasticity, polarization, and function in health and disease," *J Cell Physiol*, vol. 233, no. 9, pp. 6425–6440, Sep. 2018, doi: 10.1002/jcp.26429.
- [148] C. D. Mills, "Anatomy of a Discovery: M1 and M2 Macrophages," *Front Immunol*, vol. 6, May 2015, doi: 10.3389/fimmu.2015.00212.
- [149] N.-B. Hao, M.-H. Lü, Y.-H. Fan, Y.-L. Cao, Z.-R. Zhang, and S.-M. Yang, "Macrophages in Tumor Microenvironments and the Progression of Tumors," *Clin Dev Immunol*, vol. 2012, pp. 1–11, 2012, doi: 10.1155/2012/948098.
- [150] J. G. Hirsch, "IMMUNITY TO INFECTIOUS DISEASES: REVIEW OF SOME CONCEPTS OF METCHNIKOFF," *Bacteriol Rev*, vol. 23, no. 2, pp. 48–60, Jun. 1959, doi: 10.1128/br.23.2.48-60.1959.
- [151] J. Zhou, Z. Tang, S. Gao, C. Li, Y. Feng, and X. Zhou, "Tumor-Associated Macrophages: Recent Insights and Therapies.," *Front Oncol*, vol. 10, p. 188, 2020, doi: 10.3389/fonc.2020.00188.
- [152] C. Sloas, S. Gill, and M. Klichinsky, "Engineered CAR-Macrophages as Adoptive Immunotherapies for Solid Tumors.," *Front Immunol*, vol. 12, p. 783305, 2021, doi: 10.3389/fimmu.2021.783305.
- [153] S. H. Lee, P. M. Starkey, and S. Gordon, "Quantitative analysis of total macrophage content in adult mouse tissues. Immunochemical studies with monoclonal antibody F4/80.," *Journal of Experimental Medicine*, vol. 161, no. 3, pp. 475–489, Mar. 1985, doi: 10.1084/jem.161.3.475.
- [154] S. Wang, Q. Ye, X. Zeng, and S. Qiao, "Functions of Macrophages in the Maintenance of Intestinal Homeostasis," *J Immunol Res*, vol. 2019, pp. 1–8, Mar. 2019, doi: 10.1155/2019/1512969.
- [155] Y. R. Mahida, S. Patel, P. Gionchetti, D. Vaux, and D. P. Jewell, "Macrophage subpopulations in lamina propria of normal and inflamed colon and terminal ileum.," *Gut*, vol. 30, no. 6, pp. 826–834, Jun. 1989, doi: 10.1136/gut.30.6.826.
- [156] G. Rogler *et al.*, "Isolation and phenotypic characterization of colonic macrophages," *Clin Exp Immunol*, vol. 112, no. 2, pp. 205–215, Dec. 2001, doi: 10.1046/j.1365-2249.1998.00557.x.

- [157] A. A. Kühl, U. Erben, L. I. Kredel, and B. Siegmund, "Diversity of Intestinal Macrophages in Inflammatory Bowel Diseases," *Front Immunol*, vol. 6, Dec. 2015, doi: 10.3389/fimmu.2015.00613.
- [158] J. Farache, E. Zigmond, G. Shakhar, and S. Jung, "Contributions of dendritic cells and macrophages to intestinal homeostasis and immune defense," *Immunol Cell Biol*, vol. 91, no. 3, pp. 232–239, Mar. 2013, doi: 10.1038/icb.2012.79.
- [159] O. Schulz *et al.*, "Intestinal CD103+, but not CX3CR1+, antigen sampling cells migrate in lymph and serve classical dendritic cell functions," *Journal of Experimental Medicine*, vol. 206, no. 13, pp. 3101–3114, Dec. 2009, doi: 10.1084/jem.20091925.
- [160] Y. Lavin, A. Mortha, A. Rahman, and M. Merad, "Regulation of macrophage development and function in peripheral tissues," *Nat Rev Immunol*, vol. 15, no. 12, pp. 731–744, Dec. 2015, doi: 10.1038/nri3920.
- [161] J. L. Schultze, "Macrophage tolerance in the gut: It is in the epigenome!," *Eur J Immunol*, vol. 46, no. 8, pp. 1838–1841, Aug. 2016, doi: 10.1002/eji.201646545.
- [162] C. Atri, F. Guerfali, and D. Laouini, "Role of Human Macrophage Polarization in Inflammation during Infectious Diseases," *Int J Mol Sci*, vol. 19, no. 6, p. 1801, Jun. 2018, doi: 10.3390/ijms19061801.
- [163] A. Shapouri-Moghaddam *et al.*, "Macrophage plasticity, polarization, and function in health and disease," *J Cell Physiol*, vol. 233, no. 9, pp. 6425–6440, Sep. 2018, doi: 10.1002/jcp.26429.
- [164] A. A. Tarique, J. Logan, E. Thomas, P. G. Holt, P. D. Sly, and E. Fantino, "Phenotypic, Functional, and Plasticity Features of Classical and Alternatively Activated Human Macrophages," *Am J Respir Cell Mol Biol*, vol. 53, no. 5, pp. 676–688, Nov. 2015, doi: 10.1165/rcmb.2015-0012OC.
- [165] M. Beyer *et al.*, "High-resolution transcriptome of human macrophages.," *PLoS One*, vol. 7, no. 9, p. e45466, 2012, doi: 10.1371/journal.pone.0045466.
- [166] P. Italiani and D. Boraschi, "From Monocytes to M1/M2 Macrophages: Phenotypical vs. Functional Differentiation.," *Front Immunol*, vol. 5, p. 514, 2014, doi: 10.3389/fimmu.2014.00514.
- [167] K. Y. Gerrick, E. R. Gerrick, A. Gupta, S. J. Wheelan, S. Yegnasubramanian, and E. M. Jaffee, "Transcriptional profiling identifies novel regulators of macrophage polarization," *PLoS One*, vol. 13, no. 12, p. e0208602, Dec. 2018, doi: 10.1371/journal.pone.0208602.
- [168] F. O. Martinez, S. Gordon, M. Locati, and A. Mantovani, "Transcriptional Profiling of the Human Monocyte-to-Macrophage Differentiation and Polarization: New Molecules and Patterns of Gene Expression," *The Journal of Immunology*, vol. 177, no. 10, pp. 7303–7311, Nov. 2006, doi: 10.4049/jimmunol.177.10.7303.

- [169] W. Xu, X. Zhao, M. R. Daha, and C. van Kooten, "Reversible differentiation of pro- and anti-inflammatory macrophages," *Mol Immunol*, vol. 53, no. 3, pp. 179–186, Mar. 2013, doi: 10.1016/j.molimm.2012.07.005.
- [170] C. Yunna, H. Mengru, W. Lei, and C. Weidong, "Macrophage M1/M2 polarization," *Eur J Pharmacol*, vol. 877, p. 173090, Jun. 2020, doi: 10.1016/j.ejphar.2020.173090.
- [171] L. E. Smythies, "Mucosal IL-8 and TGF- recruit blood monocytes: evidence for cross-talk between the lamina propria stroma and myeloid cells," *J Leukoc Biol*, vol. 80, no. 3, pp. 492–499, Jul. 2006, doi: 10.1189/jlb.1005566.
- [172] L. E. Smythies *et al.*, "Inflammation Anergy in Human Intestinal Macrophages Is Due to Smad-induced I κ B α Expression and NF- κ B Inactivation," *Journal of Biological Chemistry*, vol. 285, no. 25, pp. 19593–19604, Jun. 2010, doi: 10.1074/jbc.M109.069955.
- [173] A. N. Zelensky and J. E. Gready, "The C-type lectin-like domain superfamily," *FEBS Journal*, vol. 272, no. 24, pp. 6179–6217, Dec. 2005, doi: 10.1111/j.1742-4658.2005.05031.x.
- [174] A. Craxton, D. Magaletti, E. J. Ryan, and E. A. Clark, "Macrophage- and dendritic cell—dependent regulation of human B-cell proliferation requires the TNF family ligand BAFF," *Blood*, vol. 101, no. 11, pp. 4464–4471, Jun. 2003, doi: 10.1182/blood-2002-10-3123.
- [175] E. R. Mann and X. Li, "Intestinal antigen-presenting cells in mucosal immune homeostasis: crosstalk between dendritic cells, macrophages and B-cells.," *World J Gastroenterol*, vol. 20, no. 29, pp. 9653–64, Aug. 2014, doi: 10.3748/wjg.v20.i29.9653.
- [176] B. Ruder and C. Becker, "At the Forefront of the Mucosal Barrier: The Role of Macrophages in the Intestine," *Cells*, vol. 9, no. 10, p. 2162, Sep. 2020, doi: 10.3390/cells9102162.
- [177] A. M. Mowat and W. W. Agace, "Regional specialization within the intestinal immune system," *Nat Rev Immunol*, vol. 14, no. 10, pp. 667–685, Oct. 2014, doi: 10.1038/nri3738.
- [178] Y. Du, L. Rong, Y. Cong, L. Shen, N. Zhang, and B. Wang, "Macrophage polarization: an effective approach to targeted therapy of inflammatory bowel disease," *Expert Opin Ther Targets*, vol. 25, no. 3, pp. 191–209, Mar. 2021, doi: 10.1080/14728222.2021.1901079.
- [179] S. M. Morris, "Arginine: beyond protein," *Am J Clin Nutr*, vol. 83, no. 2, pp. 508S–512S, Feb. 2006, doi: 10.1093/ajcn/83.2.508S.
- [180] R. H. Böger and S. M. Bode-Böger, "The Clinical Pharmacology of L-Arginine," *Annu Rev Pharmacol Toxicol*, vol. 41, no. 1, pp. 79–99, Apr. 2001, doi: 10.1146/annurev.pharmtox.41.1.79.
- [181] J. B. Hibbs, R. R. Taintor, and Z. Vavrin, "Macrophage Cytotoxicity: Role for L-Arginine Deiminase and Imino Nitrogen Oxidation to Nitrite," *Science (1979)*, vol. 235, no. 4787, pp. 473–476, Jan. 1987, doi: 10.1126/science.2432665.

- [182] G. WU and S. M. MORRIS, "Arginine metabolism: nitric oxide and beyond," *Biochemical Journal*, vol. 336, no. 1, pp. 1–17, Nov. 1998, doi: 10.1042/bj3360001.
- [183] M. Rath, I. MÄßler, P. Kropf, E. I. Closs, and M. Munder, "Metabolism via Arginase or Nitric Oxide Synthase: Two Competing Arginine Pathways in Macrophages," *Front Immunol*, vol. 5, Oct. 2014, doi: 10.3389/fimmu.2014.00532.
- [184] C. P. Jenkinson, W. W. Grody, and S. D. Cederbaum, "Comparative properties of arginases," *Comp Biochem Physiol B Biochem Mol Biol*, vol. 114, no. 1, pp. 107–132, May 1996, doi: 10.1016/0305-0491(95)02138-8.
- [185] M. Munder, "Arginase: an emerging key player in the mammalian immune system," *Br J Pharmacol*, vol. 158, no. 3, pp. 638–651, Oct. 2009, doi: 10.1111/j.1476-5381.2009.00291.x.
- [186] A.-L. Pauleau, R. Rutschman, R. Lang, A. Pernis, S. S. Watowich, and P. J. Murray, "Enhancer-Mediated Control of Macrophage-Specific Arginase I Expression," *The Journal of Immunology*, vol. 172, no. 12, pp. 7565–7573, Jun. 2004, doi: 10.4049/jimmunol.172.12.7565.
- [187] A. Erdely *et al.*, "Inhibition of phosphodiesterase 4 amplifies cytokine-dependent induction of arginase in macrophages," *American Journal of Physiology-Lung Cellular and Molecular Physiology*, vol. 290, no. 3, pp. L534–L539, Mar. 2006, doi: 10.1152/ajplung.00326.2005.
- [188] K. E. Sheldon, H. Shandilya, D. Kepka-Lenhart, M. Poljakovic, A. Ghosh, and S. M. Morris, "Shaping the Murine Macrophage Phenotype: IL-4 and Cyclic AMP Synergistically Activate the Arginase I Promoter," *The Journal of Immunology*, vol. 191, no. 5, pp. 2290–2298, Sep. 2013, doi: 10.4049/jimmunol.1202102.
- [189] K. A. Shirey *et al.*, "Control of RSV-induced lung injury by alternatively activated macrophages is IL-4R α -, TLR4-, and IFN- β -dependent," *Mucosal Immunol*, vol. 3, no. 3, pp. 291–300, May 2010, doi: 10.1038/mi.2010.6.
- [190] K. C. el Kasmi *et al.*, "Toll-like receptor-induced arginase 1 in macrophages thwarts effective immunity against intracellular pathogens," *Nat Immunol*, vol. 9, no. 12, pp. 1399–1406, Dec. 2008, doi: 10.1038/ni.1671.
- [191] J. E. Albina, C. D. Mills, W. L. Henry, and M. D. Caldwell, "Temporal expression of different pathways of 1-arginine metabolism in healing wounds," *J Immunol*, vol. 144, no. 10, pp. 3877–80, May 1990.
- [192] J. E. Albina *et al.*, "Arginine metabolism in wounds," *American Journal of Physiology-Endocrinology and Metabolism*, vol. 254, no. 4, pp. E459–E467, Apr. 1988, doi: 10.1152/ajpendo.1988.254.4.E459.
- [193] C. D. Mills, J. Shearer, R. Evans, and M. D. Caldwell, "Macrophage arginine metabolism and the inhibition or stimulation of cancer," *J Immunol*, vol. 149, no. 8, pp. 2709–14, Oct. 1992.

- [194] O. A. Guryanova *et al.*, “Dnmt3a regulates myeloproliferation and liver-specific expansion of hematopoietic stem and progenitor cells,” *Leukemia*, vol. 30, no. 5, pp. 1133–1142, May 2016, doi: 10.1038/leu.2015.358.
- [195] A. C. Kramer *et al.*, “Dnmt3a regulates T-cell development and suppresses T-ALL transformation,” *Leukemia*, vol. 31, no. 11, pp. 2479–2490, Nov. 2017, doi: 10.1038/leu.2017.89.
- [196] M. I. Love, W. Huber, and S. Anders, “Moderated estimation of fold change and dispersion for RNA-seq data with DESeq2,” *Genome Biol*, vol. 15, no. 12, p. 550, Dec. 2014, doi: 10.1186/s13059-014-0550-8.
- [197] B. E. Clausen, C. Burkhardt, W. Reith, R. Renkawitz, and I. Förster, “Conditional gene targeting in macrophages and granulocytes using LysMcre mice,” *Transgenic Res*, vol. 8, no. 4, pp. 265–277, 1999, doi: 10.1023/A:1008942828960.
- [198] J. Shi, L. Hua, D. Harmer, P. Li, and G. Ren, “Cre Driver Mice Targeting Macrophages.,” *Methods Mol Biol*, vol. 1784, pp. 263–275, 2018, doi: 10.1007/978-1-4939-7837-3_24.
- [199] D. Lucas, “Structural organization of the bone marrow and its role in hematopoiesis.,” *Curr Opin Hematol*, vol. 28, no. 1, pp. 36–42, 2021, doi: 10.1097/MOH.0000000000000621.
- [200] C. J. Gamper, A. T. Agoston, W. G. Nelson, and J. D. Powell, “Identification of DNA Methyltransferase 3a as a T Cell Receptor-Induced Regulator of Th1 and Th2 Differentiation,” *The Journal of Immunology*, vol. 183, no. 4, pp. 2267–2276, Aug. 2009, doi: 10.4049/jimmunol.0802960.
- [201] M. S. Kim, Y. R. Kim, N. J. Yoo, and S. H. Lee, “Mutational analysis of *DNMT3A* gene in acute leukemias and common solid cancers,” *APMIS*, vol. 121, no. 2, pp. 85–94, Feb. 2013, doi: 10.1111/j.1600-0463.2012.02940.x.
- [202] E. N. Elliott, K. L. Sheaffer, and K. H. Kaestner, “The ‘de novo’ DNA methyltransferase Dnmt3b compensates the Dnmt1-deficient intestinal epithelium,” *Elife*, vol. 5, Jan. 2016, doi: 10.7554/eLife.12975.
- [203] G. Genovese *et al.*, “Clonal Hematopoiesis and Blood-Cancer Risk Inferred from Blood DNA Sequence,” *New England Journal of Medicine*, vol. 371, no. 26, pp. 2477–2487, Dec. 2014, doi: 10.1056/NEJMoa1409405.
- [204] A. Mayle *et al.*, “Dnmt3a loss predisposes murine hematopoietic stem cells to malignant transformation,” *Blood*, vol. 125, no. 4, pp. 629–638, Jan. 2015, doi: 10.1182/blood-2014-08-594648.
- [205] B. Dykstra and G. de Haan, “Hematopoietic stem cell aging and self-renewal,” *Cell Tissue Res*, vol. 331, no. 1, pp. 91–101, Jan. 2008, doi: 10.1007/s00441-007-0529-9.

- [206] D. S. Lind, "Arginine and Cancer," *J Nutr*, vol. 134, no. 10, pp. 2837S-2841S, Oct. 2004, doi: 10.1093/jn/134.10.2837S.
- [207] C.-L. Chen, S.-C. Hsu, D. K. Ann, Y. Yen, and H.-J. Kung, "Arginine Signaling and Cancer Metabolism," *Cancers (Basel)*, vol. 13, no. 14, p. 3541, Jul. 2021, doi: 10.3390/cancers13143541.
- [208] G. Jeyabalan *et al.*, "Arginase blockade protects against hepatic damage in warm ischemia-reperfusion," *Nitric Oxide*, vol. 19, no. 1, pp. 29–35, Aug. 2008, doi: 10.1016/j.niox.2008.04.002.
- [209] A. Das *et al.*, "Monocyte and Macrophage Plasticity in Tissue Repair and Regeneration," *Am J Pathol*, vol. 185, no. 10, pp. 2596–2606, Oct. 2015, doi: 10.1016/j.ajpath.2015.06.001.
- [210] Y. R. Na, M. Stakenborg, S. H. Seok, and G. Matteoli, "Macrophages in intestinal inflammation and resolution: a potential therapeutic target in IBD," *Nat Rev Gastroenterol Hepatol*, vol. 16, no. 9, pp. 531–543, Sep. 2019, doi: 10.1038/s41575-019-0172-4.
- [211] A. Salmaninejad *et al.*, "Tumor-associated macrophages: role in cancer development and therapeutic implications," *Cellular Oncology*, vol. 42, no. 5, pp. 591–608, Oct. 2019, doi: 10.1007/s13402-019-00453-z.
- [212] N. T. Ventham *et al.*, "Integrative epigenome-wide analysis demonstrates that DNA methylation may mediate genetic risk in inflammatory bowel disease," *Nat Commun*, vol. 7, no. 1, p. 13507, Dec. 2016, doi: 10.1038/ncomms13507.
- [213] E. McDermott *et al.*, "DNA Methylation Profiling in Inflammatory Bowel Disease Provides New Insights into Disease Pathogenesis," *J Crohns Colitis*, vol. 10, no. 1, pp. 77–86, Jan. 2016, doi: 10.1093/ecco-jcc/jjv176.
- [214] I. Agliata *et al.*, "The DNA methylome of inflammatory bowel disease (IBD) reflects intrinsic and extrinsic factors in intestinal mucosal cells," *Epigenetics*, vol. 15, no. 10, pp. 1068–1082, Oct. 2020, doi: 10.1080/15592294.2020.1748916.
- [215] G. Cavalli and E. Heard, "Advances in epigenetics link genetics to the environment and disease," *Nature*, vol. 571, no. 7766, pp. 489–499, Jul. 2019, doi: 10.1038/s41586-019-1411-0.
- [216] D. A. Khavari, G. L. Sen, and J. L. Rinn, "DNA methylation and epigenetic control of cellular differentiation," *Cell Cycle*, vol. 9, no. 19, pp. 3880–3883, Oct. 2010, doi: 10.4161/cc.9.19.13385.
- [217] M. Suelves, E. Carrió, Y. Núñez-Álvarez, and M. A. Peinado, "DNA methylation dynamics in cellular commitment and differentiation," *Brief Funct Genomics*, p. elw017, Jun. 2016, doi: 10.1093/bfpg/elw017.

- [218] E. R. Nimmo *et al.*, “Genome-wide methylation profiling in Crohn’s disease identifies altered epigenetic regulation of key host defense mechanisms including the Th17 pathway,” *Inflamm Bowel Dis*, vol. 18, no. 5, pp. 889–899, May 2012, doi: 10.1002/ibd.21912.
- [219] Antonella Fazio, “Role of DNA methyltransferase 3A (DNMT3A) in intestinal epithelial cells during homeostasis and inflammation,” 2019.
- [220] M. A. Odenwald and J. R. Turner, “The intestinal epithelial barrier: a therapeutic target?,” *Nat Rev Gastroenterol Hepatol*, vol. 14, no. 1, pp. 9–21, Jan. 2017, doi: 10.1038/nrgastro.2016.169.
- [221] W. Choi, S. Yeruva, and J. R. Turner, “Contributions of intestinal epithelial barriers to health and disease,” *Exp Cell Res*, vol. 358, no. 1, pp. 71–77, Sep. 2017, doi: 10.1016/j.yexcr.2017.03.036.
- [222] Kim, “MUC2 gene promoter methylation in mucinous and non-mucinous colorectal cancer tissues,” *Int J Oncol*, vol. 36, no. 4, Mar. 2010, doi: 10.3892/ijo_00000552.
- [223] Y. Liu, X. Yu, J. Zhao, H. Zhang, Q. Zhai, and W. Chen, “The role of MUC2 mucin in intestinal homeostasis and the impact of dietary components on MUC2 expression,” *Int J Biol Macromol*, vol. 164, pp. 884–891, Dec. 2020, doi: 10.1016/j.ijbiomac.2020.07.191.
- [224] A. Vincent, M. Ducourouble, and I. van Seuningen, “Epigenetic regulation of the human mucin gene *MUC4* in epithelial cancer cell lines involves both DNA methylation and histone modifications mediated by DNA methyltransferases and histone deacetylases,” *The FASEB Journal*, vol. 22, no. 8, pp. 3035–3045, Aug. 2008, doi: 10.1096/fj.07-103390.
- [225] K. Fyderek *et al.*, “Mucosal bacterial microflora and mucus layer thickness in adolescents with inflammatory bowel disease,” *World J Gastroenterol*, vol. 15, no. 42, p. 5287, 2009, doi: 10.3748/wjg.15.5287.
- [226] H. Schmitz* *et al.*, “Altered tight junction structure contributes to the impaired epithelial barrier function in ulcerative colitis,” *Gastroenterology*, vol. 116, no. 2, pp. 301–309, Feb. 1999, doi: 10.1016/S0016-5085(99)70126-5.
- [227] J. D. Söderholm *et al.*, “Epithelial permeability to proteins in the noninflamed ileum of Crohn’s disease?,” *Gastroenterology*, vol. 117, no. 1, pp. 65–72, Jul. 1999, doi: 10.1016/S0016-5085(99)70551-2.
- [228] J. Landy *et al.*, “Tight junctions in inflammatory bowel diseases and inflammatory bowel disease associated colorectal cancer,” *World J Gastroenterol*, vol. 22, no. 11, p. 3117, 2016, doi: 10.3748/wjg.v22.i11.3117.
- [229] S. Mehta, A. Nijhuis, T. Kumagai, J. Lindsay, and A. Silver, “Defects in the adherens junction complex (E-cadherin/ β -catenin) in inflammatory bowel disease,” *Cell Tissue Res*, vol. 360, no. 3, pp. 749–760, Jun. 2015, doi: 10.1007/s00441-014-1994-6.

- [230] A. J. Karayiannakis *et al.*, “Expression of catenins and E-cadherin during epithelial restitution in inflammatory bowel disease,” *J Pathol*, vol. 185, no. 4, pp. 413–418, Aug. 1998, doi: 10.1002/(SICI)1096-9896(199808)185:4<413::AID-PATH125>3.0.CO;2-K.
- [231] T. Kucharzik, S. v. Walsh, J. Chen, C. A. Parkos, and A. Nusrat, “Neutrophil Transmigration in Inflammatory Bowel Disease Is Associated with Differential Expression of Epithelial Intercellular Junction Proteins,” *Am J Pathol*, vol. 159, no. 6, pp. 2001–2009, Dec. 2001, doi: 10.1016/S0002-9440(10)63051-9.
- [232] M. E. v. Johansson, “Mucus Layers in Inflammatory Bowel Disease,” *Inflamm Bowel Dis*, vol. 20, no. 11, pp. 2124–2131, Nov. 2014, doi: 10.1097/MIB.000000000000117.
- [233] J. K. Gustafsson and M. E. v. Johansson, “The role of goblet cells and mucus in intestinal homeostasis,” *Nat Rev Gastroenterol Hepatol*, Sep. 2022, doi: 10.1038/s41575-022-00675-x.
- [234] J. Wyatt, H. Vogelsang, W. Hübl, T. Waldhoer, and H. Lochs, “Intestinal permeability and the prediction of relapse in Crohn’s disease,” *The Lancet*, vol. 341, no. 8858, pp. 1437–1439, Jun. 1993, doi: 10.1016/0140-6736(93)90882-H.
- [235] R. D’Inca *et al.*, “Intestinal Permeability Test As A Predictor of Clinical Course in Crohn’s Disease,” *American Journal of Gastroenterology*, vol. 94, no. 10, pp. 2956–2960, Oct. 1999, doi: 10.1111/j.1572-0241.1999.01444.x.
- [236] C. J. Kiely, P. Pavli, and C. L. O’Brien, “The microbiome of translocated bacterial populations in patients with and without inflammatory bowel disease,” *Intern Med J*, vol. 48, no. 11, pp. 1346–1354, Nov. 2018, doi: 10.1111/imj.13998.
- [237] S. Vrakas *et al.*, “Intestinal Bacteria Composition and Translocation of Bacteria in Inflammatory Bowel Disease,” *PLoS One*, vol. 12, no. 1, p. e0170034, Jan. 2017, doi: 10.1371/journal.pone.0170034.
- [238] W. Jing *et al.*, “Association of genetic polymorphisms in DNMT3A with the progression of gastric mucosal atrophy and susceptibility to gastric cancer in Japan,” *Oncol Lett*, Jan. 2019, doi: 10.3892/ol.2019.9948.
- [239] H. Takano *et al.*, “Effect of DNMT3A polymorphisms on CpG island hypermethylation in gastric mucosa,” *BMC Med Genet*, vol. 21, no. 1, p. 205, Dec. 2020, doi: 10.1186/s12881-020-01142-7.
- [240] B. G. Jorgensen *et al.*, “DNA methylation, through DNMT1, has an essential role in the development of gastrointestinal smooth muscle cells and disease,” *Cell Death Dis*, vol. 9, no. 5, p. 474, May 2018, doi: 10.1038/s41419-018-0495-z.

- [241] S. Saito *et al.*, “DNA methylation of colon mucosa in ulcerative colitis patients: Correlation with inflammatory status,” *Inflamm Bowel Dis*, vol. 17, no. 9, pp. 1955–1965, Sep. 2011, doi: 10.1002/ibd.21573.
- [242] J. Kraiczy *et al.*, “DNA methylation defines regional identity of human intestinal epithelial organoids and undergoes dynamic changes during development,” *Gut*, vol. 68, no. 1, pp. 49–61, Jan. 2019, doi: 10.1136/gutjnl-2017-314817.
- [243] S. Al-Ghadban, S. Kaissi, F. R. Homaidan, H. Y. Naim, and M. E. El-Sabban, “Cross-talk between intestinal epithelial cells and immune cells in inflammatory bowel disease,” *Sci Rep*, vol. 6, no. 1, p. 29783, Jul. 2016, doi: 10.1038/srep29783.
- [244] A. Geremia, P. Biancheri, P. Allan, G. R. Corazza, and A. di Sabatino, “Innate and adaptive immunity in inflammatory bowel disease,” *Autoimmun Rev*, vol. 13, no. 1, pp. 3–10, Jan. 2014, doi: 10.1016/j.autrev.2013.06.004.
- [245] S. J. Galli, N. Borregaard, and T. A. Wynn, “Phenotypic and functional plasticity of cells of innate immunity: macrophages, mast cells and neutrophils,” *Nat Immunol*, vol. 12, no. 11, pp. 1035–44, Oct. 2011, doi: 10.1038/ni.2109.
- [246] P. J. Murray, “Macrophage Polarization,” *Annu Rev Physiol*, vol. 79, no. 1, pp. 541–566, Feb. 2017, doi: 10.1146/annurev-physiol-022516-034339.
- [247] X. Yang, X. Wang, D. Liu, L. Yu, B. Xue, and H. Shi, “Epigenetic Regulation of Macrophage Polarization by DNA Methyltransferase 3b,” *Molecular Endocrinology*, vol. 28, no. 4, pp. 565–574, Apr. 2014, doi: 10.1210/me.2013-1293.
- [248] M. Kaneda *et al.*, “Essential role for de novo DNA methyltransferase Dnmt3a in paternal and maternal imprinting,” *Nature*, vol. 429, no. 6994, pp. 900–3, Jun. 2004, doi: 10.1038/nature02633.
- [249] Z. Wu *et al.*, “Dnmt3a regulates both proliferation and differentiation of mouse neural stem cells,” *J Neurosci Res*, vol. 90, no. 10, pp. 1883–1891, Oct. 2012, doi: 10.1002/jnr.23077.
- [250] M. Okano, D. W. Bell, D. A. Haber, and E. Li, “DNA methyltransferases Dnmt3a and Dnmt3b are essential for de novo methylation and mammalian development,” *Cell*, vol. 99, no. 3, pp. 247–57, Oct. 1999, doi: 10.1016/s0092-8674(00)81656-6.
- [251] H. Wu *et al.*, “Dnmt3a-dependent nonpromoter DNA methylation facilitates transcription of neurogenic genes,” *Science*, vol. 329, no. 5990, pp. 444–8, Jul. 2010, doi: 10.1126/science.1190485.
- [252] Z. Yang and X.-F. Ming, “Functions of Arginase Isoforms in Macrophage Inflammatory Responses: Impact on Cardiovascular Diseases and Metabolic Disorders,” *Front Immunol*, vol. 5, Oct. 2014, doi: 10.3389/fimmu.2014.00533.

- [253] A. H. Cull *et al.*, “Overexpression of Arginase 1 is linked to DNMT3A and TET2 mutations in lower-grade myelodysplastic syndromes and chronic myelomonocytic leukemia,” *Leuk Res*, vol. 65, pp. 5–13, Feb. 2018, doi: 10.1016/j.leukres.2017.12.003.
- [254] P. B. Ampomah *et al.*, “Macrophages use apoptotic cell-derived methionine and DNMT3A during efferocytosis to promote tissue resolution,” *Nat Metab*, vol. 4, no. 4, pp. 444–457, Apr. 2022, doi: 10.1038/s42255-022-00551-7.
- [255] I. Cobo, T. Tanaka, C. K. Glass, and C. Yeang, “Clonal hematopoiesis driven by DNMT3A and TET2 mutations: role in monocyte and macrophage biology and atherosclerotic cardiovascular disease,” *Curr Opin Hematol*, vol. 29, no. 1, pp. 1–7, Jan. 2022, doi: 10.1097/MOH.0000000000000688.
- [256] M. Orecchioni, Y. Ghosheh, A. B. Pramod, and K. Ley, “Macrophage Polarization: Different Gene Signatures in M1(LPS+) vs. Classically and M2(LPS–) vs. Alternatively Activated Macrophages,” *Front Immunol*, vol. 10, May 2019, doi: 10.3389/fimmu.2019.01084.
- [257] K. A. Jablonski *et al.*, “Novel Markers to Delineate Murine M1 and M2 Macrophages,” *PLoS One*, vol. 10, no. 12, p. e0145342, Dec. 2015, doi: 10.1371/journal.pone.0145342.
- [258] C. Wu *et al.*, “IFN- γ Primes Macrophage Activation by Increasing Phosphatase and Tensin Homolog via Downregulation of miR-3473b,” *The Journal of Immunology*, vol. 193, no. 6, pp. 3036–3044, Sep. 2014, doi: 10.4049/jimmunol.1302379.
- [259] T. Schilling, F. Miralles, and C. Eder, “TRPM7 channels regulate proliferation and polarisation of macrophages,” *J Cell Sci*, Jan. 2014, doi: 10.1242/jcs.151068.
- [260] E. M. Palmieri, C. McGinity, D. A. Wink, and D. W. McVicar, “Nitric Oxide in Macrophage Immunometabolism: Hiding in Plain Sight,” *Metabolites*, vol. 10, no. 11, p. 429, Oct. 2020, doi: 10.3390/metabo10110429.
- [261] F. O. Martinez and S. Gordon, “The M1 and M2 paradigm of macrophage activation: time for reassessment,” *F1000Prime Rep*, vol. 6, Mar. 2014, doi: 10.12703/P6-13.
- [262] C. Lailier *et al.*, “ERK1/2 signaling regulates the immune microenvironment and macrophage recruitment in glioblastoma,” *Biosci Rep*, vol. 39, no. 9, Sep. 2019, doi: 10.1042/BSR20191433.
- [263] C. Dong, G. Zhao, M. Zhong, Y. Yue, L. Wu, and S. Xiong, “RNA sequencing and transcriptomal analysis of human monocyte to macrophage differentiation,” *Gene*, vol. 519, no. 2, pp. 279–287, May 2013, doi: 10.1016/j.gene.2013.02.015.
- [264] T. Lawrence and G. Natoli, “Transcriptional regulation of macrophage polarization: enabling diversity with identity,” *Nat Rev Immunol*, vol. 11, no. 11, pp. 750–761, Nov. 2011, doi: 10.1038/nri3088.

- [265] E. Derlindati *et al.*, “Transcriptomic Analysis of Human Polarized Macrophages: More than One Role of Alternative Activation?,” *PLoS One*, vol. 10, no. 3, p. e0119751, Mar. 2015, doi: 10.1371/journal.pone.0119751.
- [266] W. Qin, C. A. Spek, B. P. Scicluna, T. van der Poll, and J. Duitman, “Myeloid DNA methyltransferase3b deficiency aggravates pulmonary fibrosis by enhancing profibrotic macrophage activation,” *Respir Res*, vol. 23, no. 1, p. 162, Dec. 2022, doi: 10.1186/s12931-022-02088-5.
- [267] U. Lendeckel, S. Venz, and C. Wolke, “Macrophages: shapes and functions,” *ChemTexts*, vol. 8, no. 2, p. 12, Apr. 2022, doi: 10.1007/s40828-022-00163-4.
- [268] X. Wu *et al.*, “TNF- α mediated inflammatory macrophage polarization contributes to the pathogenesis of steroid-induced osteonecrosis in mice,” *Int J Immunopathol Pharmacol*, vol. 28, no. 3, pp. 351–361, Sep. 2015, doi: 10.1177/0394632015593228.
- [269] A. Michelucci *et al.*, “Immune-responsive gene 1 protein links metabolism to immunity by catalyzing itaconic acid production,” *Proceedings of the National Academy of Sciences*, vol. 110, no. 19, pp. 7820–7825, May 2013, doi: 10.1073/pnas.1218599110.
- [270] X. Wang, Q. Cao, L. Yu, H. Shi, B. Xue, and H. Shi, “Epigenetic regulation of macrophage polarization and inflammation by DNA methylation in obesity,” *JCI Insight*, vol. 1, no. 19, Nov. 2016, doi: 10.1172/jci.insight.87748.
- [271] D. Zhou *et al.*, “Promising landscape for regulating macrophage polarization: epigenetic viewpoint,” *Oncotarget*, vol. 8, no. 34, pp. 57693–57706, Aug. 2017, doi: 10.18632/oncotarget.17027.
- [272] F. Jönsson, C. B. Gurniak, B. Fleischer, G. Kirfel, and W. Witke, “Immunological Responses and Actin Dynamics in Macrophages Are Controlled by N-Cofilin but Are Independent from ADF,” *PLoS One*, vol. 7, no. 4, p. e36034, Apr. 2012, doi: 10.1371/journal.pone.0036034.
- [273] Y. Yang, Y. Lin, Z. Zhang, R. Xu, X. Yu, and F. Deng, “Micro/nano-net guides M2-pattern macrophage cytoskeleton distribution *via* Src–ROCK signalling for enhanced angiogenesis,” *Biomater Sci*, vol. 9, no. 9, pp. 3334–3347, 2021, doi: 10.1039/D1BM00116G.
- [274] F. Y. McWhorter, T. Wang, P. Nguyen, T. Chung, and W. F. Liu, “Modulation of macrophage phenotype by cell shape,” *Proceedings of the National Academy of Sciences*, vol. 110, no. 43, pp. 17253–17258, Oct. 2013, doi: 10.1073/pnas.1308887110.
- [275] J. Yu *et al.*, “DNMT1-PPAR γ pathway in macrophages regulates chronic inflammation and atherosclerosis development in mice,” *Sci Rep*, vol. 6, no. 1, p. 30053, Sep. 2016, doi: 10.1038/srep30053.

- [276] M. Locati, A. Mantovani, and A. Sica, "Macrophage Activation and Polarization as an Adaptive Component of Innate Immunity," 2013, pp. 163–184. doi: 10.1016/B978-0-12-417028-5.00006-5.
- [277] Y. Lin *et al.*, "Notch Signaling Modulates Macrophage Polarization and Phagocytosis Through Direct Suppression of Signal Regulatory Protein α Expression," *Front Immunol*, vol. 9, Jul. 2018, doi: 10.3389/fimmu.2018.01744.
- [278] H. M. McRae and D. C. Hargreaves, "Old macrophages lose their (circadian) rhythm," *Trends Immunol*, vol. 43, no. 4, pp. 265–267, Apr. 2022, doi: 10.1016/j.it.2022.02.005.
- [279] A. Aderem and D. M. Underhill, "MECHANISMS OF PHAGOCYTOSIS IN MACROPHAGES," *Annu Rev Immunol*, vol. 17, no. 1, pp. 593–623, Apr. 1999, doi: 10.1146/annurev.immunol.17.1.593.
- [280] J. Liu, X. Geng, J. Hou, and G. Wu, "New insights into M1/M2 macrophages: key modulators in cancer progression," *Cancer Cell Int*, vol. 21, no. 1, p. 389, Dec. 2021, doi: 10.1186/s12935-021-02089-2.
- [281] J. Schnyder and M. Baggiolini, "Role of phagocytosis in the activation of macrophages," *Journal of Experimental Medicine*, vol. 148, no. 6, pp. 1449–1457, Dec. 1978, doi: 10.1084/jem.148.6.1449.
- [282] M. Comalada, A. Yeramian, M. Modolell, J. Lloberas, and A. Celada, "Arginine and Macrophage Activation," 2012, pp. 223–235. doi: 10.1007/978-1-61779-527-5_16.
- [283] M. A. Marletta, P. S. Yoon, R. Iyengar, C. D. Leaf, and J. S. Wishnok, "Macrophage oxidation of L-arginine to nitrite and nitrate: nitric oxide is an intermediate," *Biochemistry*, vol. 27, no. 24, pp. 8706–8711, Nov. 1988, doi: 10.1021/bi00424a003.
- [284] W. Jing *et al.*, "<p>DNMT3a promotes proliferation by activating the STAT3 signaling pathway and depressing apoptosis in pancreatic cancer</p>," *Cancer Manag Res*, vol. Volume 11, pp. 6379–6396, Jul. 2019, doi: 10.2147/CMAR.S201610.
- [285] L. Yang, R. Rau, and M. A. Goodell, "DNMT3A in haematological malignancies," *Nat Rev Cancer*, vol. 15, no. 3, pp. 152–165, Mar. 2015, doi: 10.1038/nrc3895.
- [286] S. J. Park and R. Bejar, "Clonal Hematopoiesis in Aging," *Curr Stem Cell Rep*, vol. 4, no. 3, pp. 209–219, Sep. 2018, doi: 10.1007/s40778-018-0133-9.
- [287] G. A. Challen *et al.*, "Dnmt3a is essential for hematopoietic stem cell differentiation.," *Nat Genet*, vol. 44, no. 1, pp. 23–31, Dec. 2011, doi: 10.1038/ng.1009.
- [288] I. Beerman *et al.*, "Proliferation-Dependent Alterations of the DNA Methylation Landscape Underlie Hematopoietic Stem Cell Aging," *Cell Stem Cell*, vol. 12, no. 4, pp. 413–425, Apr. 2013, doi: 10.1016/j.stem.2013.01.017.

- [289] B. Chassaing, J. D. Aitken, M. Malleshappa, and M. Vijay-Kumar, "Dextran Sulfate Sodium (DSS)-Induced Colitis in Mice," *Curr Protoc Immunol*, vol. 104, no. 1, Feb. 2014, doi: 10.1002/0471142735.im1525s104.
- [290] B. Cheng, A. Rong, W. Li, X. Bi, and X. Qiu, "DNMT3a-Mediated Enterocyte Barrier Dysfunction Contributes to Ulcerative Colitis via Facilitating the Interaction of Enterocytes and B Cells," *Mediators Inflamm*, vol. 2022, pp. 1–15, May 2022, doi: 10.1155/2022/4862763.
- [291] Y. Feng *et al.*, "Dnmt3a Mutations in the Hematopoietic System Promote Colitis-Associated Colon Cancer: A Model of Clonal Hematopoiesis in Solid Tumors," *Blood*, vol. 138, no. Supplement 1, pp. 2161–2161, Nov. 2021, doi: 10.1182/blood-2021-149740.
- [292] R. Suzuki, H. Kohno, S. Sugie, H. Nakagama, and T. Tanaka, "Strain differences in the susceptibility to azoxymethane and dextran sodium sulfate-induced colon carcinogenesis in mice," *Carcinogenesis*, vol. 27, no. 1, pp. 162–169, Jan. 2005, doi: 10.1093/carcin/bgi205.
- [293] T. Tanaka, H. Kohno, R. Suzuki, Y. Yamada, S. Sugie, and H. Mori, "A novel inflammation-related mouse colon carcinogenesis model induced by azoxymethane and dextran sodium sulfate," *Cancer Sci*, vol. 94, no. 11, pp. 965–973, Nov. 2003, doi: 10.1111/j.1349-7006.2003.tb01386.x.
- [294] A. Tovy *et al.*, "Constitutive loss of DNMT3A causes morbid obesity through misregulation of adipogenesis," *Elife*, vol. 11, May 2022, doi: 10.7554/eLife.72359.
- [295] D. Kohno *et al.*, "Dnmt3a in Sim1 Neurons Is Necessary for Normal Energy Homeostasis," *Journal of Neuroscience*, vol. 34, no. 46, pp. 15288–15296, Nov. 2014, doi: 10.1523/JNEUROSCI.1316-14.2014.

9. Supplementary material

9.1 List of Figures

Figure 1-1: Domain architecture of the DNMTs enzyme family.

Figure 1-2: Hierarchical organization of hematopoietic stem cells differentiation.

Figure 1-3: Schematic representation of intestinal macrophages distribution during IBD manifestations

Figure 3-1: Lack of *Dnmt3a* leads to increased gut permeability and bacterial translocation.

Figure 3- 2: *Dnmt3a* is downregulated upon inflammatory conditions.

Figure 3- 3: Deletion of *Dnmt3a* in CD11b+ myeloid cells isolated from intestinal lamina propria.

Figure 3- 4: *Dnmt3a* deletion in *Dnmt3a*^{LysM} derived BMDM.

Figure 3- 5: Proportions of CD11b+ events in ex vivo differentiated BMDM do not change between *Dnmt3a*^{fl/fl} and *Dnmt3a*^{LysM} mice.

Figure 3- 6: DNMT3A protein expression varies during wild type BMDMs polarization.

Figure 3- 7: Venn diagrams summarizing unique DEGs in young and old *Dnmt3a*^{fl/fl} vs *Dnmt3a*^{LysM} BMDM.

Figure 3- 8: Absence of *Dnmt3a* results in a complex dysregulated transcriptional signature.

Figure 3- 9: GO enrichment analysis for the 50 most up- and downregulated genes between resting-M1, Resting-M2 and M1-M2 for young and old wild type vs *Dnmt3a*^{LysM} BMDM.

Figure 3- 10: Lack of *Dnmt3a* leads to impaired polarization marker genes expression.

Figure 3-11: *Dnmt3a*-null BMDM undergo cytoskeletal organization towards M1 phenotype and display improper M2 phenotype.

Figure 3-12: Lack of *Dnmt3a* results in increased phagocytotic ability of M2 BMDMs and decreases it in M1 BMDMs.

Figure 3-13: Arginase and nitric oxide synthase activity is dysregulated in old *Dnmt3a*^{LysM} mice.

Figure 3-14: *Dnmt3a* promotes IEC monolayer regeneration after wounding.

Figure 3-15: Lack of *Dnmt3a* in M2 macrophages results in less tissue proliferation.

Figure 3-16: *Dnmt3a* expression in M2 polarized BMDMs is required to induce IEC proliferation and promotes IEC-derived tumorous cell expansion.

Figure 3-17: Basal phenotyping of *Dnmt3a*^{LysM} mouse line.

Figure 3-18: Spleen and liver of *Dnmt3a*^{LysM} mice have higher proliferation rates.

Figure 3-19: Increased frequencies of HSCs in the spleen of older *Dnmt3a*^{LysM} mice.

Figure 3-20: Lack of *Dnmt3a* in myeloid cells results in impaired splenic immune cell composition.

Figure 3-21: Acute DSS colitis model impacts *Dnmt3a*^{LysM} mice on DAI score but not in overall or organ weight or length of intestines in young female mice.

Figure 3-22: Splenic immune cell composition and small intestinal lamina propria immune phenotyping after acute DSS colitis.

Figure 3-23: Conditional deletion of *Dnmt3a* in myeloid lineage determines a subtle increase in body weight and disease activity upon chronic/AOM inflammation.

Figure 3-24: Immune cell composition of spleen, colonic and small intestinal lamina propria do not change in *Dnmt3a*^{LysM} mice after chronic DSS-induced inflammation.

9.2 List of Tables

Table 1: Reagents and volumes used for cDNA synthesis.

Table 2: cDNA synthesis program.

Table 3: Reagents and amount used for protein quantification reaction.

Table 4: List of reagents used for SDS-Polyacrylamide Gel Electrophoresis.

Table 5: Composition of buffer used for protein transfer.

Table 6: List of primary antibodies used for immunoblotting.

Table 7: Disease activity scoring parameters.

Table 8: Hybridization solution preparation.

Table 9: FISH washing buffer composition.

Table 10: List of antibodies used for basal immune phenotyping panel.

Table 11: Antibodies used for flow cytometry analysis of stem cell markers.

Supplementary tables

Supplementary table 1: List of top 50 unique up-and downregulated genes for Old KO, M1 vs M2.

Supplementary table 2: List of top 50 unique up-and downregulated genes for Old WT, M1 vs M2.

Supplementary table 3: List of top 50 unique up-and downregulated genes for Old KO,resting vs M1.

Supplementary table 4: List of top 50 unique up-and downregulated genes for Old WT,resting vs M1.

Supplementary table 5: List of top 50 unique up-and downregulated genes for Old KO,resting vs M2.

Supplementary table 6: List of top 50 unique up-and downregulated genes for Old WT,resting vs M2.

Supplementary table 7: List of top 50 unique up-and downregulated genes for Young KO,M1 vs M2.

Supplementary table 8: List of top 50 unique up-and downregulated genes for Young WT,M1 vs M2.

Supplementary table 9: List of top 50 unique up-and downregulated genes for Young KO,resting vs M1.

Supplementary table 10: List of top 50 unique up-and downregulated genes for Young WT, rest. vs M1.

Supplementary table 11: List of top 50 unique up-and downregulated genes for Young KO, rest. vs M2.

Supplementary table 12: List of top 50 unique up-and downregulated genes for Young WT, rest. vs M2.

Supplementary table 13: List of buffers and solutions.

Supplementary table 14: List of cell culture media.

Supplementary table 15: List of used reagents.

Supplementary table 16: Devices used in this study.

Supplementary table 17: List of applied kits.

Supplementary table 18: List of software.

Supplementary table 19: List of antibodies and fluorescent markers.

Supplementary table 20: List of used consumables.

Supplementary table 21: Primer sequence and assays.

9.3 Abbreviations

A	Ampere
Ab	Antibody
ABx	Antibiotics
ADC	Arginine decarboxylase
ADD	ATRX-DNMT3-DNMT3L
AF	Alexa fluor
AGAT	Arginine:glycine aminotransferase
AML	Acute myeloid leukemia
AOM	Azoxymethane
APC	Adenomatous polyposis coli
APC	Allophycocyanin
APCs	Antigen presenting cells
APS	Ammonium persulfate
ARG	Arginase
ARG-1	Arginase 1
ARG-2	Arginase 2
ATG16L1	Autophagy related 16 like 1
AZA	Azathioprine
BAFF	B-cell activating factor
BAH	Bromo adjacent homology domain
BL/6	Black 6
BMDM	Bone marrow derived macrophage
BMDMs	Bone marrow derived macrophages
BSA	Bovine serum albumin
BV	Brilliant violet
C5	Carbon-5
C57BL/6	C57 black 6
Cas9	C RISPR associated protein 9
CASP1	Caspase 1
CCND1	Cyclin D1
CCR9	C-C chemokine receptor type 9
CD	Crohn's disease
CD	Cluster of differnetiation
Cdh1	Cadherin 1
cDNA	Complementary DNA
CEACAM6	CEA cell adhesion molecule 6
CEBP/β	CCAAT/enhancer-binding protein beta
CGIs	CpG islands
CH	Clonal hematopoiesis
c-kit	tyrosine-protein kinase kit
CLP	Common lymphoid progenitor
CLR	C-type-lectin receptors
CMP	Common myeloid progenitor
CRC	Colorectal cancer
Cre	Cre recombinase
CRISPR	Clustered Regularly Interspaced Short Palindromic Repeats
Ct	Cycle threshold
Ctnnb1	Catenin b1

Cy3	Cyanine 3
DAB	3,3'-Diaminobenzidine
DAI	Disease activity index
DAPI	4',6-diamidino-2-phenylindole
DC	Dendritic cells
DEGs	Differentially expressed genes
DMAP	DNMT1-associated protein
DMEM	Dulbecco's modified eagle medium
DMPs	Differentially methylated positions
DNA	Deoxyribonucleic acid
DNAm	DNA methylation
DNMT1	DNA methyltransferase 1
DNMT2	DNA methyltransferase 2
DNMT3A	DNA methyltransferase 3A
Dnmt3a1	DNA methyltransferase 3A isoform 1
Dnmt3a2	DNA methyltransferase 3A isoform 2
Dnmt3aos	DNA methyltransferase opposite strand
DNMT3B	DNA methyltransferase 3B
DNMT3L	DNA methyltransferase 3L
Dnmts	DNA methyltransferases
DNMTs	DNA methyltransferases
DRAQ5	1, 5-bis{[2- (di-methylamino)ethyl]amino}-4, 8-dihydroxyanthracene-9,10-dione
DSS	Dextran sodium sulfate
DTT	Dithiothreitol
ECL	Enhanced chemiluminescence
EDTA	Ethylenediaminetetraacetic acid
eNOS	Endothelial nitric oxide synthase
ER	Endoplasmic reticulum
ESCs	Embryonic stem cells
FACS	Fluorescence-activated cell sorting
FAD	Flavin-adenine nucleotide
FADD	FAS-associated death domain protein
Fc	Fragment crystallizable region
FCS	Fetal calf medium
FCS	Forward scatter
FISH	Fluorescent <i>in situ</i> hybridization
FITC	Fluorescein isothiocyanate
Fl	Floxed
Flp	Flippase recombinase
FMN	Flavin mononucleotide
FRT	Flippase recognition target
FWB	FACS washing buffer
GM-CSF	Granulocyte-macrophage colony-stimulating factor
GO	Gene ontology
GRSs	generic risk scores
GvHD	Graft-versus-host disease
GWAS	genome wide association analysis
h	Hours
H&E	Hematoxylin and Eosin
H ₂ O	Water
HCl	Hydrogen chloride

HGF	Hepatocyte growth factor
HRP	Horseradish peroxidase
HSCs	Hematopoietic stem cells
IBD	inflammatory bowel disease
ICAM-1	Intercellular adhesion molecule –1
IECs	Intestinal epithelial cells
IF	Immunofluorescence
IFNAR1	interferon alpha and beta receptor subunit 1
IFNG	interferon gamma
IFNGR2	Interferon gamma receptor 2
IFN- γ	Interferon gamma
IFN- γ	Interferon gamma
IL	Interleukin
IL-10	Interleukin 10
IL-12	Interleukin 12
IL-13	Interleukin 13
IL-18	Interleukin 18
IL-1 β	Interleukin 1 beta
IL-22	Interleukin 22
IL-23	Interleukin 23
IL-23R	Interleukin 23 receptor
IL-4	Interleukin 4
iNOS	Inducible nitric oxide synthase
iNOS	Inducible nitric oxide synthase
IRF	interferon regulatory factor 5
JAK	Janus tyrosine kinase
JAK2	Janus kinase 2
kDa	Kilo Dalton
KO	Knock out
Lin-	Lineage negative
Lin+	Lineage positive
lncRNA	long-noncoding RNAs
LoxP	Locus of Crossover in P1
LP	Lamina propria
LPS	Lipopolisaccharide
Lyz2	lysozyme 2
M1 M ϕ	M1 macrophages
M2 M ϕ	M2 macrophages
MACS	Magnetic Activated Cell Sorting
M-CSF	Macrophage colony-stimulating factor
MEM	Minimal essential medium
mESCs	mouse Embryonic stem cells
MHCII	major histocompatibility complex class II
Min	multiple intestinal neoplasia
min	Minutes
miRNA	micro RNAs
MLN	Mesenteric lymph nodes
mRNA	Messenger RNA
MTase	Methyltransferase
Muc2	Mucin 2
MWB	MACS washing buffer

NaCl	Sodium chloride
NF- κ B	nuclear factor kappa-light-chain enhancer of activated B cells
NK	Natural killer
NLRs	nucleotid-binding oligomerization domain-containing protein (NOD)-like receptors
nNOS	Neuronal nitric oxide synthase
NO	Nitric oxide
NOD2	Nucleotide-binding oligomerization domain containing protein-2
NOS	Nitric oxide synthase
NOS2	Nitric oxide synthase 2
Ocln	Occludin
p	p-value
PAS	Periodic acid–Schiff
PB	Pacific blue
PBS	Phosphate-buffered saline
PCR	Polymerase chain reaction
PE	Phycoerythrin
PGE2	Prostaglandin E2
pH	Potential of hydrogen
PRRs	Pattern recognition receptors
PTGDS	prostacyclin synthase
PTGIS	prostaglandin D2 synthase
PVDF	Polyvinylidene difluoride
PWWP	Pro-Trp-Trp-Pro
R M ϕ	Resting macrophages
rDNA	Ribosomal DNA
Retnla	Retnla resistin like alpha
RFTS	Replication Focus Targeting Sequence
RIP3	Receptor-interacting protein 3
RIPA	Radio-Immunoprecipitation Assay (buffer)
RLRs	retinoic acid-inducible gene-I-like
RLT	RNeasy Lysis Buffer
RNA	ribonucleic acid
RPM	Revolutions per minute
RPMI	Roswell Park Memorial Institute
RT-qPCR	Real time quantitative polymerase chain reaction
SAM	S-adenosyl-methionine
SB	Sample buffer
Sca-1	Stem cells antigen-1
SDS	Sodium dodecyl sulfate
SDS-PAGE	Sodium dodecyl sulfate polyacrylamide gel electrophoresis
Sec	Second
SEM	Standard error of the mean
SFM	Serum-free medium
SNPs	single nucleotides polymorphisms
SSC	Side scatter
STAT	Signal transducer and activator of transcription
STAT1	Signal transducer and activator of transcription 1
STAT4	Signal transducer and activator of transcription 4
STAT6	Signal transducer and activator of transcription 6
TAM	tumo associated macrophages
TBS-T	Tris-buffered saline-Tween

TEER	Transepithelial electrical resistance
TEMED	Tetramethylethylenediamine
TGF- β	Transforming growth factor beta
Th1	T helper (response type) 1
Th2	T helper (response type) 2
TLRs	Toll-like receptors
TLR2	Toll-like receptor 2
TLR4	Toll-like receptor 4
TLR5	Toll-like receptor 5
TNF	Tumor necrosis factor
TNF- α	Tumor necrosis factor alpha
TREM-1	Triggering receptor expressed on myeloid cells 1
TSS	Transcription start site
UC	Ulcerative colitis
V	Volt
Vil	Villin
Wnt	Wingless and Int-1
WNT2B	wingless-type mouse mammary tumor virus integration site family, member 2B
WT	Wild type
Zo-1	Zonula occludens 1
μm	Micrometers
$^{\circ}\text{C}$	Celsius

9.4 Supplementary tables

Supplementary table 1: List of top 50 unique up- and downregulated genes for Old KO, M1 vs M2

Gene symbol	log2FC_KO	padj_KO	Gene symbol	log2FC_KO	padj_KO
Btbd11	6,43769876	7,2624E-07	Orm2	-8,88626779	2,0432E-21
Ocstamp	5,92705273	0,01791663	Ifi205	-8,67557092	4,4964E-09
Msx3	5,89465348	0,0413933	Ms4a4c	-8,49049596	1,1002E-07
St8sia1	5,72424616	1,5448E-05	Pydc3	-7,69020289	3,8061E-06
Col1a1	5,61142366	0,00944119	Apol9b	-7,59510938	1,1629E-07
Gm44206	5,51579018	4,7213E-10	Slfn1	-7,10905772	1,0561E-05
Cpa3	5,21948953	9,6692E-05	Gm4955	-6,90726645	2,5022E-12
Ngp	4,8929114	0,01009253	Pydc4	-6,8628664	2,2507E-12
Sema6d	4,88396034	0,00086148	Ifit3b	-6,3710592	0,00070318
Ighm	4,81034029	5,9551E-07	Irf7	-6,12643587	3,0272E-12
Cbr2	4,75270287	1,5333E-07	Ifit3	-5,9662319	2,7602E-05
Siglecfl	4,72285343	2,1229E-06	Orm3	-5,94771488	0,00105064
Ramp1	4,55468137	6,4552E-10	Gm21451	-5,68873371	0,00010149
Gm27177	4,5331978	0,00038378	Ifit1bl1	-5,60783413	0,00158015
Ms4a2	4,43638708	0,0073671	Apol9a	-5,58716657	5,5486E-05
Sfrp5	4,40396469	0,00254102	Gm27221	-5,37455036	0,00355599
Tceal7	4,38784666	4,3682E-05	Slfn4	-5,22474216	3,9737E-10
Cyp11a1	4,28850993	0,00120146	Ifi44	-4,66245998	0,00333763
Npas4	4,19667353	0,00098559	Ifit1	-4,46964472	7,1196E-06
Tns4	4,13605529	6,2414E-06	1700007K13Rik	-4,31214096	0,00317101
Cacna2d1	4,12568273	0,00875663	Oasl1	-4,23656393	3,0733E-05
Fads2	4,1158683	0,00129509	Adamts7	-3,85424425	8,5064E-05
Ube2c	3,99812425	0,00013165	4930551O13Rik	-3,81718525	0,00131343
2700081O15Rik	3,93133986	0,00030522	Oas3	-3,68688385	8,318E-05
Al427809	3,91770852	3,3263E-05	Ifit2	-3,68656278	0,02478111
Ptx3	3,82051304	0,0036941	Gm42836	-3,60909072	0,03000367
Gm36569	3,75652278	5,139E-05	Isg15	-3,60423964	1,126E-05
Prep1	3,72300465	0,00087509	Trim69	-3,5795848	0,02915116
Klrb1a	3,70728171	0,02594595	Hecw2	-3,55544356	0,00046276
Lpl	3,70472115	1,838E-08	Pyhin1	-3,54179028	2,2878E-05
Cyp1b1	3,67978247	0,00013908	Rtp4	-3,35371911	0,00031493
Gm15513	3,62766966	4,7159E-05	Zbp1	-3,31807201	7,215E-06
Folr1	3,58763767	0,00048381	Gm17110	-3,12900871	0,01879991
Kcnj10	3,5831802	0,00059652	Oasl2	-3,10727796	0,00085349
Cobll1	3,53504335	0,00773732	Zdhhc2	-3,09449141	0,00380952
Maob	3,53169198	0,00631159	Pla2g4b	-3,09279401	0,00581358
Gzma	3,50496135	0,04729338	Usp18	-3,00088584	0,00019585
Ccl9	3,47453252	6,7918E-05	Stx1a	-2,93077886	0,00134989
Rundc3a	3,46990412	0,00826023	Mnda	-2,92691902	0,00023022
Gfi1b	3,43322058	0,00595699	Spaca6	-2,85570601	0,00131343
Ltf	3,42566014	7,6497E-06	Ptpv	-2,81219581	0,00085349
Tmem176a	3,41007305	0,00219982	Prr33	-2,80886505	0,02074228
Jsrp1	3,37996687	0,03005574	Sh2d6	-2,79182732	0,01971549
Zfyve28	3,35664756	5,254E-06	Tnfsf4	-2,75835241	0,00264084
Lgi4	3,3428905	5,9097E-05	Gm26772	-2,67128873	0,01130377
Gm9920	3,3248617	0,00368753	Cd200r2	-2,57684508	0,03819663
Jchain	3,3126389	0,00600263	Sema3c	-2,56235841	0,00108147
Nes	3,30290521	0,00017162	2810029C07Rik	-2,5532686	0,00372864
Aspa	3,28899749	0,00597929	Fabp3	-2,55126749	0,00859254
Gm20425	3,23656231	0,00125737	Ly6e	-2,55002309	0,00250286

Supplementary table 2: List of top 50 unique up- and downregulated genes for Old WT, M1 vs M2

Gene symbol	log2FC_WT	Padj_WT	Gene symbol	log2FC_WT	Padj_WT
Amica1	5,22147146	0,00016795	Tmem265	-7,49037932	0,00052839
Ffar4	4,84040447	0,00046755	Krt16	-6,84998798	0,03101783
Ccl24	4,81928858	0,01611755	Gm13833	-6,68140116	2,9104E-06
P2ry13	4,48792878	4,8834E-06	Nrip3	-5,69237776	1,7179E-07
Myb	4,44095901	0,00186687	Hspb1	-5,62033349	1,8613E-12
Cyp2r1	4,43891729	0,00143335	Alpk2	-5,40204091	0,00016304
Dock3	4,40204347	1,3874E-05	Gm15859	-5,02734456	0,00200051
Al464131	4,34220435	0,01131016	Gm15650	-4,92360343	0,00081929
Tceal5	4,28136494	0,00437659	D030047H15Rik	-4,77884684	2,0961E-05
Gm26637	4,13747942	0,0001338	Insl3	-4,74082519	0,00543388
Tuba8	4,02241545	2,7823E-05	Tgtp1	-4,46337768	6,8612E-24
Cd200r3	3,95322014	0,00020271	Gstp2	-4,46315018	0,00245604
Gm14440	3,83670933	0,01664686	Wnk2	-4,41991656	0,01831504
Fgd2	3,7480739	5,0421E-08	Tmem44	-3,76263398	0,00223565
Ccl7	3,73866808	0,0202376	Ghr	-3,61559786	0,00014271
Angpt1	3,73084959	0,00188567	Cxcr1	-3,59006487	0,00289076
Mn1	3,71659838	0,01305087	4933423P22Rik	-3,49078729	0,00349405
Klra9	3,7000446	0,00931123	Gm5475	-3,481635	5,3249E-05
Olr1	3,69810597	0,00374896	Pdzd3	-3,47685709	0,00930998
Selp	3,68971299	0,00116196	Gm42726	-3,46353267	0,0068022
Zfp213	3,67011922	1,8551E-06	Hrc	-3,4357968	0,00368331
Zfp518b	3,66360359	1,4888E-09	Lcn2	-3,4130248	2,0254E-05
Inpp4b	3,58625839	0,00237144	1700084C06Rik	-3,40326701	0,00069998
Frk	3,47252201	0,00216054	Gm19705	-3,34712188	0,00247657
Nrg1	3,470049	0,00049704	Acta1	-3,32915237	0,04305968
P2ry12	3,3901788	0,00216054	Pram1	-3,30409914	0,00199729
F5	3,35562165	0,00036581	Klrk1	-3,26415207	9,6628E-07
Slc16a13	3,35481114	6,2435E-06	Aox1	-3,19985203	0,00016472
Kdm8	3,27825822	0,00089975	Gm42884	-3,15791808	0,02344279
Zfp784	3,25230355	0,00487858	Gm16796	-3,06904055	0,02147604
Ppp1r3c	3,16009296	0,03438371	Smpdl3b	-3,06705582	0,00011106
Ddx4	3,15369216	0,00060629	2810030D12Rik	-3,04587364	0,00441535
Gpr171	3,11137677	0,00035467	Lefty1	-3,04266795	1,3252E-05
Kbtbd8	3,10643305	0,01244982	Gm15440	-3,01652946	0,00103601
Zfp11	3,09180516	0,00225882	Gm29358	-2,9528757	0,02293877
Fbxo10	3,08916366	0,00026202	Gm26664	-2,93128197	0,00948944
Map1a	3,07937552	0,0028039	Pdk4	-2,93051182	0,00321677
Igkv5-43	3,0637287	0,02110723	A930006K02Rik	-2,91873923	0,01896875
4932438H23Rik	3,05750161	0,01225452	Gm26865	-2,90115947	0,04255821
Acacb	3,05300246	0,00430438	Gprasp2	-2,89451488	0,01386703
Sigirr	3,04991462	0,01596737	Mgat3	-2,88642234	0,00993225
Mzf1	3,02565448	0,02683098	Siglece	-2,88489518	0,00403433
Fam83h	3,01464454	0,01198123	D430001F17Rik	-2,87737011	0,01721769
1110002J07Rik	2,96008938	0,00331305	Tnfrsf12a	-2,86255285	8,5016E-06
Glis2	2,94684253	0,03010668	Gm12031	-2,8473481	0,00642408
Setmar	2,94603123	0,00176126	Slamf9	-2,84510262	2,8462E-06
Lipt1	2,90332049	0,0086336	Gm16104	-2,82765196	4,6873E-05
Sema6b	2,89969631	3,8875E-08	Fcor	-2,81647631	0,00026309
Igkv4-91	2,86264631	0,01346393	Adamts13	-2,77633359	0,0101565
Zfp458	2,84708202	0,02455208	Rasd2	-2,75471709	0,01061632

Supplementary table 3: List of top 50 unique up- and downregulated genes for Old KO,resting vs M1

Gene symbol	log2FC_KO	Padj_KO	Gene symbol	log2FC_KO	Padj_KO
Orm3	6,33501144	9,6319E-05	Dnmt3aos	-4,16281655	8,9279E-07
Gm21451	6,29402645	4,6836E-05	Il18r1	-3,55959345	0,00634886
Socs3	3,42342146	1,0098E-05	Prkg1	-3,43419803	1,6878E-05
Pla2g4b	3,38614138	0,00069036	Lamb3	-3,39528057	0,00267093
Mef2b	2,99695817	0,01239326	Cldn15	-3,32785572	0,00123022
Gm28035	2,89533627	0,00481772	Cobll1	-3,30164277	0,00737512
Pla2g3	2,83094659	0,0047074	Pgm5	-3,21965465	0,00036876
Lif	2,71250902	0,00010874	Prss57	-3,17463864	0,00056573
Vps37d	2,69418218	0,00346933	Penk	-3,09429346	7,1285E-06
Misp	2,69312891	0,001931	Cyp2s1	-3,06709115	0,00212981
Dnm3	2,64333265	0,01792723	Bicd1	-2,99862411	0,00262449
Cav1	2,60571595	0,00063009	Mgp	-2,96351583	0,00801293
Spaca6	2,60538015	0,00046388	Lanc13	-2,90072804	0,00178617
B230303O12Rik	2,572632	0,00096013	Il1b	-2,85848457	0,00647544
Ly6g6d	2,55795037	0,04566917	Ctnnal1	-2,83496262	0,00062575
Sh2d6	2,54933	0,02930033	Nt5e	-2,75074109	0,00250261
Gm14023	2,53968103	0,00262984	Folr1	-2,74799911	0,02226124
Gm128	2,51136888	0,01428315	Camk4	-2,73899391	0,04628162
Gm20708	2,50461602	0,01636755	Zfp354c	-2,71637952	0,0224437
Soat2	2,4752706	0,00029807	Ccdc40	-2,71497331	0,01438984
RP24-285L8.3	2,37553098	0,00030309	Tubb2b	-2,66717834	9,8323E-05
Col9a3	2,35284714	0,01242703	Gm13431	-2,6647414	0,03982954
4930422M22Rik	2,35115283	0,01071788	Pcdhga12	-2,63085975	0,03925551
Gm15751	2,2842738	0,00450729	Chek1	-2,61978179	0,00152052
Dapk2	2,26091221	0,04751535	Cd300ld4	-2,57220512	0,00065936
Gm28037	2,25980099	0,02869933	Proser2	-2,5695777	0,0014409
Fndc7	2,24384844	0,01472625	Hba-a2	-2,48399407	0,00179433
Gm20522	2,12468488	0,00200132	Capn3	-2,44980069	0,0138561
Slc7a11	2,11694143	0,02194344	Igfbp5	-2,44132507	0,00787077
Syt8	2,09785055	0,00221436	Hbb-bs	-2,4404074	0,01818148
Gm8093	2,09340424	0,01993642	Nrgn	-2,39719337	0,00355811
Ip6k3	2,07005125	0,0101931	Stbd1	-2,38875037	0,03762976
Grik5	2,06297807	5,8507E-05	Mex3a	-2,37665295	0,02850332
C920006O11Rik	2,05830177	4,0257E-05	Cables1	-2,36559164	0,00290083
Sgk1	2,02921505	0,00124737	8030453O22Rik	-2,33292401	0,01266332
Il12rb1	2,02183912	0,01876247	Pik3c2b	-2,28988333	0,02050886
Slamf6	2,00992217	0,00717706	Ccdc18	-2,22291556	0,00696782
Ptpv	1,995542	0,00563602	Gata2	-2,18608875	0,01153798
Efna1	1,98610462	0,01379975	Mir99ahg	-2,15893075	0,03886393
Enah	1,89951151	0,00483497	Lipg	-2,15714699	0,01472625
Azin2	1,86556873	0,00447834	Mgam	-2,15425909	0,03932966
Gsto2	1,8457061	0,01845702	Mcam	-2,11374074	0,0243506
Rab33a	1,83789061	0,03057379	C430049B03Rik	-2,09670846	0,03706874
Fbxo32	1,83310524	0,01074022	Ahrr	-2,06822122	0,00380429
Gm26773	1,83296675	0,02877571	Tpx2	-2,06742327	1,97E-05
Lck	1,82812652	0,00832556	Lcn2	-2,06586603	0,01174028
Gm27010	1,78747877	0,04236858	Dnmt3b	-2,06434092	0,0023306
2310010J17Rik	1,78414537	0,03703144	Peg10	-2,0563828	0,04594098
Gm4262	1,74694224	0,03878478	Kif18a	-2,04594052	0,00114193
Gm11537	1,73666661	0,02781008	Pla2r1	-2,0441409	0,02442971

Supplementary table 4: List of top 50 unique up- and downregulated genes for Old WT,resting vs M1

Gene symbol	log2FC_WT	padj_WT	Gene symbol	log2FC_WT	padj_WT
Hamp	10,4087941	0,00187224	Gm45062	-7,59904189	2,4133E-11
Krt16	8,23362281	0,01638201	Pcdhga8	-5,55116322	0,00297486
Gm13833	7,76728447	3,1758E-13	Igkv6-23	-5,3149508	5,6092E-08
Ccdc155	7,2557407	0,00051681	Kif26b	-5,1605588	0,00038669
Nrip3	6,40236874	8,214E-13	Igkv15-103	-4,94404712	4,631E-06
Insl3	5,97859927	1,7381E-07	Igkv4-72	-4,87075445	0,00050752
Alpk2	5,74472097	8,2953E-09	Gm28048	-4,79601928	0,04079912
Gm26609	5,57009291	1,0165E-07	Igkv1-117	-4,7158075	1,1944E-09
Btbd16	5,14542332	7,6474E-05	Gm15675	-4,67711677	0,00022235
D430001F17Rik	4,87539149	1,302E-07	1700047M11Rik	-4,67025827	0,00038397
Tgtp1	4,65074028	1,8461E-14	Wfikkn1	-4,59902568	9,6553E-06
BC023105	4,55713713	6,155E-07	Ighv4-1	-4,59180374	5,6816E-08
Pappa2	4,50272602	2,5088E-10	Ighv1-64	-4,58568811	0,00020937
Gm15853	4,46342206	2,6955E-18	Nlrp1b	-4,52311608	0,00072828
Gstp2	4,4603436	2,4971E-05	Cyp2r1	-4,50335288	6,8197E-05
Gm43813	4,32446615	9,1771E-08	Igkv16-104	-4,45712055	0,00019615
Gbp11	4,24667866	7,7292E-08	Cxcl1	-4,44828219	0,00552988
Ppargc1a	3,96191483	4,5137E-05	Igkv6-15	-4,4318219	0,00071424
1110028F11Rik	3,86447684	0,00122104	Gm4117	-4,42742735	6,521E-07
Upp1	3,74372064	3,8967E-10	Prom1	-4,38730207	0,0002573
Hist1h2br	3,72443347	5,7503E-05	Igkv5-43	-4,38349712	5,9115E-06
Pdzd3	3,60040641	0,00015044	Pcdhgb5	-4,31216185	0,00043887
Gm21972	3,52005941	2,9881E-05	Igkv8-24	-4,30002071	0,00161893
Gm26853	3,49416005	0,00019505	Igkv10-96	-4,2102481	1,2569E-07
Ido1	3,46780008	0,02517287	Homez	-4,20624284	4,4423E-16
Tsix	3,44754995	4,7782E-14	Igkv6-17	-4,1755471	0,00055535
Btbd18	3,38542426	0,00103076	Ighv11-2	-4,11761572	3,2596E-11
Slc1a2	3,38100464	0,00434747	Ighv1-55	-4,09531983	1,844E-07
Timp1	3,36336657	2,3185E-14	Npff	-4,04972849	0,00186017
Rsg1	3,31617796	4,3054E-07	Iglv2	-4,03442912	0,00023929
Tmem44	3,2993763	0,00043572	Il5ra	-4,03352351	0,00054482
Gm15473	3,29810816	0,00334485	Igha	-4,02270069	1,1717E-09
Dgki	3,26013182	0,00029495	Ighv14-4	-4,00981333	0,00108438
Gbp4	3,25209946	0,004449	2010300C02Rik	-3,89354123	5,1229E-05
1700084C06Rik	3,23455494	0,00015489	Igkv2-137	-3,8658592	0,00720768
Pdk4	3,21806254	2,5012E-05	Ighv1-53	-3,81603053	0,00016397
Hist1h2be	3,18139939	7,8345E-08	Ptpcap	-3,80562819	1,0872E-06
Gm4841	3,14472781	0,00017356	P2ry10	-3,78467234	0,00121162
Gm27221	3,1429704	0,03330337	Igkv17-121	-3,75689626	0,00259351
Wwc1	3,13625933	0,00011646	Smim5	-3,70096633	0,00154442
Gm17110	3,12055946	0,00053643	Cxcl3	-3,7001311	0,00202355
Tex14	3,08028332	0,00053643	Ighg1	-3,68064354	0,04144032
Hsp90aa1	3,07333845	3,722E-08	Ighg2c	-3,67804052	0,00649035
Gm44732	3,04037795	2,9144E-06	Igkv3-4	-3,60317799	0,00010579
1810019N24Rik	3,03208096	0,00061251	Ighv1-26	-3,59541691	4,9072E-05
Gm28551	3,02963405	0,00482232	Gm15513	-3,56730326	0,02742702
Luc7l3	2,94604344	1,9128E-08	Zfp784	-3,55109494	1,7805E-05
Rasd2	2,92886372	0,00039776	Hba-a1	-3,53725065	0,03821011
Aim1l	2,87997996	2,0629E-05	Igkv5-39	-3,53467275	0,0288767
Stard13	2,87592286	3,6922E-05	Ighv8-8	-3,52552877	0,01542089

Supplementary table 5: List of top 50 unique up- and downregulated genes for Old KO,resting vs M2

Gene symbol	log2FC_KO	padj_KO	Gene symbol	log2FC_KO	padj_KO
Gm27177	7,44275963	0,00091961	CtsG	-4,75966253	0,00099351
Ocstamp	5,47286161	0,0018581	Ms4a4c	-4,62445279	0,00235923
Slc36a2	4,92267382	0,000252	Slc6a17	-4,60781629	0,00057886
Ogn	4,69346714	4,9975E-05	Pydc3	-4,18266424	0,00752123
Gm26702	4,68408719	0,00085697	Ccl2	-3,75417571	0,00016318
Cfap161	3,99981355	4,4382E-05	Hbb-bs	-3,73116563	9,712E-06
Itgax	3,85005506	0,00470459	Dnmt3l	-3,66388671	0,00655157
Trf	3,79660006	0,00419589	Nxpe2	-3,64622936	0,00024486
Gm16565	3,55216691	0,00189793	Ifit3	-3,63536041	0,00060338
Ppp1r3c	3,54894618	0,00406629	Gm6634	-3,58024286	0,00022685
Slc4a11	3,48674345	0,00786246	Adgrl4	-3,5387212	1,9346E-06
Dkk3	3,44886391	0,00023576	Slfn1	-3,44370017	0,03572987
Efemp1	3,42412827	5,4967E-06	Tnfsf14	-3,41554272	1,2639E-05
Plxdc2	3,37335827	0,00742813	Gfi1	-3,38585852	3,3354E-06
Gm6209	3,33089841	0,0436225	Slfn4	-3,29183187	1,063E-06
Ksr2	3,3121359	0,01730332	Trim30b	-3,25761616	9,346E-05
Slco2b1	3,28188671	0,00305942	Tlr5	-3,185949	0,00022709
Cemip	3,2497038	2,4326E-10	Adgrg7	-3,16395707	0,01340951
Map2	3,21961931	0,0001769	Muc13	-3,12554106	0,00360959
Mgll	3,1636001	0,00857217	Nwd1	-3,01664487	0,00513081
Edn1	3,14946038	0,00600065	Ifit1	-3,00517352	2,5999E-05
Sorbs2	3,10644886	0,01028871	Tnfsf9	-2,99592818	4,905E-05
Adamts5	3,04941896	2,3608E-07	Rtp4	-2,97506348	2,1032E-06
Gfra2	3,01203296	0,03210361	Rbm44	-2,94598596	0,00018107
Fn1	3,01133224	0,01558269	Rragb	-2,93259745	0,00141547
Gm2115	2,99034252	0,0031996	Cpt1b	-2,87219934	0,0031759
B3gnt7	2,96297636	8,2672E-08	Ifi44	-2,85843662	0,02682826
Clcf1	2,92407701	2,1158E-07	Tppp	-2,85033295	0,00835489
Slc9a3r2	2,8382634	0,00377829	Tie1	-2,82964979	0,00039988
1500009L16Rik	2,82223521	0,01900147	Il18rap	-2,826874	2,5605E-05
Btbd17	2,81154302	0,03527504	Dnah8	-2,82361127	0,00074631
Cyp2ab1	2,73068023	0,04597197	Pydc4	-2,79674625	0,04969201
Trim29	2,69356037	0,00179919	B230208H11Rik	-2,77040961	0,00093786
Mfge8	2,67955232	0,02875918	Scml2	-2,76707889	0,00600065
Fndc7	2,67526304	5,1328E-05	Trpc6	-2,76400725	6,39E-09
Nnmt	2,66487683	0,00399118	Erg	-2,73904617	4,281E-05
Mmp19	2,64104331	1,0005E-06	Ilgp1	-2,72799578	0,02255809
Batf3	2,56488237	0,00024218	Trim30c	-2,70846913	0,00088489
Col1a2	2,55584375	3,0046E-08	Acod1	-2,70561608	1,0734E-05
Shisa9	2,54670363	1,3197E-07	Oas2	-2,68074685	4,5842E-05
Rtn4rl2	2,51820406	0,02745068	Slc35d3	-2,66685767	0,00069708
Mrc2	2,51324607	1,65E-10	Itih5	-2,65894185	0,00084965
Fcgr2b	2,39766526	1,8936E-09	Mmp25	-2,5886568	0,00088503
Dnm3	2,39621003	0,00429217	Bcl6b	-2,58764922	0,02118135
Rspo2	2,37891848	0,00473324	2010110K18Rik	-2,5727276	0,01376143
B230303O12Rik	2,37017385	1,7589E-05	Chst13	-2,55470232	0,03540746
Micalcl	2,3643208	3,9589E-05	Ppm1e	-2,54145035	0,00066364
Cd6	2,3487805	0,01573942	Id1	-2,53007435	0,0065178
Lama5	2,34722998	0,00109796	Nrg2	-2,52799445	0,00469583
Col24a1	2,34533101	0,03669469	Peak1os	-2,51454551	2,9437E-05

Supplementary table 6: List of top 50 unique up- and downregulated genes for Old WT,resting vs M2

Gene symbol	log2FC_WT	padj_WT	Gene symbol	log2FC_WT	padj_WT
Ccl8	6,43196136	0,00225629	Gm45062	-8,1644923	0,00052801
Tceal5	5,68718768	1,1457E-09	Upb1	-4,66474921	6,5065E-06
Pgf	5,17577051	3,1687E-12	Wnt10a	-4,19090449	0,00776757
Crabp2	4,38289726	0,00276249	Sox7	-3,97997992	4,906E-05
Ddx4	3,76748855	1,2134E-07	Gm12744	-3,68585382	7,9609E-06
Adipoq	3,70512293	0,01491358	Serpnb12	-3,65177915	0,01868576
Nyap2	3,36805262	0,00049228	Dpp4	-3,63069807	0,00157211
Gbp11	3,34764902	0,00995838	Ighg3	-3,53553678	0,0025124
Nrg1	3,32804987	6,7469E-06	Apold1	-3,33670803	0,00213429
Fam71f2	3,14421549	0,03009604	Gpx3	-3,20207579	0,00010919
H2-Q6	3,04361247	4,8603E-05	Chp2	-3,15553689	0,00973887
Tarm1	3,02769203	1,0251E-10	Ly6d	-3,10175817	0,00093898
Ccl24	3,02190234	0,01953385	Dcstamp	-3,09141913	0,02240506
Efcc1	2,9430669	5,8391E-09	Tns4	-3,08689683	0,00136536
Clic5	2,93391692	0,00028306	Aldoc	-2,99021147	7,0404E-06
Stard13	2,8888584	3,162E-06	2010300C02Rik	-2,95863946	0,00457156
Ccl12	2,84173179	0,00019774	Btbd11	-2,9506552	0,01565709
D630024D03Rik	2,68940184	4,3105E-07	Siglecfl	-2,88824562	0,00182872
Htra4	2,67574279	2,2919E-05	Igkv5-39	-2,88740671	0,01809677
Car2	2,67057295	0,00013171	1700047M11Rik	-2,8177736	0,00181263
Soat2	2,64489493	1,8611E-05	Cadm3	-2,80471321	0,00474216
Cst7	2,63856646	0,00265566	Fxyd2	-2,77264204	8,9713E-09
AA467197	2,61315305	0,00057484	Prg2	-2,70001895	0,00545462
Inadl	2,60580055	0,0282411	5031425F14Rik	-2,69713393	0,00022491
Dnase1l3	2,47730702	0,04885995	Gm3571	-2,67216365	0,00168556
Ttyh1	2,40109247	0,03390959	Cxcl3	-2,67187577	0,00034708
Serpina3g	2,38144328	0,0176637	Celsr2	-2,65829817	0,00058507
Prps1	2,36252216	0,00695574	S100a4	-2,65095687	4,7529E-07
Ffar4	2,33989351	0,03246583	Npas4	-2,646467	0,02225725
Gm15880	2,33488454	0,02252606	Socs3	-2,64512987	0,00022698
Dnah12	2,32058146	0,04129613	Zan	-2,63363364	0,00992495
Tmie	2,31000567	0,01236783	Efr3b	-2,55627369	0,00433992
Gm16315	2,26108588	0,00216363	Slc13a3	-2,45082343	0,00370841
Angptl3	2,23387141	1,7505E-07	RP23-381H23.1	-2,44104047	0,00816639
Rtn4r	2,21992813	0,00018394	Cecr2	-2,42834813	0,00929964
Gbp8	2,18353239	0,04251336	Fcrls	-2,41362511	8,0462E-05
5033417F24Rik	2,17049476	0,00210658	Ighg2c	-2,40322832	0,0147097
Gm21887	2,15460926	0,00090828	Gm20658	-2,38933517	0,00075966
Gja1	2,14764246	0,00159092	Zfp618	-2,37282836	0,04977185
Tnfrsf9	2,13923484	0,00572192	Mamdc2	-2,36144398	0,03620691
Pla1a	2,12659689	0,00353771	Nuak1	-2,28302193	4,703E-05
H2-Q5	2,07376081	0,01198012	Gm28800	-2,28064787	0,04776901
Rasgrp1	2,06016729	0,00457589	Fhl1	-2,27997238	0,00024486
Gm26698	2,04374581	0,0268216	Gm20695	-2,27737026	0,00379676
Cystm1	2,0381183	0,00213451	Ramp1	-2,26824858	0,00620456
Gm6325	2,02376353	0,00645165	Gm5150	-2,26787743	0,0069897
Gm26512	1,94674994	0,02107028	Fsdp	-2,24377882	0,00725398
Ms4a4a	1,91724208	0,04071874	Smim5	-2,23731245	0,00011026
BC094916	1,9095692	0,01296208	Lpl	-2,23696437	0,02285388
Mcf2l	1,90345321	0,01140251	Mpz	-2,21889161	0,03531318

Supplementary table 7: List of top 50 unique up- and downregulated genes for Young KO,M1 vs M2

Gene symbol	log2FC_KO	padj_KO	Gene symbol	log2FC_KO	padj_KO
Blk	7,4977261	0,00066365	Gm4117	-6,07614877	4,5682E-06
Egr3	6,72306797	0,00599277	Pcp4	-5,93608619	0,00318362
Acacb	6,42536418	0,01522642	Hba-a2	-5,12794068	2,0026E-11
Ogn	6,38753678	0,01778812	F830016B08Rik	-5,01739697	0,00240516
Pax5	5,89321806	0,0004372	Arhgap8	-4,79754228	0,04706615
Shisa8	5,79512191	0,01439912	Slc6a19	-4,22074667	1,7809E-05
Ms4a1	5,62557547	0,0015021	Pbbp	-3,84117282	1,0505E-08
Cd79a	5,570463	1,8391E-05	Iigp1	-3,76973079	0,04872412
Atp2a1	5,46687071	0,02657787	Gbp5	-3,58079243	2,3905E-10
Tnfrsf13c	5,39842693	0,00395402	Mgarp	-3,54281804	0,00681541
Gm8369	4,90365267	0,0087841	Olfr56	-3,49272933	0,00011871
Gm14440	4,83104867	0,00067514	Ly6a	-3,45667931	1,8465E-19
H2afy2	4,75840792	0,03758976	Gm10634	-3,42285655	0,04743435
Pygm	4,73765562	0,01834798	Gbp8	-3,27347334	3,2326E-10
Hdhd3	4,61648785	0,04152344	Dnase1l3	-3,27016189	5,2621E-05
Spib	4,55998272	1,5688E-05	Gbp9	-3,26982128	1,0865E-08
Pou2af1	4,398209	0,01522642	Gp9	-3,21921901	0,01074548
Tex14	4,34819097	0,04853955	Prkca	-3,1861394	0,0116296
Satb1	4,32124811	0,01439647	Il27	-3,17555422	0,00274253
9330102E08Rik	4,15760358	0,02747927	Ccdc148	-2,98644641	0,01652376
TINCR	4,13190968	0,00401203	Samd14	-2,89950428	0,02797138
Cd19	4,01351711	0,00155808	Gbp11	-2,89731681	0,02011299
Ddx4	4,00287252	8,1523E-05	Ak4	-2,88158662	9,5196E-08
Srl	3,98599359	0,02900156	4931431C16Rik	-2,83933584	0,01488829
Gm26561	3,91838144	0,0154026	C920021L13Rik	-2,7712765	3,5772E-06
Igf1os	3,79525836	0,02960228	Alox12	-2,66112453	0,01504446
Tgfb3	3,72171075	0,02033526	Smpd13b	-2,65942897	0,00927352
Vwa7	3,63882063	0,04528657	Snca	-2,65525798	0,03086923
Gm14421	3,56066136	0,00754529	Irgm1	-2,60080827	2,1336E-13
Rad9b	3,5354122	0,00708301	3010003L21Rik	-2,56197744	0,01845989
Aldh1l2	3,39761794	0,00663626	Il12rb1	-2,54166626	0,00043783
Ddr2	3,36101016	0,03070179	Rgs2	-2,45344034	4,1997E-15
B230303O12Rik	3,31667327	0,01753596	Rab26os	-2,44484465	0,00306395
Irf4	3,31595926	0,00849919	1500026H17Rik	-2,39446395	0,00024629
Chac1	3,222237	0,02844629	3110056K07Rik	-2,39413058	2,6116E-08
Iglc2	3,21761939	0,00379421	Bach1	-2,38578301	1,047E-17
Mrc2	3,20058017	0,00317468	Hba-a1	-2,37933843	0,00270673
Kdelr3	3,18530563	0,04741871	H2-DMa	-2,37831298	6,8917E-11
Zfp41	3,17551113	0,00670889	Prg4	-2,37551651	0,04934231
Col20a1	3,1658553	0,00059886	Cd69	-2,36728159	1,7624E-08
Lgals4	3,15463568	0,02556715	Tnfsf13os	-2,35655917	0,0441389
Gm14306	3,14123421	2,2822E-07	Ccne1	-2,35632741	6,4697E-06
Cd79b	3,1400906	0,01407724	Htra4	-2,35476964	0,00455007
Mzb1	3,11355416	0,03711642	Irf1	-2,33779651	4,1783E-09
4930556M19Rik	2,94883647	0,04106346	Cd38	-2,32837178	0,00157735
Col11a2	2,91940595	2,4111E-06	Icam1	-2,31839559	7,8745E-12
Fam161b	2,91737663	0,01008368	H2-Ab1	-2,31742433	6,8353E-10
Gtf2h3	2,90892786	2,8684E-05	Gm16712	-2,29643431	0,01984023
Cxcl12	2,89728786	0,02033526	Socs1	-2,29333665	1,7839E-05
Dync2h1	2,86304603	0,00058004	Clic5	-2,28277472	4,5E-06

Supplementary table 8: List of top 50 unique up- and downregulated genes for Young WT,M1 vs M2

Gene symbol	log2FC_WT	padj_WT	Gene symbol	log2FC_WT	padj_WT
Gm27177	4,29265092	0,00337237	Gm28048	-7,40449977	0,00461222
Adcy3	4,16349341	3,0345E-16	Zfp969	-7,06862621	0,00070611
C5ar2	4,13882914	1,8533E-05	Gm17034	-6,39572155	4,6468E-05
Mamdc2	4,05293683	2,1895E-05	Saa1	-5,8680023	0,00015328
Slc9a9	3,84346813	1,0682E-15	Ifi205	-5,24271679	0,03088893
C030034L19Rik	3,7437086	0,00492319	8430408G22Rik	-5,16504043	4,9306E-07
Gm996	3,61622579	0,00024326	Bpifc	-5,09081074	0,00610771
Gm2004	3,55818894	0,02129846	Serpina3f	-5,00819959	0,00094635
Cysltrl	3,52747317	5,8658E-05	Apol9b	-5,00311433	0,00096909
Il6ra	3,52373324	0,00024326	Gm13822	-4,94433422	0,00548075
Tifab	3,47697918	5,0277E-05	B430010I23Rik	-4,708669	0,0115972
Pdgfc	3,43751544	3,1491E-12	Gm15935	-4,55411224	0,00076302
Mmp27	3,43633118	5,0232E-08	Unc93a	-4,54102723	0,03111306
C5ar1	3,41535251	1,1362E-20	Efcab6	-4,51788649	0,04744112
Dhrs9	3,36943589	3,9509E-07	Inhba	-4,48241585	1,0468E-06
Cnr2	3,35607059	1,6827E-05	5033430I15Rik	-4,25963797	0,00032804
Gpr155	3,3233994	0,00030774	Dusp14	-4,24119506	0,00043304
Mertk	3,27248983	1,1452E-08	Gm26626	-4,21154839	0,00162475
Il16	3,21901321	9,2148E-05	Btbd16	-4,2070089	4,3612E-05
Cnrip1	3,18495291	3,5365E-06	Gem	-4,1553276	2,7163E-05
Mblac2	3,15965955	0,00040873	Gm20406	-4,1525798	0,00133956
Gemin4	3,12626344	0,02234318	Apol9a	-4,10017842	0,03511273
Itgax	3,11423345	5,6258E-10	Gm4876	-4,07532196	8,0877E-05
Fam13a	3,10765044	0,01093664	Gm9992	-4,02326438	0,00904598
Map2k7	3,07205734	0,0217279	Xcr1	-4,0006851	0,00191414
Tfrc	3,04626396	0,00402376	Gm13571	-3,95396929	0,00013685
Shisa9	3,01772653	4,0371E-06	Stx1a	-3,87817979	6,1421E-05
Aatk	3,0134851	3,7137E-05	RP23-385F3.2	-3,87351153	0,00054156
Tmem51	3,00775879	0,00085191	Cxcr1	-3,8706391	0,00013437
Cfh	2,97928229	3,0192E-06	Gm20732	-3,86987727	0,01146581
Ptpro	2,92562686	6,4639E-05	Eif4ebp3	-3,84526299	0,00293354
Hlcs	2,9227026	0,00127029	Crlf1	-3,83909625	0,00208136
Prdm1	2,92076661	0,00022657	Gm15956	-3,83074305	0,00830502
Abcg2	2,89387315	1,2294E-05	Ctf2	-3,80935709	0,00143571
Ptgs1	2,88744925	0,00102356	Orm2	-3,75686612	2,9818E-11
Adap2os	2,88094158	0,00118252	Gm3513	-3,71333761	0,01063194
Ap5b1	2,87267201	0,00065689	Gm17590	-3,70153361	0,01283911
Dnajc28	2,85300293	0,01839232	Drd1	-3,681243	0,00067963
Zfand4	2,85083568	0,02195364	Ccdc155	-3,64901772	0,00246522
Pdcd1lg2	2,83453643	0,00373199	Orm1	-3,64092369	6,7783E-08
Ablim1	2,79811543	0,00221057	Sstr5	-3,63907996	0,00695298
Engase	2,77795258	0,00018349	C1qtnf4	-3,5745662	0,01589458
Zfp395	2,77147785	1,1401E-06	Gfy	-3,45756384	0,0282466
Jade2	2,74013807	0,00141065	Hecw2	-3,45184792	0,00025153
Plxnb3	2,73457591	0,00054582	Il9r	-3,39135761	0,01962897
Arhgef10l	2,73436986	4,0512E-08	Cacna1b	-3,318819	0,00020177
Trem1	2,7087244	1,4228E-05	Ngp	-3,29982737	0,00019554
Rnf150	2,70847897	0,00084699	4933433G15Rik	-3,28237615	0,00470198
Itipr1l1	2,68450645	0,00743343	Il10	-3,20294697	0,01897642
Erb3	2,6726826	0,01905356	Gm15473	-3,18528178	0,02508951

Supplementary table 9: List of top 50 unique up- and downregulated genes for Young KO,resting vs M1

Gene symbol	log2FC_KO	padj_KO	Gene symbol	log2FC_KO	padj_KO
Pcp4	7,62104157	1,2017E-05	Blk	-7,58883198	9,7174E-05
Gm43079	4,93461544	0,00796024	Aff3	-6,94752371	0,00142441
Gm20708	4,62965751	0,02395397	Epdr1	-6,92594103	0,0021537
Slc6a19	4,5700384	4,9027E-09	Cdh1	-6,8897643	0,00171566
Htra4	4,50432423	5,7885E-11	P2ry10	-6,86038713	0,00270677
Arg1	3,80783922	0,00069502	Klrd1	-6,79780751	0,00316945
Cyp2ab1	3,66186177	0,01042413	Ddr1	-6,73311634	0,00384147
Pla2g4b	3,40922439	0,0196074	Ccl24	-6,67287383	0,00511099
Jsrp1	3,29060144	0,01301279	Itgad	-6,64457319	0,00359275
Dnm1	3,22745583	5,1644E-06	Fat4	-6,50365789	0,00803951
Ak4	3,149731	6,3367E-17	Smim5	-6,46439732	0,00937142
Gm16794	3,12400328	0,00059953	Vegfc	-6,45176882	0,0102643
Gm15122	3,09551464	0,00168823	Lad1	-6,3975859	0,01164519
Nxf2	3,08862117	0,04561157	Actr3b	-6,39103649	0,01215756
Gm26635	3,08404371	0,00996357	Col5a3	-6,23631574	3,8813E-06
Gm10863	3,02534954	0,00036231	Il5ra	-6,18572423	0,01666071
Gm15541	3,00661086	0,03232627	Gm45062	-6,17621337	1,4722E-05
Gm43714	2,9943217	0,00049995	Slc36a2	-6,15093031	0,0225671
3010003L21Rik	2,90316941	0,00178453	Kcna2	-6,1420157	0,02145628
Ankrd61	2,89922636	0,03023807	Cd300e	-6,13829256	0,00079469
Dnase1l3	2,84981752	1,0864E-05	Myl10	-6,08626147	0,02477509
Tgtp2	2,8091817	0,04287678	Gimap3	-6,07048929	0,02078965
5730405O15Ri	2,77782786	0,0089406	Tbxa2r	-6,04917054	0,02353108
5330438D12Rik	2,75559252	0,00012582	Siglecg	-5,97868938	1,5695E-05
Gbp8	2,71266956	6,1901E-09	Itgb8	-5,87444602	0,04263285
BC049715	2,67348996	0,00075093	Timd4	-5,84428958	0,03771003
Cep97	2,61028796	7,8308E-08	Slc35d3	-5,82666644	0,04395523
4933412A08Rik	2,59737176	0,03570198	Apol7c	-5,68536891	1,2925E-07
Gm15567	2,59372358	0,01877829	Tnfrsf13c	-5,54813335	0,00082875
Zbtb26	2,58614956	3,2284E-10	Gfi1	-5,5106928	0,01068212
Tmem240	2,56228884	0,00027613	Gm35339	-5,44059859	0,01624251
Dancr	2,55371982	0,00047803	Adgrl1	-5,42923998	0,00215938
Gm17108	2,48329295	0,03631871	5830444B04Rik	-5,40700839	0,01411734
Ly6a	2,44317251	2,1911E-11	Chil3	-5,18655925	3,1039E-32
2310031A07Rik	2,44311065	0,0462174	Arhgef37	-5,16417523	0,00137703
Hba-a2	2,30936595	0,00030005	Reck	-5,06641865	0,03307504
Id1	2,30259391	5,5718E-05	Dhtkd1	-5,03685626	0,03430544
Gramd1c	2,29717178	0,01599668	Gm26606	-5,01056991	0,03734126
Spdya	2,2955138	0,0281356	Lyzl4	-4,985971	0,01094987
Gm16754	2,29310263	0,00241409	Cxcl2	-4,92821622	0,00222074
Socs1	2,27848196	2,332E-06	Itgam	-4,79098693	0,00199142
Ggn	2,27181168	0,00089998	Adcy2	-4,72147997	0,00728091
Gm9725	2,25994409	0,0290458	Ccdc40	-4,71698363	0,02064983
Prg4	2,2477754	0,01945717	Tnfsf10	-4,61690775	2,7418E-08
Snhg4	2,24217098	3,3847E-07	Ncam1	-4,6167276	0,01252523
Spef2	2,20985002	0,01626385	Ptx3	-4,5500521	0,0341476
Gm12940	2,1520922	7,181E-06	Ninl	-4,53915989	2,4123E-05
A230072C01Rik	2,14441648	0,01871314	Gm26797	-4,53852109	0,00299739
1110035H17Rik	2,13459233	0,04536195	Siglece	-4,5266525	1,3717E-17
D130020L05Rik	2,09961212	0,00379995	Cecr2	-4,51376862	0,00260812

Supplementary table 10: List of top 50 unique up-and downregulated genes for Young WT, resting vs M1

Gene symbol	log2FC_WT	padj_WT	Gene symbol	log2FC_WT	padj_WT
U90926	8,9715895	1,6118E-06	Rab39	-6,61353019	8,1673E-07
Btbd16	7,62415831	1,128E-12	Tns4	-5,91237731	3,3567E-08
D6ErtD527e	5,33658912	1,179E-10	1700047M11Rik	-5,61277875	0,00037552
Prss50	4,98752563	6,0898E-21	Pcdhgb5	-5,40635978	6,8185E-05
Aloxe3	4,85248465	2,2306E-07	Rgs7bp	-5,39884824	7,9668E-05
Cxcr1	4,6595402	1,5268E-08	Abcc2	-5,36986382	8,2859E-05
Apol9b	4,55854333	0,03342493	Pcdhgb6	-5,13152424	2,5109E-05
Pdk4	4,55303153	2,6465E-08	Camk2a	-4,97603078	9,7717E-08
Acta1	4,36832866	8,1094E-07	Slc13a2	-4,97023378	0,00052529
Camk2n1	4,23531893	9,0773E-16	Gm4117	-4,76063256	0,00022033
Gm20406	4,18631094	1,4033E-05	5830416119Rik	-4,55745585	0,00151816
Il9r	4,14071586	0,00013495	Clca3a1	-4,50189138	0,00652276
Col27a1	4,05624264	4,9901E-11	Tmc3	-4,42986086	0,00160428
Ankmy1	4,05418169	2,5697E-06	Lgi4	-4,34442077	0,00393312
Ramp3	3,98925489	0,00025284	Epor	-4,1035262	7,2883E-05
Prss46	3,97716184	1,0364E-20	Bach2os	-4,06650322	0,00070749
Tspan18	3,9724885	1,0798E-05	Gm9949	-4,039529	0,00061705
Atp13a4	3,87434674	6,0003E-08	P2rx1	-3,92780617	8,0015E-05
Tcp10b	3,8716456	0,00011932	Armcx4	-3,91818935	9,6502E-05
RP24-155I9.3	3,76481213	1,6428E-08	Clec1a	-3,87464197	0,00160822
Gm17024	3,74283843	3,1377E-05	Trem14	-3,78792745	0,00563509
AW822252	3,72006084	0,00581037	Ceacam10	-3,77580168	0,00232038
Il6	3,71198814	0,00116483	2900005J15Rik	-3,75527099	0,00285273
Pappa2	3,61443796	0,00033317	Nat8f4	-3,66644317	0,0023239
Gm13421	3,60454002	3,8867E-07	Gbgt1	-3,66147283	1,5431E-05
Apol9a	3,59289318	0,00422594	Gm1976	-3,63886105	0,00087574
Tmeff1	3,51159494	9,4834E-12	Nek3	-3,49164042	0,00043476
Pcdh1	3,479569	2,5735E-10	Gspt2	-3,44547418	0,00384792
Gm42890	3,40275126	5,2199E-08	Mpz	-3,445437	0,00017375
Saxo2	3,39871892	0,00473807	Gm19719	-3,33306144	7,0953E-05
A330074K22Rik	3,38806922	5,3519E-13	Il20rb	-3,29217086	0,00265312
Ugt1a6b	3,31239891	1,7968E-27	Coro2b	-3,2684764	0,01120499
Gm26896	3,27722945	1,8193E-06	Atg9b	-3,26430465	1,2785E-05
Rdh9	3,26411146	5,8815E-06	Tspan2	-3,25352174	0,00054859
Dixdc1	3,2555439	0,00414327	Sult6b1	-3,22490124	0,00574982
2210418O10Rik	3,20170816	5,2444E-08	Gm42878	-3,18201767	0,00472047
Spic	3,18386787	9,2855E-07	Gnaz	-3,14308443	0,00055558
Gm26542	3,17904119	0,00024548	Gm28800	-3,14264347	0,00414492
Klrk1	3,14474683	0,00279	Ehd3	-3,11900189	0,00235814
Megf11	3,1231315	0,00112714	Gm20257	-3,10406167	0,00327918
1700086P04Rik	3,10676412	0,00059351	Hoxb3	-3,05942013	0,0109558
AV099323	3,08221707	1,7695E-07	Palm3	-3,04279599	0,00110978
Cyb561	3,06574486	4,1012E-05	Klhdc8b	-3,03599789	2,2744E-05
2200002D01Rik	3,06338583	0,00025886	Mpl	-3,01667081	0,01062273
RP23-344G11.4	3,05830779	7,8453E-05	Zfand4	-2,98635378	0,00275438
Gng3	3,03193536	0,00241475	Fam174b	-2,98386081	0,00478021
Six5	2,99833188	3,3923E-09	Vipr1	-2,95241793	0,00237472
Zfp9	2,9593431	1,021E-07	Pacsin1	-2,92759076	0,00617249
Gm44592	2,95903176	0,00316363	Fbxo48	-2,91505964	0,00913995
Spata33	2,92636998	0,00014968	Ckap2	-2,88201081	1,5665E-07

Supplementary table 11: List of top 50 unique up- and downregulated genes for Young KO, resting vs M2

Gene symbol	log2FC_KO	padj_KO	Gene symbol	log2FC_KO	padj_KO
Tmem265	9,68269007	0,03010011	Apol7c	-7,6288085	2,9777E-11
Gm4767	9,63825279	0,03090885	Pard3b	-7,17626329	0,00020389
Gm3513	8,49158825	1,0699E-05	Akr1c18	-7,15601003	0,00023265
Gfy	8,3469247	3,2375E-05	Csgalnact1	-7,04596965	0,00035865
Gm3764	7,57121152	0,00099628	Kif26b	-7,02487472	0,00035426
Gzma	7,43206502	0,00164011	Gm16194	-6,95961088	0,00050994
Gm15056	6,86378039	4,9885E-15	Tmem176b	-6,75782744	6,972E-213
Slc6a20b	6,61845432	5,1583E-06	Gm26581	-6,72945244	0,00120777
Vgf	5,6516147	0,00024056	Asgr2	-6,67001938	0,00150441
1810062G17Rik	5,27728664	2,3546E-05	Cxcl5	-6,60079735	0,00010154
Mt2	5,19010572	1,538E-185	Cxcl2	-6,43452935	1,223E-96
Hrc	5,17824723	0,00376221	Tmem254a	-6,33497832	0,04520702
Coch	5,14735273	0,0002691	Fgf13	-6,22117061	0,00059993
Efcab6	5,14178407	6,9635E-07	Gm11772	-6,13394402	0,00864371
Gm20708	4,97993525	6,9944E-06	Rgs11	-6,02814565	1,8598E-08
Gm28373	4,97371723	9,7543E-12	Gpr141	-6,00579252	1,0251E-42
A330069E16Rik	4,76817808	1,04E-33	Il1b	-5,98365242	4,5573E-22
Gm11527	4,71873818	1,2751E-06	Tmem246	-5,97758285	0,01168887
Ifrd1	4,59974687	1,409E-222	Gpr18	-5,9564653	1,768E-05
Gm12522	4,50983006	5,1803E-10	F5	-5,93768594	9,7597E-19
B430219N15Rik	4,43491252	0,00022731	Mmp9	-5,82875298	1,3712E-76
Gm17098	4,33623135	2,1938E-06	1700047M11Rik	-5,65506947	0,00262728
Hecw2	4,31342692	3,0734E-09	Fcrla	-5,63426356	8,1567E-07
Lncpint	4,27613466	3,6828E-05	Cmklr1	-5,62241489	2,274E-71
Mesp2	4,22223257	0,00305836	Cxcl1	-5,52951935	1,5621E-23
Rasd2	4,1396466	1,4597E-07	Tmprss4	-5,45837651	0,00025006
Gm26508	4,10907278	0,00960142	Slc13a2	-5,34841704	0,00805646
Pla2g5	4,10520626	1,1805E-27	Tmem176a	-5,3440597	7,69E-128
Cst7	4,0712561	2,1423E-71	Cplx2	-5,27533509	0,00508511
4930481B07Rik	3,96932385	0,00015583	Clec4a2	-5,25905417	1,1058E-13
Pla2g4b	3,95548679	2,1127E-07	Ceacam19	-5,2540126	1,7717E-18
4632427E13Rik	3,94645434	4,8886E-21	Itgb8	-5,20011795	0,01050494
Tnnc1	3,89314755	2,9877E-10	Gm15675	-5,12890688	0,00010429
Gm17200	3,88071423	0,00260986	Stab2	-5,09890678	2,0477E-14
Arhgap27os1	3,87607599	3,9703E-09	Zfp300	-5,08583646	0,01592399
Gm14416	3,85559123	0,01290653	Itga2	-5,07999518	0,01465306
Stx1a	3,80633953	8,1333E-28	St8sia1	-5,07912891	0,00064012
2810029C07Rik	3,7896314	0,00023052	Tlr5	-5,06706177	0,01856674
Cxcl9	3,7863008	1,3319E-30	Cfh	-5,01191951	0,00013388
Sdcbp2	3,77889897	3,5536E-06	Klk1b11	-5,00632945	2,0781E-06
2010015M23Rik	3,69828058	0,00160064	Slc13a3	-4,99267565	1,7381E-62
Gm17024	3,69255807	2,942E-06	Kynu	-4,98859724	4,2459E-06
Gdf15	3,67774599	5,5734E-92	Gbgt1	-4,98007352	6,8366E-10
Gm7008	3,66950334	4,5514E-49	Sardh	-4,96567101	4,792E-05
Gm2004	3,66384098	0,00295018	Lpcat2	-4,96245412	2,8839E-96
Gm7496	3,65115351	0,00231096	Rab44	-4,94814858	2,386E-16
Traf4	3,65113853	4,3883E-34	Gm5150	-4,91978867	6,6377E-18
Gm10501	3,61927577	1,521E-05	Hp	-4,91555888	2,4569E-64
Gm43079	3,56078873	0,04069248	Ace	-4,8945012	0,01898173
Gm13684	3,54042106	0,00642376	Klrb1a	-4,88792438	0,02170297

Supplementary table 12: List of top 50 unique up- and downregulated genes for Young WT, resting vs M2

Gene symbol	log2FC_WT	padj_WT	Gene symbol	log2FC_WT	padj_WT
Sspo	3,65783178	0,00144029	F730016J06Rik	-6,75806318	1,0784E-09
Susd2	3,5353158	7,8373E-05	Mrgpra2b	-6,50322521	1,0758E-05
Greb1	3,41276321	7,1449E-05	Ms4a3	-6,20116111	1,2606E-07
Dpep1	3,29400828	0,00017489	Prss57	-6,12582245	0,00026587
Gm996	3,28517547	2,1828E-09	Abca13	-5,61761174	9,2487E-12
Dnah2	2,97700233	1,3203E-06	2010110K18Rik	-5,53631233	0,00024423
Wdr38	2,97171313	6,7856E-07	Mogat2	-5,30400731	1,276E-06
Dixdc1	2,91698575	0,0010871	Gm12744	-5,25575115	4,5312E-06
Kcnn3	2,75628245	0,00079602	Rag1	-4,90492494	0,00351393
Vnn3	2,74509237	0,00817042	Cd300lg	-4,74532742	2,4058E-07
Axin2	2,72571423	8,4601E-06	Crispld2	-4,54577858	5,8452E-09
Nrg1	2,68957588	0,01204472	D130058E05Rik	-4,36143144	0,00036807
Slit3	2,66481432	4,5836E-05	Lrg1	-4,06306065	0,00059357
Adamts13	2,64353543	0,00247078	Serpinb12	-4,00298126	6,7355E-05
Prl2c2	2,60649943	0,01546349	Gm28048	-3,87315035	0,0113427
4931431C16Rik	2,58907109	0,03118751	Serpinb10	-3,79841541	1,8884E-07
Zfp786	2,57044191	0,00359053	lfnlr1	-3,74161167	2,6965E-06
Mgat3	2,53254165	0,00495638	Galnt3	-3,6993344	1,3195E-05
Acpp	2,43910093	0,00068956	Steap4	-3,36052533	0,03025904
Il1r1	2,37350056	1,3689E-10	Kcnb1	-3,30234146	2,381E-10
Prelp	2,32917649	0,00068208	Ccdc92	-3,2397862	0,02122531
Car11	2,32366535	0,00028789	1700006J14Rik	-3,23160866	0,00156688
Gm5345	2,32341196	5,6223E-07	Zfp831	-3,22611657	0,00288051
Ntn4	2,31247608	0,03746968	Gm3571	-3,21360528	0,00023137
Lif	2,2474137	2,3814E-05	Lamb3	-3,17876755	0,00052797
Fgf7	2,23135562	8,7954E-05	BC065397	-3,11095064	0,00250659
Olr1	2,20693342	1,8385E-07	Cyp2s1	-3,07365971	0,00867688
Dll4	2,20195708	0,01049625	Dkk2	-3,0662586	0,04304842
Dyx1c1	2,19542644	0,00644606	Mpz	-3,04627268	1,5373E-05
Gm6297	2,15861466	0,01158856	Slco4a1	-2,9481451	3,8544E-07
Pagr1b	2,10035902	0,01114032	Ppm1e	-2,87587732	0,00052914
4930550C14Rik	2,08284659	0,01844599	Gm9949	-2,79929818	3,0201E-06
Rbm20	2,05904785	0,0220307	Aff3	-2,79542969	0,01124766
Aicda	2,00019146	0,03028068	Mbnl3	-2,72815964	8,5828E-06
Gnb3	1,98281305	0,03347631	Pla2g4c	-2,71954812	0,00773852
Sult2b1	1,94916944	0,00264825	Chdh	-2,5896245	2,0111E-05
Dzank1	1,94847702	0,01447305	Lockd	-2,47949654	0,00113702
Hpx	1,94148017	0,00874697	Dnah14	-2,39864322	2,2973E-05
Slc16a14	1,93184748	0,00532325	Phf24	-2,38644459	0,02122019
Mttp	1,88790785	2,0111E-05	Gm17383	-2,36851251	0,01114032
Fam110c	1,86552043	0,00340264	Bcl6b	-2,35087354	0,00304362
4933406C10Rik	1,86015915	0,03517701	Gm16793	-2,26700011	0,00537133
4930480K23Rik	1,85407379	0,00505362	Nid2	-2,24964723	0,00268013
Srcin1	1,80850342	0,02849113	Smim5	-2,22985277	0,02059288
Lefty1	1,79818645	0,00034488	Txlnb	-2,19482587	0,00299587
Zfp334	1,77496657	0,00226983	Cenpk	-2,10774827	0,00017166
Gm15541	1,76281549	0,03341191	Kcnk5	-2,10058271	0,0207511
BC034090	1,76046004	0,03804902	Gm16104	-2,03384359	0,0053842
Cideb	1,7494459	0,00012896	Cngb1	-2,03231693	0,03099833
Plxnb1	1,73574784	0,03485404	Stxbp6	-2,02600311	0,04630421

Supplementary table 13: List of buffers and solutions

Buffer/solution	Composition or company
10x TBS	200mM Tris (pH 7.6), 1.37M sodium chloride
10x TGS buffer	25mM Tris (pH 8.3), 192 mM glycine, 0.1 % (w/v) SDS
5x SDS loading dye	250mM Tris, 10% (w/v) SDS, 50% (v/v) glycerol, 500mM DTT
Anode buffer 1	30 mM Tris, 20 % (v/v) methanol
Anode buffer 2	300 mM Tris, 20 % (v/v) methanol
Blocking solution	5 % (w/v) non-fat dry milk in TTBS
Cathode buffer	25 mM Tris, 20 % (v/v) methanol, 40 mM 6-amino-n-caproic acid
Carnoy fixative	60% ethanol, 30% chloroform, 10% glacial acetic acid, 1 g ferric chloride
ECL substrate	GE Healthcare, Freiburg, Germany, cat. nr. RPN2109
FCS	PAA Lab/GE Healthcare, Freiburg, Germany, cat. nr. PAA A15-151
Loading gel	0.5 M Tris (pH 6.8), 0.4 % (w/v) SDS
MOPS SDS Running Buffer (20X)	Novex/Life Technologies, Darmstadt, Germany, cat. nr. NP001
PBS	8 g/l sodium chloride, 0.2 g/l potassium chloride, 1.56 g/l disodium phosphate, 0.24 g/l monopotassium phosphate, pH 7.4
RIPA buffer	150 mM sodium chloride, 1 % (v/v) NP40, 0.5 % (w/v) deoxycholic acid, 0.1 % (w/v) SDS, 50 mM Tris (pH 8.0)
Separation buffer	1.5 M Tris (pH 8.8), 0.4 % (w/v) SDS
1% Formalin	10x Formalin (1:10) in PBS
Smart Ladder	Eurogentec, Cologne, Germany, cat. nr. MW-1700-10
Stacking buffer	0.5 M Tris (pH 8.8), 0.4 % (w/v) SDS
Stripping buffer	62.5 mM Tris (pH 6.8), 2 % (w/v) SDS
TTBS	1x TBS, 0.1 % (v/v) Tween20
TripLE® Express	Gibco (Life technologies (Darmstadt, Germany))
FACS washing buffer (FWB)	0.5 % (w/v) BSA in PBS
MACS washing buffer (MWB)	1x PBS supplemented with 2mM EDTA, and 0.5% (v/v) BSA
Hybridization solution	Distilled water supplemented with 0.9M NaCl, 10mM Tris-HCL (pH 7.4), 0.1% SDS, Formamide 35%.
FISH washing buffer	Distilled water supplemented with 0.9M NaCl and 20mM Tris-HCL pH7.4
Lymphoprep 250ml	Progen Biotechnik GmbH 1114544

Supplementary table 14: List of cell culture media

Medium	Composition or company
BMDM medium	DMEM and Macrophage SFM medium (1:1) supplemented with 10 % (v/v) FCS, 5 % (v/v) Penicillin/Streptomycin, 5 % (v/v) Amphotericin
DMEM cell culture medium	Gibco (Darmstadt, Germany)
Hank's Balanced Salt Solution (HBSS)	Gibco (Darmstadt, Germany)
DMEM Glutamax	Gibco/Life Technologies, Darmstadt, Germany cat. nr. 61965-059
IntestiCult™ GM (Mouse organoids)	Stemcell cat nr. 6005
IntestiCult™-SF GM (Human organoids)	Stemcell cat nr. 100-0340

Supplementary table 15: List of used reagents

Reagent	Producer
1 % Eosin solution	Roth (Karlsruhe, Germany)
10 % Formalin	Sigma Aldrich (Munich, Germany)
10 x BD FACS Lysing Solution	BD Biosciences (Heidelberg, Germany)
30 % Bis-acrylamide (37.5:1)	Bio-Rad (Munich, Germany)
Hydrogen peroxide (H ₂ O ₂)	Sigma Aldrich (Munich, Germany)
6-aminocaproic acid	Sigma Aldrich (Munich, Germany)
Agarose	Biozym (Hessisch Oldendorf, Germany)
Agarose Ammonium persulfate (APS)	Sigma Aldrich (Munich, Germany)
Azoxymethane (AOM)	Sigma Aldrich (Munich, Germany)_A5486
Blotting grade blocker (non-fat dry milk)	Bio-Rad (Munich, Germany)
Bovine serum albumin (BSA)	Roth (Karlsruhe, Germany)
CD11b MicroBeads (human and mouse)	Miltenyi BioTec (Bergisch Gladbach, Germany)
Citric acid	Roth (Karlsruhe, Germany)
Deoxynucleotide triphosphates (dNTPs)	Thermo Scientific (Darmstadt, Germany)
Dimethyl sulfoxide (DMSO)	Sigma Aldrich (Munich, Germany)
Dithiothreitol (DTT)	Sigma Aldrich (Munich, Germany)
ECL™ Western Blotting Detection Reagents	GE Healthcare (Hamburg, Germany)
Ethanol	Roth (Karlsruhe, Germany)
Ethylenediaminetetraacetic acid (EDTA)	Sigma Aldrich (Munich, Germany)
Fc-receptor block (anti-CD16/32)	BD Biosciences (Heidelberg, Germany)
Fetal calf serum (FCS)	Merck Millipore (Darmstadt, Germany)
FITC-Dextran	Sigma Aldrich (Munich, Germany)
Ficol	Sigma Aldrich (Munich, Germany)
Hematoxylin solution	Th Geyer (Renningen, Germany)
Recombinant murine Interleukin 13 (IL-13)	PeproTech cat. Nr 210-13
Interleukin 4 (IL-4)	Immunotools cat. Nr. 12340045
Interferon γ (IFNγ) (recombinant mouse)	Immunotools Cat. Nr 1234536
Lipopolysaccharid (Escherichia coli, F515)	Sigma cat nr. L2880-10MG

rm M-CSF	Immunotools cat. Nr. 12343125
Matrigel®	BD bioscience (Heidelberg, Germany)
Methanol	Roth (Karlsruhe, Germany)
Nuclease-free water	Qiagen (Hilden, Germany)
Paraffin	Thermo Scientific (Darmstadt, Germany)
Penicillin-Streptomycin (10,000 U/mL)	Life Technologies (Darmstadt, Germany)
Pierce ECLTM Plus Western Blotting substrate	Thermo Scientific (Darmstadt, Germany)
Protease and phosphatase inhibitor	Thermo Scientific (Darmstadt, Germany)
Proteinase K	Thermo Scientific (Darmstadt, Germany)
Roti-Histo-Kit mounting medium	Roth (Karlsruhe, Germany)
Sodium chloride (NaCl)	Merck Millipore (Darmstadt, Germany)
Sodium dodecyl sulfate (SDS)	Roth (Karlsruhe, Germany)
Sodium hydroxide (NaOH)	Merck Millipore (Darmstadt, Germany)
SYBR® Select Master Mix	Applied Biosystems (Darmstadt, Germany)
TaqMan Gene Expression Master Mix	Applied Biosystems (Darmstadt, Germany)
Tris	Merck Millipore (Darmstadt, Germany)
Tween 20	Roth (Karlsruhe, Germany)
Xylene	Thermo Scientific (Darmstadt, Germany)
β-Mercaptoethanol	Sigma Aldrich (Munich, Germany)

Supplementary table 16: Devices used in this study

Device	Company
100-1000 µL pipette	Eppendorf, Hamburg, Germany
10-100 µL pipette	Eppendorf, Hamburg, Germany
10-200 µL multi-channel pipette	Eppendorf, Hamburg, Germany
1-10 µL pipette	Eppendorf, Hamburg, Germany
7900 HT Fast Real-Time PCR System	Applied Biosystems/Life Technologies, Darmstadt, Germany
96-well thermocycler	Applied Biosystems/Life Technologies, Darmstadt, Germany
ABI PRISM® 3700 sequencer	Applied Biosystems/Life Technologies, Darmstadt, Germany
Assistant Mini-Centrifuge SPROUT	Heathrow Scientific, Nottingham, United Kingdom
Axio Imager.Z1	Zeiss, Jena, Germany
Balance	PeqLab, Erlangen, Germany
Cellometer Auto T4 Plus	PeqLab Biotechnologie GmbH, Erlangen, Germany
Megafuge 16R	Thermo Scientific, Bremen, Germany
Fresco 21	Thermo Scientific, Bremen, Germany
Certomat MV, vortex mixer	B. Braun Biotech Internat., Melsungen, Germany
ChemiDoc MP Imaging System	Bio Rad, Munich, Germany

Confocal microscope: TCS SP5	Leica Microsystems, Wetzlar, Germany
Electrophoresis chamber Multigel G44	Tecan (Männedorf, Switzerland)
Electronic pipet filler	Eppendorf, Hamburg, Germany
Adjustable volume pipette	Eppendorf, Hamburg, Germany
SA3800 Spectral analyzer	SONY Biotechnology
GeneAmp PCR System 9700	Applied Biosystems- Life Technologies, (Darmstadt, Germany)
Gentle-MACS™ Dissociator	Miltenyi Biotec (Bergisch Gladbach, Germany)
HiSeq3000	Illumina (San Diego, United States)
Incubator for cell culture	Binder (Tuttlingen, Germany)
IBIDI culture inserts 2 wells	Ibidi (Gräfeling, Germany)
Laminar flow workbench HERA Safe KS	Thermo Scientific (Bremen, Germany)
Leica RM 2255 microtome	Leica Microsystems (Wetzlar, Germany)
Magnetic stirrer C-MAG HS 7 IKAMAG	IKA, Staufen, Germany
Microplate reader Infinite M200 Pro	Tecan, Männedorf, Switzerland
Mini-Sub Cell GT	Bio-Rad, Munich, Germany
NanoDrop ND-1000 spectrophotometer	PeqLab Biotechnologie GmbH, Erlangen, Germany
RM2255 microtome	(Leica, Wetzlar, Germany)
Sonificator Sonopuls	Eppendorf (Hamburg, Germany)
Tecan Infinite F200 pro plate reader	Tecan, Männedorf, Switzerland
Thermomixer compact 5350	Eppendorf, Hamburg, Germany
Trans-Blot® Turbo™ Transfer System	Bio-Rad, Munich, Germany
Tube roller SRT6	Stuart Equipment (Staffordshire, United Kingdom)
VIIA 7 PCR system	ThermoFisher (Waltham, MA)
Vortex-Genie 2 Variable Speed	Sartorius (Göttingen, Germany)
Water bath 1013	GFL (Burgwedel, Germany)
Water purification system	TKA (Niederelbert, Germany)

Supplementary table 17: List of applied kits

Kit	Company
Maxima H Minus First Strand cDNA Synthesis Kit	Thermo Scientific (Bremen, Germany)
BIO-RAD DC protein assay	BIO-RAD (Munich, Germany)
QIAshredder	Qiagen (Hilden, Germany)
RNeasy Mini Kit	Qiagen (Hilden, Germany)
Taqman Universal PCR MasterMix	Life Technologies (Darmstadt, Germany)
Arginase activity Kit	Sigma- Aldrich (St. Luis, USA)
Nitric Oxide Synthase Activity Assay Kit)	Abcam (ab211083)
DNeasy PowerSoil Kit (100)	Qiagen (Hilden, Germany)
DNeasy Blood and Tissue kit	Qiagen (Hilden, Germany)
Phagocytosis Assay Kit (Green Zymosan)	Abcam ab234053
Lineage Cell Depletion Kit, mouse	Miltenyi Biotec 130-090-858
LP dissociation Kit for mouse	Milenty BioTech (Bergisch Gladbach, Germany)
Vectastain Elite ABC Kit	Vector Labs (Peterborough, United Kingdom)

Supplementary table 18: List of software

Software	Developer or Company
Imagej 1.53e	Wayne Rasband, National Institutes of Health, USA
SA3800	SONY biotechnology
ZEN 3.4.91.00000 (Blue edition)	Carl Zeiss Microscopy GmbH
Gel analyzer 2010a Freeware	Copyright 2010 by Dr. Istvan Lazar
Image Lab Version 6.1.0 build 7 St. ed.	Bio-Rad, Munich, Germany
GraphPad Prism version 9.3.1	GraphPad Software Inc., La Jolla, USA
i-control TM 1.9	Tecan, Männedorf, Switzerland
AxioVision Rel 4.9	Carl Zeiss, Oberkochen, Germany
R Statistical Software	v.4.2.0; R Core Team 2022

Supplementary table 19: List of antibodies and fluorescent markers

Antibody/fluorescent marker	provider
Anti Arginase 1 (ARG1)	ThermoFischer #PA5-29645
iNOS (D6B6S) Rabbit mAb	Cell signaling #13120
Human/Mouse DNMT3A Antibody	RnD systems #MAB63151
E-cadherin (E-Cad)-AF488	BD Biosciences #610182
DAPI	Sigma Aldrich, #D9542
Rhodamine/Phalloidin	Invitrogen™ #R415

Supplementary table 20: List of used consumables

Consumable	Company
0.5 mL/1.5 mL/2.0 mL tubes	Sarstedt (Nümbrecht, Germany)
100ml culture flasks	Schott, Mainz, Germany
1.5 mL/2.0 mL safe seal tubes	Sarstedt (Nümbrecht, Germany)
1-10-20 mL syringe	BD Biosciences (Heidelberg, Germany)
1-10 µL/10-100 µL/100-1000 µL pipette (filter) tips	Sarstedt (Nümbrecht, Germany)
15 cm/10 mL petri dish	Sarstedt (Nümbrecht, Germany)
15 mL/50 mL tubes	Sarstedt (Nümbrecht, Germany)
18G/20G/26G needles	BD Biosciences (Heidelberg, Germany)
384-well plates	Life Technologies (Darmstadt, Germany)
40 µm/70 µm cell strainer	BD Biosciences (Heidelberg, Germany)
5 mL/10 mL/25 mL serological pipettes	Sarstedt (Nümbrecht, Germany)
6-well/12-well/96-well plate (flat bottom)	Sarstedt (Nümbrecht, Germany)
96-well V-bottom plate	BD Biosciences (Heidelberg, Germany)
cell scraper	Sarstedt (Nümbrecht, Germany)
coverslips (24x50mm)	Geyer (Renningen, Germany)
FACS tubes	Greiner (Frickenhäusen, Germany)
EDTA tubes	Sarstedt (Nümbrecht, Germany)
MACS MS columns	Miltenyi BioTec (Bergisch Gladbach, Germany)
Nunc Lab-Tek II Chamber Slide 8-wells	Thermo Scientific (Darmstadt, Germany)
Culture-Inserts 2 Well for self-insertion	IBIDI Cat. Nr. 80209
Surgical disposable scalpels	B. Braun, Melsungen, Germany
Roti-Histo-Kit mounting medium	Roth, Karlsruhe, Germany
Roti-Labo 0.22µm syringe filter	Roth, Karlsruhe, Germany
Polyvinylidene difluoride (PVDF) membranes	Bio-Rad, Munich, Germany
6.5 mm Transwell® 0.4 µm pore Insert	Corning, Cat. Nr. 3470

Supplementary table 21: Primer sequence and assays

Target	Sequence
Dnmt3a (ms)	F: CAGCAGCTCCTCTCTGGAGCGTTTT R: GCTCCAGAGAGGAGCTGCTGCGGTG
Dnmt3b (ms)	F: AGGAGTGCATTATCGTTAATGTTTT R: ATTAACGATAATGCACTCCTCGGTG
Tnf (ms)	F: TCACACTCAGATCATCTTCTC R: AGACTCCTCCCAGGTATATG
Retnla (ms)	F: CCTTCTCATCTGCATCTCCC R: GGGATAGTTAGCTGGATTGGC
Arg-1 (ms)	F: AACACTCCCCTGACAACCAG R: GTTCCCCAGGGTCTACGTCT
Cxcl1 (ms)	F: AACCGAAGTCATAGCCACAC R: GTTGGATTTGTCAGTGTTCAGC
Cxcl10 (ms)	F: AAGTGCTGCCGTATTTTCT R: TCTTTTTTCATCGTGGCAATG

lrg-1 (ms)	F: ACGGCTTGAAAGTGAACCAC R: GTGCTGGAGGTGTTGGAAC
DNMT3A (human)	TaqMan 01027166
DNMT3B (human)	TaqMan 00171876
CXCL10 (human)	TaqMan 00171042
CCND1 (human)	TaqMan 00432359

9.5 Curriculum vitae

PERSONAL DATA

First and last name: Dora Bordoni

Date of birth: 17.02.1992

Place of birth: Sondrio, Italy

Nationality: Italian

CONTACTS

E-mail: dorabordoni@gmail.com

EDUCATION - RESEARCH EXPERIENCE

- | | |
|-------------------|---|
| 09/2018-12/2022 | <p>Christian-Albrechts-University Kiel, Germany
PhD student at Institute of Clinical Molecular Biology</p> <p>Dissertation title: "On the role of DNA methyltransferase 3A (DNMT3A) in myeloid cells in intestinal homeostasis and inflammatory responses"
Leading scientist: Prof. Dr. Philip Rosenstiel</p> |
| 06/2015-10/2017 | <p>University of Gent, Belgium
Master of Science in Biochemistry and Biotechnology</p> <p><u>Master project 1: Study of the importance of ER stress and autophagy in the pathology of multiple sclerosis</u>
Leading scientist: Prof. Geert Van Loo</p> <p><u>Master project 2: Growth regulating protein complexes in Zea mays</u>
Leading scientist: Prof. Geert De Jaeger</p> <p><u>Master thesis title: Characterizing the dynamics of growth regulatory protein complexes in maize</u>
Leading scientist: Prof. Geert De Jaeger</p> |
| 09/2011-02/2015 | <p>University of Milan, Italy
Bachelor in Veterinary Biotechnology</p> <p><u>Bachelor Thesis: Determination of genes encoding for antigens of <i>E.coli</i> in GM <i>Nicotiana tabacum</i></u>
Leading scientists: Prof. Antonella Baldi and Dr. Luciana Rossi</p> |
| 09/2007 - 07/2011 | <p>High school - Scientific lyceum "C. Donegani", Sondrio, Italy</p> |

SCIENTIFIC CONTRIBUTION

Antonella Fazio*, **Dora Bordoni***, Jan W.P. Kuiper, Saskia Weber-Stiehl, Stephanie T. Stengel, Philipp Arnold, David Ellinghaus, Go Ito, Florian Tran, Berith Messner, Anna Henning, Joana P. Bernardes, Robert Häsler, Anne Luzius, Simon Imm, Finn Hinrichsen, Andre Franke, Samuel Huber, Susanna Nikolaus, Konrad Aden, Stefan Schreiber, Felix Sommer, Gioacchino Natoli, Neha Mishra and Philip Rosenstiel

* Shared first authorship

DNA methyltransferase 3A controls intestinal epithelial barrier function and regeneration in the colon. *Nature Communications*, 2022

Antonella Fazio, **Dora Bordoni** and Philip Rosenstiel

Inflammatory Bowel Disease and Epigenetics. Book chapter in *Molecular Genetics of Inflammatory Bowel Disease*

Neha Mishra, Konrad Aden, Johanna I. Blase, Nathan Baran, **Dora Bordoni**, Florian Tran, Claudio Conrad, Diana Avalos, Charlot Jaeckel, Michael Scherer⁴, Signe B. Sørensen, Silja H. Overgaard, Berenice Schulte, Susanna Nikolaus, Guillaume Rey, Gilles Gasparoni, Paul A. Lyons, Joachim L. Schultze, Jörn Walter, Vibeke Andersen, SYSCID Consortium, Emmanouil T. Dermitzakis, Stefan Schreiber, Philip Rosenstiel

Longitudinal multi-omics analysis identifies early blood-based predictors of anti-TNF therapy response in inflammatory bowel disease. *Gastroenterology*, 2022

Felix Wottawa, **Dora Bordoni**, Nathan Baran, Philip Rosenstiel, Konrad Aden

The role of cGAS/STING in intestinal immunity. *European Journal of Immunology*, 2021

Finn Hinrichsen Jacob Hamm, Magdalena Westermann, Lena Schröder, Kensuke Shima, Neha Mishra, Alesia Walker, Nina Sommer, Kenneth Klischies, Daniela Prasse, Johannes Zimmermann, Sina Kaiser, **Dora Bordoni**, Antonella Fazio, Georgios Marinos, Georg Laue Simon Imm Valentina Tremaroli, Marijana Basic, Robert Häsler, Ruth A.Schmitz Stefan Krautwald Andrea Wolf, Bärbel Stecher, Philippe Schmitt-Kopplin , Christoph Kaleta, Jan Rupp, Fredrik Bäckhed, Philip Rosenstiel, Felix Sommer

Microbial regulation of hexokinase 2 links mitochondrial metabolism and cell death in colitis. *Cell metabolism*, 2021

Joana P Bernardes, Neha Mishra, Florian Tran, Thomas Bahmer, Lena Best, Johanna I Blase, **Dora Bordoni**, ..., Stefan Schreiber, Joachim L Schultze, Philip Rosenstiel, HCA Lung Biological Network; Deutsche COVID-19 Omics Initiative (DeCOI)

Longitudinal Multi-omics Analyses Identify Responses of Megakaryocytes, Erythroid Cells, and Plasmablasts as Hallmarks of Severe COVID-19. *Immunity*, 2020

Lena Schröder, Sina Kaiser, Burkhardt Flemer, Jacob Hamm, Finn Hinrichsen, **Dora Bordoni**, Philip Rosenstiel, Felix Sommer

Nutritional Targeting of the Microbiome as Potential Therapy for Malnutrition and Chronic Inflammation. *Nutrients*, 2020

Stephanie T. Stengel, Antonella Fazio, Simone Lipinski, Martin T. Jahn, Konrad Aden, Go Ito, Felix Wottawa, Jan W. P. Kuiper, Olivia I. Coleman, Florian Tran, **Dora Bordoni**, Joana P. Bernardes, Marlene Jentzsch, Anne Luzius, Sandra Bierwirth, Berith Messner, Anna Henning, Lina Welz, Nassim Kakavand, Maren Falk-Paulsen, Simon Imm, Finn Hinrichsen, Matthias Zilbauer, Stefan Schreiber, Arthur Kaser, Richard Blumberg, Dirk Haller, Philip Rosenstiel

Activating Transcription Factor 6 Mediates Inflammatory Signals in Intestinal Epithelial Cells Upon Endoplasmic Reticulum Stress. *Gastroenterology*, 2020

9.6 Eidesstattliche Erklärung

Hiermit erkläre ich, Dora Bordoni, an Eides statt, dass ich die vorliegende Arbeit unter der wissenschaftlichen Leitung von Prof. Dr. Philip Rosenstiel selbstständig und ohne fremde Hilfe verfasst habe. Die Abhandlung stellt nach Form und Inhalt meine eigene Arbeit dar und ich habe außer der Beratung meiner Betreuer, Prof. Dr. Philip Rosenstiel keine weitere Hilfe in Anspruch genommen.

Weiterhin habe ich keine anderen als die von mir angegebenen Quellen und Hilfsmittel benutzt und die den verwendeten Werken wörtlich und inhaltlich entnommenen Stellen als solche kenntlich gemacht. Die Arbeit wurde unter der Einhaltung der Regeln guter wissenschaftlicher Praxis der Deutschen Forschungsgemeinschaft erstellt. Auszüge der Dissertation wurden bereits in wissenschaftlichen Artikeln veröffentlicht.

Ich versichere, dass ich weder an der Christian-Albrechts-Universität zu Kiel noch anderweitig versucht habe, eine Dissertation einzureichen oder mich einer Promotionsprüfung zu unterziehen.

Hiermit erkläre ich, dass mir kein akademischer Grad entzogen wurde.

Kiel, den